



NATIONAL WATER USE QUANTIFICATION OF INDIGENOUS FORESTS USING REMOTELY SENSED EVAPOTRANSPIRATION DATA

Report to the
WATER RESEARCH COMMISSION

by

**A van Niekerk¹, G Stephenson¹, C Jarmain^{1,4}, J du Plessis¹, B Davids¹,
C Higgs¹, A Watson², L Mucina^{1,3}**

¹ Centre for Geographical Analysis, Geography and Environmental Studies, Stellenbosch University

² School of Climate Studies, Stellenbosch University

³ Harry Butler Institute, Murdoch University

⁴ Department of Biological Sciences, Faculty of Science and Engineering, University of Limerick, Limerick, Republic of Ireland

WRC Report No. 3131/1/24
ISBN 978-0-6392-0605-9

April 2024



Obtainable from

Water Research Commission
Bloukrans Building, Lynnwood Bridge Office Park
4 Daventry Street
Lynnwood Manor
PRETORIA

orders@wrc.org.za or download from www.wrc.org.za

This is the final report of WRC project no. C2020/2021-00510.

DISCLAIMER

This report has been reviewed by the Water Research Commission (WRC) and approved for publication. Approval does not signify that the contents necessarily reflect the views and policies of the WRC, nor does mention of trade names or commercial products constitute endorsement or recommendation for use.

EXECUTIVE SUMMARY

BACKGROUND AND RATIONALE

Indigenous forests (known in other parts of the world as ‘natural forests’) are a multilayered vegetation structure comprised of largely evergreen or semideciduous trees (often endemic or sub-endemic) with a crown cover of over 75%. Bushes and shrub plant species may also be present, but graminoid species are rare (Von Maltitz *et al.*, 2003). Although indigenous forests cover less than 0.4% of South Africa's total land area, they are home to more than 1 700 indigenous tree and shrub species belonging to about 370 genera and 97 families (Dye *et al.*, 2008b). Forestry activities in indigenous forests involve protecting, developing and managing this critical natural and cultural resource. However, the indigenous forests in South Africa are highly fragmented and diverse, which complicates their effective management.

South Africa is classified as a water-scarce country, with an estimated average annual rainfall ranging between 451 and 495 mm, depending on the source quoted. An estimated 21% of SA is considered arid, receiving less than 200 mm/yr of rainfall, with 44% regarded as semi-arid, receiving between 200 and 500 mm/yr (Annandale *et al.*, 2011). The recent droughts experienced in Southern Africa drew renewed attention to the water scarcity in the region and have intensified the competition for water resources among land uses. The chief competitors are urban settlements, agriculture and forestry.

In a recently completed Water Research Commission (WRC) report, titled *THE APPLICATION OF NATIONAL SCALE REMOTELY SENSED EVAPOTRANSPIRATION (ET) ESTIMATES TO QUANTIFY WATER USE AND DIFFERENCES BETWEEN PLANTATIONS IN COMMERCIAL FORESTRY REGIONS OF SOUTH AFRICA* (Van Niekerk *et al.*, 2023) (WRC Report No. 29661/23), the value of Earth observation (EO) methods for estimating water use by plantation forests at regional (national) scales was demonstrated. EO methods were also used to quantify the water use of different commercial forest genera (e.g. *Eucalyptus*, *Pinus* and *Acacia*). Other factors impacting water use, such as plantation age, species (clone/hybrid), climate and terrain, were also investigated. One of the recommendations of that project was to carry out a similar study on indigenous forests as this will assist in better understanding the impact of afforestation and deforestation on stream-flow reduction. It will also assist in understanding how environmental and topographic factors influence water use of trees at regional scales.

METHODOLOGY

This project aimed to quantify and characterise the water use (evapotranspiration) of indigenous forests throughout South Africa. The first step towards achieving this aim was to produce a geographical database of indigenous forests in South Africa. The knowledge review revealed that the most up-to-date and accurate indigenous forest map was the recently produced IF2021 (Mucina *et al.*, 2022),

consisting of 21 forest types (in South Africa). Despite its overall quality, upon close examination, the IF2021 exhibited spatial accuracy inconsistencies stemming from digitisation at different spatial scales. The project team consequently set out to improve the IF2021 for this project by using a fully automated knowledge-based image classification (KBIC) procedure developed to differentiate indigenous forests from other land covers. The KBIC makes use of a range of EO data, including multispectral satellite imagery (Sentinel-2), very high spatial resolution (50 cm) and low spectral (RGB) aerial imagery, as well as a 2 m resolution digital surface model (DSM). The KBIC procedure was applied to areas with known indigenous forests to produce a highly accurate indigenous forest cover map, internally referred to as IF2022, which was further refined through manual correction into the IF2023. The IF2023 was subsequently disaggregated into forest types using the IF2021 forest type classification as basis. A proximity-based geospatial methodology was developed for this purpose. The resulting map is called IF2024. The final step in the indigenous forest mapping procedure was to manually check and edit the IF2024, facilitated by an online geographic information system (GIS) web application developed in-house for this purpose.

The second project objective was to determine indigenous forests' consumptive water use (actual ET) using existing remote sensing (RS) data. The WaPOR product (FAO 2024) was deemed the most suitable for this purpose and monthly WaPOR ET values from 2009 to 2023 were extracted for each forest type in the IF2024. The extracted WaPOR data were compared to historical field-based measurements for verification purposes (Objective 3). Unfortunately, such data were scant, and only a handful of historical measurements could be directly related to the extracted WaPOR ET data. Nevertheless, the information helped us understand the uncertainties in the WaPOR ET data.

The final objective of this project was to describe, analyse and interpret location-specific differences in water use between indigenous forest types at specific locations in South Africa. A total of 24 readily available climate, terrain and soil characteristics were collated at national scale and compared to the ET values for all forest types. Univariate statistical analyses (correlation analyses and regression modelling) were conducted to find relationships between each environmental variable and the ET values extracted per forest patch. In addition, multivariate machine learning modelling was used to determine which environmental factors are the most important drivers of forest water use. The results of these analyses were interpreted within the ecological and biophysical context of the various forest types.

MAIN FINDINGS

One of the main findings of this project is that there is a dire need for an up-to-date and accurate indigenous forest map of South Africa. The absence of such a map makes studies about water use impossible. More importantly, without such a map, there is no way to assess whether our forests are being managed sustainably and determine the rate at which forests are lost. Based on international trends and the growing pressures relating to reporting greenhouse gas emissions from different land uses, an accurate and up-to-date indigenous forest map will be critical to quantify the carbon stocks and fluxes of forests and their relationship to biodiversity. This project updated and refined the latest indigenous forest map (Mucina *et al.*, 2022), the IF2021. The refined map, called IF2024, is an

invaluable resource, not only for this project, but for future research.

Using the IF2024 and long-term WaPOR ET data, we found that the median ET of all indigenous forests is 989 mm/yr, with medians per forest type ranging from 296 mm/yr (Arid Zone Riparian Woodland, ARF1) to 1 338 mm/yr (Subtropical Indian Ocean Mangrove, AMAN1). Comparing WaPOR ET estimates to previous field-based ET estimates showed varying results. For instance, the annual ET for Cape Afrotemperate Forest was estimated as 933 mm/yr and 1 175 mm/yr in previous studies, while the median WaPOR ET for this forest type is 1 224 mm/yr. In contrast, the ET for Subtropical Scarp Forest was estimated by Dye *et al.* (2008c) to be 668 mm/yr, while the WaPOR ET median for this forest type is 1 054 mm/yr. The ET of Arid Zone Riparian Woodland was estimated by Dye *et al.* (2008c) to be 1 094 mm/yr, while the median ET of this forest type is 296 mm/yr according to the WaPOR data. These large deviations are concerning and cannot be explained. Therefore, the absolute ET estimates produced in this research project should be interpreted by taking these uncertainties into account.

Given that the focus of this project was on studying regional water use variations and relating these variations to a selection of environmental factors, the WaPOR ET data was used as it provides a long-term ET dataset that has been proven useful in past studies. More importantly, it provides ET data at regional scales. Univariate statistical analyses and multivariate machine learning were used to better understand the regional variations in indigenous forests' water use and relate these variations to environmental conditions. None of the univariate statistical methods produced strong models, which suggests that water use of indigenous forests is complex and not determined by a single factor considered, or that other important controlling variable(s) were not included in this analysis. The fact that we relied on readily available long-term mean environmental conditions in this analysis, likely contributed to the weak models.

Multivariate (random forest regression) machine learning (using the WaPOR ET as the target variable and 24 climatic, terrain and soil-related variables as predictors) produced a very strong model ($R^2 = 0.98$). The random forest algorithm identified long-term mean annual rainfall as the most important driver of water use. This finding was not surprising, given the importance of soil water availability in driving ET. Summer solar radiation was identified as the second most important driver of forest ET. Where sufficient soil moisture is available and if plant physiological thresholds are not exceeded, increased solar radiation will increase transpiration and evaporation since more energy is available to drive these processes. The other climate-related variables that were identified as being important drivers of forest water use included heat units (3rd), solar radiation during winter (4th) and vapour pressure deficit (7th).

Various terrain-related variables were also compared to the WaPOR ET values extracted per forest type. Terrain morphology was identified as the most important terrain-related variable (ranked 8th overall), positive topographic openness (9th), elevation (10th) and negative topographic openness (11th). However, finding consistent relationships between terrain-based variables and water use was difficult. The relationships depend on the forest type, likely because forest types are composed of many different species.

The analysis also showed soil depth and soil clay content as variables impacting forest water use, with soil clay content being the fifth most important variable, and soil depth the seventh. As with terrain-related variables, it was challenging to find consistent patterns in the relationship between soil characteristics and forest water use, likely related to the resolution and accuracy of the soil maps. In some cases, such as Southern Mistbelt Forest and Northern Mistbelt Forest, water use of forests was consistently lower in shallow soils compared to deeper soils, highlighting the importance of soil water over the soil profile.

This study illustrated the value of using EO data in studying how water use varies among forest types, within the same forest type, regions, and over time. It further showed the benefits of coupling this with machine learning, and that the complex interrelationships between EO-based forest ET and GIS-based environmental conditions can be modelled to a high accuracy (235 mm/yr). To our knowledge, this finding is novel and a contribution to new knowledge.

RECOMMENDATIONS

Despite the increasing availability of ET data products internationally, high spatial resolution and accurate datasets remain lacking for areas with complex vegetation and contrasting climatic conditions. Based on the comparison of the WaPOR data to published ET data of indigenous forests, it is recommended that the WaPOR-based ET estimates be interpreted and used with caution, as in most cases, WaPOR tended to overestimate ET, likely due to the relative coarse resolution of the product (250 m) compared to the high spatial variation of the target classes (forest patches). We also encourage closer collaboration between SA researchers and the providers of international ET data products, and feedback to data providers, so that these valuable and costly data sources can be improved. The available field-based measurements against which it could be compared (for verification purposes) are scant and insufficient to properly assess its accuracy. More field-based measurements of ET, within indigenous forests, are needed. Ideally, several forest types should be targeted (the results of this project can be used to assist with selection). The expansion of the EFTEON data network could in future prove very valuable.

Despite the uncertainties in the WaPOR ET data, the range of analyses carried out in this project highlighted the intricate relationships between environmental conditions and water use of forests. Future studies should consider analysing individual forest types separately as this might reduce the large variations in ET observed. Ideally, such an undertaking should include field-based ET measurements.

The long-term climate data used in this study (Schulze, 2007) were last updated in 2007. It is critical that fundamental climate spatial data such as long-term monthly rainfall, temperature, solar radiation, vapour deficit and relative humidity be updated. The potential of atmospheric reanalysis data (e.g. ERA5 from ECMWF) should be investigated and if deemed suitable, data should be extracted for use in future studies, or integrated with other climatic data sets. The lack of accessible weather station data is holding South African research back. Urgent interventions are needed to ensure that data and research findings

are open access.

We strongly recommend that South Africa develop capacity in digital soil mapping, complemented by country-wide soil sampling. Many hydrological and carbon balance models need high-resolution soil type and property maps. Soil properties (like soil water holding capacity) are highly variable across the landscape and expensive to quantify, but collaboration with private laboratory services should be explored. Such maps will be invaluable for water use studies (but were not available for this study), and can also inform decisions on crop plantings and water use efficiencies in agriculture.

The indigenous forest map refined in this study is an invaluable resource for protecting and managing our indigenous forests. It is recommended that verification and editing processes continue beyond the end of this project. Ideally, indigenous forest mapping should be operationalised and updated on a frequent (e.g. annual or bi-annual) basis.

Information on the water use of different indigenous forest types generated as part of this project, complement ET information generated in past studies which should prove very valuable for water resource planning in South Africa. We encourage the use of the ET data generated here (for indigenous forest types), not as much to contrast it against other vegetation types or commercial forestry plantations, but to encourage the allocation of water in catchment management plans to support the ecological functioning of this important land use type.

Apart from contributing to new knowledge, this project significantly contributed to developing human capacity. Four post-graduate students directly benefitted from this project. In addition, several undergraduate students, as well as two interns from the Gert Sibande District Municipality in Mpumalanga, assisted with the forest mapping component of the project. These students were exposed to advanced remote sensing and geospatial techniques, including object-based image analysis and machine learning.

ACKNOWLEDGEMENTS

This report would not have been possible without the help of others. In particular, the project team would like to thank the following reference group members for their invaluable inputs and sage advice during the course of the project:

Dr L Nhamo	Water Research Commission (Chairman 2023-2024)
Prof NS Mpandeli	Water Research Commission (Chairman 2021-2022)
Dr SN Hlophe-Ginindza	Water Research Commission
Ms M Kapari	Water Research Commission
Dr R Heath	Forestry South Africa
Dr J Magidi	Tshwane University of Technology
Dr N Majози	Council for Scientific and Industrial Research
Prof P Chirwa	University of Pretoria

In addition, the project team is grateful to:

- The Water Research Commission for funding this research.
- Dr R Heath for his valuable insights during the reference group meetings and continued support relating to water use research of forests.
- Dr M Toucher (née Warburton) for sharing her research.
- Mr V Ndyafi of Stellenbosch University who contributed to this research project.
- Ms J Eichhoff for producing most of the maps included in this and previous reports.
- Ms L McCarthy, Mr D Timpson, Ms N Ngubo, Mr N Fourie, M Z Lourens, Mr E Burger and M J O Kennedy for their assistance in the indigenous forest mapping.
- Drs P Dye, C Everson and Prof A Clulow for references to past and present studies on ET.

Finally, the project team would like to extend their gratitude to both Prof. NS Mpandeli and Dr L Nhamo for the professional way in which they managed this project. The project would not have materialised had it not been for their vision and understanding of the importance of water utilisation in the forestry sector.

TABLE OF CONTENTS

TABLE OF CONTENTS.....	I
EXECUTIVE SUMMARY.....	I
ACKNOWLEDGEMENTS.....	VI
LIST OF TABLES.....	X
LIST OF FIGURES.....	XII
LIST OF ACRONYMS.....	XVI
1 INTRODUCTION AND OBJECTIVES.....	1
1.1 Introduction.....	1
1.2 Aims.....	1
1.3 Research and development activities and report structure.....	2
2 KNOWLEDGE REVIEW.....	3
2.1 Land and water use by indigenous forests in South Africa.....	3
2.1.1 Indigenous forest land cover.....	3
2.1.2 Water use of indigenous forests.....	5
2.2 Forest water use estimation methods.....	6
2.2.1 Field-based methods.....	6
2.2.2 Earth observation methods.....	7
2.3 The ETLook model and WaPOR data.....	9
2.4 Technologies and techniques used in estimating land and water use by indigenous forests.....	11
2.4.1 GIS and its use for spatial modelling.....	12
2.4.2 Earth observation.....	13
2.4.2.1 Multispectral remote sensing.....	13
2.4.2.2 Thermal remote sensing.....	15
2.4.2.3 Microwave remote sensing (RADAR).....	15
2.5 Combining GIS and Earth observation for forest water use estimations.....	16
2.5.1 Image transformations.....	16
2.5.2 Image classification approaches.....	18
2.5.2.1 Unsupervised classification.....	19
2.5.2.2 Supervised classification.....	19
2.5.2.3 Knowledge-based approaches.....	22
2.5.3 Object-based image analysis.....	22
2.5.4 Cloud-computing for remote sensing.....	23
2.5.5 Image classification for forests.....	23
3 METHODS AND MATERIALS.....	25
3.1 Indigenous forest classification scheme.....	25
3.2 Overview of forest types.....	25
3.2.1 Cape Milkwood Woodland (ACF1).....	26
3.2.2 Subtropical Dune Woodland (ACF2).....	27
3.2.3 Subtropical Indian Ocean Mangrove (AMAN1).....	29
3.2.4 Tropical Indian Ocean Mangrove (AMAN2).....	29
3.2.5 Arid Zone Riparian Woodland (ARF1).....	30

3.2.6	Cape Alluvial Woodland (ARF2)	30
3.2.7	Highland Alluvial Woodland (ARF3)	30
3.2.8	Subtropical Riparian Woodland (ARF4)	31
3.2.9	East African Swamp Forest (ASF1)	31
3.2.10	Cape Talus Forest (ATF1)	32
3.2.11	Bushveld Talus Forest (ATF3)	32
3.2.12	Drakensberg Afrotperate Forest (ATF4)	32
3.2.13	Northern Highveld Afrotperate Forest (ATF5)	33
3.2.14	Cape Afrotperate Forest (AF1)	33
3.2.15	Southern Mistbelt Forest (AF2)	34
3.2.16	Northern Mistbelt Forest (AF3)	35
3.2.17	African Subtropical Coastal Forest (STFa2)	35
3.2.18	Subtropical Scarp Forest (STFa4)	36
3.2.19	Albany Coastal Forest (STFa5)	36
3.2.20	Southern African Dry Forest (TDFa2)	37
3.2.21	Southern African Dry Thicket (TDFa3)	37
3.3	Indigenous forest type mapping	38
3.3.1	Draft indigenous forest mapping	40
3.3.2	Indigenous forest map refinement	44
3.3.3	Indigenous forest type classification	48
3.3.4	Validation of forest type classification	50
3.4	Indigenous forests water use analyses	52
3.4.1	Environmental variable selection and preparation	52
3.4.2	Water use data extraction	56
3.5	Multivariate machine learning analyses	56
4	RESULTS AND DISCUSSIONS	58
4.1	Forest types	58
4.1.1	Extent (coverage) per forest type	58
4.1.2	Modelling forest types using machine learning	58
4.2	Forest water use	60
4.2.1	Water use per forest type	60
4.2.2	Drivers of forest water use	64
4.2.3	Water use of indigenous forests and climate	65
4.2.3.1	Mean annual rainfall	66
4.2.3.2	Solar radiation	77
4.2.3.3	Heat units (degree days)	81
4.2.3.4	Vapour pressure deficit	85
4.2.3.5	Relative humidity	90
4.2.4	Water use compared to terrain characteristics	94
4.2.4.1	Terrain morphology	94
4.2.4.2	Topographic openness	96
4.2.4.3	Elevation	100
4.2.4.4	Slope gradient	104
4.2.4.5	Topographic position index	107
4.2.5	Water use compared to soil characteristics	110

4.2.5.1	Soil depth	111
4.2.5.2	Soil clay percentage.....	114
4.2.6	Indigenous forest water use validation.....	118
4.2.6.1	Comparison to literature and reference evapotranspiration .	118
4.2.6.2	Comparison to agriculture.....	123
4.2.6.3	Comparison to commercial forestry	124
5	SYNTHESIS	125
5.1	Revisiting the project aim and objectives	125
5.2	Main findings.....	126
5.3	Study limitations and proposals for future research.....	127
5.4	Recommendations	129
	REFERENCES	131
	APPENDIX I: CAPACITY BUILDING	143
	APPENDIX II: PUBLICATIONS	145
	APPENDIX III: ACCESS TO DATA GENERATED THROUGH THIS PROJECT	146
	APPENDIX IV: SUPPLEMENTARY MATERIAL	147

LIST OF TABLES

Table 2-1	Examples of research on water use by indigenous forests in South Africa, including studies involving measurement and modelling.....	6
Table 2-2	Sentinel-2 sensor characteristics.....	14
Table 3-1	Forest types and their respective zonal biomes	26
Table 3-2	A list of variables considered in the analysis and a reference to the variable source....	53
Table 3-3	Reclassified terrain morphology units.....	54
Table 3-4	Reclassification of terrain variables	55
Table 4-1	Forest type area classified in IF2024 and total area of IF2021	58
Table 4-2	Environmental variable importance for classifying forest types	59
Table 4-3	Evapotranspiration statistics per forest type for the period January 2009 to June 2023, as estimated using 250 m resolution WaPOR data	61
Table 4-4	Most important variables for mean annual ET identified by random forest regression modelling	65
Table 4-5	Long-term rainfall per forest type.....	67
Table 4-6	Percentage of indigenous forest type area that occur within each of the assigned rainfall classes (low, medium, high and very high). See Table 3-4 (Section 3.4.1) for a description of these classes.	67
Table 4-7	Mean and standard deviation of solar radiation during summer (Feb) and winter (July) per forest type.....	79
Table 4-8	Solar radiation (February) % class cover per forest type	79
Table 4-9	Solar radiation (July) % class cover per forest type	80
Table 4-10	Mean and standard deviation of annual heat units (degree days) per forest type	83
Table 4-11	Annual heat units (degree days) % class cover	83
Table 4-12	Vapour pressure deficit % class cover (Feb).....	86
Table 4-13	Vapour pressure deficit % class cover (July)	87
Table 4-14	Mean and standard deviation of vapour pressure deficit per forest type during summer (February) and winter (July)	88
Table 4-15	Mean annual relativity % class cover	92
Table 4-16	Mean and standard deviation of annual relative humidity per fores type.....	92
Table 4-17	Terrain morphology type count per forest type (>50% in bold and shaded)	95
Table 4-18	Mean and standard deviation of topographic openness (positive and negative) for each forest type	98
Table 4-19	TNO % class cover per forest type.....	99
Table 4-20	TPO % class cover per forest type	99
Table 4-21	Mean and standard deviation of elevation per forest type	102
Table 4-22	Elevation % class cover per forest type	102
Table 4-23	Mean and standard deviation of slope gradient per forest type	105
Table 4-24	Mean slope % class cover per forest type.....	106
Table 4-25	Mean and standard deviation of topographic position index per forest type	109

Table 4-26	Topographic position index % class cover per forest type	109
Table 4-27	Mean and standard deviation of soil classes per forest type	112
Table 4-28	Soil depth % class cover per forest type	112
Table 4-29	Mean and standard deviation of soil clay % per forest type	116
Table 4-30	Soil clay % class cover per forest type	116
Table 4-31	List of South African studies estimating transpiration (T) and evapotranspiration (ET) from forest types. ET/T estimates are shown where available in mm, alternatively in L.	121
Table 4-32	Estimated water use (ET) statistics for selected crop types (Van Niekerk <i>et al.</i> , 2018)	123
Table 4-33	Summary statistics of evapotranspiration (ET) for selected Acacia, Eucalyptus and Pinus compartments from 1 Jan 2009 to 31 Dec 2020 (Van Niekerk <i>et al.</i> , 2023)	124

LIST OF FIGURES

Figure 1-1	Activities (steps) of Phases 1 and 2	2
Figure 2-1	Indigenous forest types as per the 2018 Vegetation Map South Africa (borders exaggerated for visual clarity).....	4
Figure 2-2	ETLook model equations (Van Niekerk <i>et al.</i> , 2018).....	10
Figure 2-3	Schematic representation of the ETLook model for energy balance computations of bare soil and vegetation (Van Niekerk <i>et al.</i> , 2018).	10
Figure 3-1	ACF1 Cape Milkwood Woodland at De Hoop (left) and ACF2 Subtropical Dune Woodland at Mtunzini (right) (Credit: L. Mucina).....	27
Figure 3-2	Distribution and location per forest type in South Africa.....	28
Figure 3-3	AMAN1 Subtropical Indian Ocean Mangrove, KZN LaMercy (Credit: L Mucina).....	29
Figure 3-4	AMAN2 Tropical Indian Ocean Mangrove, Kosi Bay (Credit: T. Riddin).....	30
Figure 3-5	ASF1 East African Swamp Forest at Mkuzi (left), ATF1 Cape Talus Forest Langeberg at Tradouw Pass (middle), ATF3 Bushveld Talus Forest at Strydom Pass (right) (Credit: L. Mucina).....	32
Figure 3-6	ATF4 Drakensberg Afrotropical Forest, Golden Gate Highlands NP (Credit: L. Mucina).....	33
Figure 3-7	AF1 Cape Afrotropical Forest, Knysna (Credit: L. Mucina)	34
Figure 3-8	AF2 Southern Mistbelt Forest at Zuurberg (left) and AF3 Northern Mistbelt Forest at Graskop (right) (Credit: L. Mucina).....	35
Figure 3-9	STFa2 African Subtropical Coastal Forest at Margate (left), STFa4 Subtropical Scarp Forest at Oribi Gorge (middle), STFa5 Albany Coastal Forest at Alexandria Forest (right) (Credit: L. Mucina)	36
Figure 3-10	TDFa2 Southern African Dry Forest at Tembe (left) and TDFa3 Southern African Dry Thicket at Tembe (right) (Credit: L. Mucina).....	37
Figure 3-11	Generalised and missing indigenous forest polygons near Hogsback, Eastern Cape	38
Figure 3-12	Non-forest patches that could be removed in Ngoya Forest, KwaZulu-Natal	39
Figure 3-13	Workflow and product development of indigenous forest type mapping.....	40
Figure 3-14	Aerial photograph of an area north of Richards Bay	41
Figure 3-15	Sentinel-2 natural colour composite image (RGB) of an area north of Richards Bay....	41
Figure 3-16	Classified <i>Water</i> (blue) overlain onto an aerial photograph of an area north of Richards Bay	41
Figure 3-17	Woody vegetation (orange and pink) overlain onto a hillshade of the Digital Elevation Model of South Africa (DEMSEA).....	42
Figure 3-18	Planted forests (purple), Natural woody vegetation (red), Other (yellow) and Water (blue) classified using KBIC (overlain onto a hillshade of the DEMSEA)	42
Figure 3-19	Relative area (ha) of indigenous forests within each quarter degree tile	43
Figure 3-20	<i>Indigenous forest</i> classification progress to date	44

Figure 3-21	Examples (yellow lines) of where object boundaries do not match the <i>Indigenous forest</i> (green) patch boundary and where subdivision (splitting) of objects is required	45
Figure 3-22	Example of where Indigenous forests (green) are distinctly less smooth (in terms of texture) compared to planted forests (red) and other land covers (yellow)	46
Figure 3-23	Example of where <i>Indigenous forest</i> object with less than 75% tree coverage must be manually reclassified to <i>Other</i>	46
Figure 3-24	Examples of <i>Indigenous forest</i> objects in urban areas that must be manually assigned to <i>Plantation</i> or <i>Other</i> based on their contiguous size or content (e.g. buildings), respectively	47
Figure 3-25	Comparison of IF2021 and IF2023	48
Figure 3-26	<i>Indigenous Forest</i> and <i>Uncertain</i> IF2024 classes (solid fill) compared to the IF2021 near Hluhluwe, KwaZulu-Natal	49
Figure 3-27	<i>Indigenous Forest</i> and <i>Uncertain</i> IF2024 classes (solid fill) compared to the IF2021 near St Lucia, KwaZulu-Natal	49
Figure 3-28	Web application showing IF2021 (red) and IF024 forest type polygons (predefined colours)	50
Figure 3-29	Functionality on the web application allowing for polygons to be reclassified	51
Figure 3-30	Functionality on the web application allowing users to select polygons and view their attributes	51
Figure 3-31	Functionality on the web application allowing users to swipe the classified feature classes to see the aerial image below	52
Figure 4-1	Correlation among environmental variables	60
Figure 4-2	Histograms showing the frequency distribution of ET for a subset of forest types (subset A), with the frequency (Y-axis) showing the percentage of pixels per range of annual ET (X-axis)	62
Figure 4-3	Histograms showing the frequency distribution of ET for a subset of forest types (subset B), with the frequency (Y-axis) showing the percentage of pixels per range of annual ET (X-axis)	63
Figure 4-4	Monthly mean ET per forest type for zonal forest types for the period 2009 to 2023	64
Figure 4-5	Monthly mean ET per forest type for azonal forest types for the period 2009 to 2023	64
Figure 4-6	Scatterplot showing the relationship between the mean annual rainfall (Schulze, 2007) and mean annual ET of indigenous forests	66
Figure 4-7	Long-term mean annual rainfall classes for South Africa	68
Figure 4-8	Evapotranspiration per rainfall class for ACF1 Cape Milkwood Woodland	69
Figure 4-9	Evapotranspiration per rainfall class for ACF2 Subtropical Dune Woodland	69
Figure 4-10	Evapotranspiration per rainfall class for AF1 Cape Afrotropical Forest	69
Figure 4-11	Evapotranspiration per rainfall class for AF2 Southern Mistbelt Forest	70

Figure 4-12	Evapotranspiration per rainfall class for AF3 Northern Mistbelt Forest.....	70
Figure 4-13	Evapotranspiration per rainfall class for AMAN1 Subtropical Indian Ocean Mangrove	70
Figure 4-14	Evapotranspiration per rainfall class for AMAN2 Tropical Indian Ocean Mangrove	71
Figure 4-15	Evapotranspiration per rainfall class for ARF1 Arid Zone Riparian Woodland	71
Figure 4-16	Evapotranspiration per rainfall class for ARF2 Cape Alluvial Woodland.....	71
Figure 4-17	Evapotranspiration per rainfall class for ARF3 Highland Alluvial Woodland	72
Figure 4-18	Evapotranspiration per rainfall class for ARF4 Subtropical Riparian Woodland	72
Figure 4-19	Evapotranspiration per rainfall class for ASF1 East African Swamp Forest	72
Figure 4-20	Evapotranspiration per rainfall class for ATF1 Cape Talus Forest.....	73
Figure 4-21	Evapotranspiration per rainfall class for ATF3 Bushveld Talus Forest	73
Figure 4-22	Evapotranspiration per rainfall class for ATF4 Drakensberg Afrotemperate Forest	73
Figure 4-23	Evapotranspiration per rainfall class for ATF5 Northern Highveld Afrotemperate Forest.....	74
Figure 4-24	Evapotranspiration per rainfall class for STFa2 African Subtropical Coastal Forest	74
Figure 4-25	Evapotranspiration per rainfall class for STFa4 Subtropical Scarp Forest	74
Figure 4-26	Evapotranspiration per rainfall class for STFa5 Albany Coastal Forest.....	75
Figure 4-27	Evapotranspiration per rainfall class for TDFa2 Albany Coastal Forest.....	75
Figure 4-28	Evapotranspiration per rainfall class for TDFa3 Southern African Dry Thicket.....	75
Figure 4-29	Monthly and annual precipitation from 2009 to 2023 at St Lucia (Source: CHIRPS).....	76
Figure 4-30	Monthly and annual precipitation from 2009 to 2023 at Sabie (Source: CHIRPS)	76
Figure 4-31	Monthly and annual precipitation from 2009 to 2023 at Knysna (Source: CHIRPS).....	77
Figure 4-32	Long-term solar radiation classes for February (left) and July (right).....	78
Figure 4-33	Linear regression between forest water use and long-term solar radiation during summer (left), winter (middle) and all year (right).....	80
Figure 4-34	Evapotranspiration per solar radiation class during winter for ARF1	81
Figure 4-35	Evapotranspiration per solar radiation class during winter for ARF4	81
Figure 4-36	Annual heat units (degree days) classes for South Africa	82
Figure 4-37	Linear regression between forest water use and heat units (degree days).	84
Figure 4-38	Evapotranspiration per heat unit class for AF3	84
Figure 4-39	Evapotranspiration per heat unit class for ARF1	85
Figure 4-40	Evapotranspiration per heat unit class for ARF2	85
Figure 4-41	Average vapour pressure deficit classes for February (left) and July (right).....	86
Figure 4-42	Linear regression between forest water use and long-term vapour pressure deficit during summer (left) and winter (right)	88
Figure 4-43	Evapotranspiration per vapour pressure deficit class during summer for AF2	89
Figure 4-44	Evapotranspiration per vapour pressure deficit class during summer for AF3	90
Figure 4-45	Annual relative humidity classes for South Africa	91
Figure 4-46	Linear regression between forest water use and long-term annual relative humidity	93
Figure 4-47	Evapotranspiration per annual relative humidity class for ASF1	93

Figure 4-48 Simplified terrain morphology classes	94
Figure 4-49 Evapotranspiration per terrain morphology class for ARF1	95
Figure 4-50 Evapotranspiration per terrain morphology class for ARF2	96
Figure 4-51 Positive (left) and negative (right) topographic openness along two profiles (Li & McCarty, 2019)	97
Figure 4-52 Area of Nyonga forest, with aerial view (a), Topographic positive openness (b), and Topographic negative openness (c)	97
Figure 4-53 Linear regression between forest water use and positive (left) and negative (right) topographic openness, abbreviated as TPO and TNO respectively	100
Figure 4-54 Evapotranspiration per topographic negative openness class for AF3	100
Figure 4-55 Elevation classes of South Africa	101
Figure 4-56 Linear regression between forest water use and elevation	103
Figure 4-57 Evapotranspiration per elevation class for AF3	103
Figure 4-58 Slope gradient classes of South Africa	104
Figure 4-59 Evapotranspiration per slope gradient class for AF1	106
Figure 4-60 Evapotranspiration per slope gradient class for AF2	107
Figure 4-61 Evapotranspiration per slope gradient class for AF3	107
Figure 4-62 Ngoya forest area, with aerial image view (a) and topographic position index (b)	108
Figure 4-63 Evapotranspiration per TPI class for STFa2	110
Figure 4-64 Evapotranspiration per TPI class for STFa4	110
Figure 4-65 Soil depth classes of South Africa	111
Figure 4-66 Linear regression between forest water use and soil depth	113
Figure 4-67 Evapotranspiration per soil depth class for AF2	113
Figure 4-68 Evapotranspiration per soil depth class for AF3	114
Figure 4-69 Soil clay % classes of South Africa	115
Figure 4-70 Linear regression between forest water use and soil clay	117
Figure 4-71 Evapotranspiration per soil clay % class for AF2	117
Figure 4-72 Examples of forested pixels with evapotranspiration values exceeding 1600 mm/yr ..	119
Figure 4-73 WaPOR actual evapotranspiration (ET Actual) extracted at two locations (Mixed and Forest) compared to reference evapotranspiration (ETo) obtained from a nearby a weather station	120

LIST OF ACRONYMS

AETI	Actual evapotranspiration and interception
AG	Azonal ecosystem group
ALEXI	Atmosphere-Land EXchange Inverse
ANN	Artificial neural networks
aRB	Azonal regional biome
CART	Classification and Regression Tree
CB	Continental biome
CSA	Climate Smart Agriculture
DEMOSA	Digital Elevation Model of South Africa
DFFE	Department of Forestry, Fisheries and the Environment
DL	Deep learning
DSM	Digital surface model
DT	Decision tree
DWAF	Department of Water Affairs and Forestry
EO	Earth observation
ET	Evapotranspiration
EVI	Enhanced vegetation index
GB	Global biome
GDD	Growing degree days
GIS	Geographical information systems
HR	High resolution
IAHS	International Association of Hydrological Sciences
KBIC	Knowledge-based image classification
LAI	Leaf area index
LST	Land surface temperature
MMU	Minimum mapping units
MRS	Multiresolution segmentation
NDMI	Normalised difference moisture index
NDVI	Normalised difference vegetation index
NDWI	Normalised difference water index
NFB	National field boundaries
NN	Neural networks
OBIA	Object-based image analysis
OLI	Operational land imager
PM	Penman-Monteith
RB	Regional biome
RF	Random forest

RGB	Red, green and blue
RH	Relative humidity
RMSE	Root mean square error
RS	Remote sensing
SA	South Africa
SANBI	South African National Biodiversity Institute
SANLC	South Africa National Land Cover
SANSA	South African National Space Agency
SAR	Synthetic aperture radar
SEBAL	Surface Energy Balance Algorithm for Land
SEBS	Surface Energy Balance System
SFRA	Stream-flow reduction activities
SUDEM	Stellenbosch University Digital Elevation Model
SVM	Support vector machine
TNO	Topographic negative openness
TPI	Topographic position index
TPO	Topographic positive openness
TSEB	Two-Source Energy Balance
VHR	Very high resolution
VIL	Variable importance list
VITT	Vegetation Index/Temperature Trapezoid
VPD	Vapour pressure deficit
WaPOR	Water Productivity Open access Portal
WRC	Water Research Commission
WUE	Water use efficiency
ZB	Zonobiome

This page was intentionally left blank

1 INTRODUCTION AND OBJECTIVES

1.1 Introduction

Indigenous forests (known in other parts of the world as 'natural forests') are a multilayered vegetation structure comprised of largely evergreen or semideciduous trees (often endemic or sub-endemic) with a crown cover of over 75%. Bushes and shrubs plant species may also be present, but graminoid species are rare (Von Maltitz *et al.*, 2003). Although indigenous forests cover less than 0.4% of South Africa's total land area, they are home to more than 1 700 indigenous tree and shrub species belonging to about 370 genera and 97 families (Dye *et al.*, 2008b). Forestry activities in indigenous forests involve protecting, developing and managing this critical natural and cultural resource. However, the indigenous forests in South Africa are highly fragmented and diverse, which complicates their effective management.

South Africa is classified as a water-scarce country, with an estimated average annual rainfall ranging between 451 and 495 mm, depending on the source quoted. An estimated 21% of SA is considered arid, receiving less than 200 mm/yr of rainfall, with 44% regarded as semi-arid, receiving between 200 and 500 mm/yr (Annandale *et al.*, 2011). The recent droughts experienced in Southern Africa drew renewed attention to the water scarcity in the region and have intensified the competition for water resources among land uses. The chief competitors are urban settlements, agriculture and forestry.

In a recently completed Water Research Commission (WRC) report, titled *THE APPLICATION OF NATIONAL SCALE REMOTELY SENSED EVAPOTRANSPIRATION (ET) ESTIMATES TO QUANTIFY WATER USE AND DIFFERENCES BETWEEN PLANTATIONS IN COMMERCIAL FORESTRY REGIONS OF SOUTH AFRICA* (Van Niekerk *et al.*, 2023), the value of Earth observation (EO) methods for estimating water use by plantation forests at regional (national) scales was demonstrated. EO methods were also used to quantify the water use of different commercial forest genera (e.g. *Eucalyptus*, *Pinus* and *Acacia*). Other factors impacting water use, such as plantation age, species (clone/hybrid), climate and terrain, were also investigated. One of the recommendations of that project was to carry out a similar study on indigenous forests as this will assist in better understanding the impact of afforestation and deforestation on stream-flow reduction. It will also assist in understanding how environmental and topographic factors influence water use of trees at regional scales.

1.2 Aims

This project (C2020/2021-00510) aims to quantify and characterise the water use (evapotranspiration) of indigenous forests throughout South Africa. The specific objectives are to:

1. Produce a geographical database of indigenous forests in South Africa;
2. Determine consumptive water use (actual ET) of indigenous forests using existing remote sensing (RS) data;

3. Validate (ground truth) RS-based consumptive water use of indigenous forests using historical field-based measurements; and
4. Describe, analyse and interpret location-specific differences in water use between indigenous forest types at specific locations in South Africa.

1.3 Research and development activities and report structure

The project was carried out in two phases, namely:

5. Indigenous forest mapping; and
6. Quantify and analyse consumptive water use (actual ET) of indigenous forests.

Figure 1-1 depicts the project phases and the corresponding activities. The steps within each Phase are numbered from 1-3. These steps are used in subsequent sections (e.g. the first activity in Phase 1 is *Draft indigenous forest mapping*, which is labelled as Phase 1.1).

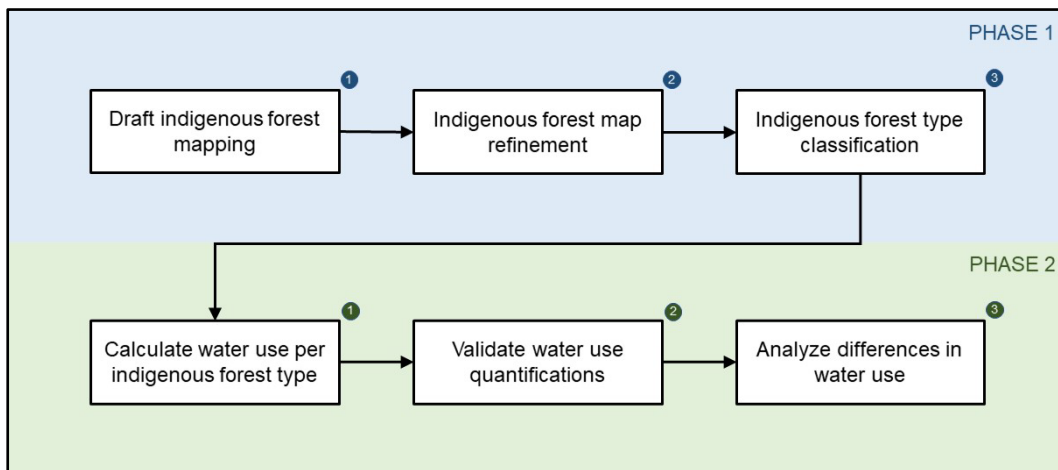


Figure 1-1 Activities (steps) of Phases 1 and 2

2 KNOWLEDGE REVIEW

2.1 Land and water use by indigenous forests in South Africa

2.1.1 Indigenous forest land cover

The South African government, forestry management authorities, and scientists in general have done much to manage and conserve South Africa's indigenous forests. Indigenous forests (known in other parts of the world as 'natural') are a multilayered vegetation structure comprised of largely evergreen or semideciduous trees (often endemic or sub-endemic) with a crown cover of over 75%. Bush and shrub plant species may also be present, but graminoid species are rare (Von Maltitz *et al.*, 2003). Indigenous forests are the crown jewel of South Africa's biodiversity-rich natural environment and deserve our full attention in terms of conservation and sustainable use. Recognising this, the Department of Water Affairs and Forestry (DWAF), now called the Department of Forestry, Fisheries and the Environment (DFFE), contracted a country-wide classification of indigenous forests, which was finalised and published in 2003 (Von Maltitz *et al.*, 2003).

The most recent inventory of indigenous forests is the 2018 account of the classification of selected subtropical forests of South Africa (Von Maltitz *et al.*, 2003).

According to the 2006 Vegetation Map of South Africa (Mucina & Rutherford, 2006), the indigenous forests of South Africa cover 4 981 km² or just over 0.4% of the area of the country. Twelve zonal, intrazonal and azonal forest types are mapped and classified, as shown in Figure 2-1, with 26 forest sub-types classified in total. National Biodiversity Assessment (SANBI 2018) relies heavily on two major sources of information on the variability and extent of the indigenous forests, namely the CSIR report to DWAF (Von Maltitz *et al.*, 2003) and its improved and simplified version published by Mucina and Rutherford (2006) as a chapter of the book (and associated map) entitled 'Vegetation of South Africa, Lesotho and Swaziland'. These two reports were followed by a detailed account of some selected subtropical forest types (Mucina, 2018), which was a result of a project contracted by DWAF and submitted in 2007 (Mucina *et al.*, 2007).

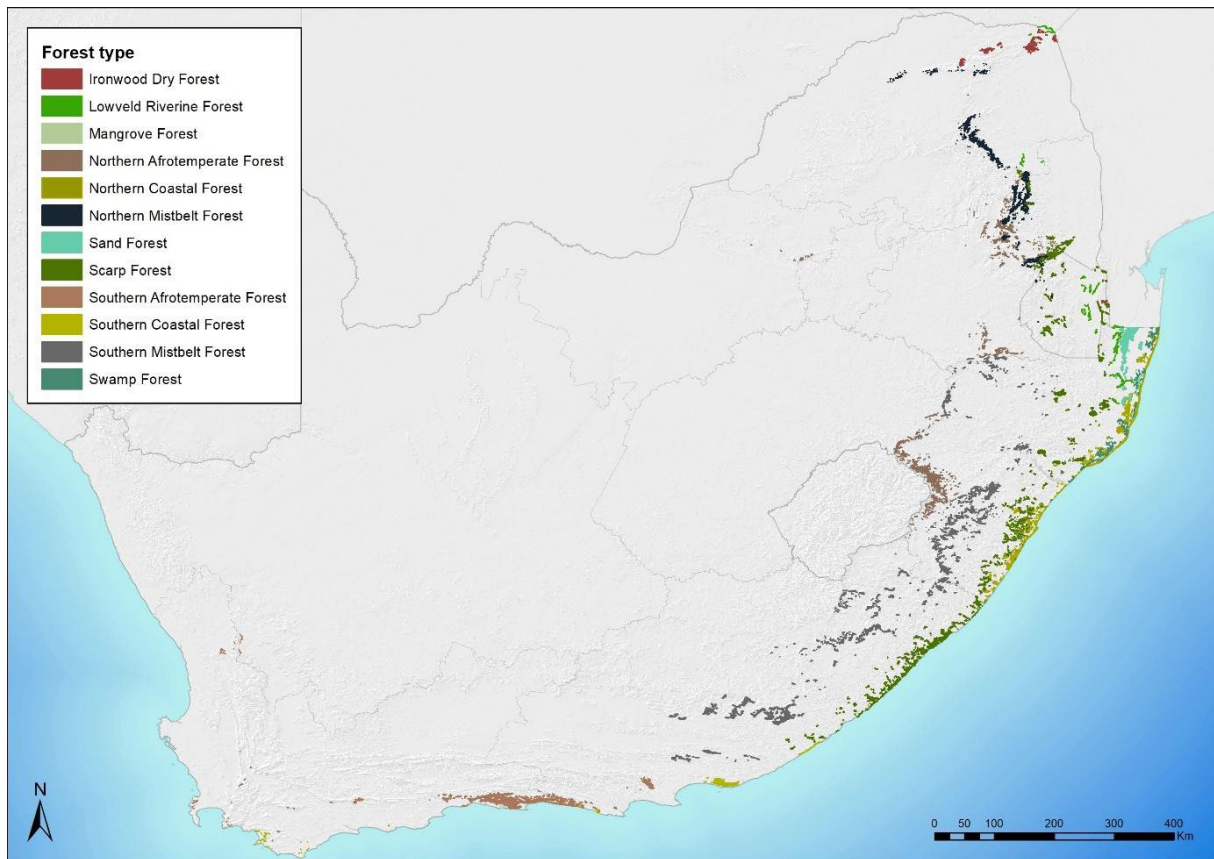


Figure 2-1 Indigenous forest types as per the 2018 Vegetation Map South Africa (borders exaggerated for visual clarity)

A recently completed study of forest biomes (Mucina *et al.*, 2022) revealed gaps in the mapping of the extant indigenous forests. Previous forest surveys have largely neglected one important segment of the forest cover – the riparian woodlands and thickets accompanying intermittent or permanent rivers and streams. Von Maltitz *et al.* (2003) and subsequently Mucina and Rutherford (2006) recognised one such type – Lowveld Riparian Forests – but the authors of both reports acknowledged that there are many more. Mucina *et al.* (2022) devoted much attention to riparian woodlands (mapped many patches riparian forests and thickets), but more work is still needed to map the true extent of these forest/woodland structures in South Africa. Improved knowledge of the locations and extents of these forest/woodlands would be not only critical for water use estimations (i.e. this project) but also for sustainable water use, given that they are most vulnerable to alien plant infestations.

Although much attention has been paid to indigenous forests, there are other forests (or forest-like vegetation structures) that have received less attention. These ‘spontaneous non-indigenous’ forests consist wholly or partly of alien invasive trees (and shrubs). In some cases, they are remnants of indigenous forests that have, as a result of alien plant invasions, changed in terms of floristic composition, structure, and functioning. Mapping such forests is vital for understanding the hydrological dynamics of landscapes since their function (in terms of water retention and utilisation) are likely similar to those of indigenous and plantation forests.

While the VegMap2006 (and its later versions published in 2012 and 2018) is a useful product, it is now

over six years old. It is also not without criticism, with Mucina *et al.* (2022) noting that the mapping precision is “in need of a major improvement” and that many forest and thicket patches visible on remotely sensed imagery were not captured. Additionally, many riparian indigenous forests have been invaded by woody alien vegetation, forming novel forest ecosystems. Mucina *et al.* (2022) also argued that there are gaps in the established national forest classification system used in South Africa, especially at the *Forest type* level.

To address some of these limitations, and in accordance with the aim of this project, an update of the indigenous forest map was undertaken by Mucina *et al.* (2022), including a reassessment and revision of the classification of forest types in Southern Africa, the improvement of the spatial accuracy of the boundaries of indigenous forests and the expansion of the map to include Mozambique and Zimbabwe. For reference, this product is referred to as IF2021 hereafter.

2.1.2 Water use of indigenous forests

Research on the water consumption (evapotranspiration or ET) of indigenous forests in South Africa is limited (spatial and temporal extent), but notable works are listed in Table 2-1. The studies undertaken by Everson *et al.* (2019), Everson *et al.* (2011), Pearton (2017), Gush and Dye (2009) and Clulow *et al.* (2013) involved mainly sap flow measurements to understand transpiration only. Only the two studies by Dye *et al.* (2008b) and Gush *et al.* (2015) have quantified both the transpiration and ET, and then only in selected indigenous forests in the Eastern Cape, KwaZulu-Natal, Mpumalanga and Limpopo Provinces.

Long-term ET and other data sets have been collected for many years using an open-path eddy covariance system over an indigenous forest at Skukuza in the Kruger National Park as part of the SAFARI 2000 campaign (Scholes *et al.*, 2001). The goal of the experiment was to investigate the interactions between land surface and atmosphere in southern Africa by connecting ground data on carbon dioxide, water, and energy fluxes with RS data generated by EO satellites (Scholes *et al.*, 2001; Shugart *et al.*, 2004). The dominant vegetation type in the study area is the broadleaf Combretum savanna on high ground and fine-leaved Acacia savanna in the valleys. High temporal resolution data of evapotranspiration and other energy balance components (i.e. net radiation, soil heat flux, profile soil moisture, leaf area index, etc.) were collected for more than 10 years.

In recent years, the Expanded Freshwater Terrestrial Environmental Observation Network¹ (EFTEON) has instrumented several sites representing a range of vegetation types, to monitor carbon dioxide and water vapour fluxes (i.e. evapotranspiration). These include a new savanna site (Spioenkop with thickening savanna dominated with V. Karoo), a new fynbos site (Jonkershoek) and a grassy savanna site (Maputaland) with forest patches and Lala palm (Fieg, 2024). This network will also upgrade the existing flux towers in the Kruger National Park.

¹ <https://www.saeon.ac.za/weather-stations/>

Table 2-1 Examples of research on water use by indigenous forests in South Africa, including studies involving measurement and modelling.

Study	Title
Scholes <i>et al.</i> (2001)	Long-term water and carbon flux measurements at Skukuza, Kruger National Park
Jarmain <i>et al.</i> (2004)	Improving the basis for predicting total evaporation from natural veld types in South Africa: A focus on Moist Upland Grassland, Valley Thicket and Coastal Bushveld/Grassland.
Dye <i>et al.</i> (2008b)	Water use in relation to biomass of indigenous tree species in woodland, forest and /or plantation conditions
Dye <i>et al.</i> (2008a)	The potential of woodlands and reed beds for control of acid mine drainage in the Witwatersrand Gold Fields
Gush and Dye (2009)	Water use efficiency within a selection of indigenous and exotic tree species in South Africa as determined using sap flow and biomass measurements
Everson <i>et al.</i> (2011)	Water use of grasslands, agroforestry systems and indigenous forests
Clulow <i>et al.</i> (2013)	Water use dynamics of a peat swamp forest and a dune forest in Maputaland, South Africa
Gush <i>et al.</i> (2015)	Water Use and Socio-Economic Benefit of the Biomass of Indigenous Trees
Pearton (2017)	An assessment of the water use of indigenous and introduced tree spp. and varying land uses around Vasi Pan, Maputaland, KwaZulu-Natal
Dye <i>et al.</i> (2018)	Evapotranspiration from mine-affected riparian sites along the Vaal River in central South Africa
Everson <i>et al.</i> (2019)	Quantifying the water use of dominant land uses in the Maputaland coastal plain
Scott-Shaw <i>et al.</i> (2017)	Water use dynamics of an alien-invaded riparian forest within the summer rainfall zone of South Africa

There is a need to extrapolate results from these studies to other indigenous forest types to gain a national perspective of the hydrological impacts of indigenous forests and for comparisons with the hydrological impacts (e.g. stream-flow reduction) of commercial forests and other land uses. There is also a need to understand how indigenous forests' water use is influenced by environmental conditions (climate and soils) and their species composition. For example, Gush and Dye (2009) have shown that during winter, the difference in water use between indigenous and plantation forests is marginal, although plantation forests use considerably more water during summer, mainly attributed to considerably higher growth rates and hence larger transpiring leaf areas.

Although this foundational research outlined above is critical for understanding the water use of indigenous tree species, the (sap flow, eddy covariance and scintillometry) methods on which they rely are very expensive to carry out and are thus limited to specific forests/species and often over relatively short periods of time. It is therefore difficult to translate the findings of these studies to other forests/species and/or other regions.

2.2 Forest water use estimation methods

Several methods are available to estimate forestry water use (ET or transpiration). Some of the methods capture the process of transpiration only, while others capture transpiration and evaporation (from the soil surface and water intercepted by the canopy), which are all included in the ET term. The methods estimate water use at individual plant/tree, stand or larger (catchment) levels and involve measurements and/or modelling. The following subsections provide a brief overview of these methods.

2.2.1 Field-based methods

Field-based (point-based) methods for measuring or estimating ET have been reviewed in previous

work (Verstraeten *et al.*, 2008; Savage *et al.*, 2010; Amani & Shafizadeh-Moghadam, 2023). These methods include point, plant, field and landscape scales and are mostly based on the mass water balance, energy balance or a combination thereof. Examples include lysimetry, pan methods (e.g. class A pan), atmometers (e.g. ETgage), the eddy covariance method, and a range of aerodynamic methods that estimate sensible heat from which evaporation is estimated as a residual, using the shortened energy balance equation (Jarman *et al.*, 2009a). The latter method includes the one-sensor eddy covariance, Bowen ratio, surface renewal, scintillometry and other methods. Some methods are used to estimate transpiration directly, e.g. the sap flow and heat pulse velocity methods (Jarman *et al.*, 2009c). Many of these methods have been used to estimate ET in SA as part of WRC-funded projects. See for example Bristow and De Jager (1981); Green and Clothier (1988); Dye *et al.* (1997); Savage *et al.* (1997); Savage *et al.* (2004); Jarman *et al.* (2009a) and Jarman *et al.* (2014). The above-mentioned methods are point-, field- or stand-based. As such, their ET estimates have a limited spatial “footprint”. When applying the water balance method to a larger area, i.e. a catchment area, it can provide an estimate of ET from a larger spatial “footprint”. Table 2-1 lists some of the South African studies that used these methods, often in combination with modelling, to study forestry water use.

2.2.2 Earth observation methods

The increased availability of spatially referenced GIS and EO data (Laipelt *et al.*, 2021) enables crop water use or ET estimation at pixel level and at high resolutions (e.g. 20 to 1 000 m). Such data can be aggregated and employed at different spatial scales and used over large areas. Because satellite data are frequently collected, estimates can be made regularly, and temporal trends studied. Such spatial and temporal coverage can contribute greatly towards improved water management from national and/or regional levels down to individual land uses.

Estimates of ET, including water consumption by vegetation, relate to the vaporisation of water from the land surface into the lower part of the atmospheric boundary layer. ET consists of evaporation of water from the soil, evaporation of intercepted water and transpiration losses by plants. The sum of all these losses is often referred to as consumptive water use. The water volumes lost through the processes encompassed in ET form part of the hydrological cycle where no water is truly lost but merely changes in form.

Advances in the interpretation of EO information enable the spatial estimation of ET plant water use, biomass and yield production and associated water use efficiency (WUE) for each pixel of a satellite image, without having to rely on generalised plant coefficients. Different methods have been developed to provide information at a range of temporal and spatial scales and for various applications. Several review papers describe methods used to spatially estimate ET, including Choudhury (1997), Courault *et al.* (2005), Kustas and Norman (1996), Verstraeten *et al.* (2005), Verstraeten *et al.* (2008) and Gibson *et al.* (2013), Zhang *et al.* (2016), and Amani and Shafizadeh-Moghadam (2023). Numerous models have been developed for agricultural (field scale) and forestry applications. They are typically based on the surface energy balance, Peman-Monteith or Priestly-Taylor formulations, Vegetation index with Land surface temperature or Statistical and empirical approaches (Amani & Shafizadeh-Moghadam,

2023). Examples include the Surface Energy Balance Algorithm for Land (SEBAL); Surface Energy Balance System (SEBS); Mapping Evapotranspiration with high Resolution and Internalised Calibration (METRIC_{tm}); Vegetation Index/Temperature Trapezoid (VITT); Two-Source Energy Balance (TSEB); the Atmosphere-Land EXchange Inverse (ALEXI/disALEXI); Normalised Difference Vegetation Index Diurnal Surface Temperature Variation (NDVI-DSTV) triangle model, ETLook and several others. These methods either estimate ET as the residual of a shortened energy balance equation using land surface temperature (LST) estimates or use a WUE relationship to determine ET. Some of the models are used operationally for field-scale agricultural water management², but most are used primarily in research applications. A selection of the models (SEBAL, SEBS, VITT and METRIC_{tm}) was reviewed by Jarman et al. (2009b). The review included an assessment of each model's accuracy in estimating ET and their potential for operational applications in SA. It was found that some of the components of the energy balance (such as net radiation) were accurately simulated, but that the other energy balance components and ET were generally more complex. SEBAL and METRIC estimates of ET were generally lower than measured ET, while SEBS commonly overestimated ET. The VITT model yielded the least accurate evaporation estimates. Laipelt *et al.* (2021) demonstrated the use of the SEBAL algorithm and the Google Earth Engine platform to monitor ET over a long period of time. Their reported accuracy (RMSE) for the ET estimations was 0.67 mm/day.

Other EO-based models have been developed and provide ET estimates at lower spatial resolutions (often ~1 to 3 km) but higher temporal resolutions (30 min to daily). A number of these models use Meteosat Second Generation satellite data and provide ET data at 30-minute intervals at a resolution of 1-3 km³. ET data from HYLARSMET⁴ and MODIS⁵ are estimated daily for the entire globe at a 1 km resolution. The global water cycle monitor⁵ from Princeton University also estimates ET at a daily time step⁶, while the ALEXI model⁷ can be used to estimate energy fluxes and other parameters daily, e.g. at a 10 km spatial resolution. Other available data products include ECOSTRESS PT-JPL, GLEAM, and SSEBop, but not all these data products are available for SA.

New approaches and models are continually being developed and tested, and existing methodologies are being improved. Amani and Shafizadeh-Moghadam (2023) provide a good, updated overview of available EO and other approaches and associated models. For instance, the ETLook model (Pelgrum et al., 2011) is used in the FAO-based Water Productivity through Open access of Remotely sensed derived data (WaPOR)⁸ initiative, which provides free access to satellite-based data on agricultural productivity in Africa and the Near East for the period 2009-2021. This project will make use of the ETLook data (as provided through WaPOR) as is and no ET modelling will be carried out as part of this study. The following section provides more information about the ETLook model as well as the WaPOR

² For instance, www.mijnakker.nl; fruitlook.co.za; www.idwr.idaho.gov/GeographicInfo/METRIC/et.htm

³ <http://landsaf.meteo.pt/> and <http://www.ears.nl/>

⁴ http://sahg.ukzn.ac.za/soil_moisture/et/

⁵ http://modis.gsfc.nasa.gov/data/dataproduct/dataproducts.php?MOD_NUMBER=16

⁶ http://hydrology.princeton.edu/~justin/research/project_global_monitor/

⁷ http://alfi.soils.wisc.edu/cgi-bin/anderson/alexi_server.pl?region=SMEX02MOD

⁸ <http://www.fao.org/in-action/remote-sensing-for-water-productivity/database/database-dissemination-wapor/en/>

data.

2.3 The ETLook model and WaPOR data

Surface energy balance models such as the SEBAL (Bastiaanssen *et al.*, 1998; Bastiaanssen *et al.*, 2005) and ETLook models (Pelgrum *et al.*, 2011; Bastiaanssen *et al.*, 2012) eliminate the need for generalised crop information (e.g. coefficients) in describing ET.

SEBAL is intended for catchment-level crop growth monitoring studies and not for application over extensive areas with widely varying climatic conditions (e.g. SA). The ETLook model addresses this limitation of SEBAL (Pelgrum *et al.*, 2011; Bastiaanssen *et al.*, 2012). With ETLook, the daily energy balances and biomass production of extensive areas can be estimated, making it ideally suited for the present study. ETLook was released in 2009 and is used extensively in the Nile Basin, China, India, Pakistan, Australia, Syria, Morocco, Iran, Ukraine, Poland, Canada and the Netherlands by eLEAF. The results from a validation study carried out in the Indus Basin were presented at a conference of the International Association of Hydrological Sciences (IAHS), showing a good correlation between ETLook, actual ET and other actual ET measurements in the basin (Pelgrum *et al.*, 2011). ETLook has also, since 2016, replaced the SEBAL model in the FruitLook initiative (Goudriaan, 2014).

ETLook (Pelgrum *et al.*, 2011) is a two-layer energy balance model that calculates evaporation (E) from soil and water surfaces and transpiration (T) from canopies using transport resistances in conjunction with the Penman-Monteith (PM) equation (Figure 2-2). The PM equation used to estimate ET is solved separately here for vegetation and (bare) soil processes, and hence, T and E are split.

A basic structure of the ETLook model is illustrated in Figure 2-3. Separate and physically defined aerodynamic and evaporation resistances for bare soil and canopies are incorporated. The soil resistance (r_{soil}) is a function of the soil water content in the topsoil and is therefore characterised by a strong reflectance of microwave signals. Topsoil water content values can be obtained at daily intervals from radar-based satellite EOs. The canopy resistance (r_{canopy}) is a function of the leaf area index (LAI; [$\text{m}^2 \text{ leaf} / \text{m}^2 \text{ soil}$]) and four dimensionless stress factors. These stress factors indicate the influence of radiation, temperature, vapour pressure (meteorological conditions) and soil water content in the subsoil. The aerodynamic canopy ($r_{\text{a,canopy}}$) and aerodynamic soil resistance ($r_{\text{a,soil}}$) are functions of wind speed and surface roughness. An iteration procedure is carried out to correct for unstable conditions. The Monin-Obukhov Similarity Theory (Monin & Obukhov, 1954) is used to parameterise the effects of shear stress and buoyancy. In ETLook, both the actual (T_{act}) and potential (T_{pot}) transpiration fluxes are calculated. The difference ($T_{\text{pot}} - T_{\text{act}}$) expresses vegetation water stress induced by the limited availability of soil water content in the root zone (Pelgrum *et al.*, 2011). ETLook requires precipitation interception as input, which is calculated from spatial (interpolated) precipitation and NDVI data.

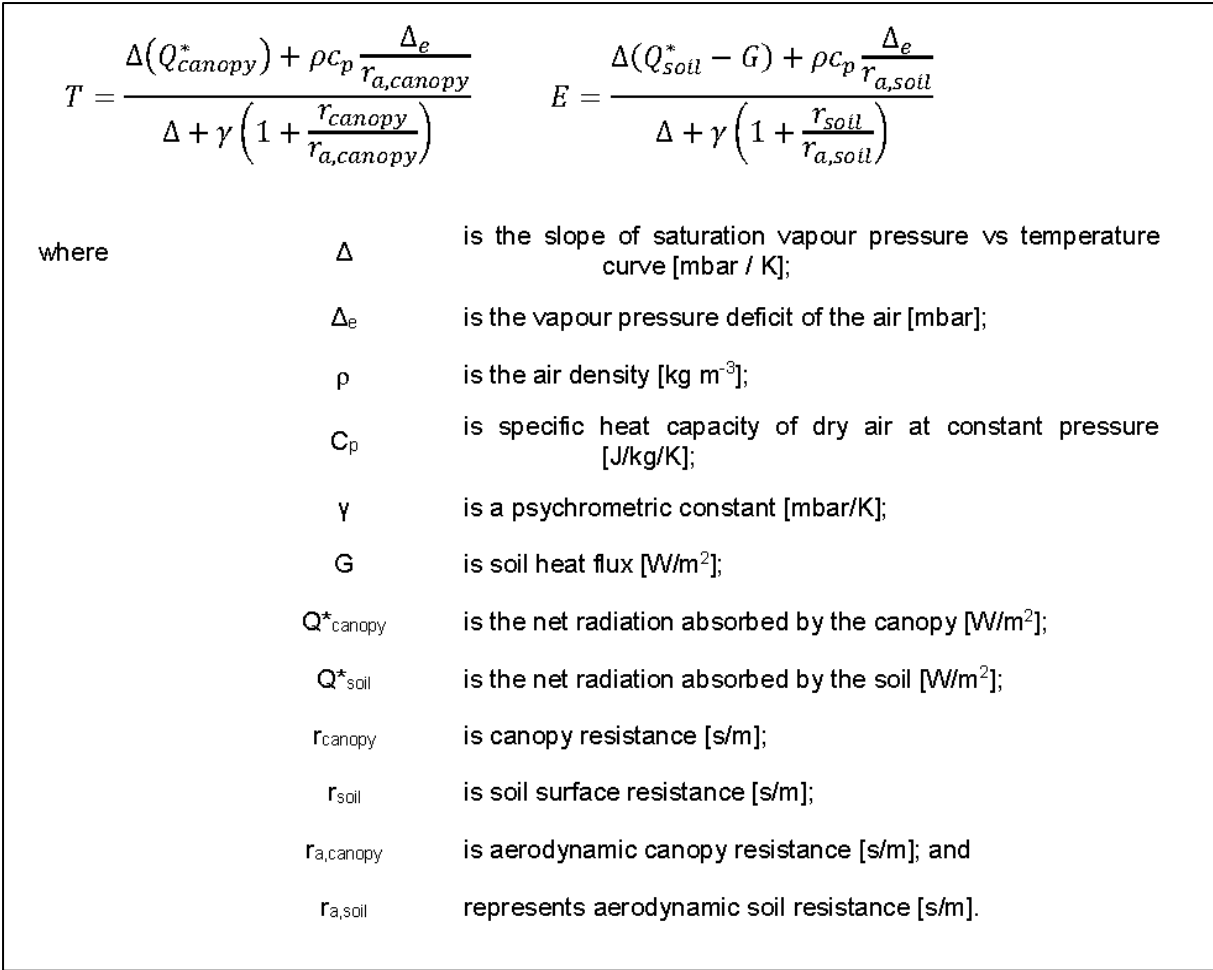


Figure 2-2 ETLook model equations (Van Niekerk et al., 2018).

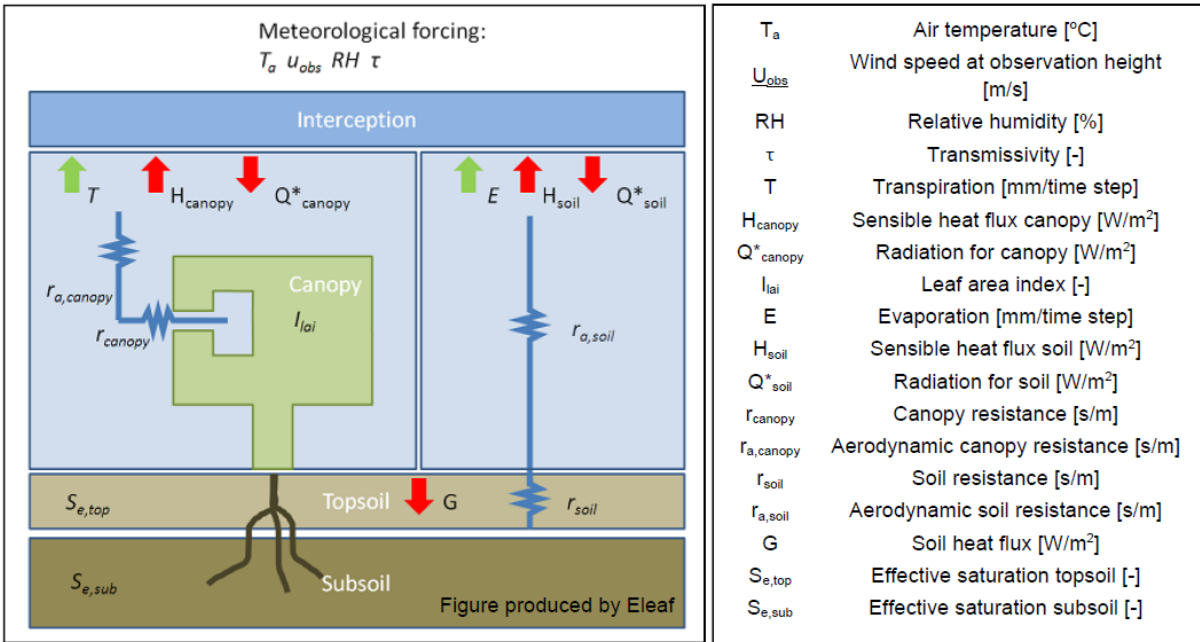


Figure 2-3 Schematic representation of the ETLook model for energy balance computations of bare soil and vegetation (Van Niekerk et al., 2018).

The biophysical datasets required in the ETLook PM equation include surface albedo, surface emissivity, surface roughness, surface LAI and surface canopy resistance. The meteorological datasets used as input include air temperature [T_a], relative humidity [RH], wind [u_{obs}] and transmissivity [τ]. Due to atmospheric interferences (reflection, absorption, scattering), not all solar radiation at the top of the atmosphere is transmitted through the atmosphere towards the land surface; only a fraction will reach the evaporating surface of the land under clear conditions. Typically, 75% of all radiation reaches the land surface, and it will reduce to 25% when heavy clouds prevail. The exact position of the sun, in combination with transmissivity values, determines the net solar radiation that reaches the crops or surface where ET takes place. The biophysical parameters required in ETLook are retrieved from satellite measurements, while the meteorological data (with the exclusion of transmissivity, which was obtained from MSG) was retrieved from meteorological stations. Van Niekerk *et al.* (2018) provide detailed information about datasets used for the implementation of ETLook.

As noted in Section 2.2.2, the ETLook model was used to develop the FAO-led WaPOR initiative to support land and water productivity monitoring using ET and biomass production data. Its data portal⁹ (FAO 2024) has three levels of EO-based data products. Level 1 (v2) provides 250 m resolution data for Africa and the Middle East¹⁰. Level 2 provides 100 m data for a number of selected countries, including Morocco, Tunisia, Kenya and Mozambique, as well as the Jordan/Litani River basin, the Nile Basin, the Awash Basin and the Niger inner Delta. Level 3 provides 20 m resolution data for eight selected irrigation schemes in Ethiopia, Jordan and Tunisia.

The Level 1 (v2) product was employed in this study. As it also uses the ETLook model, the WaPOR product is very similar to the actual ET product described and successfully used by Van Niekerk *et al.* (2018) to quantify the water use of irrigated agricultural crops. In that study, water use was also differentiated for different crop types and in different regions throughout South Africa. The results were verified and validated through an extensive stakeholder engagement exercise and by comparing the water use estimates with those quantified in previous studies. The Level 1 (v2) WaPOR product was also used by Van Niekerk *et al.* (2023) to characterise the variations in water use among commercial plantation genera at a national scale. The results showed that the water use estimations of the genera closely matched those of previous field-based studies and compared favourably to several other ET products.

2.4 Technologies and techniques used in estimating land and water use by indigenous forests

It is clear from the previous sections that water use estimations require reliable, accurate and up-to-date data. These data are often needed for large areas, which necessitates the use of geospatial technologies such as GIS and EO. This section provides an overview of the geospatial techniques and technologies that are relevant to this project. The review starts with GIS and spatial modelling, as these are the fundamental technologies that will be used to map and quantify water use by indigenous forests.

⁹ <https://data.apps.fao.org/wapor/?lang=en>

¹⁰ WaPOR Level 1 v3 at 100 m resolution was released between 23 October and 29 November 2023.

This is followed by an introductory overview of concepts such as multispectral, thermal and microwave EO. The section concludes with a short overview of image classification and object-based image analysis techniques.

2.4.1 GIS and its use for spatial modelling

GIS is used to manage and analyse spatially referenced or geographical data and provides a unique platform capable of integrating large volumes of spatial data for analysis (Heywood *et al.*, 2006). The use of GIS offers a quick and easy way to monitor and manage resources, which is not possible with traditional methods.

Over the last two decades, GIS has emerged as a mature technology with a particular value in answering questions about spatial location, patterns, trends, conditions and their implications. Using GIS, datasets of different formats at varying scales can be incorporated into a single database, which can be stored as vector and/or raster data. Spatial modelling involves using such data to construct models to predict spatial outcomes that simulate the dynamics of natural processes (O'Sullivan & Unwin, 2010). Spatial modelling in GIS embraces techniques and models that apply quantitative structures to systems in which the variables of interest vary across space. Spatio-temporal models simulate change over time using equations that represent real-world processes while taking spatial patterns and spatial interaction in the system into account (Karszenberg *et al.*, 2008). Such spatial and temporal process models can be used for decision-making regarding spatial phenomena (also known as spatial decision support systems) but are also used to evaluate our understanding of complex spatial systems (Heywood *et al.*, 2006). Models can be used to establish (*a priori*) theory or explore (*a posteriori*) theory (Hardisty *et al.*, 1993). When modelling in GIS, the questions of validation and the roles of scale and accuracy need to be carefully considered (Goodchild, 2005).

There are numerous examples of where GIS has been used in forest management. Recent examples include Akumu *et al.* (2019), who developed a GIS-based modelling procedure to predict and map relative soil moisture classes in a forested landscape. They used a rule-based GIS model to develop a technique to predict soil moisture classes (dry, fresh, moist and wet) based on soil textural classes derived from quaternary geology maps and water-receiving areas derived from topographic attributes generated from a digital elevation model. Choudhary *et al.* (2018) used land cover/land use, vegetation, soil, geology and geomorphology spatial data to assess and classify land vulnerability from a multidisciplinary approach based on EO and GIS techniques. San Juan and Domingo-Santos (2018) assessed the use of GIS and LiDAR for the inventory, monitoring, analysis and modelling of natural forest resources, and provided an overview of their use in sustainable forest management. In a comprehensive literature study, Beckline *et al.* (2017) examined and demonstrated both the need for and the shift towards GIS and RS in tropical forest management. Sonti (2015) explored the potential application of GIS technology in forest management in general and a range of forest applications in Kenya, Cameroon and the Congo in particular, concluding that forest management can strongly benefit from the use of GIS. Dincă *et al.* (2014) used a GIS model to develop an improved forest soil map and

database for Romania, and Zambelli *et al.* (2012) developed a GIS decision support system for regional forest management to evaluate biomass availability for energy production in northern Italy.

From the preceding discussion it should be clear that GIS and spatial modelling has become invaluable for managing forests and for improving our understanding of where forests are located, how they function and how they are changing.

2.4.2 Earth observation

2.4.2.1 Multispectral remote sensing

A wide variety of multispectral EO imagery is freely or commercially available. The choice of the appropriate sensor for a given application depends on the following image factors:

- spatial resolution (also known as the pixel size), which is a measure of the level of detail that can be recognised using the imagery;
- spectral resolution, which refers to the number of spectral bands available;
- temporal resolution (also known as revisit cycle), which denotes the time interval between image acquisitions for the same area;
- swath width (also called image extent or scene footprint), which describes the area covered by one scene; and
- cost per image.

A number of multispectral satellite platforms are being considered for use in this research (a list of multispectral satellites is provided in Deliverable 1). The low spatial resolutions of the freely available MODIS (250-1 000 m) and AVHRR (1 km) satellite imagery are unsuitable for detailed mapping exercises (e.g. mapping the boundaries of indigenous forest patches). The sub-metre resolutions of very high resolution (VHR) sensors such as IKONOS, Quickbird, Worldview and GeoEye (in the panchromatic bands) are more suitable for analysing the structural properties of indigenous forest canopy. Examples of such images can be seen on online applications (apps) such as Google Earth, Bing Maps, HERE and ArcGIS Online. VHR imagery provided through such apps can be used for visual interpretations and manual digitising of forest patches. However, such manual (qualitative) approaches for identifying and delineating the millions of forest patches in South Africa would be extremely tedious and costly, if not impossible. Automated (quantitative) approaches such as image classification (see Section 2.5.2) for an overview) are more viable, but such methods require access to the raw imagery as the near-infrared bands (which are not provided by apps) would be needed (Cho *et al.*, 2015). However, acquiring the thousands of images required for national coverage would be prohibitively expensive.

The imagery provided by high-resolution (HR) multispectral sensors, such as those mounted on the Landsat, SPOT and Sentinel-2 satellites, are more suitable when sub-metre detail is not required. As well as being freely available, these sensors have large swaths, resulting in larger image extents

(compared to VHR imagery) and fewer images, which are consequently required to cover a large area. The highest resolution images within this subgroup of sensors are those provided by the SPOT family of satellites, which have been recording HR satellite imagery for almost 30 years. The South African National Space Agency (SANSA) and Airbus Defence, the owner of the SPOT satellite series, have in place a licence agreement allowing the use of SPOT imagery for government and research purposes. Although the 1.5 m spatial resolution of SPOT 6 & 7 would be relatively suitable for forest mapping, the following factors impede their value:

- The spectral resolution is limited to three bands in the visible spectrum (RGB) and only one band in the infrared (IR) range of the EMS (VNIR), thereby limiting its use for forest mapping;
- The agreement between SANSA and Airbus Defence stipulates that a limited number of scenes may be made available for research (or governmental) purposes, resulting in patchy spatial coverage of South Africa;
- Suitable image scenes must be manually identified through the SANSA-EO online catalogue¹¹. The image is then extracted by SANSA and placed on an FTP server (which is often not instantaneous). The primary consequence of these factors is that SPOT imagery cannot easily be incorporated into an automated EO processing workflow, which significantly decreases the cost-effectiveness of their use.

The Sentinel-2 programme, developed by the European Space Agency, forms part of the European Union's comprehensive Copernicus EO programme aimed at performing terrestrial observations in support of services such as forest and agricultural monitoring, land cover change detection and natural disaster management. The platform comprises two identical HR multispectral satellites: Sentinel-2A (launched on 23 June 2015) and Sentinel-2B (launched on 7 March 2017). The spatial and spectral characteristics of the Sentinel-2 sensors are provided in Table 2-2.

Table 2-2 Sentinel-2 sensor characteristics

Sentinel-2 Bands	Central Wavelength (µm)	Resolution (m)
Band 1 – Coastal aerosol	0.443	60
Band 2 – Blue	0.490	10
Band 3 – Green	0.560	10
Band 4 – Red	0.665	10
Band 5 – Vegetation Red Edge	0.705	20
Band 6 – Vegetation Red Edge	0.740	20
Band 7 – Vegetation Red Edge	0.783	20
Band 8 – NIR	0.842	10
Band 8A – Vegetation Red Edge	0.865	20
Band 9 – Water vapour	0.945	60
Band 10 – SWIR – Cirrus	1.375	60
Band 11 – SWIR	1.610	20
Band 12 – SWIR	2.190	20

¹¹ <http://catalogue.sansa.org.za/>

The Landsat sensor is the most commonly used HR data, with Landsat satellites continuously capturing images of the earth's surface since 1972. The Landsat Data Continuity Mission, run by the North American Space Agency and the United States Geological Survey, comprises ~40 years of imagery, all of which is freely available. To date, eight (8) Landsat missions (Landsat 1-8) have been launched, with the latest being Landsat-8 (launched in 2013). Landsat08 carries two instruments, the operational land imager (OLI) and thermal infrared (TIR) sensor (see next section for more about thermal RS). The OLI sensor detects seven multispectral bands at 30 m resolution and a panchromatic band at 15 m resolution. Landsat 5 TM was decommissioned in 2013, and the scan-line corrector of Landsat 7 ETM+ has been inoperative since 2003, resulting in gaps in the imagery between 2003 and 2013. However, the continuity and high spectral resolution among Landsat TM, ETM+ and OLI are highly beneficial for multitemporal analysis, which will be employed in this research.

2.4.2.2 Thermal remote sensing

Thermal RS deals with the acquisition, processing and interpretation of data acquired primarily in the thermal infrared (TIR) region of the EM spectrum (3 to 35 μm). In thermal RS, the radiation from the surface of the earth is 'emitted', as opposed to multispectral RS, where the radiation is 'reflected'. A commonly studied aspect in the domain of thermal RS is LST. LST provides information on the temporal and spatial variations of the surface equilibrium state (Li *et al.*, 2013b) and is an important observation, particularly in the estimation of land surface atmospheric fluxes. However, the strong heterogeneity of land surface characteristics such as vegetation, topography and soil lead to a rapidly changing LST in both space and time, resulting in RS satellite data offering the only possibility for measuring LST over the entire globe with sufficiently high temporal resolution (Kalma *et al.*, 2008; Li *et al.*, 2013b). For example, when using an energy balance approach to estimate evapotranspiration (Section 2.2.2), LST is used in the estimation of net radiation and to estimate the sensible heat flux. Although there were early doubts as to whether satellite-based radiometric temperature could be used in the estimation of evapotranspiration (Kalma *et al.*, 2008), it has since been established that to estimate evapotranspiration with a better than 10% accuracy, LST must be retrieved at an accuracy of 1 K or better (Li *et al.*, 2013b). This reinforces the need to obtain accurate LST for critical observations in hydrology (e.g. ET).

2.4.2.3 Microwave remote sensing (RADAR)

Microwave RS functions by detecting energy backscattered from the earth's surface in the microwave region of the electromagnetic spectrum. This region ranges in frequency from 0.3 to 300 GHz, which corresponds to wavelengths of 3 mm to 30 cm. The long wavelengths of microwave radiation mean that it experiences very little atmospheric attenuation, making it possible for imaging radars to capture image scenes even in cloudy conditions. This makes radar imagery particularly powerful for obtaining unbroken time series of data, especially in tropical or cloudy regions. Most imaging radars are active sensors (in that they provide their own source of microwave illumination), which means that they can capture imagery both day and night, thereby doubling the imaging capacity per orbit.

Synthetic aperture radar (SAR) is a type of microwave sensor that provides a dramatically improved spatial resolution over conventional real aperture radar systems. A list of popular SAR systems is provided in Appendix B. While archived scenes for decommissioned sensors such as ERS-1, ERS-2, ENVISAT, ALOS-1 and RADARSAT-1 are available, several radar satellites are currently in operation. Some of these satellites offer HR, fully polarimetric (HH, HV, VH and VV) capabilities. Examples include RADARSAT-2, TerraSAR-X and COSMO-Skymed. The most reliable and commonly used SAR sensors currently active are RADARSAT-2, TerraSAR/TanDEM-X, ALOS PALSAR-2, Cosmo-SkyMed and Sentinel-1A. These sensors provide a mixture of spatial resolutions (1-100 m), wavelengths (X, C and L bands) and revisit periods (11-24 days). Despite not having full polarimetric capabilities, Sentinel-1 has gained much popularity for a range of applications, including forestry (e.g. Mngadi *et al.*, 2019; Dostálová *et al.*, 2021), mainly because it is freely available from ESA.

2.5 Combining GIS and Earth observation for forest water use estimations

GIS, spatial modelling and EO can be combined to estimate the water used by indigenous forests. The most effective approach involves three main steps:

1. Use RS and GIS to map forests;
7. Use RS and spatial modelling to estimate actual ET;
8. Use GIS to extract ET values for each individual forest patch.

These steps are repeated for each time step (e.g. month) to generate temporal and seasonal profiles of water use over a period (e.g. decade). The forest patches and extracted ET values can also be grouped (categorised) into forest types, climatic regions, slope classes, etc. to gain an understanding of how such environmental factors affect water use.

The following subsections provide a brief overview of some of the principal techniques that will be employed in this project. The overview starts with image classification, which can be used to differentiate among land covers (e.g. forests from urban areas), for delineating individual forest patches, and for grouping patches into classes (e.g. forest types). This is followed by an introduction to object-based image analysis (OBIA), which has been shown to improve image classification results. In addition, Mucina *et al.* (2018) demonstrated the value of OBIA for forest type classification, using a combination of terrain analysis and machine learning techniques.

2.5.1 Image transformations

In RS, image transformations refer to a broad range of techniques used to modify and analyse data captured from aerial or satellite sensors. These transformations are applied to raw or pre-processed image data to enhance features, highlight specific information, or prepare the data for further analysis.

Section 2.4.2.1 explained the value of multispectral imagery for various applications. Although individual spectral bands are often used in image classification and modelling tasks, different spectral bands are often combined to observe subtle characteristics of features on the earth's surface. For instance,

vegetation indices (VIs) are popular for studies related to vegetation mapping. VIs are linear combinations or ratios using two or more spectral bands (Huete *et al.*, 2002). VIs aim to maximise the vegetation signal while minimising background signals (Jackson & Huete, 1991). There are many different VIs, each intended for different applications.

The normalised difference vegetation index (NDVI) is the most popular as it can be used to quantify the health and density of vegetation (Xu *et al.*, 2022) and is calculated by:

$$NDVI = \frac{\rho_{NIR} - \rho_R}{\rho_{NIR} + \rho_R} \quad \text{Equation 2-1}$$

where ρ_{NIR} is the near-infrared image band; and
 ρ_R is the red image band.

It is also useful to only consider the brightness of a target feature. For instance, woody and grassy vegetation may have similar NDVI values but are different in terms of their brightness (total reflectance in the visible region of the electromagnetic spectrum (EMS)). Woody vegetation, especially trees with a sizeable proportion of shadows between leaves, have lower brightness characteristics than grasses (almost no shadows). Consequently, brightness is often a popular image transformation can be calculated as follows:

$$Brightness = \left(\left(\frac{\rho_R}{3} \right) + \left(\frac{\rho_G}{3} \right) + \left(\frac{\rho_B}{3} \right) \right) * 1 \quad \text{Equation 2-2}$$

where ρ_R is the red image band;
 ρ_G is the green image band; and
 ρ_B is the blue image band.

If more than one source of multispectral imagery is available, then it is often useful to calculate it for each source. For instance, in Section 3.3.3 brightness was calculated from aerial imagery (the resulting index was called NGIB) and from Sentinel-2 imagery (the resulting index was called S2B) in the mapping of indigenous forests (and three other land covers).

Another popular index used in vegetation mapping is the normalised difference water index (NDWI), which exploits the (relatively) higher reflectance of water in the green region of the visible spectrum and the low reflectance of water in the shortwave IR (SWIR) region. The NDWI is calculated:

$$NDWI = \frac{\rho G - \rho SWIR}{\rho G + \rho SWIR}$$

Equation 2-3

where ρG is the green image band; and
 $\rho SWIR$ is the shortwave infrared image band.

The normalised difference moisture index (NDMI) is used to determine vegetation water content. It is calculated (Equation 2-4) by combining the SWIR band (low spectral reflectance of moisture) with the near IR (NIR) band (high reflectance of vegetation). The NDMI is also sensitive to the mesophyll structure of leaves (Morell-Monzó *et al.*, 2020).

$$NDMI = \frac{\rho NIR - \rho SWIR}{\rho SWIR + \rho SWIR}$$

Equation 2-4

where ρNIR is the near-infrared image band; and
 $\rho SWIR$ is the shortwave infrared image band.

Given that Sentinel-2 imagery has two SWIR bands, it is common practice to swap out the NIR band with the other SWIR band (which we call NDMI2 in Section 3.3.3). There are countless other indices that can be generated from the combinations of bands, especially if more than two bands are combined.

2.5.2 Image classification approaches

Digital image classification methodologies (image classifiers) involve a set of computer procedures that assign image pixels or objects to classes representing information categories relevant to the user based on a diverse selection of inherent image features (Campbell, 2007). The development of image classifiers has been subject to ongoing research since the introduction of RS. A wide variety of classifier types and forms exists, each with its own strengths and weaknesses relative to applications to which they may be applied (Lawrence & Wright, 2001; Mather, 2004). When deciding on a classification method for an application, a user must weigh the importance of several factors. The efficacy of classification methods is usually assessed based on the accuracies of the final classification products using statistical metrics. However, the demand for human expertise, the time and expense of preparing and running the classifier, and the degree of automation required are aspects which must also be considered (Pal & Mather, 2003). It should also be noted that the accuracies of different classification methodologies are often specific to the application to which they are put (Lui *et al.*, 2002). It is, therefore, important that the user understands the types of classifiers available to judge which is better suited to the application at hand.

Conventional methods of image classification consist of unsupervised and supervised procedures, which rely strongly on a variety of statistical algorithms employed in spectral feature space. Although widely used in operational applications, these more traditional classifiers are not without their limitations.

The progression of digital image analysis techniques combined with the advancement of computer hardware and software has led to the development and increased implementation of more advanced classifiers, which utilise a greater degree of data mining for image pattern recognition (Tseng *et al.*, 2008). This is done by incorporating techniques such as machine learning, logical structures and expert knowledge into the classification procedures (Brown de Colstoun *et al.*, 2003; Mather, 2004). The following sections focus on the common methods used for discriminating land cover in remotely sensed imagery.

2.5.2.1 Unsupervised classification

Unsupervised classification is the clustering of image pixels into groups based on spectral information. This classification technique entails two distinct steps, namely the automatic classification of pixels into a user-specified number of image classes according to their spectral properties and the manual assigning of the classes into information classes (Campbell, 2007). Although the automated nature of the spectral delineation renders this classification method less user-intensive, it cannot be completely considered truly unsupervised in nature. According to Mather (2004:203), it is an “exploratory” technique where repeated unsupervised area delineations with different parameters allow a user to ascertain which real-world classes are spectrally distinct and which are spectrally similar. This understanding of image features can inform the construction of the set of real-world classes to be used in the classification, rendering unsupervised classification extremely useful where *a priori* information regarding the study area or the classification structure is unavailable or not predetermined. Conversely, where a real-world class structure is already established, it is rare that it will correspond with the automatically delineated spectral classes, resulting in the lowering of the accuracy of the outcome (Campbell, 2007). This is especially true for HR imagery, where features of interest commonly comprise multiple spectral classes shared by more than one information class. This is the primary disadvantage of unsupervised classification, and for this reason, its use is often limited in operational applications. An additional disadvantage is that spectral classes may change over time, which reduces their value for automated classification methods (Olaode *et al.*, 2014).

2.5.2.2 Supervised classification

Supervised classification is defined by the application of *a priori* information of real-world classes to determine the identity of unknown image elements. Data for the real-world classes are acquired from an external source and serve as input to the classifier in the form of designated and labelled regions called “training areas” or “training data”. Training data contains statistical information regarding the spectral properties of each class, which is used by a classification algorithm to identify the class of unknown pixels (Mather, 2004; Campbell, 2007). Classification algorithms are widely varied but are all designed to compare the features of each of the classes with those of an unknown pixel in geometric space and assign a class based on the results of that comparison. Traditionally, the most widely used algorithm is the maximum likelihood classification (MaxL) algorithm due to its ready accessibility, robustness, strong theoretical foundation, and high accuracy for a wide range of RS applications (Bolstad & Lillisand, 1991; Albert, 2002; Brown de Colstoun *et al.*, 2003; Pal & Mather, 2003; Tseng *et*

al., 2008). Because of these traits, several studies have used MaxL as the benchmark to compare more recently developed classification methods (Hepner *et al.*, 1990; Gumbricht *et al.*, 1996; Lui *et al.*, 2002; Neusch T & Grussenmeyer, 2003; Pal & Mather, 2003; Hagner & Reese, 2007; Nangendo *et al.*, 2007).

Recent improvements in image resolution (spatial and spectral), increases in data availability, and the integration of contextual and ancillary data have prompted the use of more powerful classifiers which incorporate elements of machine learning (Tseng *et al.*, 2008). While more traditional classifiers (such as MaxL) estimate parameters to a data distribution, ML classifiers are non-parametric and therefore do not make assumptions about the distribution of data (Jain *et al.*, 2000; Hubert-Moy *et al.*, 2001). This is especially advantageous when working with geospatial data, which, in most cases, is not normally distributed. Additionally, ML techniques can easily be automated, allow for combinations of categorical and continuous input variables, and can capture hierarchical and non-linear relationships (Hladik & Alber, 2014).

Several ML algorithms are available in RS, namely k-nearest neighbour (kNN) (Franco-Lopez *et al.*, 2001; Ying & Bo, 2009; Falkowski *et al.*, 2010), support vector machine (SVM) (Lizarazo, 2008; Li *et al.*, 2010; Petropoulos *et al.*, 2012), decision tree (DT) (Punia *et al.*, 2011; Gómez *et al.*, 2012; Hladik & Alber, 2014) and random forest (RF) (Gislason *et al.*, 2006; Chang *et al.*, 2008; Rodriguez-Galiano *et al.*, 2012).

kNN is a non-parametric, distance-based classifier that labels each unknown instance based on its k neighbouring known instances. A class is assigned to the unknown instance, which is best represented by the training samples among the k neighbours (Cover & Hart, 1967; Gibson & Power, 2000). The kNN algorithm is effective in classifying data that are not normally distributed but has the disadvantage of assigning equal weight to all variables even though certain variables may have higher priority. This can result in incorrect class assignments and diffuse clusters (Cunningham & Delany, 2007). To avoid this, only odd k-values (e.g. 1, 3 and 5) should be used, as suggested by Campbell (2007). However, the higher the k-value, the more training data are required (Xie *et al.*, 2019).

The efficiency of SVM classifiers for RS applications has been demonstrated by Lizarazo (2008) and Petropoulos *et al.* (2012). Myburgh and Van Niekerk (2013) showed that SVM produces more accurate results than kNN and MaxL for land cover mapping using SPOT-5 imagery. SVM determines the optimal separating hyperplane between classes (Novack *et al.*, 2011) by focussing on the training samples close to the edge (support vector) of the class descriptors (Tzotsos & Argialas, 2008). In cases where the relationship between classes and features is non-linear, the radial basis function kernel is often applied. See Vapnik (1995) and Huang *et al.* (2002) for a detailed mathematical formulation of SVM.

A DT identifies relationships between a continuous response variable, known as the dependent variable, and multiple continuous variables, known as the independent variables. DTs hierarchically split a dataset into increasingly homogeneous subsets known as nodes (Lawrence & Wright, 2001; Gómez *et al.*, 2012). By recursively splitting the feature datasets, a leaf node is reached, with the class associated with the node assigned to the observation (Pal & Mather, 2003). According to Novack *et al.*

(2011), each node is limited to a split in feature space orthogonal to the axis of the selected feature. Each branch of the DT consists of divisions (or rules) of the most probable class. Applying these rules will assign the class to an unknown instance (Lawrence & Wright, 2001). The main disadvantage of DT is that a large training dataset is needed, and it is prone to overfitting (Baatuuwie & Van Leeuwen, 2011).

There has been a notable increase in the use of the RF classifier for RS applications (Gislason *et al.*, 2006; Lawrence, 2006; Duro *et al.*, 2012; Immitzer *et al.*, 2012), and it has been shown to be effective for many classification tasks (Lawrence & Wright, 2001; Rodriguez-Galiano *et al.*, 2012). RF, an enhancement of DTs (Immitzer *et al.*, 2012), generates each DT by using a random vector sampled independently from the input vector. A vote is cast by each of the generated DTs (Breiman, 2001; Pal, 2005; Bosch *et al.*, 2007). Each classifier contributes a single vote to the assignment of the most popular class of the input variable (Breiman, 2001; Rodriguez-Galiano *et al.*, 2012). RF makes use of bagging (Breiman, 1996), a method which generates a training set for feature selection. This allows RF classifiers to have a low (even lower than DT classifiers) sensitivity to training set size (Rodriguez-Galiano *et al.*, 2012). Two parameters are required to be set, namely the number of trees and the number of active (predictive) variables. Rodriguez-Galiano *et al.* (2012) showed that stability in accuracy is achieved at 100 trees and that a small number of split variables are optimal for reducing generalisation errors and correlations between trees. A more detailed discussion of the RF classifier can be found in Breiman (1996), Breiman (2001), Pal (2005) and Rodriguez-Galiano *et al.* (2012).

Artificial neural networks (ANNs) were one of the first classifiers to draw on the field of ML in RS (Hepner *et al.*, 1990) but were not widely employed due to their non-intuitive usability and black-box nature. However, neural networks (NN) have recently benefitted from developments in deep learning (DL) technology, and RS is seeing the increased application of NNs, including convolutional NNs, multi-layer perceptron NNs, autoencoders and deep belief networks (Heydari & Mountrakis, 2019). ANNs are more complex than traditional statistical classifiers as they can model non-linear relationships. They contain three elements: an input layer, hidden layers and an output layer. The input layer contains the source data (imagery), hidden layers represent weights of association between classes and pixel values, and there can be many hidden layers. The output layer represents the classes for the desired output, which is defined by the training data during model building. The input data are passed through the network, and weights are adjusted until the expected classification (defined by the training data) is achieved. Once the NN is established, the input data can be replaced with other data. The disadvantages of ANNs are that they are complex and prone to overfitting (Han *et al.*, 2018). DL occurs when a multilayered NN is formed, creating a deeper network than conventional NNs (Devi Mahalakshmi and Geethanjali, 2019). A convolutional NN (CNN) contains convolutional layers, max-pooling layers and fully connected layers. Filters are applied to the convolutional layers, the dimensionality of the data is reduced in the max-pooling layers, and the fully connected layers ensure that all of the input data in one layer are connected to all of the units of the next layer (Devi Mahalakshmi and Geethanjali, 2019). NNs are advantageous as they can accept various numerical data, even if the data does not have a statistical distribution, allowing them to process ancillary data to remotely sensed data (Mather, 2004). A major

disadvantage of NNs is that a large amount of training data and computing power are required (Han *et al.*, 2018).

2.5.2.3 Knowledge-based approaches

Knowledge-based image classification (KBIC), also known as expert system or rule-based classification, applies a set of rules defined by an expert to classify remotely sensed images (Peled & Gilichinsky, 2010). KBIC consists of a knowledge base containing a set of rules (e.g. if-then statements), an inference engine that stores information about how to apply the rules and a database that contains the transformed or raw input datasets. The rules defined in KBIC are based on the expert knowledge of the user, ancillary data and spectral information, mimicking how humans differentiate between classes on the earth's surface (Cohen & Shoshany, 2002). An example of a rule would be to assign all pixels with NDVI values greater than 0.3 to a Vegetation class, as it is well-known that growing vegetation has relatively high NDVI values. An example based on literature would be to assign all pixels with NDWI values of greater than zero to a *Water* class (Bangira *et al.*, 2019)

Apart from not requiring training data, KBIC is advantageous in that the rules are transparent (open for scrutiny) and can be easily updated/modified and applied to other areas and/or data (Peled & Gilichinsky, 2010). Existing datasets, such as the South Africa National Land Cover (SANLC) products, can also easily be incorporated into the set of rules (ruleset). The challenge, however, is to find rules that generalise well (i.e. will work in areas with very different conditions).

2.5.3 Object-based image analysis

The development of classification methodologies has been enhanced by the advent of OBIA. Traditional methods of image analysis consider each pixel as an individual unit, with little cognisance of its topological relations to its neighbours or the class structure it represents (Lira & Maletti, 2002; Van Coillie *et al.*, 2007). This individuality of pixels renders them susceptible to data noise, atmospheric effects and surface variation (Wicks *et al.*, 2002) and limits the usability of spectral, textural and relational information (Rego & Koch, 2003; Lennartz & Congalton, 2004; Oruc *et al.*, 2004). Considering these factors, Blaschke *et al.* (2000) argue that no form of per-pixel classification can really yield reliable, robust, and accurate results. The increased availability of fine spatial resolution satellite imagery has exposed further limitations of per-pixel techniques, as for many applications, the pixels of these images are significantly smaller than the real-life objects of interest. In such cases, pixels often demonstrate spatial autocorrelation – the concept that features nearby are more similar than features further away – and will, therefore, belong to the same classes as their neighbours (Blaschke *et al.*, 2000; Lang, 2008). In contrast, OBIA operates on predefined areas of the image, derived either from an external source or, more commonly, from region-partitioning processes based on spectral variance known as segmentation (Blaschke *et al.*, 2000). According to (Benz *et al.*, 2004; Bock *et al.*, 2005; Hay *et al.*, 2005; Shiba & Itaya, 2006), OBIA uniquely offers meaningful statistical calculation of spectral and textural qualities, availability of feature qualities such as shape and object topology, intuitive spatial relations between real-world objects and image objects, and easier integration between GIS and RS environments and

flexibility among different software platforms.

2.5.4 Cloud-computing for remote sensing

Hansen and Loveland (2012) speculated that the future of large scale operational mapping lay with automated processing chains for multi-image classification, facilitated by the image standardisation of long-term satellite programmes such as Landsat (and more recently, Sentinel) that make the imagery freely available to the public. This concept has been advanced by the recent development of open access data catalogues and cloud-based computing services for geospatial analysis, such as Google Earth Engine and Amazon Web Server (Koskinen *et al.*, 2019; Mauya *et al.*, 2019). These services, which are freely available for research purposes, provide access to decades of remotely sensed data, which can be queried, manipulated, analysed and visualised using a wide variety of RS toolboxes. In addition to bypassing the need for data acquisition and on-site storage and processing, the architecture of these services allows for automated processing on a large scale in a scripting environment. In addition, Initiatives such as Digital Earth Africa¹² will facilitate continental-scale EO data analyses through online interfaces. Specifically, its vision is to "provide a routine, reliable and operational service, using Earth observations to deliver decision-ready products enabling policymakers, scientists, the private sector and civil society to address social, environmental and economic changes on the continent and develop an ecosystem for innovation across sectors."

2.5.5 Image classification for forests

The incorporation of satellite imagery in forest mapping has improved the cost efficiency, development speed, timeliness, accuracy and level of detail (McRoberts & Tomppo, 2007). Consequently, there is a large body of research in this field. McRoberts *et al.* (2002) classified four states in America into forest and non-forest areas using stratified national land cover data for training, while Hagner and Reese (2007) and (Tomppo *et al.*, 2008) classified forest types in Sweden and Finland. A land cover classification was conducted on a global level using MERIS fine resolution (300 m) data (Arino *et al.*, 2007). Defries *et al.* (2000), Hansen *et al.* (2003) and Hansen *et al.* (2005) estimated the global percentage of tree cover using different machine learning algorithms and MODIS imagery. Several studies have successfully discriminated between plantation and natural vegetation (Luck, 2018) conifers, deciduous and mixed forests (Nangendo *et al.*, 2007), and other land cover (Baatuuwie & Van Leeuwen, 2011) types using medium resolution (15-30 m) multispectral imagery. The use of VHR multispectral imagery in classifications has been shown to be useful in differentiating between forest species (Ke *et al.*, 2010; Pu *et al.*, 2011; Immitzer *et al.*, 2012; Atzberger, 2013; Cho *et al.*, 2015; Franklin *et al.*, 2017; Franklin & Ahmed, 2018; Wagner *et al.*, 2019; Xie *et al.*, 2019).

VHR hyperspectral data have been used to successfully classify exotic forests (Peerbhay *et al.*, 2013), coniferous forest species (Buddenbaum *et al.*, 2005), eucalyptus and pine plantations (Van Aardt &

¹² <https://www.digitalearthafrika.org/african-regional-data-cube>

Norris-Rogers, 2008), swamp tree species (Adam *et al.*, 2012), and forest plantation species (Voss & Sugumaran, 2008; Fagan *et al.*, 2015).

SAR-derived metrics have been used in conjunction with multispectral-derived metrics in classification algorithms to map forest plantations. SAR-derived metrics are often used to differentiate between forest and non-forest areas (Dong *et al.*, 2012; Dong *et al.*, 2013; Chen *et al.*, 2016). Airborne LiDAR has been used in classification algorithms to map tree species (Heinzel & Koch, 2011; Li *et al.*, 2013a; Martinuzzi *et al.*, 2013; Budei *et al.*, 2018) and deciduous and coniferous trees (Yao *et al.*, 2012).

As part of a previous WRC project (Van Niekerk *et al.*, 2023), multispectral imagery (Sentinel-2) was used to discriminate among plantation forest genera (Higgs & van Niekerk, 2022; 2024).

3 METHODS AND MATERIALS

3.1 Indigenous forest classification scheme

The development of IF2021 included reassessing forest type classification at multiple levels. Established reviews of forest classification do not fully address the position of the Southern African forest biome in a global context (Mucina *et al.*, 2022). Following the principles of zonality/azonality Mucina *et al.* (2022) used the Schimper-Walterian conceptual framework of biome classification (Schimper 1898), dividing the zonal and azonal forest biomes into separate hierarchical structures. Zonal biomes were assigned to a four-tier hierarchical structure as follows:

1. Zonobiomes (ZBs), with temperature regimes as the 1st-tier ecological driver;
2. Global biomes (GBs), with precipitation as the 2nd-tier ecological driver;
3. Continental biomes (CBs), with the variations within the energy-water interactions (both a function of 1st and 2nd-tier drivers), as the drivers for ecological separation at this level; and
4. Regional biomes (RBs), with the regional variations of the climate, geology and soil as the 3rd-tier ecological drivers.

The first three biome-classifications align with the established zonal biome classification methodology employed previously in South Africa. RBs, however, are a new concept, designed to replace the bioregion classifications employed at this level in the VegMap. RBs can be further broken down into vegetation units, which in this context are analogous to forest types (i.e. the typology of forest vegetation). A revision of the forest types for South Africa was recently completed (Mucina *et al.*, 2022).

Azonal units were assigned to a two-tier hierarchical structure:

1. Azonal ecosystem groups (AGs), classified as in Macintyre and Mucina (2021); and
2. Azonal regional biomes (aRBs), equivalent to zonal RBs.

More details on the comparison of the National Forest Classification developed by Von Maltitz *et al.* (2003), the classifications used in VegMap2006 (and its later incarnations) and in IF2021 can be found in Mucina *et al.* (2022).

3.2 Overview of forest types

Table 3-1 shows a breakdown of the azonal and zonal forest types that occur within South Africa (forest types outside of South Africa were excluded) and include structurally and species-diverse forest types.

Table 3-1 Forest types and their respective zonal biomes

Zonobiome/azonal	Forest type name	Code
Azonal Coastal Group	Cape Milkwood Woodland	ACF1
	Subtropical Dune Woodland	ACF2
Azonal Mangrove Group	Subtropical Indian Ocean Mangrove	AMAN1
	Tropical Indian Ocean Mangrove	AMAN2
Azonal Riparian Group	Arid Zone Riparian Woodland	ARF1
	Cape Alluvial Woodland	ARF2
	Highland Alluvial Woodland	ARF3
	Subtropical Riparian Woodland	ARF4
Azonal Swamp Group	East African Swamp Forest	ASF1
Warm Temperate Zone	Cape Talus Forest	ATF1
	Bushveld Talus Forest	ATF3
	Drakensberg Afrotperate Forest	ATF4
	Northern Highveld Afrotperate Forest	ATF5
	Cape Afrotperate Forest	AF1
	Southern Mistbelt Forest	AF2
	Northern Mistbelt Forest	AF3
Tropical Diurnal Zone	African Subtropical Coastal Forest	STFa2
	Subtropical Scarp Forest	STFa4
	Albany Coastal Forest	STFa5
Tropical Seasonal Zone	Southern African Dry Forest	TDFa2
	Southern African Dry Thicket	TDFa3

The location and distribution of each forest type as per the IF2021 is shown in Figure 3-2. Detailed descriptions for each forest type are given below (Mucina *et al.*, 2022).

3.2.1 Cape Milkwood Woodland (ACF1)

Cape Milkwood Woodland (Figure 3-1) is found primarily in the Overberg and Hessequa regions (Western Cape) as far east as the Gouritz River along the South Coast, and occasionally occurring further west in False Bay and on the Cape Peninsula. It is highly fragmented, degraded and in the past cleared for agricultural purposes. The low forests are dominated by milkwood *Sideroxylon inerme*, with sparse (if any) undergrowth when tree canopy is closed.



Figure 3-1 ACF1 Cape Milkwood Woodland at De Hoop (left) and ACF2 Subtropical Dune Woodland at Mtunzini (right) (Credit: L. Mucina)

3.2.2 Subtropical Dune Woodland (ACF2)

Subtropical Dune Woodland (Figure 3-1) is found along the coast stretching from the Albany region of the Eastern Cape as far north as Xai Xai in Mozambique. It typically occurs in the form of prolonged, interrupted patches. Vegetation is usually thicket-like, with only a single shrub layer, but more typical forest develops in dune depressions or behind the foredune, comprising a coenocline of communities spanning low scrub, thicket to low-grown forest. The main trees and shrubs include *Allophylus natalensis*, *Brachylaena discolor*, *Casearia gladiiformis*, *Coptosperma littorale*, *Cussonia arenicola*, *Diospyros rotundifolia*, *D. inhacaensis*, *Dovyalis longispina*, *Drypetes natalensis*, *Euclea natalensis* subsp. *obovata*, *E. racemosa* subsp. *sinuata*, *Eugenia capensis* subsp. *capensis*, *Grewia occidentalis* var. *litoralis*, *Guilandina bonduc*, *Gymnosporia arenicola*, *Maerua nervosa*, *Mimusops caffra*, *Osyris compressa*, *Psydrax obovata* subsp. *obovata*, *Searsia natalensis*, *Sideroxylon inerme*, *Tarenna junodii*, *Thespesia acutiloba*, *Tricalysia delagoensis*, *Vepris lanceolata* and *Zanthoxylum delagoense*.

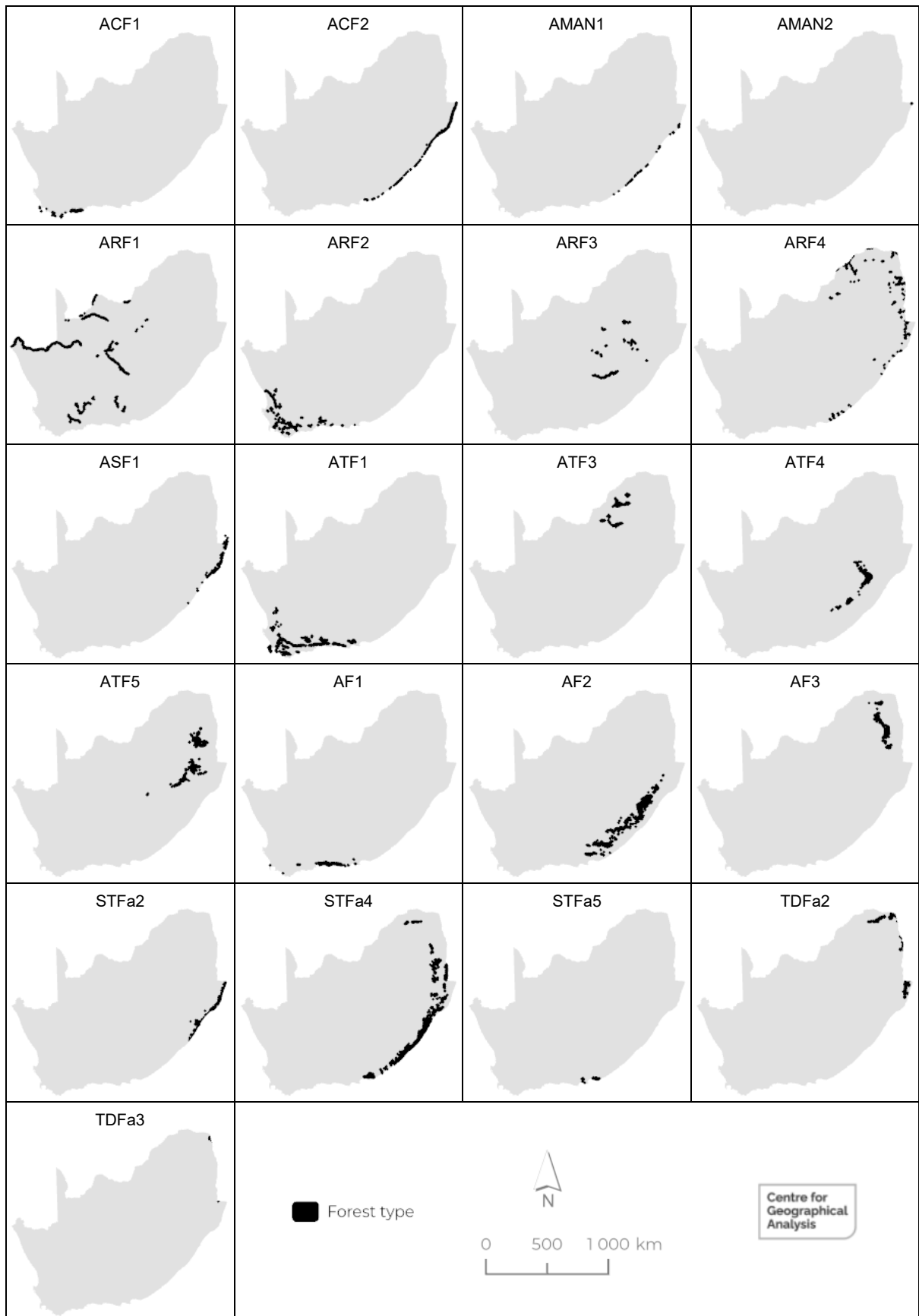


Figure 3-2 Distribution and location per forest type in South Africa

3.2.3 Subtropical Indian Ocean Mangrove (AMAN1)

Subtropical Indian Ocean Mangroves (Figure 3-3) occur in South African estuaries south of (but excluding) Kosi Bay (KwaZulu-Natal). It is species-poor and often monotypic, with the vegetation consisting of low forest and thicket dominated by *Avicennia marina* and, to a lesser extent, *Bruguiera gymnorhiza* and *Rhizophora mucronata*.



Figure 3-3 AMAN1 Subtropical Indian Ocean Mangrove, KZN La Mercy (Credit: L Mucina)

3.2.4 Tropical Indian Ocean Mangrove (AMAN2)

Tropical Indian Ocean Mangroves (Figure 3-4) occur in all South African estuaries north of and including Kosi Bay (KwaZulu-Natal). The vegetation consists of tall thickets and occasional low-grown forests dominated by *Avicennia marina* and accompanied by *Bruguiera gymnorhiza*, *Ceriops tagal*, *Heritiera littoralis*, *Lumnitzera racemosa*, *Rhizophora mucronata*, *Sonneratia alba* and *Xylocarpus granatum*.



Figure 3-4 AMAN2 Tropical Indian Ocean Mangrove, Kosi Bay (Credit: T. Riddin)

3.2.5 Arid Zone Riparian Woodland (ARF1)

Arid Zone Riparian Woodlands typically fringe or form patches in the riverbed of rarely running rivers crossing arid zonal ecosystems in Namibia, Botswana and South Africa. In South Africa, this is limited to the lower reaches of the Gariep River west of the Au-grabies Waterfalls. The vegetation consists of low, fringing ('gallery' or 'oasis') forests or open woodlands and associated thickets and scrub. The common tree dominants of the forests and tall woodlands include *Faidherbia albida*, *Searsia lancea*, *S. pendulina*, *Vachellia erioloba*, while the thickets found around the edges of the forests or replacing those in places are composed of *Euclea pseudebenus*, *Salvadora persica*, *Syzygium guineense*, *S. kuneenense*, and *Tamarix usneoides*. Low-grown scrub with halophytic *Caroxylon* spp. and *Suaeda plumosa* forms mosaics with the thickets.

3.2.6 Cape Alluvial Woodland (ARF2)

Cape Alluvial Woodlands are found in running rivers and streams of the lowland Western Cape. The vegetation consists of mid-tall fringing forests with fynbos-like sedge-rich (Cyperaceae, Restionaceae) and shrubby (Ericaceae, Fabaceae) undergrowth. Riparian thickets (with no tree overstorey) are often found fringing these riparian forests and replacing them in disturbed situations. The riparian forests and thickets in the lowlands (especially on nutrient-richer soils) have been impacted by invasive Australian, European and American trees (*Acacia*, *Quercus* and *Populus*) and numerous species of herbaceous alien flora. This regional biome is home to several iconic endemic species, such as *Brabejum stellatifolium*, *Cunonia capensis*, *Metrosideros angustifolia* and *Virgilia divaricate*.

3.2.7 Highland Alluvial Woodland (ARF3)

Highland Alluvial Woodlands are found in riparian areas of varying breadth embedded within Highveld

and Sub-Escarpment Grassland regional biomes, including major rivers such as Vaal (and its tributaries) and Gariep (above the Gariep Dam). Some patches occur also (albeit rarely) on banks of dams of various sizes in the region of occurrence. The vegetation consists mainly of woodlands with poorly closed canopy, although true forests (albeit low-grown) also occur. The prominent native trees include *Vachellia karroo*, *Searsia gerradii*; *Diospyros lycioides*. Large expanses of this riparian woodland have been invaded by alien species such as *Acacia mearnsii*, *Salix babylonica* and clonal *Populus alba* and hybrid *P. X canadensis*. The shrubby undergrowth is species-rich, and the herbaceous layer is often dominated by grasses and also supports many invasive alien species.

3.2.8 Subtropical Riparian Woodland (ARF4)

Subtropical Riparian Woodlands are found on running rivers of the southern and eastern Kalahari and all rivers crossing the Mesic Savanna (South Africa, Eswatini, Mozambique, Zimbabwe and to a lesser extent also Namibia and Botswana). The vegetation consists of discontinuous ribbons of fringing forest along rivers in flow most of the year; with a usually evergreen canopy (although *Faidherbia albida* is deciduous in summer). Common tree dominants include *Diospyros mespiliformis*, *Faidherbia albida*, *Ficus sycomorus*, *Hyphaene coriacea*, *Kigelia africana*, *Phoenix reclinata*, *Schotia brachypetala*, *Syzygium cordatum*, *Vachellia robusta* var. *clavigera*, *V. xanthophloea* and *Xanthocercis zambesiaca*; fringing riparian thickets contain prominent *Capparis tomentosa*, *Dalbergia armata*, *Entada rheedii*, *Combretum microphyllum*, *Croton megalobotrys*, *Grewia caffra*, *Maclura africana* and *Senegalia schweinfurthii*.

3.2.9 East African Swamp Forest (ASF1)

East African Swamp Forests (Figure 3-5) are found primarily on the coastal plains south of the Zambezi Delta and Maputaland in Mozambique. Rare patches are found in South Africa on the coast of KwaZulu-Natal and reach as far south as Eastern Cape. The vegetation consists of tall and mid-grown dense forests rich in lianas and understory ferns. The forest communities are usually monodominant (e.g. *Barringtonia racemosa*, *Caesaria gladiiformis*, *Ficus trichopoda*, *Raphia australis*), with other frequent trees including *Ficus lutea*, *Macaranga capensis*, *Rauvolfia caffra*, *Schefflera umbellifera*, *Shirakopsis elliptica*, and *Syzygium cordatum*.



Figure 3-5 ASF1 East African Swamp Forest at Mkuzi (left), ATF1 Cape Talus Forest Langeberg at Tradouw Pass (middle), ATF3 Bushveld Talus Forest at Strydom Pass (right) (Credit: L. Mucina)

3.2.10 Cape Talus Forest (ATF1)

Cape Talus Forests (Figure 3-5) are found in isolated patches mainly in the Western and Eastern Cape, extending along the north-south mountain chain from Bokkeveld (Hantam), through the Cederberg, and extending eastwards along the Cape Fold Mountains of Riversonderend, Langeberg, Outeniqua and Tsitsikamma, Baviaanskloof and Groot Winterhoekberge. This forest type is also found in Swartberg, Rooiberg and Kammanassie Mountains. The vegetation consists of medium-tall and especially low (scrub) forest with dominants including *Apodytes dimidiata*, *Cassine schinoides*, *Cunonia capensis*, *Ilex mitis*, *Heeria argentea*, *Kiggelaria africana*, *Podocarpus elongatus* (in the Bokkeveld area), *Rapanea melanophloeos*; *Brabejum stellatifolium*, *Platylophus trifolius*, *Virgilia* spp. The riparian thickets are tall-grown and typically composed of *Brachylaena neriifolia*, *Cliffortia* spp., *Metrosideros angustifolia*, *Phylica* spp. while the fynbos thickets are composed of *Cassine peragua*, *C. schinoides*, *Diospyros glabra*, *Heeria argentea*, *Hyphaene globosa*, *Maurocena frangula*, *Maytenus acuminata*, *M. oleoides* and *Olea europaea* subsp. *africana*.

3.2.11 Bushveld Talus Forest (ATF3)

Bushland Talus Forests (Figure 3-5) are found in isolated occurrences on the Pilanesberg and Waterberg in Limpopo in the north, West Magaliesberg in the northwest and Gauteng in the south. The vegetation consists of generally low and rarely also medium-tall forest dominated by *Buxus macowanii* (rarely), *Celtis africana*, *Diospyros lycioides*, *D. whyteana*, *Erythrina lysistemon*, *Kirkia wilmsii*, *Myrsine africana*, *Olea europaea* subsp. *africana*, *Osyris lanceolata*, *Pittosporum viridiflorum*, *Podocarpus latifolius*, *Searsia lancea*, *S. leptodictya*, *Tricalysia lanceolata* and *Widdringtonia nodiflora*.

3.2.12 Drakensberg Afrotropical Forest (ATF4)

Drakenstein Afrotropical Forests (Figure 3-6) are found in patches, mainly along the lower reaches

of the northeastern side of Drakensberg Escarpment between KwaZulu-Natal and Lesotho (and marginally northwards to the vicinity of Van Reenen's Pass), extending southwards along the Great Escarpment to the northeast Eastern Cape. The vegetation consists of low to medium-height forest, with dominants including *Halleria lucida*, *Ilex mitis*, *Kiggelaria africana*, *Maytenus acuminata*, *M. undata*, *Olinia emarginata*, *Podocarpus latifolius*, *Rapanea melanophloeos*, *Scolopia mundii*, *Pittosporum viridiflorum* and *Pterocelastrus rostratus*.



Figure 3-6 ATF4 Drakensberg Afrotropical Forest, Golden Gate Highlands NP (Credit: L. Mucina)

3.2.13 Northern Highveld Afrotropical Forest (ATF5)

Northern Highveld Afrotropical Forests are found occurring in patches along the eastern side of the low escarpment separating KwaZulu-Natal and the Free State, extending to the Highveld around Vryheid and Wakkerstroom in south Mpumalanga and also occurring further north, mainly on the western (rain shadow) flank of the Great Escarpment in north Mpumalanga (e.g. in the Lydenburg area). The vegetation consists of medium-high, multilayered forest with well-developed understory and herb layer, with dominant species including *Afrocarpus falcatus*, *Allophylus africanus*, *Celtis africana*, *Diospyros whyteana*, *Dombeya burgessiae*, *Greyia sutherlandii*, *Myrsine africana*, *Podocarpus latifolius*, *Senegalia caffra* and *Xymalos monospora*.

3.2.14 Cape Afrotropical Forest (AF1)

Cape Afrotropical Forests (Figure 3-7) present the largest continuous (albeit fragmented through historical logging) forest complex in South Africa. Known as the Knysna-Tsitsikamma forest complex, it occupies the coastal platform between approximately George and Humansdorp, with outlier forest

patches on low-elevation slopes of the Outeniqua and Langeberg ranges. The most western outlying patch is found on the eastern slopes of Table Mountain (Cape Town). The vegetation consists of tall, multi-layered forests dominated by *Apodytes dimidiata*, *Cassine peragua*, *Curtisia dentata*, *Diospyros whyteana*, *Nuxia floribunda*, *Ocotea bullata*, *Olea capensis subsp. macrocarpa*, *Podocarpus latifolius*, *Pterocelastrus tricuspidatus*, *Rapanea melanophloeos*; shrub layer hosts *Alsophila capensis* (tree fern), *Burchellia bubalina*, *Trichocladus crinitus* and *Sparmannia africana* on forest edges. Lianas (*Capparis*, *Rhoicissus*, *Scutia*, *Secamone*) are common, and the herbaceous layer is rich in ferns. *Oplismenus hirtellus* and some *Carex* species (formerly *Schoenoxiphium*) are the most important understory graminoids.



Figure 3-7 AF1 Cape Afrotropical Forest, Knysna (Credit: L. Mucina)

3.2.15 Southern Mistbelt Forest (AF2)

Southern Mistbelt Forests (Figure 3-8) are found within a fragmented distribution at middle elevations of the Kwa-Zulu Natal Midlands near Ulundi in the north and Kokstad vicinity in the south, into the Eastern Cape through areas of Mount Ayliff and Engcobo to the south Amathole and Winterberg Mountains between Stutterheim and Fort Beaufort, and with outliers as far as Somerset East and the Zuurberg. The vegetation consists of mainly tall forest dominated by *Afrocarpus falcatus*, *Calodendrum capense*, *Celtis africana*, *Kiggelaria africana*, *Podocarpus latifolius*, *Rapanea melanophloeos*, *Xymalos monospora* and *Zanthoxylum davyi*; *Podocarpus henkelii* is an important element in the KwaZulu-Natal Midlands.



Figure 3-8 AF2 Southern Mistbelt Forest at Zuurborg (left) and AF3 Northern Mistbelt Forest at Graskop (right) (Credit: L. Mucina)

3.2.16 Northern Mistbelt Forest (AF3)

Northern Mistbelt Forests (Figure 3-8) are found from the Mpumalanga Escarpment (Barberton, Long Tom Pass, Blyde and Mariepskop areas), northwards along the northeastern Escarpment as far as Soutpansberg. The vegetation consists of tall, moist, evergreen forest rich in epiphytes and comprised of *Xymalos monospora*, *Brachylaena transvaalensis*, *Bersama tysoniana*, *Cassipourea malosana*, *Chionanthus foveolatus subsp. major*, *Cryptocarya transvaalensis*, *Curtisia dentata*, *Olea capensis subsp. macrocarpa*, *Oxyanthus speciosus subsp. gerrardii*, *Maytenus acuminata var. acuminata*, *Podocarpus latifolius*, *Psydrax obovata subsp. elliptica*, *Rapanea melanophloeos*, *Rothmannia capensis*, *Schefflera umbellifera*, *Scolopia mundii*, *Searsia chirindensis*, *Syzygium gerrardii* and *Zanthoxylum davyi*.

3.2.17 African Subtropical Coastal Forest (STFa2)

African Subtropical Coastal Forests (Figure 3-9) are concentrated in the coastal (Indian Ocean) belt from south KwaZulu-Natal, stretching north to and into Mozambique. The most iconic forest complexes include Hawaan, Hlongweni (Tugela Mouth) and Dukuduku Forest (all in South Africa), Maputaland forests and Bilene forest complex (Mozambique). The vegetation consists of medium-tall semi-deciduous or occasionally evergreen forest, with some of the dominant or characteristic canopy species including *Azelia quanzensis*, *Albizia adianthifolia*, *Brachylaena discolor*, *Celtis africana*, *Chaetachme aristata*, *Dialium schlechteri*, *Diospyros inhacaensis*, *D. natalensis*, *Ficus natalensis*, *Filicium decipiens*, *Hymenocardia ulmoides*, *Lannea antiscorbutica*, *Manilkara discolor*, *Mimusops caffra*, *Morus mesozygia*, *Pteleopsis myrtifolia*, *Sclerocroton integerrimus*, *Sideroxylon inerme*, *Strychnos gerrardii* and *Vepris lanceolata*.



Figure 3-9 STFa2 African Subtropical Coastal Forest at Margate (left), STFa4 Subtropical Scarp Forest at Oribi Gorge (middle), STFa5 Albany Coastal Forest at Alexandria Forest (right) (Credit: L. Mucina)

3.2.18 Subtropical Scarp Forest (STFa4)

Subtropical Scarp Forest (Figure 3-9) occur in a narrow, fragmented belt from Albany region south of Grahamstown, along the Indian Ocean seaboard of Transkei and KwaZulu-Natal and then turning inland in two nearly parallel belts – one from north KwaZulu-Natal towards the bases of Mpumalanga Escarpment, and the other along the Lebombo range from Maputaland to Eswatini and Mozambique border areas. A special type of scarp forest occurs on the south flanks of Blouberg and Soutpansberg. The vegetation consists of usually mid-tall, evergreen or semideciduous forests, with some of the dominant or characteristic canopy taxa including *Chaetachme aristata*, *Chionanthus foveolatus* subsp. *foveolatus*, *Combretum kraussii*, *C. woodii*, *Croton sylvaticus*, *Englerophytum magalismsontanum*, *Ekebergia capensis*, *Ficus sur*, *Harpephyllum caffrum*, *Homalium dentatum*, *Macaranga capensis*, *Manilkara concolor*, *M. discolor*, *Margaritaria discoidea*, *Mimusops zeyheri*, *Philenoptera sutherlandii*, *Protorhus longifolia*, *Rawsonia lucida*, *Strychnos decussata*, *S. mitis*, *Vitellariopsis marginata* and *Trichilia dregeana*.

3.2.19 Albany Coastal Forest (STFa5)

Albany Coastal Forests (Figure 3-9) are limited to the broad coastal platform of the Albany region (Eastern Cape), with the Alexandria Forest complex the iconic flagship forest of this type. These are remnants of obviously extensive westernmost subtropical coastal forests from the past, which are heavily fragmented today. The vegetation consists of mid-tall semi-deciduous forest dominated by *Apodytes dimidiata*, *Celtis africana*, *Erythrina caffra*, *Maytenus undata*, *Mimusops obovate* and *Sideroxylon inerme*. The shrub layer is species-rich and contains species such as *Cordia caffra*, *Euclea natalensis*, *Gymnosporia buxifolia*, *Strychnos decussata* and *Teclea natalensis*, while the herb layer is usually dense and dominated by *Acalypha glabrata*, *Hypoestes aristata* and grass *Panicum deustum*.

3.2.20 Southern African Dry Forest (TDFa2)

Southern African Dry Forests (Figure 3-10) occur in diverse forms across large areas in southern Africa, though in South Africa specifically, they are found in highly localised mid- to small-size (and rarely large-scale) patches from north Limpopo and along the western piedmonts of Lebombo Mts of South Africa. The vegetation consists of short to tall deciduous forest, often with a dense, almost impenetrable shrub layer and occasionally with a near-evergreen canopy, particularly when dominated by *Androstachys johnstonii*. The canopy can be either open or closed and dominated by *Azelia quanzensis*, *Albizia forbesii*, *Androstachys johnsonii*, *Balanites maughamii*, *Brachystegia torrei*, *Cleistanthus schlechteri*, *Craibia zimmermannii*, *Dialium schlechteri*, *Drypetes mossambicensis*, *Fernandoa magnifica*, *Guibourtia conjugata*, *Erythrophleum lasianthum*, *Hymenocardia ulmoides*, *Lannea antiscorbutica*, *Lecaniodiscus fraxinifolius*, *Margaritaria discoidea*, *Millettia stuhlmannii*, *Newtonia hildebrandtii*, *Pteleopsis myrtifolia*, *Pterocarpus lucens*, *Suregada zanzibariensis*, *Tapura fischeri*, *Xeroderris stuhlmannii*, *Xylia torreana*, *Zanthoxylum delagoense* and *Z. holtzianum*.



Figure 3-10 TDFa2 Southern African Dry Forest at Tembe (left) and TDFa3 Southern African Dry Thicket at Tembe (right) (Credit: L. Mucina)

3.2.21 Southern African Dry Thicket (TDFa3)

Southern African Dry Thickets (Figure 3-10) are found in South Africa in small patches in Ndumo (KwaZulu-Natal), stretching northwards as far as Greater Limpopo Transfrontier Park. The vegetation consists of very dense thicket of 3 – 8 m with occasional scattered taller trees or pockets of taller trees with canopies of up to 15 m. The dense shrub layer results in a poorly developed ground layer, with the dominating large shrubs including *Baphia massaiensis* and *Boscia foetida* subsp. *filipes*, *Canthium armatum*, *Cassipourea mossambicensis*, *Cleistanthus schlechteri*, *Combretum celastroides*, *Coptosperma littorale*, *C. madandensis*, *Croton pseudopulchellus*, *Dialium schlechteri*, *Diospyros natalensis*, *Empogona junodii*, *Grewia microthyrsa*, *Guibourtia conjugata*, *Hyperacanthus microphyllus*,

Lagynias lasiantha, *Leptactina delagoensis*, *Markhamia zanguebarica*, *Ochna barbosae*, *Oxytenanthera abyssinica*, *Psydrax locuples*, *P. fragrantissima*, *Pteleopsis myrtifolia*, *Rytigynia celastroides*, *Sclerochiton apiculatus*, *Strychnos decussata*, *Tricalysia delagoensis*, *Uvaria lucida*, *Vitex ferruginea*, *V. patula* and *Warneckea parvifolia*. Emergents may include *Adansonia digitata*, *Azelia quanzensis*, *Balanites maughamii*, *Bombax rhodognaphalon* and *Cordyla Africana*.

3.3 Indigenous forest type mapping

The IF2021 is currently the most comprehensive map of indigenous forests of Southern Africa. Although the accuracy and level of detail of the forest patches in IF2021 are a great improvement on the VegMap2018, the manual digitising was employed often at a different scale in different areas, resulting in inconsistencies in the spatial accuracy. For example, in some areas, polygons are generalised, small patches are still excluded, or some non-forest patches (or severely degraded forests) could be removed (Figure 3-11 and Figure 3-12).

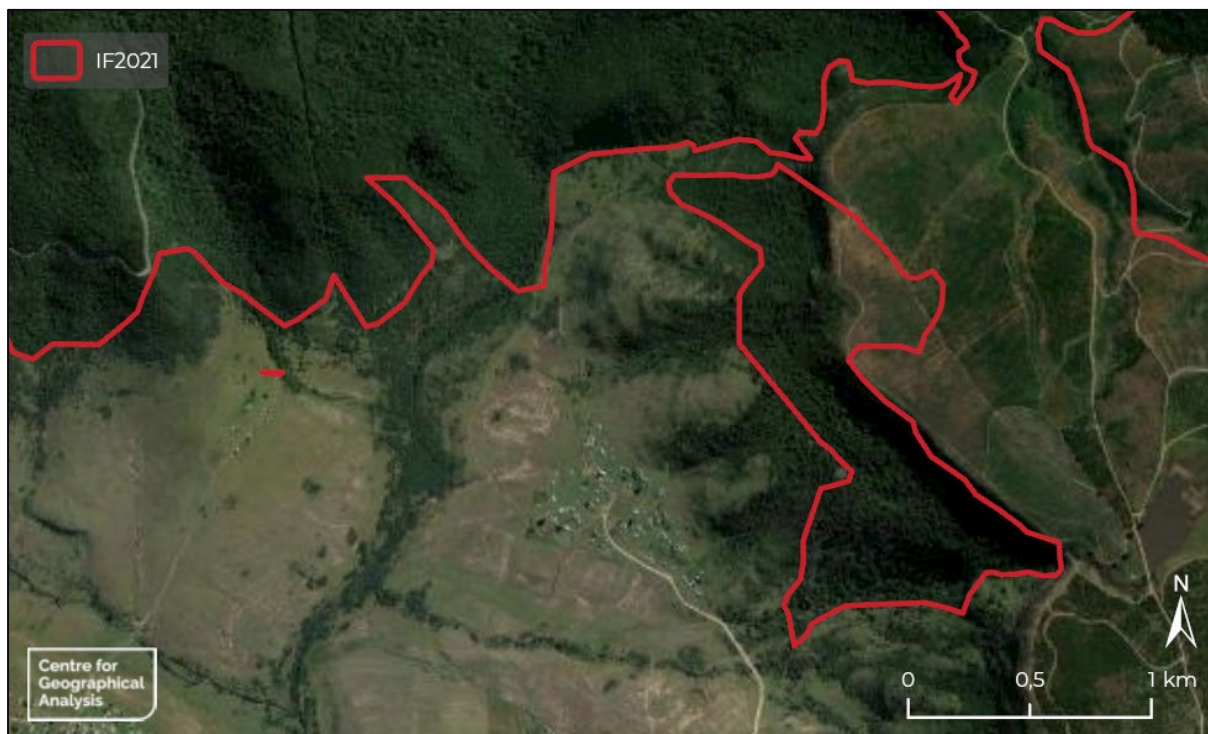


Figure 3-11 Generalised and missing indigenous forest polygons near Hogsback, Eastern Cape



Figure 3-12 Non-forest patches that could be removed in Ngoya Forest, KwaZulu-Natal

Given the inconsistencies and inaccuracies of the IF2021, Phase 1 of this research involved the mapping of indigenous forests for more accurate water use quantification and analysis per forest type. Figure 3-13 shows the workflow diagram and associated product naming convention used by the research team for Phase 1.

Phase 1.1 involved the draft indigenous forest mapping. As seen during the work done with Mucina *et al.* (2022), mapping indigenous forests for Southern Africa at a very large (detailed) scale is a task that will take many years to achieve if done manually. The mapping in this project was therefore undertaken using RS to derive draft indigenous forest maps in areas of South Africa (IF2022). Phase 1.2 involved the refinement of the draft indigenous forest mapping through manual correction in order to increase the accuracy (IF2023). Phase 1.3 involved the incorporation of the IF2021 forest types into the IF2023 indigenous forest maps to develop maps of indigenous forest types (IF2024). Validation of the mapping and classification was undertaken with expert knowledge through an online GIS application. The following sections describe these phases in more detail.

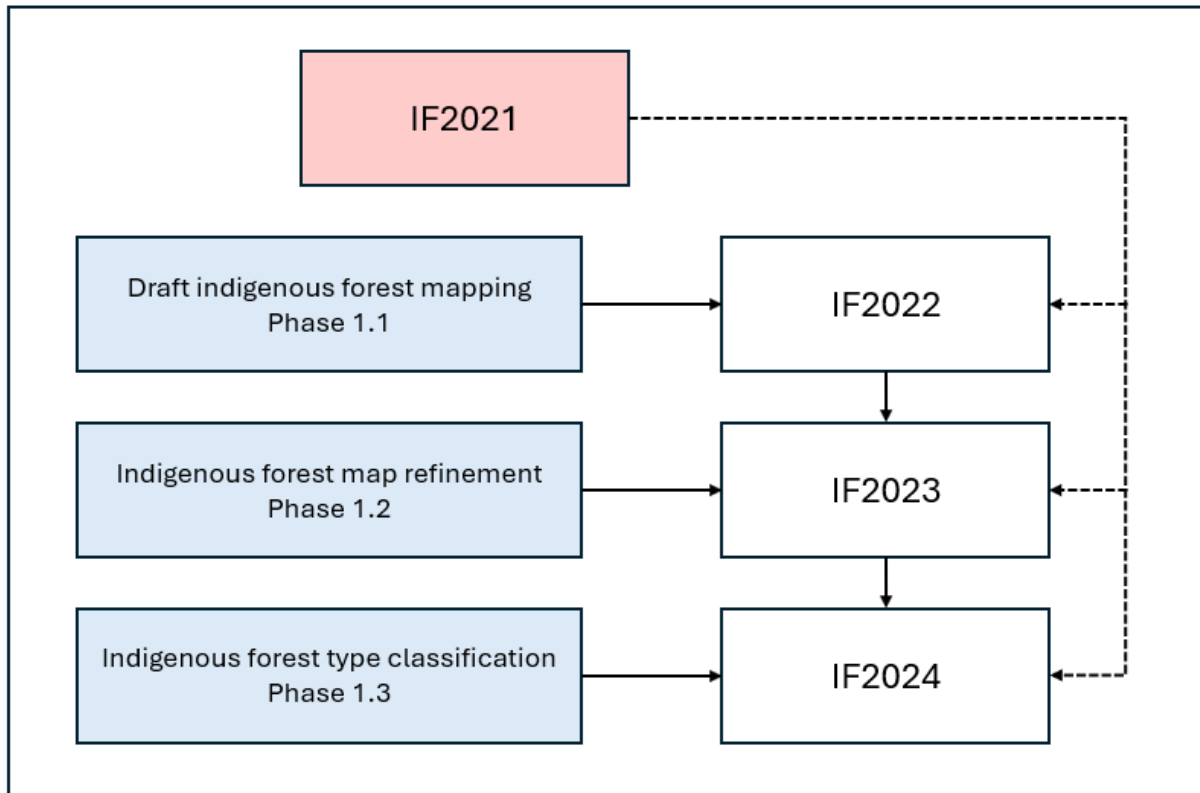


Figure 3-13 Workflow and product development of indigenous forest type mapping

3.3.1 Draft indigenous forest mapping

Given that per-pixel classification can result in undesired effects when applied to very high-resolution imagery, an OBIA approach using KBIC was taken in this study (Section 2.5.2.3 and 2.5.3). The project team has undertaken research in KBIC dating back to the early 2000s (Kidane 2005; Stephenson & Van Niekerk, 2009) and, between 2012 and 2014, applied KBIC to map land cover in the Eastern Cape (32 classes) with an average overall accuracy of over 90% (Van Niekerk *et al.*, 2014). The following section outlines the OBIA and KBIC processes used to undertake the draft indigenous forest mapping (Phase 1.1; more details can be found in Deliverable 3).

Four basic land cover types were targeted: *Plantation*, *Natural woody vegetation*, *Water* and *Other*, by applying OBIA KBIC to aerial photographs, satellite imagery and ancillary data. Figure 3-14 shows an aerial photograph composite of the northern parts of Richards Bay, which includes plantations in the northwest and in the east, woody vegetation along the coast and riparian areas, and water in the ocean and estuary. Other land cover types include built-up residential and semi-residential areas, as well as bare ground and cultivation.



Figure 3-14 Aerial photograph of an area north of Richards Bay

Figure 3-15 shows a natural colour Sentinel-2 (S2) composite image of the same area. Notice that due to its lower resolution, the image contains much less detail than the aerial photograph, but the radiometric quality of the image is higher (for instance, compare the reflection in the ocean).



Figure 3-15 Sentinel-2 natural colour composite image (RGB) of an area north of Richards Bay

The first class targeted was *Water*. *Water* class “seed” pixels were created using the satellite images using NDWI, which were then grown into *Water* objects using a region merging procedure assessed against the spectral returns of the aerial photographs. This approach worked very well for inland water bodies but not for the ocean, as wave action caused too much variation in the aerial photograph reflectance. To overcome this, a further NDWI rule was applied to the S2 imagery. The result of these rules is shown in Figure 3-16.



Figure 3-16 Classified Water (blue) overlain onto an aerial photograph of an area north of Richards Bay

The next class targeted was a generic *Woody vegetation* class comprised of both plantations and indigenous forest. Three sequential MRS segmentations were derived. The first segmentation was run on aerial photographs, and VHR digital surface model (DSM) derivatives were incorporated to accentuate surface features within objects. Subsequent segmentations incorporated aerial photograph bands and indices derived from satellite imagery to determine minimum mapping units for *Woody vegetation*. These were then classified by applying threshold rules for NDVI, NGIB, S2B, NDMI2 (Section 2.5.1) and NFB (national field boundaries). This successfully delineated large tree stands,

though some small stands were missed. Additional rules were then applied to capture these missed segments, resulting in a more comprehensive identification of tree stands (Figure 3-17).

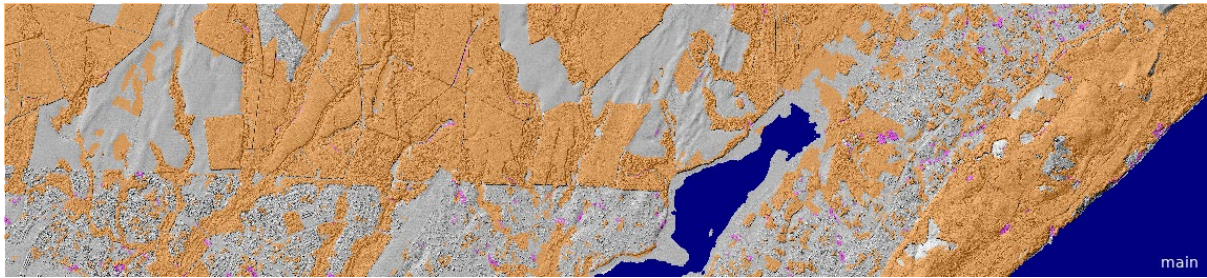


Figure 3-17 Woody vegetation (orange and pink) overlain onto a hillshade of the Digital Elevation Model of South Africa (DEMSA)

The objects belonging to the *Woody vegetation* class were then reclassified into *Plantation forests* using proximity to the SANLC and IF2021 and ancillary DEM derivatives. All remaining *Woody vegetation* objects were assigned to the *Natural woody vegetation* class, and all remaining unclassified objects were classified as *Other*. The result of this classification is shown in Figure 3-18, with *Plantations* in purple, *Natural woody vegetation* in red, *Other* in yellow and *Water* in blue.

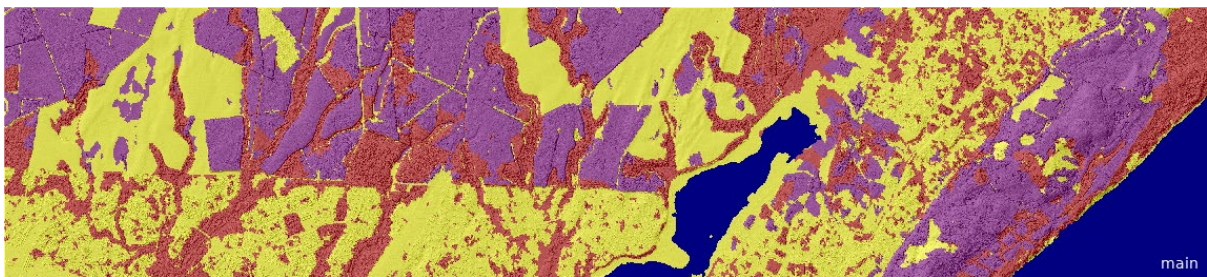


Figure 3-18 Planted forests (purple), Natural woody vegetation (red), Other (yellow) and Water (blue) classified using KBIC (overlain onto a hillshade of the DEMSA)

Given the large extent to which IFs are found in South Africa, the KBIC methodology was implemented per quarter degree tile, of which 1919 cover South Africa (Figure 3-19). Using the IF2021 as a basis, the area covered by indigenous forests was calculated within each tile. In total, 618 tiles containing indigenous forests were identified. The tiles with the largest proportion (>1000 ha) of indigenous forests were prioritised for mapping (141 tiles in total).

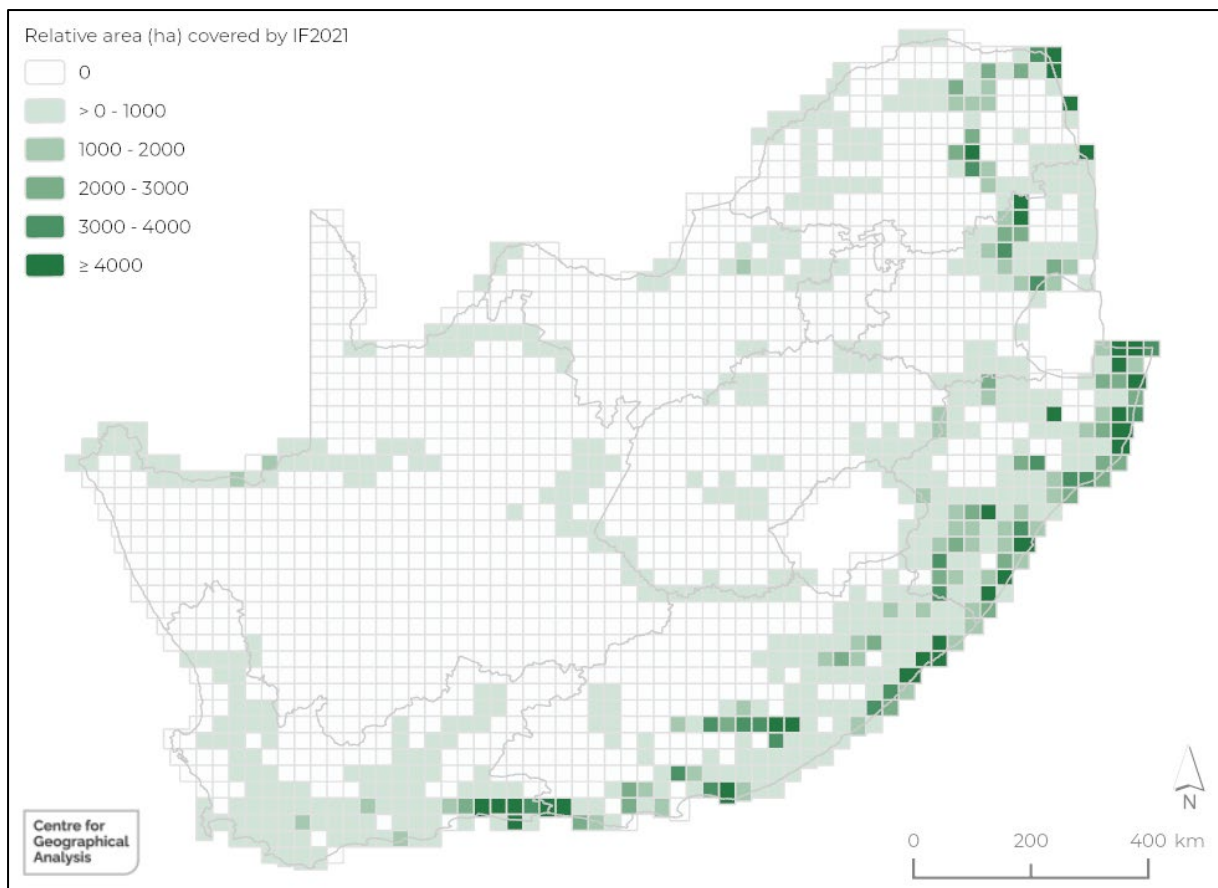


Figure 3-19 Relative area (ha) of indigenous forests within each quarter degree tile

At the time of writing this report, the KBIC was successfully applied to 91 tiles (Figure 3-20), constituting over 62% of the indigenous forest in South Africa.

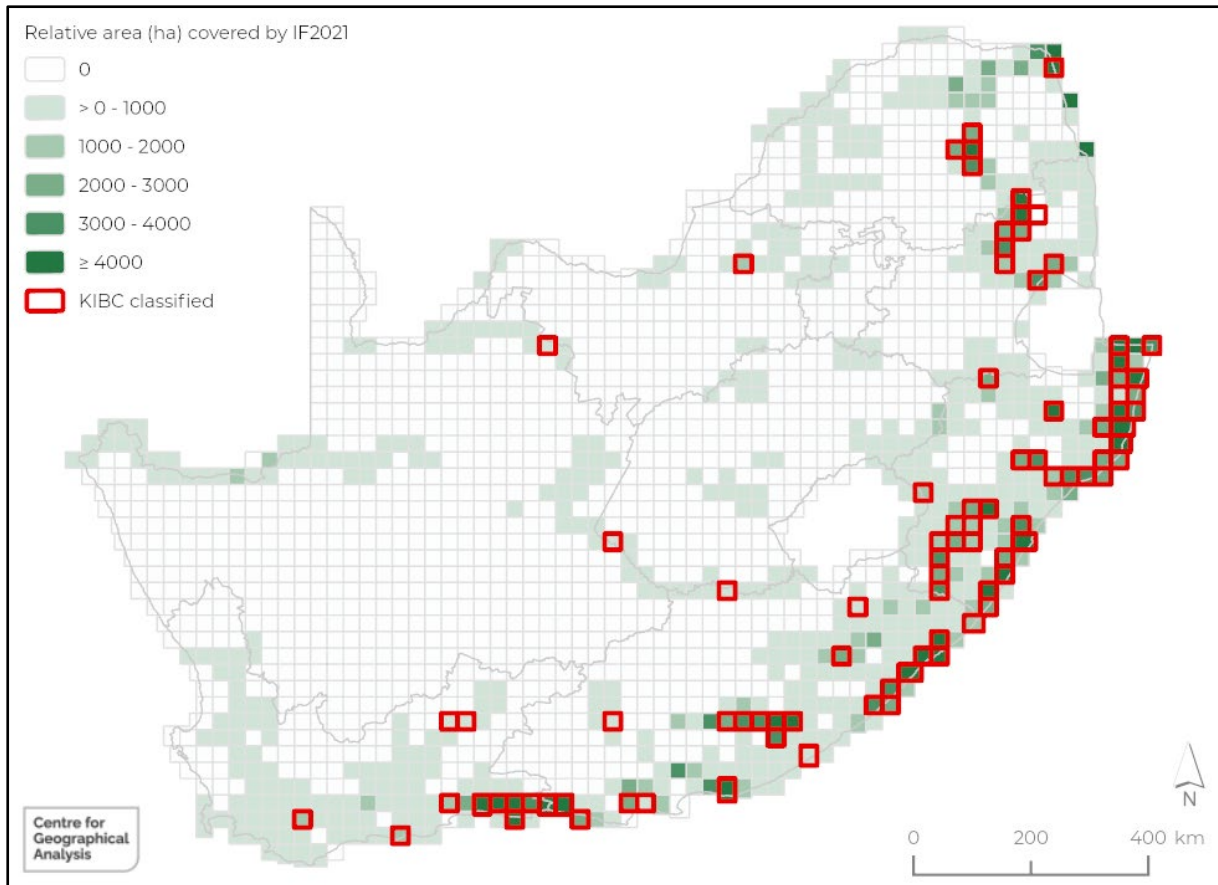


Figure 3-20 Indigenous forest classification progress to date

The overall accuracy of the IF2022 was estimated to be around 90%. Although this accuracy is high by most RS standards, it was deemed insufficient for indigenous forests water use analysis and further refinements were undertaken.

3.3.2 Indigenous forest map refinement

The refinement of the IF2022 was undertaken through manual corrections, as advised by expert knowledge. Typically, manual editing (e.g. digitising the boundaries of individual forest patches) is extremely time-consuming, but the process was streamlined by using OBIA. Image objects representing homogenous land cover units were created by applying MRS to the classified forest boundaries, NDVI, enhanced vegetation index (EVI), texture, and elevation. These objects were then used as minimum mapping units (MMUs) for the manual corrections. Using image objects instead of pixels as MMUs allows operators to select and assign multiple objects to a specific class (i.e. Indigenous forest vs. Other) without any need for any digitising.

With the assistance of Prof Mucina, the following guidelines were set for the manual class assignments:

1. Large (> 5 ha) objects with a majority proportion (>50%) of indigenous forests, but also other land cover classes such as non-woody vegetation (e.g. grass), water, bare ground, buildings, etc. must be manually split along the edge of the indigenous forest (Figure 3-21);

2. Compared to naturally occurring trees, plantations generally have a much smoother appearance in very high-resolution imagery as they are of the same age and planted in a more or less regular grid. Objects containing planted trees should be removed from the *Indigenous forest* class (Figure 3-22);
3. For an object to be assigned to the *Indigenous forest* class, it must have a natural (i.e. perceived not to be planted) tree canopy cover of greater than 75% (Figure 3-23);
4. Objects within urban areas containing tree cover of greater than 75% must be assigned to *Other* (Figure 3-24), unless they form part of a patch of trees that is larger than 50 x 50 m (quarter of a hectare).
5. Objects containing buildings and residential gardens must be assigned to *Other* (Figure 3-24);
6. Objects that contain a mixture of planted and natural trees, or where it is difficult to discern whether the trees within an object were planted or are of natural origin, must be mapped as *Indigenous forest*. I.e. err on the side of caution.

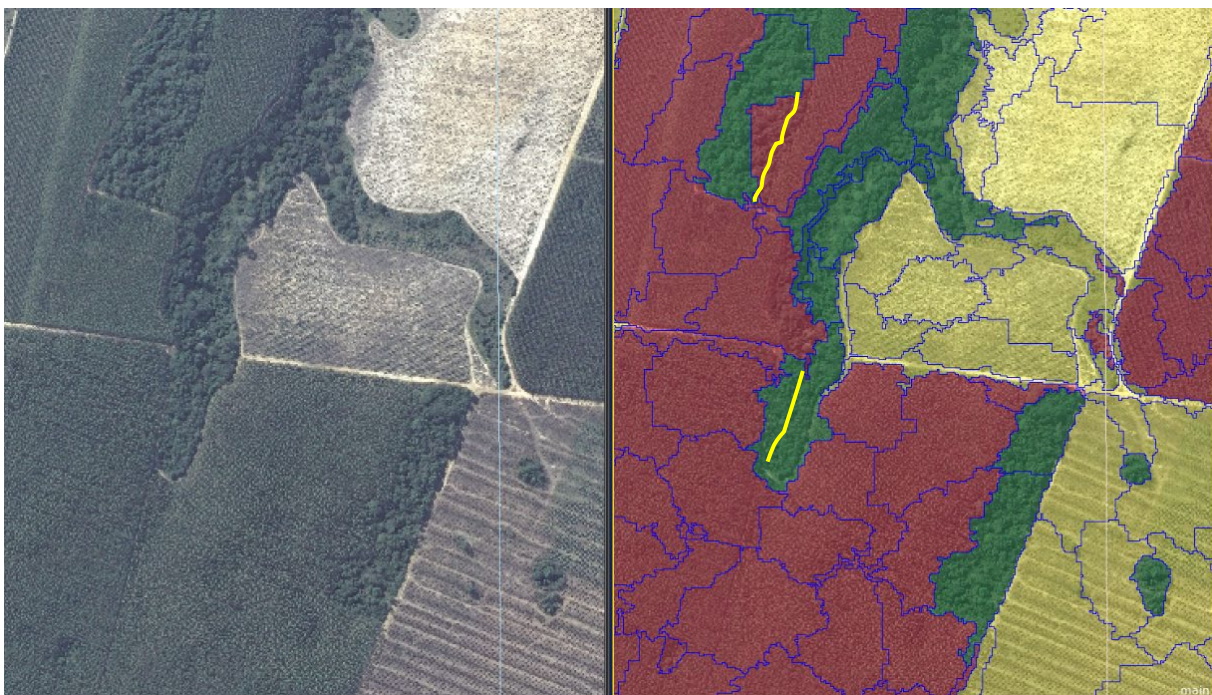


Figure 3-21 Examples (yellow lines) of where object boundaries do not match the *Indigenous forest* (green) patch boundary and where subdivision (splitting) of objects is required



Figure 3-22 Example of where Indigenous forests (green) are distinctly less smooth (in terms of texture) compared to planted forests (red) and other land covers (yellow)

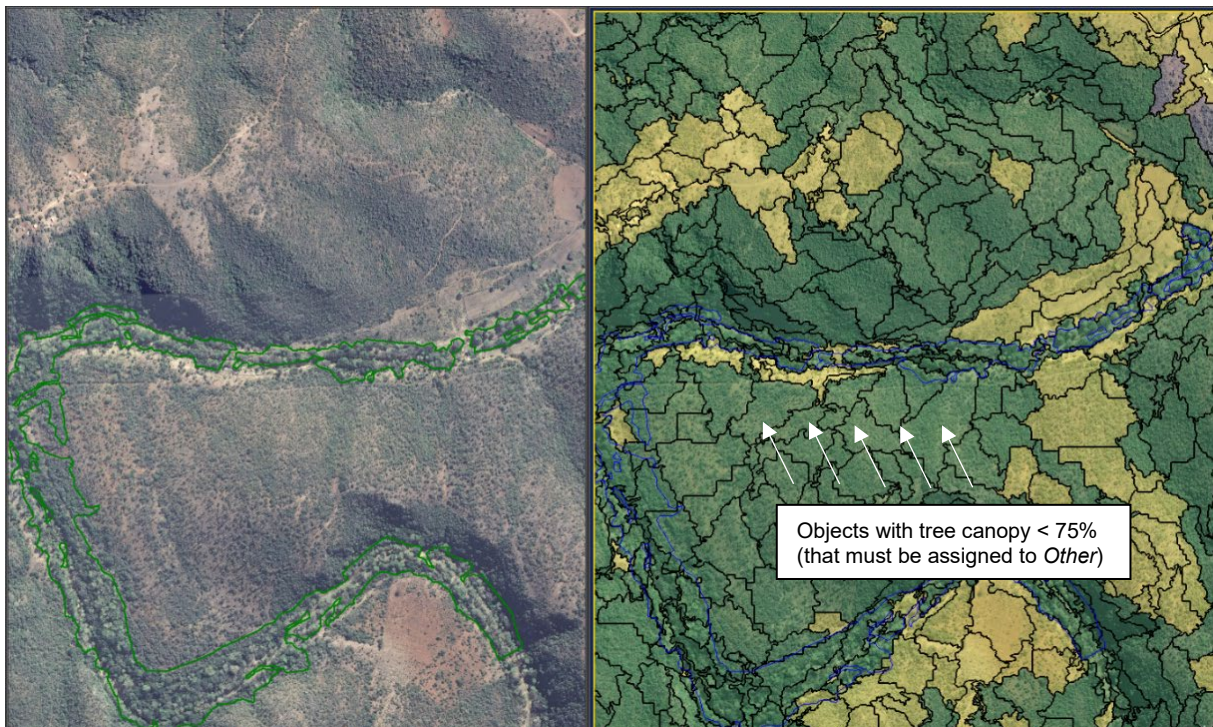


Figure 3-23 Example of where *Indigenous forest* object with less than 75% tree coverage must be manually reclassified to *Other*



Figure 3-24 Examples of *Indigenous forest* objects in urban areas that must be manually assigned to *Plantation* or *Other* based on their contiguous size or content (e.g. buildings), respectively

Despite the very high classification accuracies (>90%) achieved using the KBIC approach, each tile still required a significant amount of manual correction and verification (quality control). To date, the mapping has entailed over 1200 hours of processing and over 1000 person-hours of post-processing time, most of which was spent on manual corrections and quality control. The project team severely underestimated the time required for this process but feels that the value that this has added to the project is worth the effort. An example of the refinement is shown for the Ngoya Forest, KwaZulu-Natal in Figure 3-25.

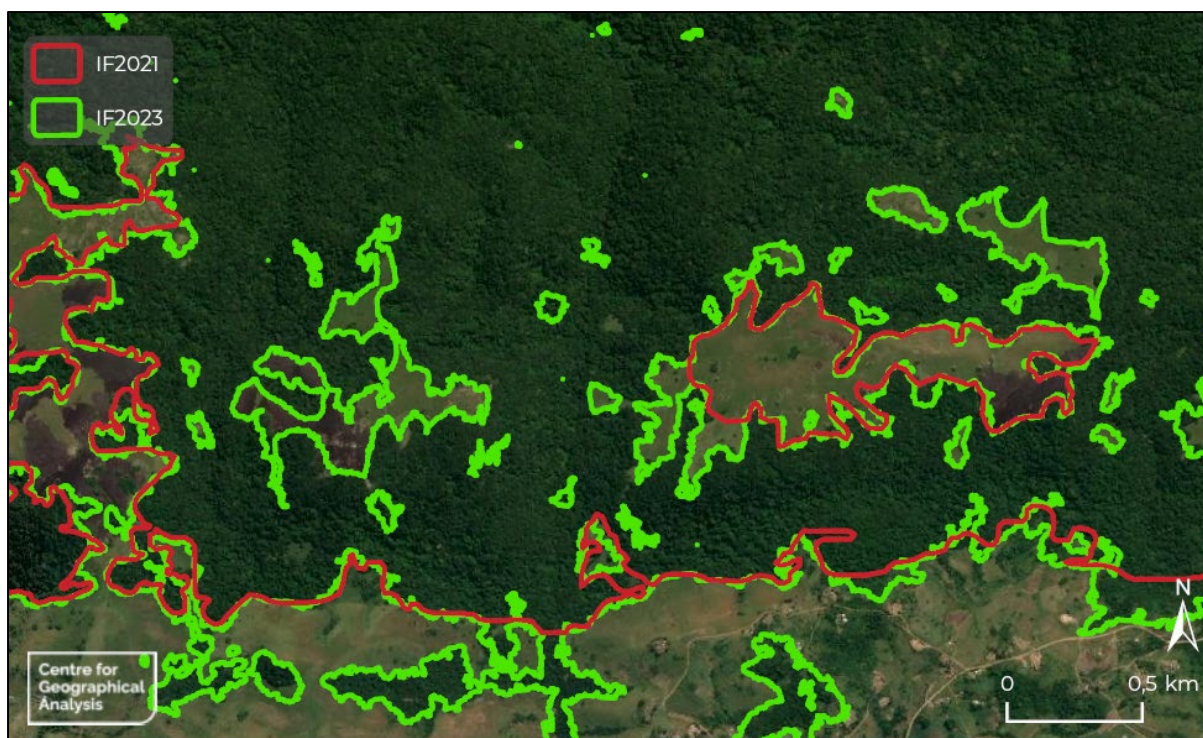


Figure 3-25 Comparison of IF2021 and IF2023

Increasing the accuracy of the national indigenous forest map was a necessary step to increase the fidelity and reduce the uncertainty of the water use extractions. At the time of this report, 56% of the indigenous forest has been edited and 47% quality controlled, providing a sufficiently large proportion (10% per class) of “pure” ET pixels (Section 2.3) per forest type for extracting water use (ET) and environmental variables (e.g. terrain and climate).

3.3.3 Indigenous forest type classification

Phase 1.3 involved the classification of the *Indigenous Forest* objects in the IF2023 product into individual forest types using proximity analysis to the forest types in the IF2021. The following methods were considered:

1. Where *Indigenous Forest* objects intersected an IF2021 forest type.
2. Where *Indigenous Forest* objects were compared to only the closest IF2021 forest type.
3. Where *Indigenous Forest* objects were compared to a ratio between the first and second closest IF2021 forest types.

The first method was found to spatially limit the classification of the forest types, while the second method resulted in the “straight line” anomalies in areas of previously unclassified indigenous forest, as shown in a previous report (Deliverable 4). The third method provided a balance between the first two methods. The distances from the aggregated objects to the closest and second closest forest type polygons in the IF2021 dataset were calculated for each IF object and calculated as a ratio. *Indigenous forest* objects in closer proximity to the IF2021 (ratio ≤ 1) were labelled as *Forest type*, while objects

further away (ratio > 0.1) were labelled as *Uncertain* for further validation. Figure 3-26 and Figure 3-27 show examples of these classifications, referred to as the IF2024, compared against the IF2021.

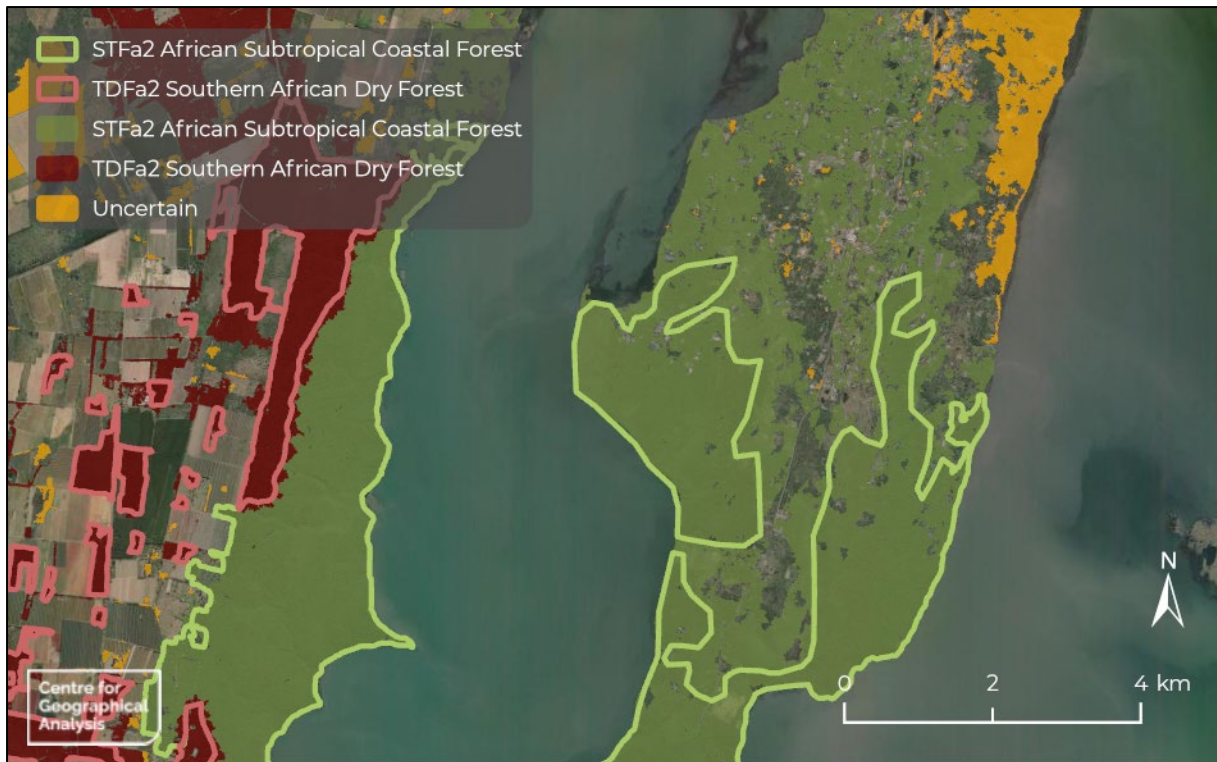


Figure 3-26 *Indigenous Forest and Uncertain IF2024 classes (solid fill) compared to the IF2021 near Hluhluwe, KwaZulu-Natal*

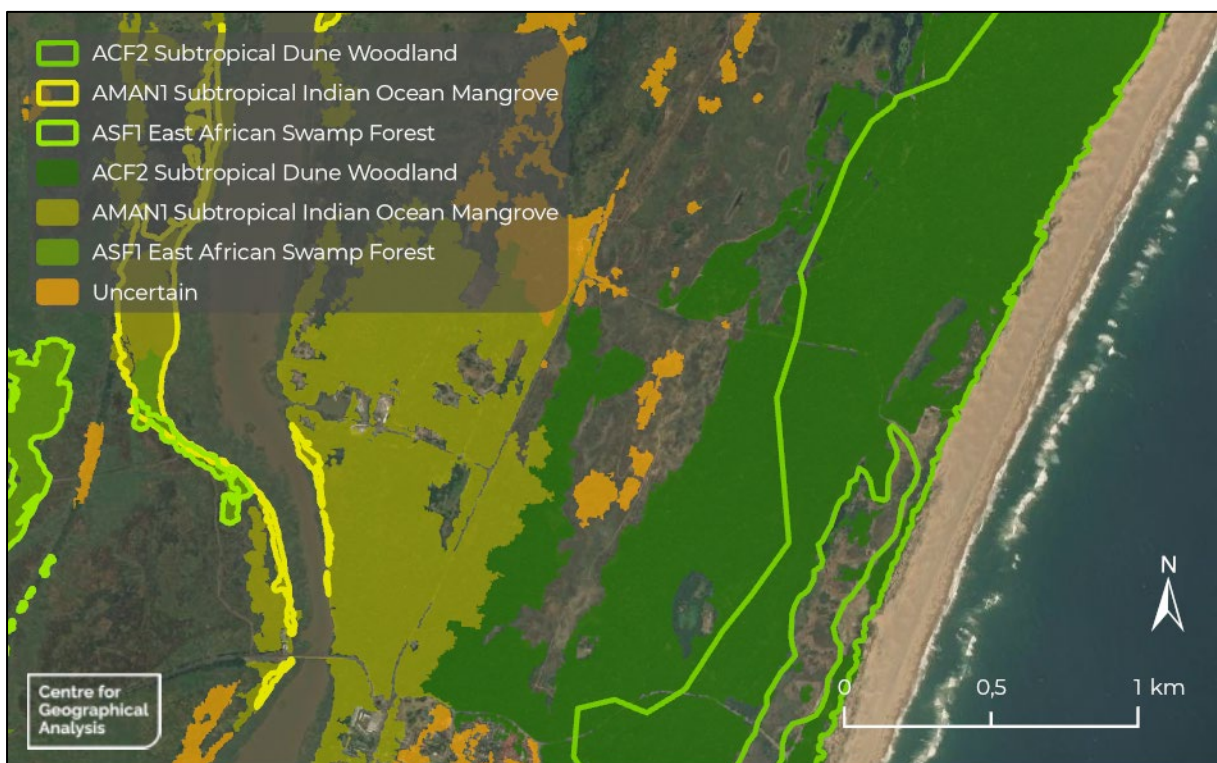


Figure 3-27 *Indigenous Forest and Uncertain IF2024 classes (solid fill) compared to the IF2021 near St Lucia, KwaZulu-Natal*

3.3.4 Validation of forest type classification

As demonstrated in the previous section, automated forest type labelling using proximity analysis is not foolproof, especially in complex regions where multiple forest types occur or which are located very far away from existing labelled forest types (IF2021). Prof Ladislav Mucina was tasked to check all labelled forest type polygons, with a particular focus on the polygons for which the forest type classification was *Uncertain*.

In order to facilitate this, ArcGIS Online (www.arcgis.com) was used to develop a web application ([IF WebApp](#)) through which the indigenous forest mapping results can be easily scrutinised. The web app shows the IF2021 *Indigenous Forest* polygons with red outlines and predefined colours to show the different forest types of the manually corrected and classified IF2024 (Figure 3-28). The polygons are overlain onto recent very high-resolution satellite imagery to assist with the validation¹³. Users of the web app can navigate (zoom and pan) through the map and toggle layers on and off. Users can also easily modify a polygon's classification, subdivide polygons using the cut tool and add new polygons using the digitising tool.



Figure 3-28 Web application showing IF2021 (red) and IF024 forest type polygons (predefined colours)

In Figure 3-29 a polygon that was incorrectly assigned to the African Subtropical Coastal Forest is reclassified to the Southern African Dry Forest class. The *Edit* tool also allows the user to cut, merge and reshape features.

¹³ Using recent satellite imagery also served to correct errors that may have occurred due to deforestation since 2016-2017 when the aerial photography used in the KBIC was acquired.

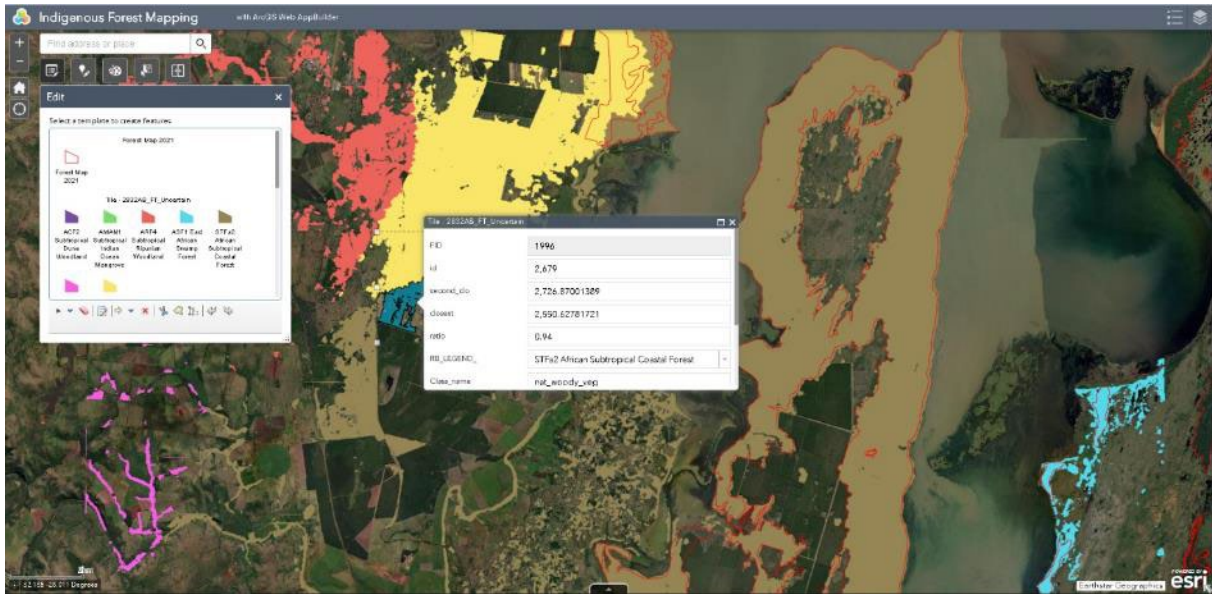


Figure 3-29 Functionality on the web application allowing for polygons to be reclassified

In Figure 3-30, the *Select* tool is used to select a polygon to check the attributes for that polygon. For instance, the editor might be interested in the ratio attribute which indicates how far the closest and second closest IF2021 polygon is to the selected polygon.



Figure 3-30 Functionality on the web application allowing users to select polygons and view their attributes

Figure 3-31 demonstrates how the *Swipe* tool can be used to study the underlying satellite imagery to validate the *Indigenous Forest* class.

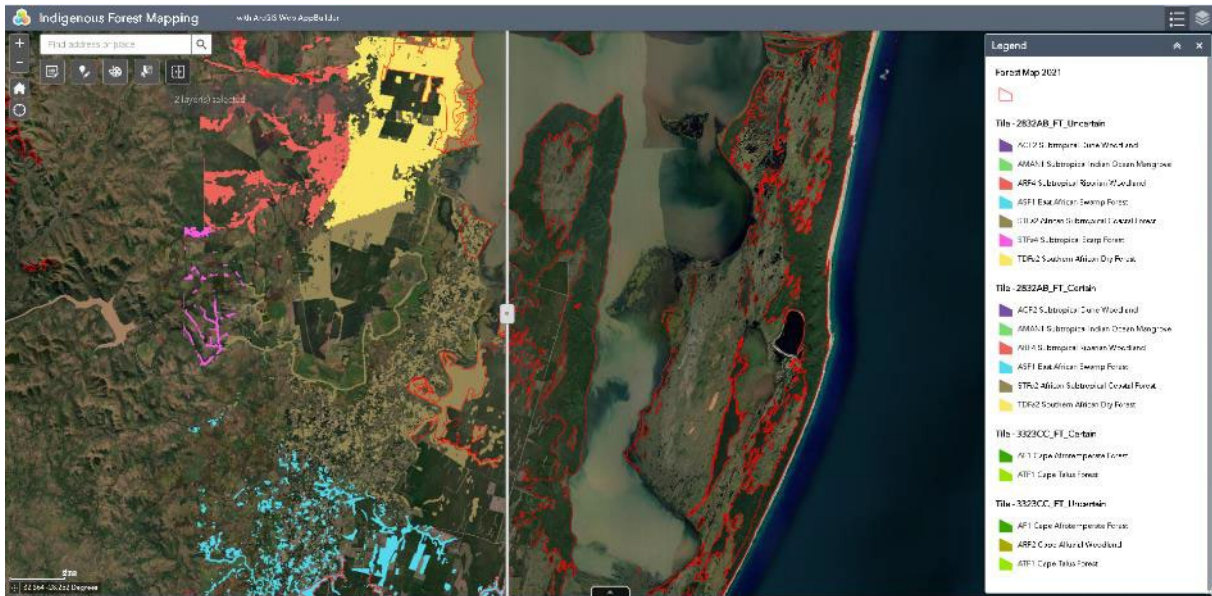


Figure 3-31 Functionality on the web application allowing users to swipe the classified feature classes to see the aerial image below

Due to the time required for validation (some validations will require field visits – not within the scope of this project), the forest type validation process will likely continue beyond the end of this project. However, this did not impact the water use quantification to any great degree, as sufficient coverage of each of the forest types was ensured to allow for meaningful statistical analysis (Section 3.4.2).

3.4 Indigenous forests water use analyses

Phase 2 of this research involved the quantification and analysis of water use of indigenous forest types and explaining evapotranspiration variations within different environments. This was undertaken by extracting actual ET per forest type for 24 different terrain, soil and climate variables (Phase 2.1), comparing water use quantifications within the context of field measurements (Phase 2.2) and analysing the differences in water use per forest type (Phase 2.3). The following sections provide more detail on the environmental variable assessment and preparation, as well as the water use calculation methodology.

3.4.1 Environmental variable selection and preparation

The 24 readily available climatic, terrain and soil variables assessed in this research are shown in Table 3-2. All terrain indices other than morphology were sourced from the Stellenbosch University Digital Elevation Model (SUDEM) developed by Van Niekerk (2016). The long-term climate variables, as well as the terrain morphological units, were sourced from the South African Atlas of Agrohydrology and Climatology (Schulze, 2007). Soil data was sourced from the Land types of South Africa: Digital map (1:250 000 scale) and soil inventory dataset, developed by the Agricultural Research Council: Institute for Soil, Climate and Water (Agricultural Research Council, 2010).

Table 3-2 A list of variables considered in the analysis and a reference to the variable source

Type	Variable	Description	Source
Terrain	Elevation (m)	Height above mean sea level (m)	Van Niekerk (2016)
	Slope gradient (degrees)	Elevation divided by pixel size, expressed in degrees	Van Niekerk (2016)
	Slope aspect	Mean downslope cardinal direction (deg)	Van Niekerk (2016)
	Terrain morphology	Terrain classification based on slope form, relief, drainage density, stream frequency and percent area with slopes < 3 degrees	Schulze (2007)
	Topographic Wetness Index	Areas prone to water accumulation or drainage based on slope and upstream contributing area	Van Niekerk (2016)
	Flow accumulation	Cumulative sum of flow entering each cell in a drainage network	Van Niekerk (2016)
	Topographic negative openness	Measure of topographic concave features in the landscape	Van Niekerk (2016)
	Topographic positive openness	Measure of topographic convex features in the landscape	Van Niekerk (2016)
	Topographic Position Index	The difference between the elevation at a central point and the mean elevation within a predetermined neighbourhood	Van Niekerk (2016)
Soil	Soil depth	Soil depth (mm)	ARC-ISCW (2010)
	Soil clay	Percent of clay content in soil (%)	ARC-ISCW (2010)
Climate	Mean annual rainfall	Long-term mean of cumulative annual rainfall (mm)	Schulze (2007)
	Mean annual temperature	Long-term mean of mean annual temperature (deg C)	Schulze (2007)
	Mean temperature in February	Long-term mean of mean temperature in February (deg C)	Schulze (2007)
	Mean temperature in July	Long-term mean of mean temperature in July (deg C)	Schulze (2007)
	Climate zones	Climate classification system based on long-term median monthly rainfall and temperatures, developed by Köppen (1931)	Schulze (2007)
	Rainfall seasonality	Predominant rainfall season, based on long-term rainfall peak concentrations.	Schulze (2007)
	Annual solar radiation	Long-term annual mean of mean daily solar radiation (ave daily MJ/m ² /day)	Schulze (2007)
	Solar radiation for February	Long-term monthly mean of daily solar radiation in February (MJ/m ² /day)	Schulze (2007)
	Solar radiation for July	Long-term monthly mean of daily solar radiation in February (MJ/m ² /day)	Schulze (2007)
	Annual relative humidity	Ratio of water vapour present in the air and maximum at a specific temperature, as a percentage. Long-term annual mean.	Schulze (2007)
	Vapour Pressure Deficit February	Difference between the actual water vapour pressure and vapour pressure saturation point at a specific temperature. Long-term mean for the month of February (kPa)	Schulze (2007)
	Vapour Pressure Deficit July	Difference between the actual water vapour pressure and vapour pressure saturation point at a specific temperature. Long-term mean for the month of July (kPa)	Schulze (2007)
	Heat units	Long-term mean of accumulated days per year within specified maximum and minimum temperature thresholds (degree days)	Schulze (2007)

Although this set of variables is comprehensive, in many cases they represent long-term mean values and at coarse resolution and may thus not necessarily represent the full set of factors (e.g. canopy structure, species diversity, seasonality, age) regulating or impacting ET.

The water use per forest type analysis required nominal categories rather than quantitative variables. Continuous environmental variables were reclassified into categories (e.g. low, medium, high) using quantile analysis, which divides a dataset into segments of equal probability or frequency. Quantiles were determined according to the range of a given variable on a national scale (e.g. 0-3478 m for elevation). Variables with existing nominal classes were retained as is, with the exception of terrain morphology, which was simplified as per Table 3-3.

Table 3-3 Reclassified terrain morphology units

Original units	Reclassified units
Dune hills with parallel crests and lowlands Extremely irregular plains Moderately undulating plains Plains Slightly undulating plains Plains and pans Slightly irregular plains Slightly irregular plains and pans Slightly irregular undulating plains (some hills) Slightly undulating plains and pans	Plains/flat
Highly dissected hills Hills Hills and lowlands Strongly undulating irregular land Undulating hills Undulating hills and lowlands irregular undulating lowlands and hills Lowlands and hills Lowlands and parallel hills Parallel hills Parallel hills and lowlands	Hilly/undulated
High mountains Highly dissected low undulating mountains Low mountains Table-lands Lowlands with mountains Mountains and lowlands Undulating mountains and lowlands	Mountainous

The reclassification of the terrain, soil and climate environmental variables applied to the water use calculations is shown in Table 3-4.

Table 3-4 Reclassification of terrain variables

Type	Variable	Classification
Terrain	Elevation (m)	Low: (0-881) Medium: (881-1224) High: (1224-3478)
	Slope gradient (degrees)	Level/gently inclined (0-5.7) Moderately inclined/steep (5.7-29.3) Very steep (29.3-88.2)
	Slope aspect	North; North-East; East; South-East; South; South-West; West; North-West
	Terrain morphology	Plains/flat Hilly/undulated Mountainous
	Topographic Wetness Index	Low: (1.37-7.17) Medium: (7.17-8.50) High: (8.50-39.0)
	Flow accumulation	Low: (0-1) Medium: (1-1224) High: (1224-103964)
	Topographic negative openness	Low: (0.00-1.22) Medium: (1.22-1.48) High: (1.48-1.72)
	Topographic positive openness	Low: (0.00-1.28) Medium: (1.28-1.50) High: (1.50-1.75)
	Topographic Position Index	Low: (-1997 – -5.37) Medium: (-5.37 – -1.87) High: (-1.87 – 1510)
Soil	Soil depth (mm)	Low: (0-331) Medium: (331-584) High: (584-1320)
	Soil clay (%)	Low: (0.0-10.2) Medium: (10.2-17.7) High: (17.7-61.7)
Climate	Mean annual rainfall (mm)	Low (< 600) Medium (600-800) High (800-1 000) Very high (> 1 000)
	Mean annual temperature (deg C)	Low: (6.0-16.6) Medium: (16.6-18.6) High: (18.6-25.0)
	Mean temperature in Feb (deg C)	Low: (9.9-21.6) Medium: (21.6-23.8) High: (23.8-29.1)
	Mean temperature in Jul (deg C)	Low: (1.70-9.8) Medium: (9.8-11.9) High: (11.9-18.8)
	Climate zones (Köppen)	Arid, hot and dry (BWh) Arid, cool and dry (BWk) Semi-arid, hot and dry (BSh) Semi-arid, cool and dry (BSk) Summers long, dry and cool (Csb) Summers long, dry and hot (Csa) Wet all seasons, summers long and hot (Cfa) Wet all seasons, summers long and cool (Cfb) Winter long, dry and hot (Cwa) Winter long, dry and cool (Cwb) Tropical wet, dry and winter season (Aw)
	Rainfall seasonality	All year Winter Early summer Mid-summer Late summer Very late summer

Table continued from previous page

	Mean annual solar radiation (ave daily MJ/m ² /day)	Low: (101-221) Medium: (221-235) High: (235-264)
	Solar radiation for Feb (ave daily MJ/m ² /day)	Low: (7.4-22.1) Medium: (22.1-23.8) High: (23.8-28.1)
	Solar radiation for Jul (ave daily MJ/m ² /day)	Low: (6.4-12.1) Medium: (12.1-13.7) High: (13.7-16.4)
	Mean annual relative humidity (%)	Low: (42.5-55.2) Medium: (55.2-63.5) High: (63.5-93.2)
	Mean Vapour Pressure Deficit Feb (kPa)	Low: (-0.57 – 0.83) Medium: (0.83-1.30) High: (1.30-2.60)
	Mean Vapour Pressure Deficit Jul (kPa)	Low: (-0.15 – 0.47) Medium: (0.47-0.63) High: (0.63-1.20)
	Total Heat units (degree days)	Low: (128-2483) Medium: (2483-3156) High: (3156-5174)

3.4.2 Water use data extraction

The Level 1 (v2) monthly ET WaPOR rasters from January 2009 to June 2023 served as the primary data for water use calculations undertaken in this study (see Section 2.3). To extract the data, the centroids of each 250 m ET WaPOR pixel were converted to a point grid. This was intersected with each forest type polygon to clip the points to areas of indigenous forest and acquire the forest types for each point. A “sample by point” algorithm was then implemented on the 174 monthly rasters to acquire the ET time series values for each forest type point. Van Niekerk *et al.* (2023) found that the mixed pixel effects resulting from this method are minimised to the point of being negligible to the overall results, and the assumption was made that it will be the case for this study.

3.5 Multivariate machine learning analyses

Machine learning (Section 2.5.2) is frequently used in RS applications to map land cover. Supervised classification (Section 2.5.2.2) is an empirical approach for mapping large areas using remotely sensed data as input. However, machine learning is also useful to gain a deeper understanding of the complex relationships among many variables, as is the case in this project. In this study, we used RF classification and regression to gain a better understanding of how environmental conditions (represented by the environmental variables collected in Section 3.4.1) affect:

1. The water use of indigenous forests; and
2. The occurrence (location) of forest types.

In the first set of experiments, RF regression was used to “model” forest water use. The purpose of this analysis was not to predict water use, but rather to identify how strongly the environmental variables contribute to (or explain) the water use of forests.

Although the water use of indigenous forests was the focus of the project, the production of a highly detailed and accurate indigenous forest map (Section 3.3) and the development of a set of analysis-ready environmental datasets (Section 3.4.1) opens many other avenues for research. For instance, the data can be analysed to gain a deeper understanding of the environmental profiles and drivers of different forest types. Annual mean ET was set as the target variable, while all the environmental variables were set as predictor variables. The resulting model's accuracy was assessed using R-squared (R^2) and root mean square error (RMSE) values. R^2 is a measure for the percentage of variance of the dependent variable that the independent variables are able to explain (a higher value indicates a better fit). RMSE is a metric that provides the average difference between predicted and actual values (the lower the value, the more accurate the predictions). A secondary output of RF regression is a list of variables that contributed most to the model. This ranking is calculated by measuring the decrease in model performance when a specific environmental variable is randomly removed (see Section 2.5.2.2 for an explanation of how the RF model uses out-of-bag sets of data in the process of model building and testing). The ranking of variables, also called the variable importance list (VIL), is very useful because it identifies the "drivers" of the target variable (annual mean ET in our case). It can also be used to eliminate variables for further consideration. However, the VIL does not take collinearity among variables into account. For instance, two variables that are highly correlated (contain the same information) may both be ranked highly. Consequently, it is advisable to consider the collinearity of variables in the interpretation of the table. A correlation matrix is usually employed for this purpose, whereby all except one of the highly correlated variables can effectively be ignored. The regression modelling results, VIL and correlation matrix are discussed in Section 4.2.2.

Although compositional and ecological analyses of indigenous forests were not within the scope of this project, the potential of the rich set of data that was collated and generated in this project is ideal for such research. To demonstrate, RF classification was applied to model the distribution of forest types, with the locations of forest types set as the target variable and the full list of environmental variables (Section 3.4.1) used as predictor variables. In other words, a machine learning model was built to predict where different indigenous forest types will occur, using only environmental characteristics (as represented by the selected variables) as input. It is important to note that the model only considers areas where indigenous forests are located, i.e. it does not differentiate indigenous forests from other land cover/uses. The accuracy was quantified using 10-fold cross-validation. This divides the training set into ten subsets, of which nine are used to train the model, and the remaining are used for testing. This process is iterated until all ten subsets have been used for testing. The mean of the ten accuracies is then used for the overall model performance. The model used 76 682 samples, of which roughly 7 670 were used for testing, and roughly 69 010 were used for training during each of the ten iterations. The results of the classification are reported in Section 4.1.2.

4 RESULTS AND DISCUSSIONS

4.1 Forest types

4.1.1 Extent (coverage) per forest type

Table 4-1 summarises the areas mapped, refined and classified for each forest type in the IF2024 compared to the total area found in the IF2021.

Table 4-1 Forest type area classified in IF2024 and total area of IF2021

Forest type	Code	IF2024 area (km ²)	IF2021 area (km ²)
Cape Milkwood Woodland	ACF1	40.9	24.7
Subtropical Dune Woodland	ACF2	181.6	273.9
Subtropical Indian Ocean Mangrove	AMAN1	39.8	25.8
Tropical Indian Ocean Mangrove	AMAN2	2.00	0.7
Arid Zone Riparian Woodland	ARF1	31.8	171.6
Cape Alluvial Woodland	ARF2	24.0	70.3
Highland Alluvial Woodland	ARF3	10.1	29.6
Subtropical Riparian Woodland	ARF4	56.9	199.3
East African Swamp Forest	ASF1	115.2	80.7
Cape Talus Forest	ATF1	132.1	228.5
Bushveld Talus Forest	ATF3	16.2	48.7
Drakensberg Afrotropical Forest	ATF4	49.1	71.4
Northern Highveld Afrotropical Forest	ATF5	36.6	220.8
Cape Afrotropical Forest	AF1	216.8	550.3
Southern Mistbelt Forest	AF2	1098.9	1011.7
Northern Mistbelt Forest	AF3	85.1	422.4
African Subtropical Coastal Forest	STFa2	447.0	282.5
Subtropical Scarp Forest	STFa4	1496.3	1027.3
Albany Coastal Forest	STFa5	133.9	117.4
Southern African Dry Forest	TDFa2	623.1	535.5
Southern African Dry Thicket	TDFa3	51.4	280.2
Total		4888.6	5673.2

Southern Mistbelt Forest (AF2) and Subtropical Scarp Forest (STFa4) cover the largest areas, comprising 53.2% of the forest types mapped. Tropical Indian Ocean Mangrove (AMAN2) covered the smallest area: 2 km² (0.07% of total forest cover). In certain cases, such as Cape Afrotropical Forest and Northern Mistbelt Forest, the IF2024 mapped area is smaller than in IF2021, reflecting the non-exhaustive nature of the mapping project. Conversely, the African Subtropical Forest and Subtropical Scarp Forest (which were mapped almost to completion) show a larger area mapped in the IF2024 compared to the IF2021. This is either due to the IF2024 mapping overestimating indigenous forest coverage, i.e. “erring on the side of caution”, or due to misclassifications or missed indigenous forest in the IF2021.

4.1.2 Modelling forest types using machine learning

The RF classification, modelling the environmental drivers of forest type (Section 3.5) produced an overall classification accuracy of 85.3%. This is remarkably high considering that there are 21 forest types. The environmental VIL is shown in Table 4-2. However, the VIL does not take collinearity among variables into account. For instance, two variables that are highly correlated (contain the same information) may both be ranked highly on the list. Consequently, it is advisable to consider the

collinearity of variables in the interpretation of the table. A correlation matrix (Figure 4-1) was produced for this purpose.

Table 4-2 Environmental variable importance for classifying forest types

Rank	Environmental variable	Feature importance (%)
1	Mean temperature in Jul (deg C)	9.3
2	Heat units (degree days)	9.2
3	Terrain morphology	9.0
4	Mean annual temperature (deg C)	8.4
5	Soil clay (%)	7.1
6	Mean temperature in Feb (deg C)	7.0
7	Vapour Pressure Deficit Jul (kPa)	6.8
8	Annual relative humidity (%)	5.8
9	Solar radiation for Jul (ave daily MJ/m ² /day)	5.3
10	Annual solar radiation (ave daily MJ/m ² /day)	5.1
11	Vapour Pressure Deficit Feb (kPa)	4.5
12	Soil depth (mm)	3.8
13	Solar radiation for Feb (ave daily MJ/m ² /day)	3.5
14	Mean annual rainfall (mm)	3.0
15	Rainfall seasonality	2.8
16	Elevation	2.6
17	Climate zones (Köppen)	2.6
18	Topographic positive openness	1.5
19	Topographic negative openness	1.2
20	Slope gradient	0.9
21	Topographic Wetness Index	0.3
22	Topographic Position Index	0.3
23	Slope aspect	0.2
24	Flow accumulation	0.2

Based on the variables included in the modelling, the strongest environmental driver is mean temperature in July (9.3%), closely followed by heat units (9.2%), terrain morphology (9.0%), and mean annual temperature (8.4%), apart from terrain morphology the strongest drivers underline the importance of temperature-related factors in the occurrence of forest types. However, all three of these temperature-related variables are highly correlated ($R^2 \geq 0.95$), which means that excluding two of these variables from the classification will likely produce similar results (a separate experiment that excludes heat units and annual temperature was carried out to test this hypothesis and the resulting model's accuracy was 85.4%). Vapour pressure deficit in July (6.8%) is also an important driver of forest types, but this variable is also strongly related ($R^2 \geq 0.84$) with the above-mentioned variables. Although winter (July) solar radiation is ranked ninth, it is poorly correlated with other (non-solar radiation-based) variables, which suggests that solar radiation is also a noteworthy driver of forest types. The fact that annual and summer (February) solar radiation is also ranked within the top 13 most important variables supports this observation.

Terrain morphology (9.0%) was the third most important variable in the modelling of forest types, demonstrating the close relationship between terrain and forest types (Mucina, 2018). Surprisingly, elevation, slope gradient and slope aspect were not as important as morphology. This is likely because morphology is a combination of these terrain variables.

Both soil-related variables, namely soil clay percentage (7.1%) and soil depth (3.8%), are listed in the

top 12 variables, suggesting that soil-related factors play an important role in the location of different forest types.

Although variables such as mean annual rainfall (3%), rainfall seasonality (2.8%) and climate zones (2.6%) are ranked low, they are not strongly correlated to each other and any other important variables. As such, they are likely contributing factors to differentiate among forest types.

	Climate Zone	Heat Units	Mean Rain Annual	Rainfall Seasonality	Rel Humidity Annual	Soil Clay	Soil Depth	Sol Rad Annual	Sol Rad Feb	Sol Rad July	Aspect	Flow Accumulation	Slope Degrees	Temp Mean	Temp Mean Feb	Temp Mean July	Terrain Morphology	TNO	TPO	TPI	TWI	VPD Feb	VPD July	Elevation
Climate Zone	1.00																							
Heat Units	0.00	1.00																						
Mean Rain Annual	0.29	-0.07	1.00																					
Rainfall Seasonality	0.14	0.08	0.34	1.00																				
Rel Humidity Annual	0.12	-0.44	0.54	0.02	1.00																			
Soil Clay	0.16	-0.50	0.43	0.40	0.31	1.00																		
Soil Depth	0.07	0.61	-0.17	0.03	-0.38	-0.53	1.00																	
Sol Rad Annual	0.09	-0.01	-0.28	0.13	-0.68	-0.01	0.26	1.00																
Sol Rad Feb	0.00	-0.21	-0.36	-0.10	-0.60	-0.06	0.13	0.91	1.00															
Sol Rad July	0.20	0.48	-0.02	0.41	-0.60	-0.05	0.46	0.74	0.42	1.00														
Aspect	-0.02	0.01	-0.02	0.01	-0.02	-0.01	0.03	0.03	0.03	0.02	1.00													
Flow Accumulation	0.01	-0.07	0.03	0.01	0.02	0.06	-0.05	0.02	0.02	0.00	-0.02	1.00												
Slope Degrees	0.05	-0.48	0.23	-0.03	0.34	0.41	-0.55	-0.12	-0.05	-0.25	0.04	-0.06	1.00											
Temp Mean	-0.01	1.00	-0.06	0.07	-0.43	-0.49	0.60	-0.03	-0.22	0.46	0.00	-0.07	-0.47	1.00										
Temp Mean Feb	-0.04	0.98	-0.15	0.02	-0.53	-0.54	0.61	0.08	-0.07	0.49	0.01	-0.06	-0.49	0.98	1.00									
Temp Mean July	0.00	0.95	0.04	0.06	-0.22	-0.44	0.50	-0.30	-0.46	0.25	0.00	-0.07	-0.41	0.95	0.90	1.00								
Terrain Morphology	-0.08	-0.64	0.29	0.05	0.49	0.61	-0.72	-0.29	-0.21	-0.41	-0.01	0.06	0.58	-0.63	-0.67	-0.50	1.00							
TNO	-0.04	0.49	-0.21	0.05	-0.35	-0.40	0.54	0.12	0.05	0.27	-0.02	0.07	-0.83	0.49	0.50	0.42	-0.56	1.00						
TPO	-0.04	0.52	-0.24	0.03	-0.35	-0.45	0.60	0.13	0.06	0.27	-0.02	-0.08	-0.79	0.51	0.53	0.44	-0.65	0.54	1.00					
TPI	-0.01	0.05	-0.03	0.01	-0.03	-0.04	0.07	0.00	0.00	0.00	-0.01	-0.10	-0.03	0.05	0.05	0.05	-0.07	-0.27	0.37	1.00				
TWI	-0.02	0.24	-0.14	0.06	-0.27	-0.19	0.31	0.18	0.13	0.23	-0.03	0.39	-0.56	0.23	0.25	0.17	-0.32	0.59	0.28	-0.24	1.00			
VPD Feb	-0.11	0.77	-0.44	-0.08	-0.86	-0.55	0.57	0.46	0.39	0.54	0.02	-0.05	-0.49	0.76	0.85	0.58	-0.71	0.50	0.52	0.05	0.30	1.00		
VPD July	-0.03	0.90	-0.21	0.12	-0.67	-0.40	0.52	0.13	-0.06	0.53	0.01	-0.05	-0.43	0.90	0.89	0.84	-0.55	0.45	0.45	0.04	0.25	0.83	1.00	
Elevation	0.12	-0.52	0.08	0.18	0.19	0.37	-0.31	0.12	0.14	-0.06	-0.01	0.04	0.27	-0.52	-0.53	-0.51	0.33	-0.27	-0.28	-0.02	-0.12	-0.41	-0.43	1.00

Figure 4-1 Correlation among environmental variables

4.2 Forest water use

4.2.1 Water use per forest type

Table 4-3 shows that the highest mean annual ET was estimated for Subtropical Indian Ocean Mangrove (AMAN1) (1 312±304 mm/yr), followed by Cape Afrotropical Forest (AF1, 1 211±144 mm/yr). The lowest mean annual ET estimate was for Arid Zone Riparian Woodland (ARF1) (402±346 mm/yr). The ranges (minimum to maximum) in annual ET per forest type for all forest types are substantial. Minimum annual ET values below 100 mm/yr were estimated for Arid Zone Riparian Woodland and Cape Milkwood Woodland. Very high maximum annual ET values (>1 300 mm/yr) were estimated for all forest types, with maximum ET estimates for six forest types exceeding 2 000 mm/yr. These very high maximum annual ET estimates are ‘hidden’ in the mean and median values, and are deemed inaccurate (overestimation). These values are likely caused by WaPOR modelling inaccuracies and not physically possible and should be treated with caution. Although a previous study (Van Niekerk *et al.*, 2018) showed ET based on EO data from waterbodies in the range of 2 000 mm/yr, these values are most likely an overestimation of ET (evaporation from water bodies is not restricted by physiological

controls like transpiration from vegetative bodies). We suggest that, when interpreting Table 4-3, the median value be used instead of the mean as the former is less sensitive to outliers. It is likely that the median values may present an overestimation of annual ET in some cases.

Table 4-3 Evapotranspiration statistics per forest type for the period January 2009 to June 2023, as estimated using 250 m resolution WaPOR data

Forest Type	Code	# of 250x250 samples	Annual ET (mm)				
			Mean	Median	Min	Max	Std Dev
Cape Milkwood Woodland	ACF1	629	541	518	61	1611	184
Subtropical Dune Woodland	ACF2	2208	1071	1120	122	2257	314
Subtropical Indian Ocean Mangrove	AMAN1	599	1312	1338	224	2198	304
Tropical Indian Ocean Mangrove	AMAN2	32	1054	1131	309	1934	347
Arid Zone Riparian Woodland	ARF1	508	402	296	29	2106	346
Cape Alluvial Woodland	ARF2	384	1016	998	368	1717	251
Highland Alluvial Woodland	ARF3	161	501	476	149	1555	199
Subtropical Riparian Woodland	ARF4	815	1044	1055	178	1727	280
East African Swamp Forest	ASF1	1777	1181	1213	199	2163	279
Cape Talus Forest	ATF1	2114	1083	1106	360	1828	222
Bushveld Talus Forest	ATF3	259	927	918	539	1399	137
Drakensberg Afrotperate Forest	ATF4	785	754	749	308	1365	157
Northern Highveld Afrotperate Forest	ATF5	586	783	763	334	1373	181
Cape Afrotperate Forest	AF1	3454	1211	1224	428	1713	144
Southern Mistbelt Forest	AF2	17583	1174	1190	248	2004	293
Northern Mistbelt Forest	AF3	1361	1171	1199	275	1768	256
African Subtropical Coastal Forest	STFa2	7100	1145	1194	194	2204	283
Subtropical Scarp Forest	STFa4	23860	1033	1054	129	1913	237
Albany Coastal Forest	STFa5	2141	1025	1027	120	1742	175
Southern African Dry Forest	TDFa2	9671	1039	1049	239	1689	195
Southern African Dry Thicket	TDFa3	667	1142	1153	443	1775	188
Total / Average		76694		989			

Table 4-3 also shows the number of samples (250x250 pixels) that were used to calculate the mean, median and standard deviation of ET per forest type. Except for Tropical Indian Ocean Mangrove (AMAN2), which in South Africa has a limited coverage (very small area in Kosi Bay), all other forest types were represented by a minimum of 150 samples. The limited number of samples in certain instances also contributes to uncertainties in the ET (specifically mean and median) that represent the water use of entire forest type classes. Figure 4-3 shows histograms (data distribution) of the annual ET for each forest type, highlighting the skewed water use distribution for some forest types.

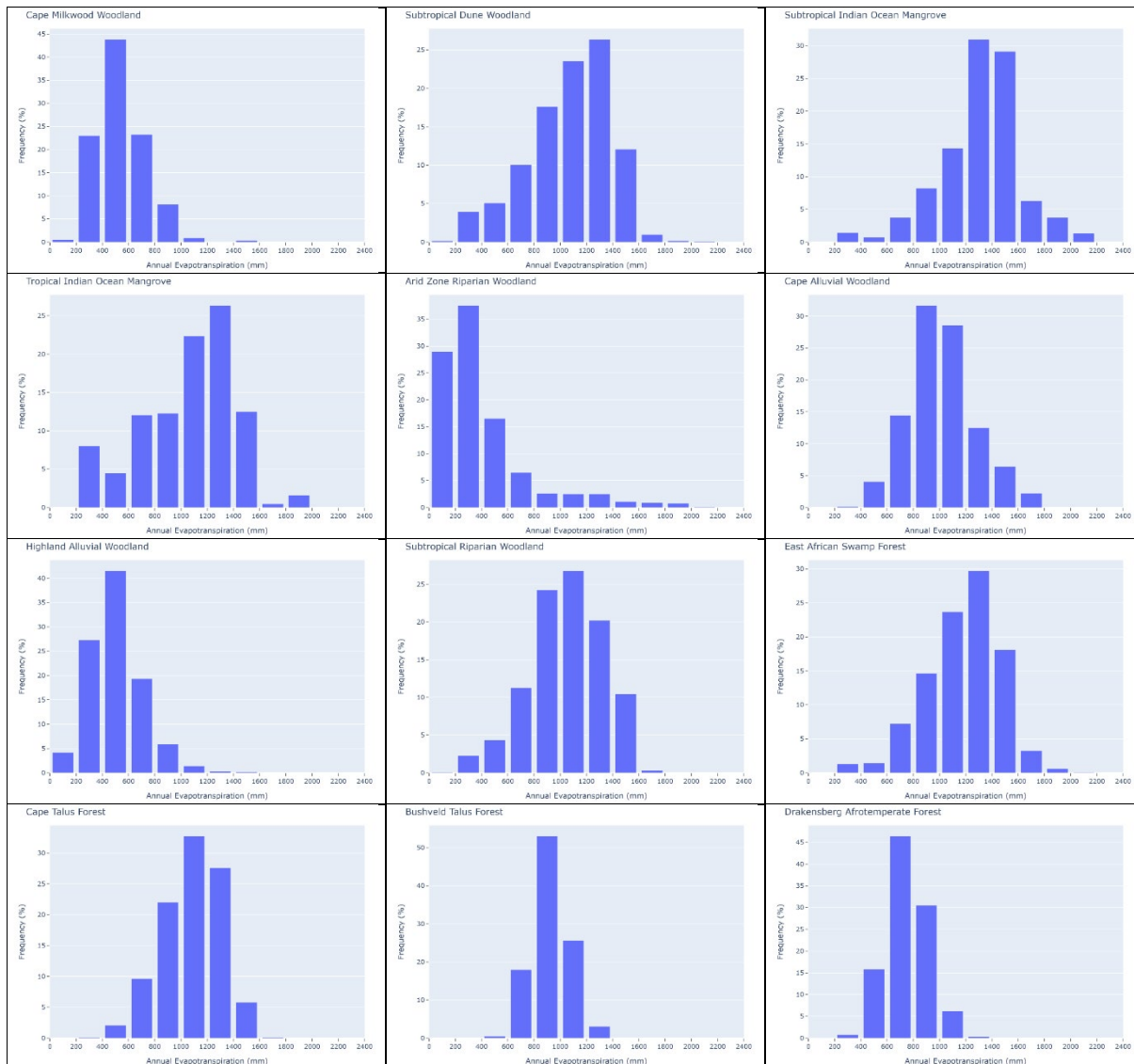


Figure 4-2 Histograms showing the frequency distribution of ET for a subset of forest types (subset A), with the frequency (Y-axis) showing the percentage of pixels per range of annual ET (X-axis)

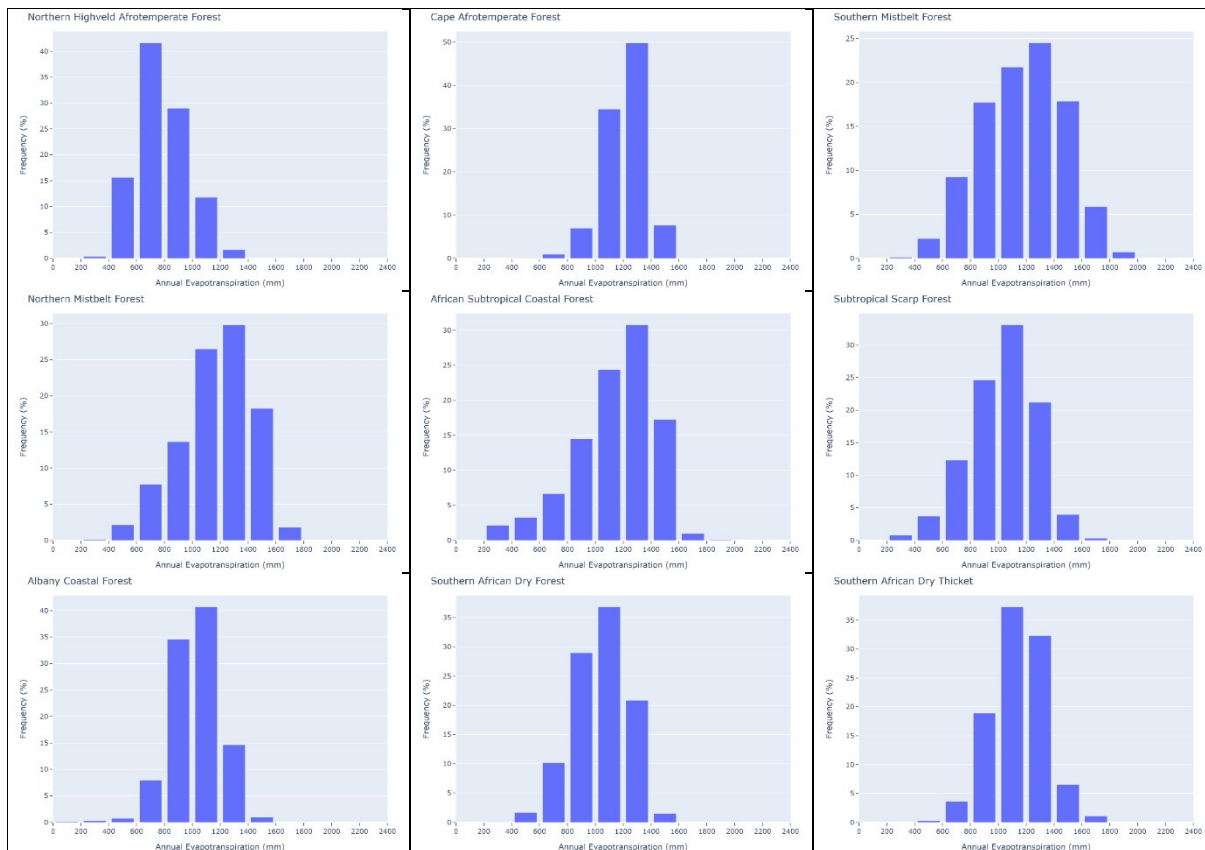


Figure 4-3 Histograms showing the frequency distribution of ET for a subset of forest types (subset B), with the frequency (Y-axis) showing the percentage of pixels per range of annual ET (X-axis)

Figure 4-4 and Figure 4-5 show the monthly ET from 2009 to 2023 as well as the average ET trend (3rd order polynomial function) for zonal and azonal forest types, respectively. Monthly ET estimates ranged between minimum values of <25 and maxima's of >160 mm for zonal forest types and between <10 and 150 mm/month for azonal forest types. The ET trend lines over the 12-year period were within a small range for all the zonal forest types. The small variation in the monthly ET over time, even during the drought period of 2015-2018, is in stark contrast to the findings by Van Niekerk *et al.* (2023), which showed that the water use of commercial forest genera (*Pinus*, *Eucalyptus* and *Acacia*) was noticeably reduced during the 2015-2018 drought. The Van Niekerk *et al.* (2023) water use estimations represented homogeneous, even-aged single-genus plantations, which contrast greatly with the indigenous forests considered in this study; these forests are heterogeneous in structure, age and species. It is likely that indigenous forests have adapted to local conditions and are, as such, likely less sensitive to extreme conditions such as droughts.

Figure 4-4 and Figure 4-5 indicate that the difference in monthly ET among the azonal forest types is substantially larger than that of zonal forest types, but there are small interannual differences. This likely reflects the species and age diversity of indigenous forests, but our limited understanding of ET dynamics of these vegetation types(s) makes interpreting the results difficult. Individual water use profiles (graphs) per forest type are included in Appendix IV.

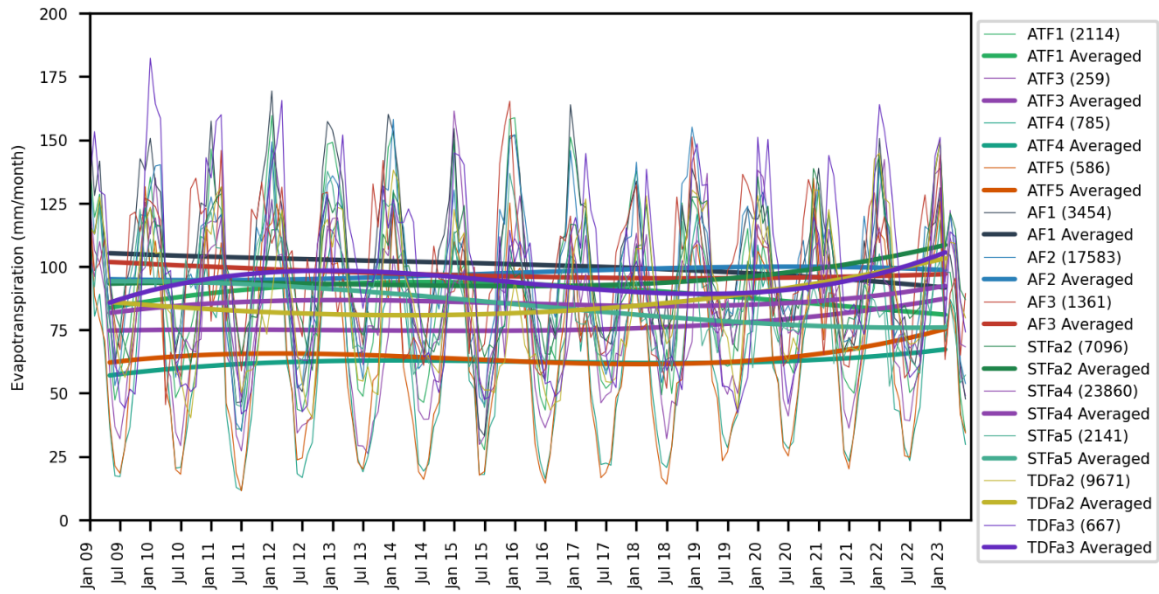


Figure 4-4 Monthly mean ET per forest type for zonal forest types for the period 2009 to 2023.

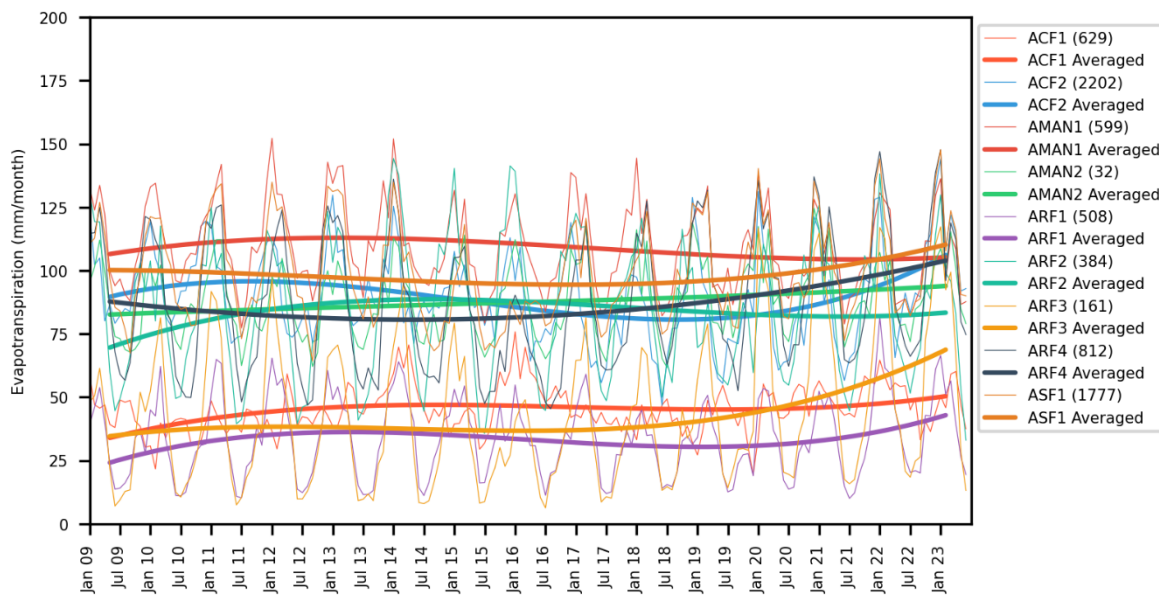


Figure 4-5 Monthly mean ET per forest type for azonal forest types for the period 2009 to 2023

4.2.2 Drivers of forest water use

RF regression modelling was used to identify the main environmental drivers of water use based on the climatic, terrain and soil variables (Table 3-2) that were considered. Mean annual ET was set as the target variable, while the long-term mean climatic and environmental variables considered were used as predictor variables. The resulting model is very strong ($R^2 = 0.98$) and predicted forest water use to an accuracy (RMSE) of 235 mm/yr. This strong model was unexpected and demonstrates the strong

relationship between water use and environmental conditions when all indigenous forest types are considered. For this modelling, indigenous forests were considered as one class, so the model does not distinguish between forest types.

Based on the VIL (Table 4-4), the strongest driver of indigenous forest water use is long-term mean annual rainfall, followed closely by summer solar radiation (February) and heat units. None of these variables are strongly collinear ($R^2 < 0.4$) (Figure 4-1), which indicates that each of these variables is individually important. The fourth most important variable in the model is winter solar radiation (July), which is only moderately ($R^2 = 0.42$) correlated to summer (February) solar radiation, indicating that winter solar radiation is an important factor in water use. Soil depth and clay content are both listed within the top ten variables, confirming that soil conditions are important drivers of forest water use. The most important terrain-based variable is terrain morphology, followed closely by topographic positive openness (TPO), elevation and topographic negative openness (TNO).

Table 4-4 Most important variables for mean annual ET identified by random forest regression modelling

Rank	Variable	Importance
1	Mean Annual Rainfall	12.68
2	Solar Radiation February	12.62
3	Heat Units	11.16
4	Solar Radiation July	10.83
5	Soil Clay	5.13
6	Vapour Pressure Deficit July	4.44
7	Soil Depth	4.22
8	Terrain Morphology	4.11
9	Topographic Openness (+)	3.75
10	Elevation	3.68
11	Topographic Openness (-)	3.42
12	Annual Solar Radiation	3.37
13	Mean Annual Relative Humidity	3.30
14	Slope gradient	2.48
15	Vapour Pressure Deficit February	2.38
16	Temperature Mean July	2.35
17	Topographic Position Index	2.29
18	Topographic Wetness Index	1.80
19	Aspect	1.54
20	Rainfall Seasonality	1.32
21	Temperature Mean February	1.30
22	Flow Accumulation	1.01
23	Climate Zone	0.43
24	Mean Annual Temperature	0.39

The RF regression modelling was used to inform which variables should be studied in greater depth. In the following subsections, the impact of the most important climatic, terrain and soil variables on indigenous forest water use is scrutinised. Data on the other variables are included in Appendix IV.

4.2.3 Water use of indigenous forests and climate

The impact of climatic conditions, such as temperature and rainfall, on the water use of plants is well-known (Campbell & Norman, 2000) and there are many climatic characteristics that can potentially affect forest water use. In this study, a total of 13 such variables were considered and analysed. For

the sake of brevity, the results of only the five most important climate variables (as determined by the machine learning analysis, Section 4.2.2) are included in this section. The data relating to the other eight variables can be found in Appendix IV.

4.2.3.1 Mean annual rainfall

Mean long-term annual rainfall was identified as the most important driver of forest water use (Table 4-4). Fitting a regression model (2nd order polynomial) to long-term mean rainfall and mean annual ET data (Figure 4-6), shows a weak relationship ($R^2=0.05$). This suggests a complex link between ET and rainfall, but the fact that long-term mean rainfall data were used rather than rainfall from the corresponding study period may also have contributed to this weak model. We acknowledge that it is difficult to analyse these complex relationships using univariate statistical techniques such as correlation and regression. The RF machine learning algorithm was, however, able to exploit this complex relationship.

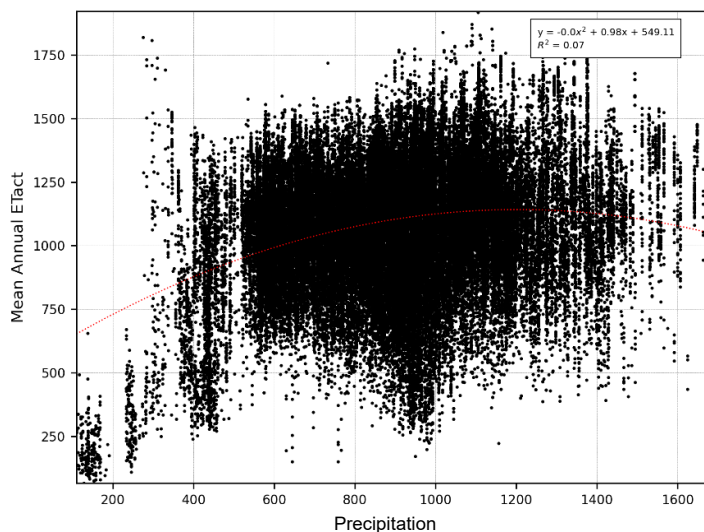


Figure 4-6 Scatterplot showing the relationship between the mean annual rainfall (Schulze, 2007) and mean annual ET of indigenous forests

Table 4-5 lists each forest type's long-term mean and standard deviation of annual rainfall. Northern Mistbelt Forest (AF3) is found in a high rainfall region with a mean annual rainfall of $1\ 183 \pm 228$ mm/yr, while Arid Zone Riparian Woodland (ARF1) is in a low rainfall region (223 ± 71 mm/yr). The direct impact of rainfall and subsequently water availability on ET is shown in Table 4-3.

Table 4-6 shows the percentage of each forest type within the mean annual rainfall classes used in the analysis (Table 3-2), while Figure 4-7 shows the geographical distribution of these classes. For example, indigenous forests of type Cape Milkwood Woodland, Arid Zone Riparian Woodland, Cape Alluvial Woodland and Highland Alluvial Woodland are found in low (< 600 mm/yr) rainfall regions, as opposed to Subtropical Indian Ocean Mangrove and Tropical Indian Ocean Mangrove which mostly occur in high (800-1 000 mm/yr) rainfall regions. Substantial areas (50-75%) of Northern Mistbelt Forest, East African Swamp Forest and Subtropical Scarp Forest occur in very high rainfall regions (>1 000 mm/yr).

Table 4-5 Long-term rainfall per forest type

Forest Type	Code	Annual Rain (mm)	
		Mean	Standard Deviation
Arid Zone Riparian Woodland	ARF1	223	71
Cape Alluvial Woodland	ARF2	403	38
Cape Milkwood Woodland	ACF1	417	35
Highland Alluvial Woodland	ARF3	451	72
Southern African Dry Thicket	TDFa3	566	43
Bushveld Talus Forest	ATF3	588	9
Cape Talus Forest	ATF1	619	229
Southern African Dry Forest	TDFa2	714	88
Albany Coastal Forest	STFa5	723	58
Subtropical Riparian Woodland	ARF4	758	151
Tropical Indian Ocean Mangrove	AMAN2	871	13
African Subtropical Coastal Forest	STFa2	890	127
Cape Afrotropical Forest	AF1	920	123
Southern Mistbelt Forest	AF2	937	237
Northern Highveld Afrotropical Forest	ATF5	952	98
Subtropical Scarp Forest	STFa4	1007	212
Drakensberg Afrotropical Forest	ATF4	1009	241
East African Swamp Forest	ASF1	1037	157
Subtropical Dune Woodland	ACF2	1044	171
Subtropical Indian Ocean Mangrove	AMAN1	1134	69
Northern Mistbelt Forest	AF3	1183	228

Table 4-6 Percentage of indigenous forest type area that occur within each of the assigned rainfall classes (low, medium, high and very high). See Table 3-4 (Section 3.4.1) for a description of these classes.

Forest Type	Code	Low	Medium	High	V. High
Cape Milkwood Woodland	ACF1	100	0	0	0
Subtropical Dune Woodland	ACF2	0	4	46	49
Subtropical Indian Ocean Mangrove	AMAN1	0	0	1	99
Tropical Indian Ocean Mangrove	AMAN2	0	0	100	0
Arid Zone Riparian Woodland	ARF1	100	0	0	0
Cape Alluvial Woodland	ARF2	100	0	0	0
Highland Alluvial Woodland	ARF3	98	0	2	0
Subtropical Riparian Woodland	ARF4	21	48	23	7
East African Swamp Forest	ASF1	0	2	42	55
Cape Talus Forest	ATF1	62	19	12	7
Bushveld Talus Forest	ATF3	89	11	0	0
Drakensberg Afrotropical Forest	ATF4	0	30	24	46
Northern Highveld Afrotropical Forest	ATF5	1	3	67	29
Cape Afrotropical Forest	AF1	0	16	60	24
Southern Mistbelt Forest	AF2	5	28	29	38
Northern Mistbelt Forest	AF3	0	2	23	75
African Subtropical Coastal Forest	STFa2	0	25	58	17
Subtropical Scarp Forest	STFa4	6	7	36	52
Albany Coastal Forest	STFa5	0	89	10	0
Southern African Dry Forest	TDFa2	12	72	16	0
Southern African Dry Thicket	TDFa3	86	14	0	0

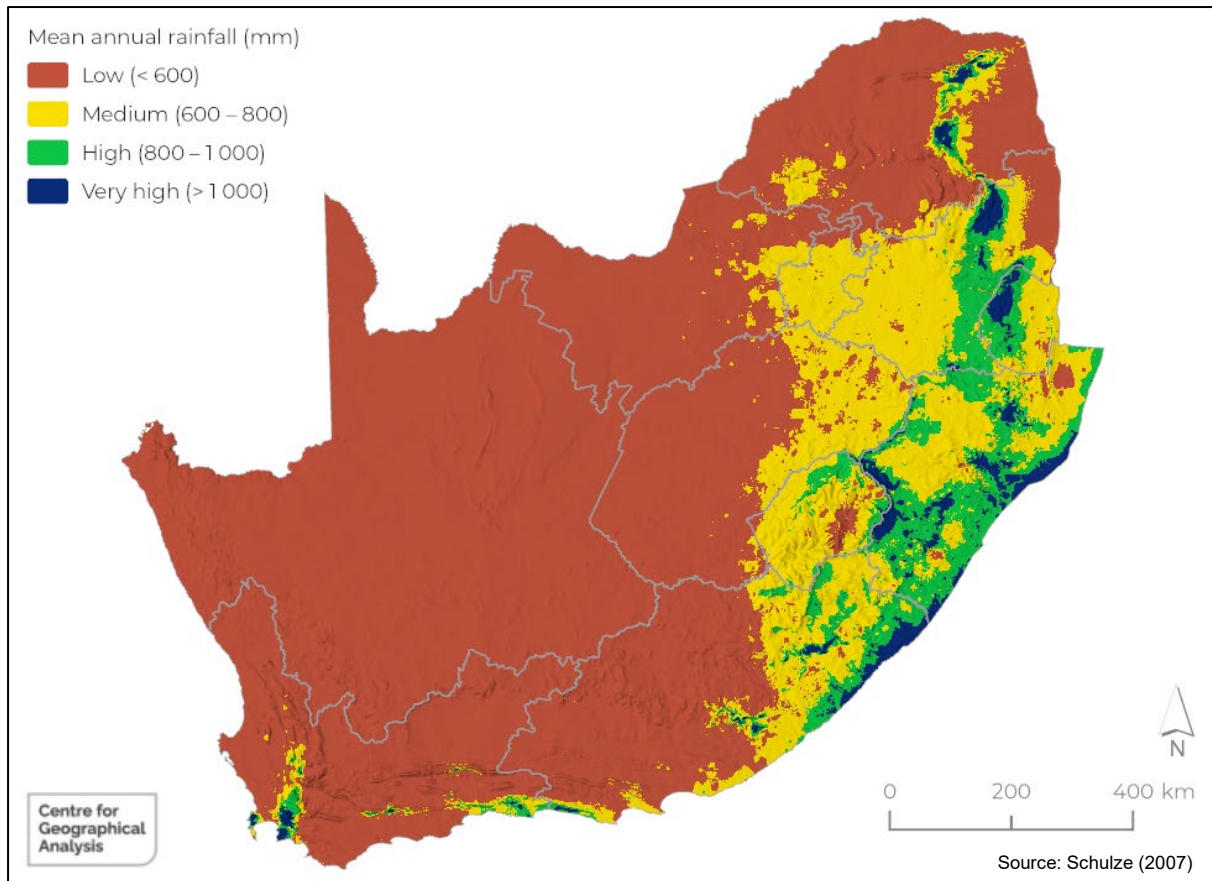


Figure 4-7 Long-term mean annual rainfall classes for South Africa

Figure 4-8 to Figure 4-28 show more details of the seasonal water use per forest type per rainfall region. For instance, the monthly ET of Subtropical Dune Woodland (ACF2) from 2009 to 2023 is shown in Figure 4-9. This forest type occurs in the medium, high, and very high rainfall regions, and there is a substantial difference in the water use of forests in the medium rainfall region from that in the high and very high rainfall regions. Similarly, the variation in water use of Subtropical Riparian Woodland (ARF4) forests occurring in the very high rainfall region is substantially higher than those occurring in the other regions (Figure 4-18).

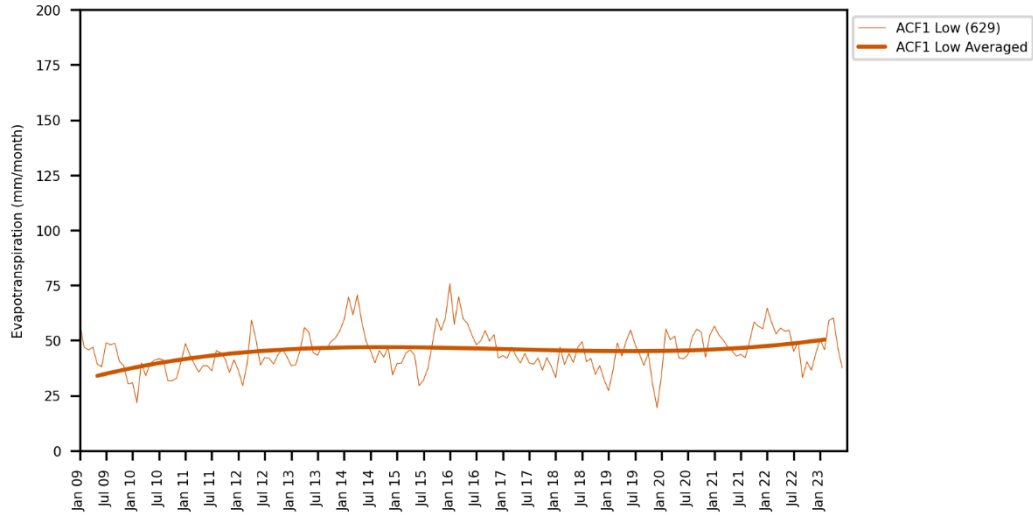


Figure 4-8 Evapotranspiration per rainfall class for ACF1 Cape Milkwood Woodland

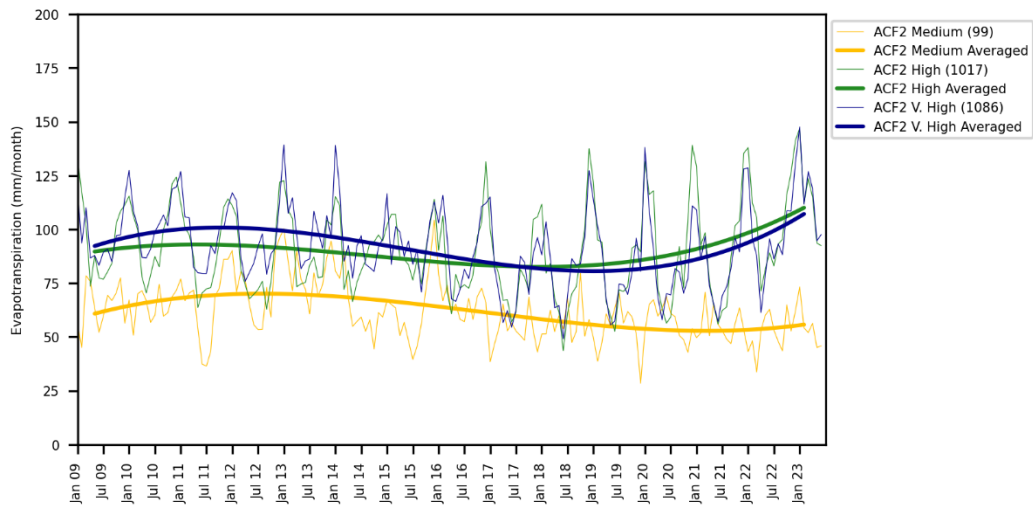


Figure 4-9 Evapotranspiration per rainfall class for ACF2 Subtropical Dune Woodland

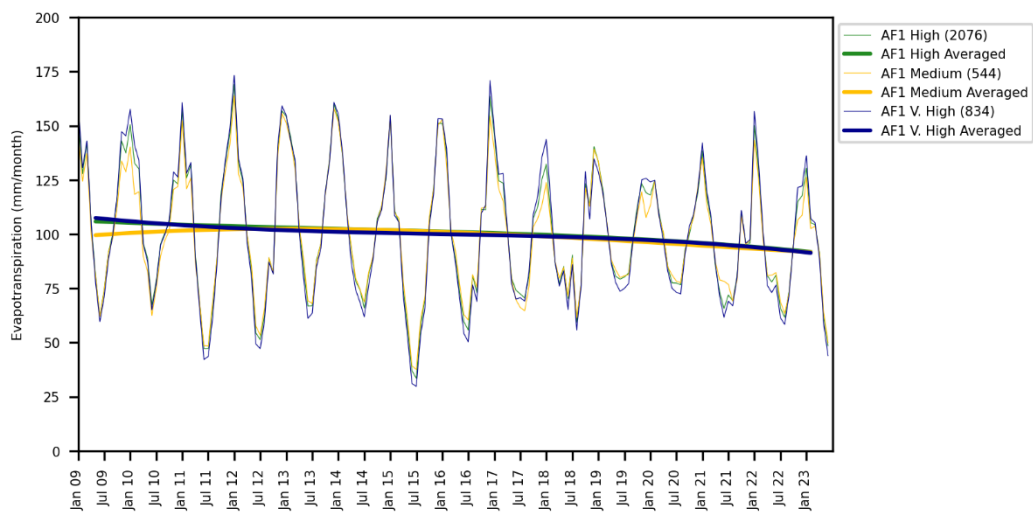


Figure 4-10 Evapotranspiration per rainfall class for AF1 Cape Afrotemperate Forest

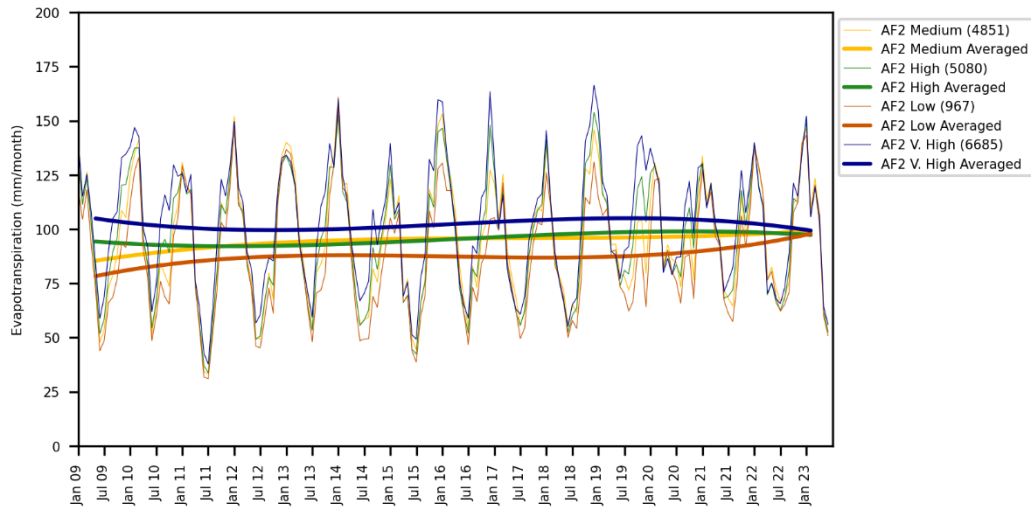


Figure 4-11 Evapotranspiration per rainfall class for AF2 Southern Mistbelt Forest

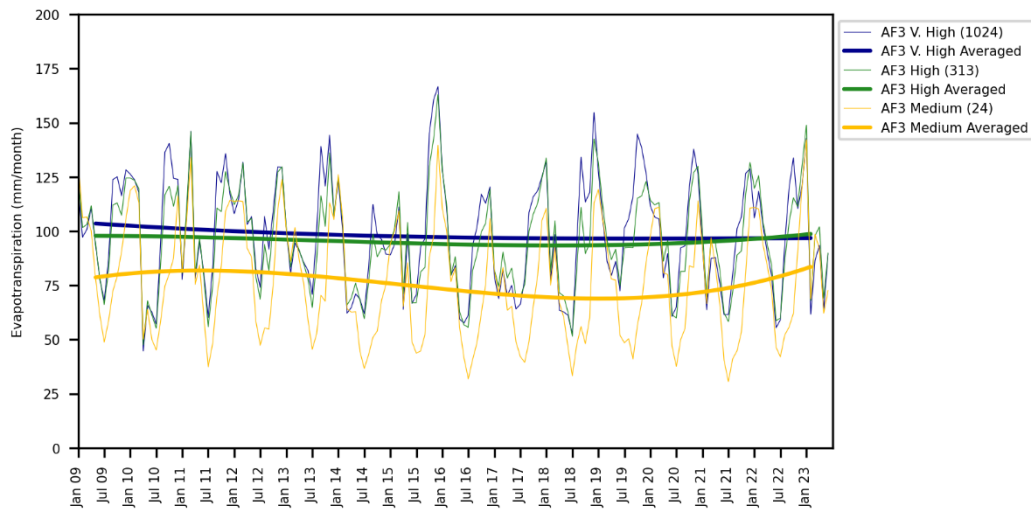


Figure 4-12 Evapotranspiration per rainfall class for AF3 Northern Mistbelt Forest

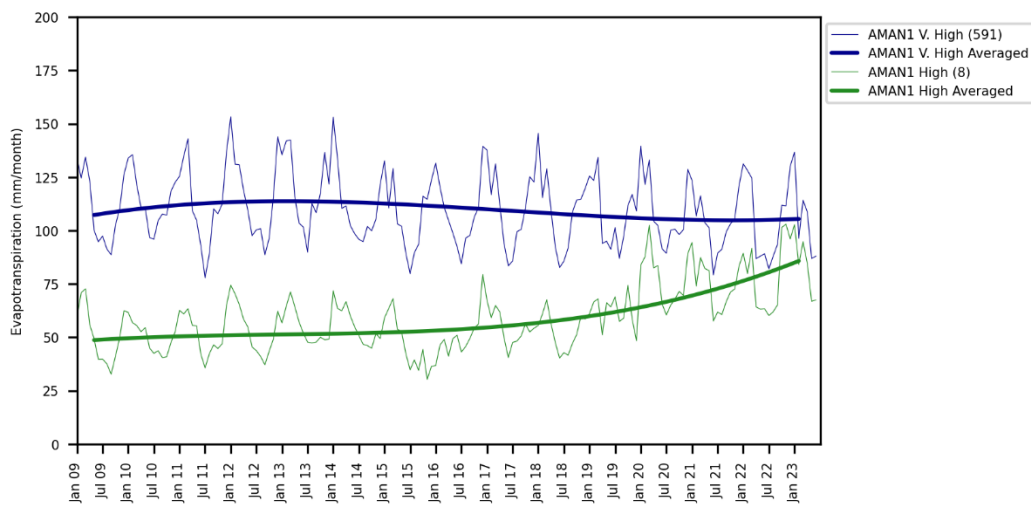


Figure 4-13 Evapotranspiration per rainfall class for AMAN1 Subtropical Indian Ocean Mangrove

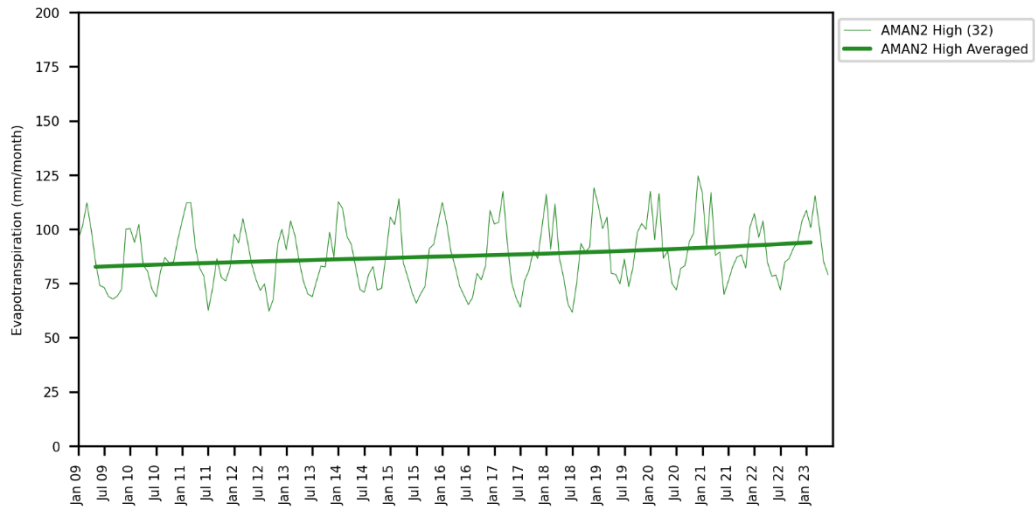


Figure 4-14 Evapotranspiration per rainfall class for AMAN2 Tropical Indian Ocean Mangrove

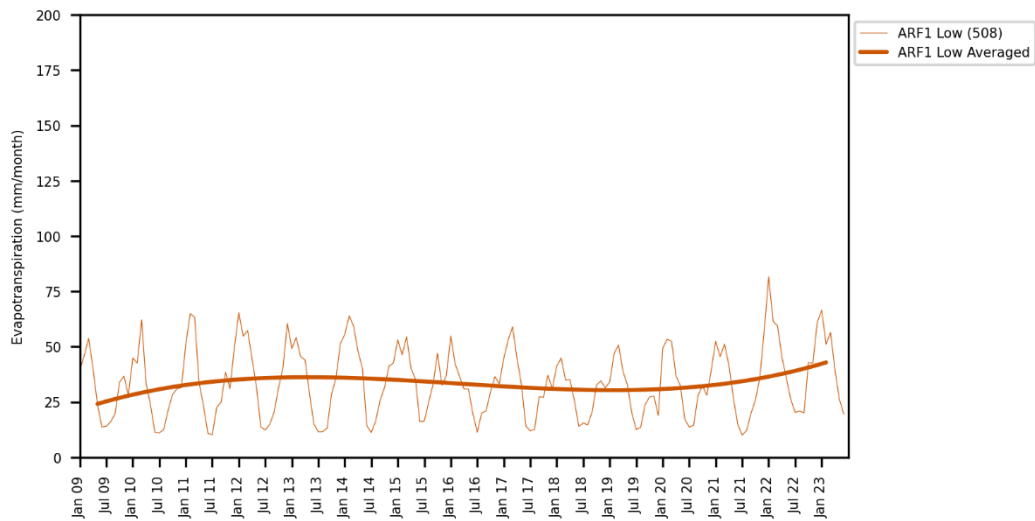


Figure 4-15 Evapotranspiration per rainfall class for ARF1 Arid Zone Riparian Woodland

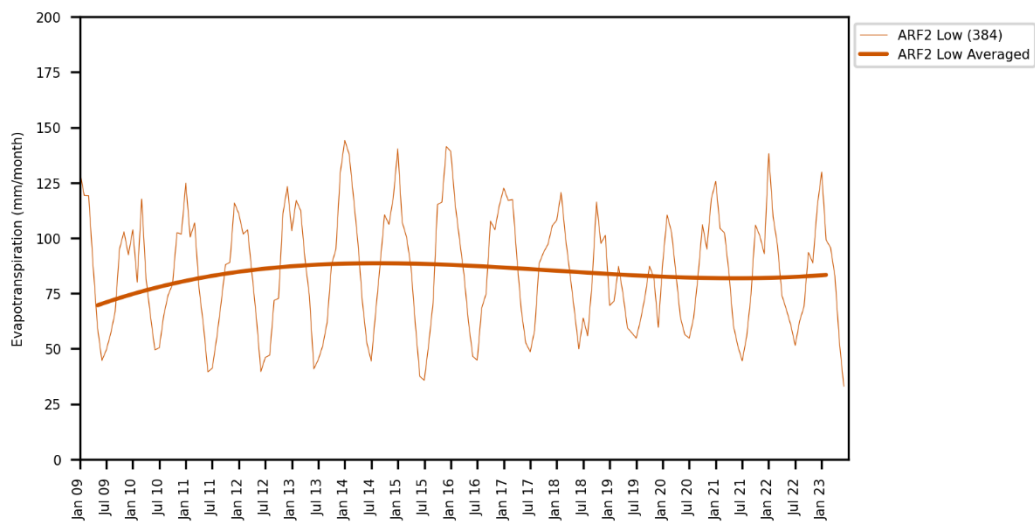


Figure 4-16 Evapotranspiration per rainfall class for ARF2 Cape Alluvial Woodland

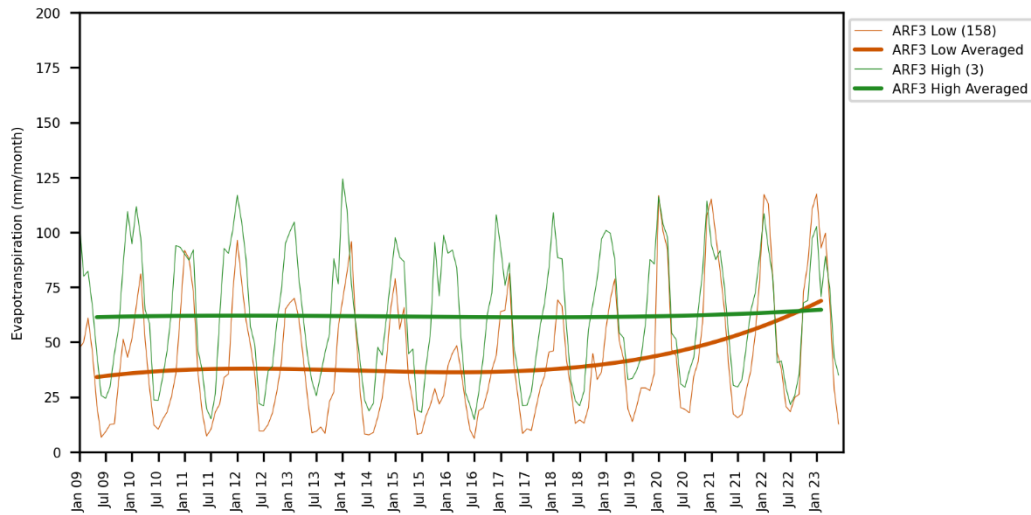


Figure 4-17 Evapotranspiration per rainfall class for ARF3 Highland Alluvial Woodland

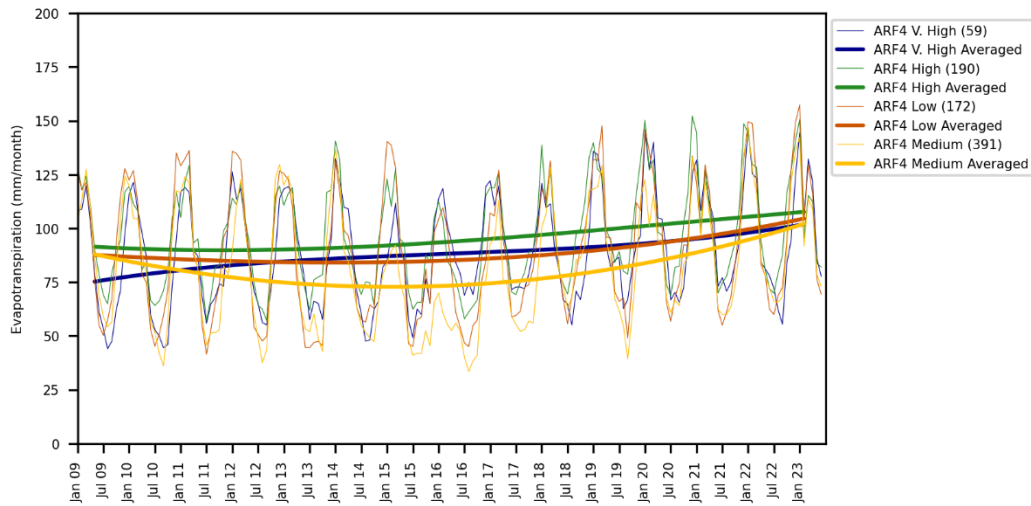


Figure 4-18 Evapotranspiration per rainfall class for ARF4 Subtropical Riparian Woodland

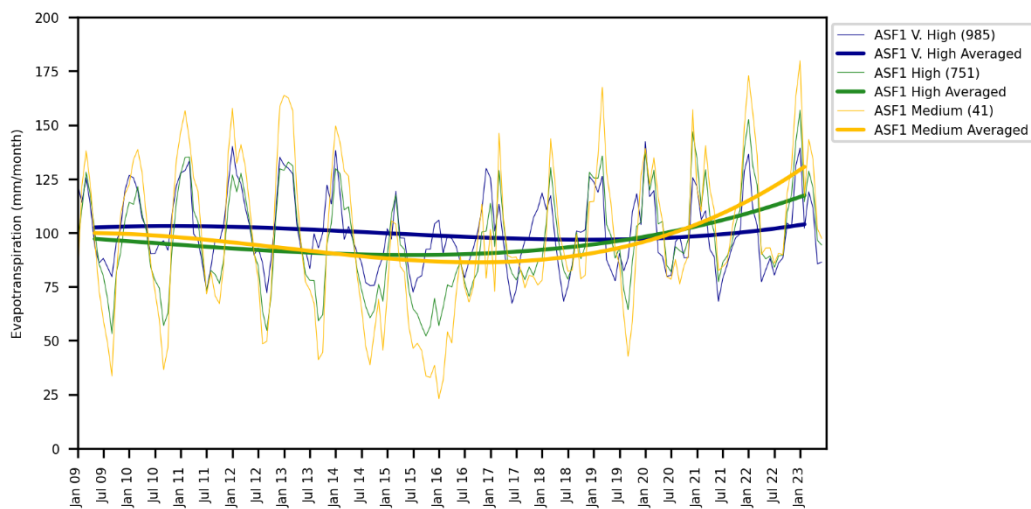


Figure 4-19 Evapotranspiration per rainfall class for ASF1 East African Swamp Forest

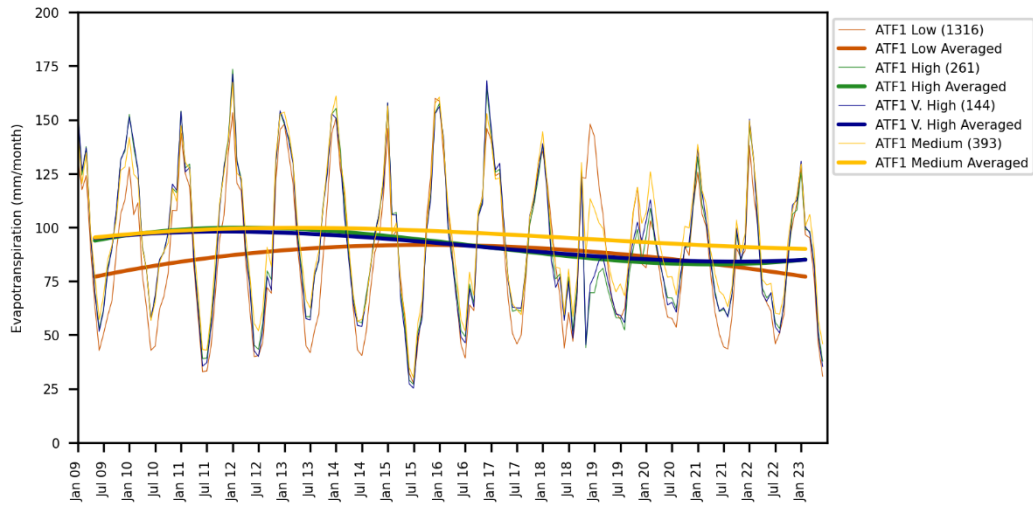


Figure 4-20 Evapotranspiration per rainfall class for ATF1 Cape Talus Forest

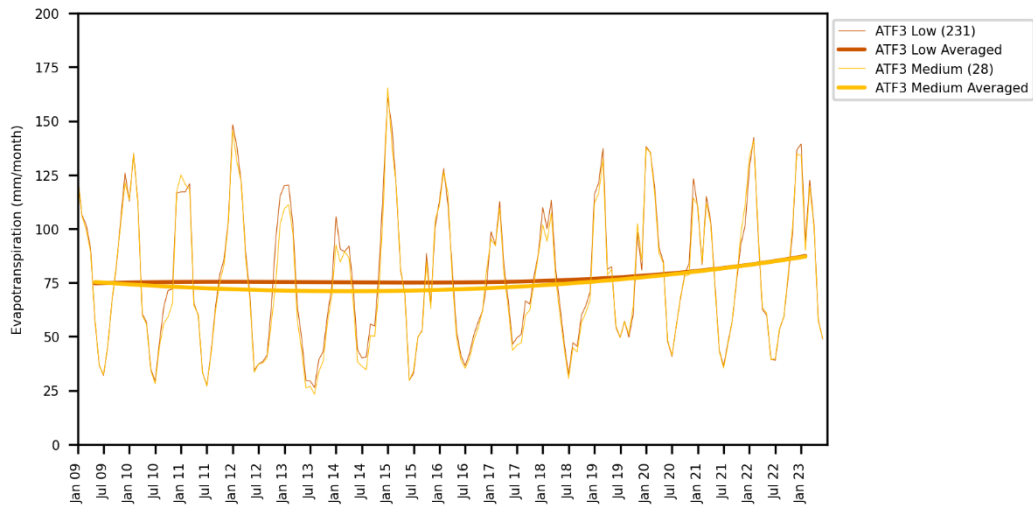


Figure 4-21 Evapotranspiration per rainfall class for ATF3 Bushveld Talus Forest

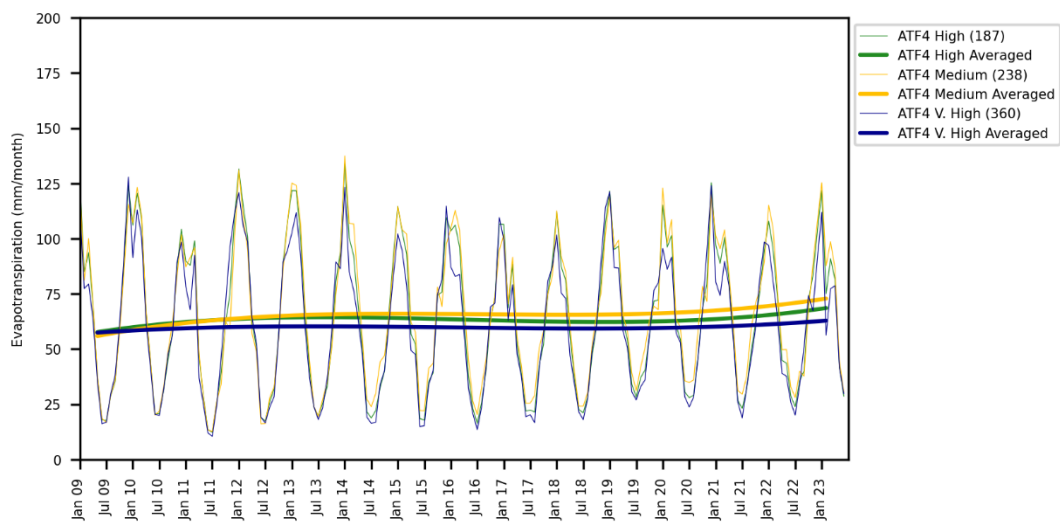


Figure 4-22 Evapotranspiration per rainfall class for ATF4 Drakensberg Afrotemperate Forest

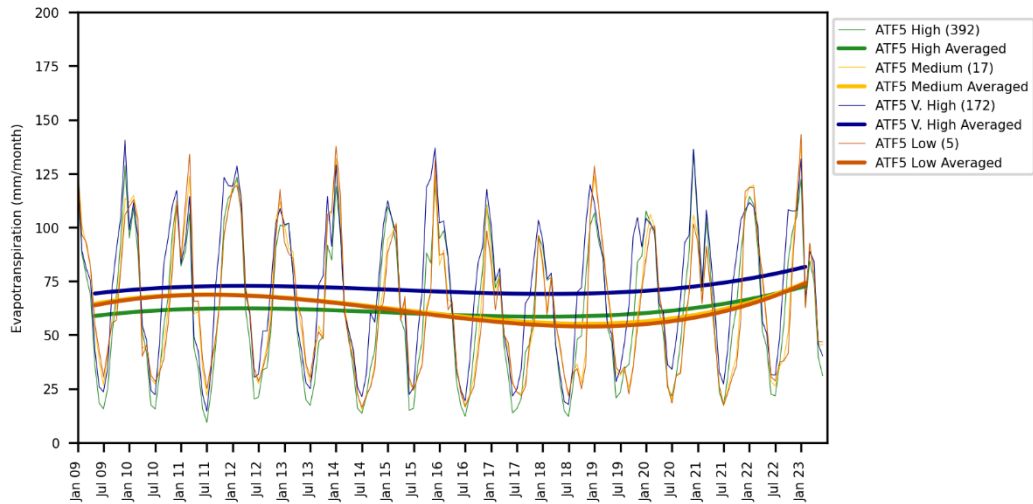


Figure 4-23 Evapotranspiration per rainfall class for ATF5 Northern Highveld Afrotemperate Forest

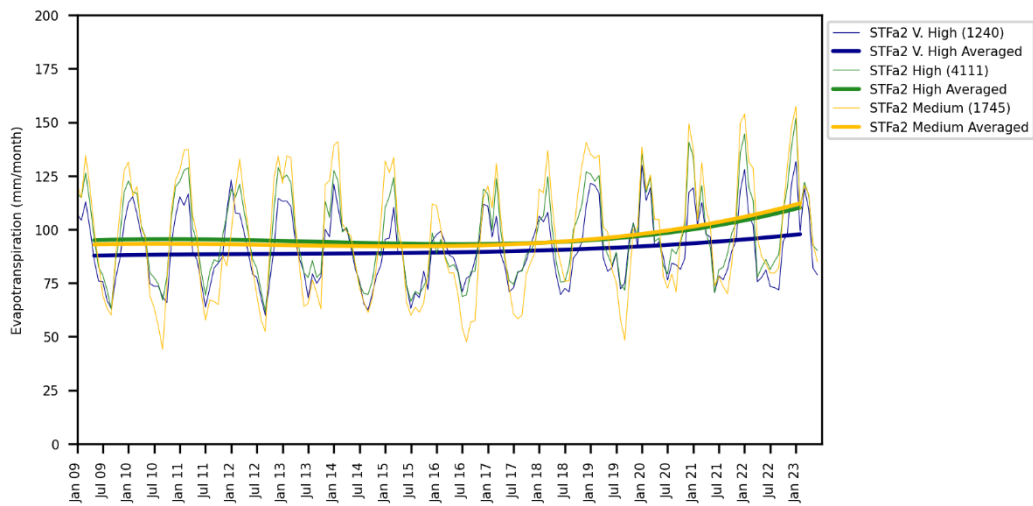


Figure 4-24 Evapotranspiration per rainfall class for STFa2 African Subtropical Coastal Forest

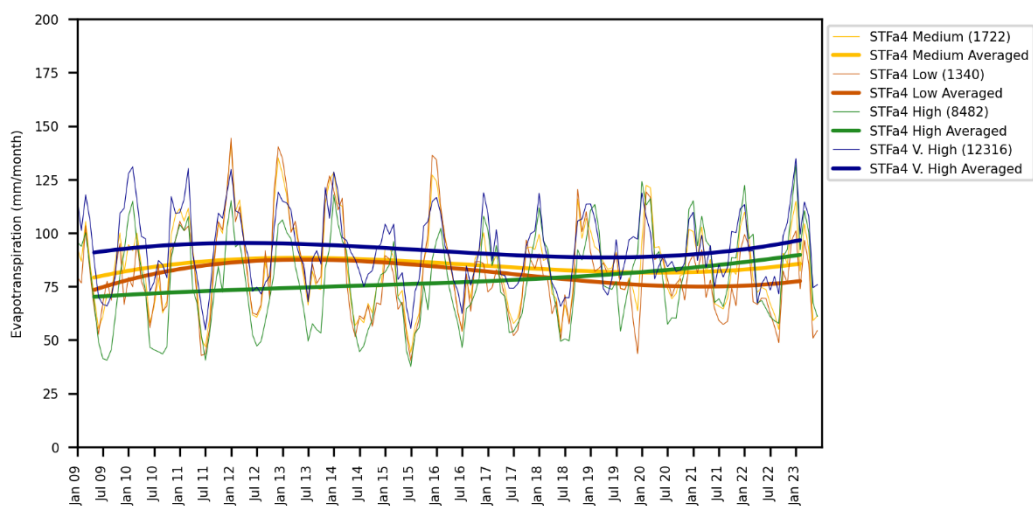


Figure 4-25 Evapotranspiration per rainfall class for STFa4 Subtropical Scarp Forest

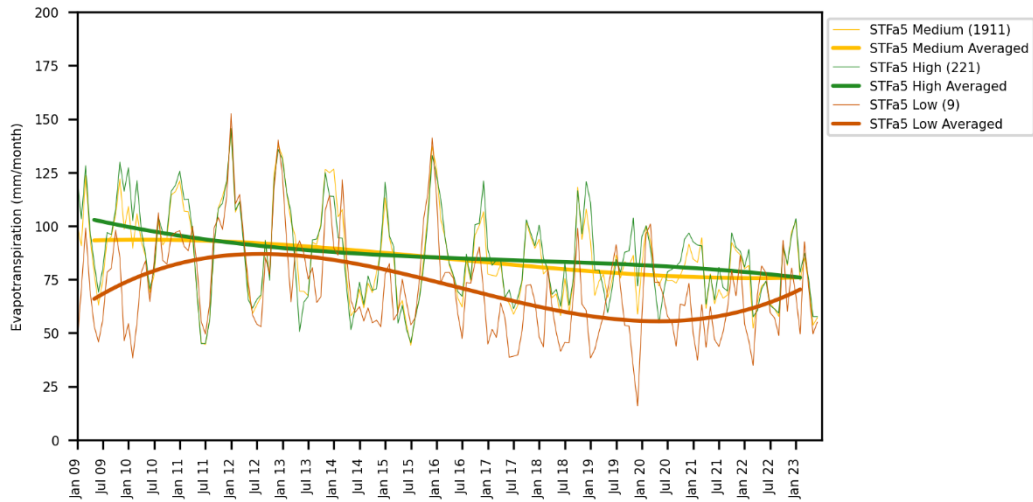


Figure 4-26 Evapotranspiration per rainfall class for STFa5 Albany Coastal Forest

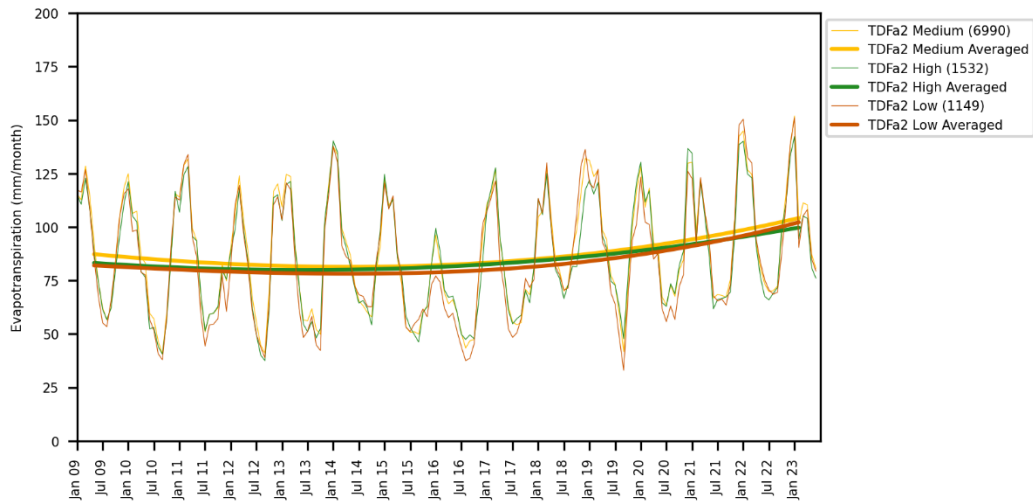


Figure 4-27 Evapotranspiration per rainfall class for TDFa2 Albany Coastal Forest

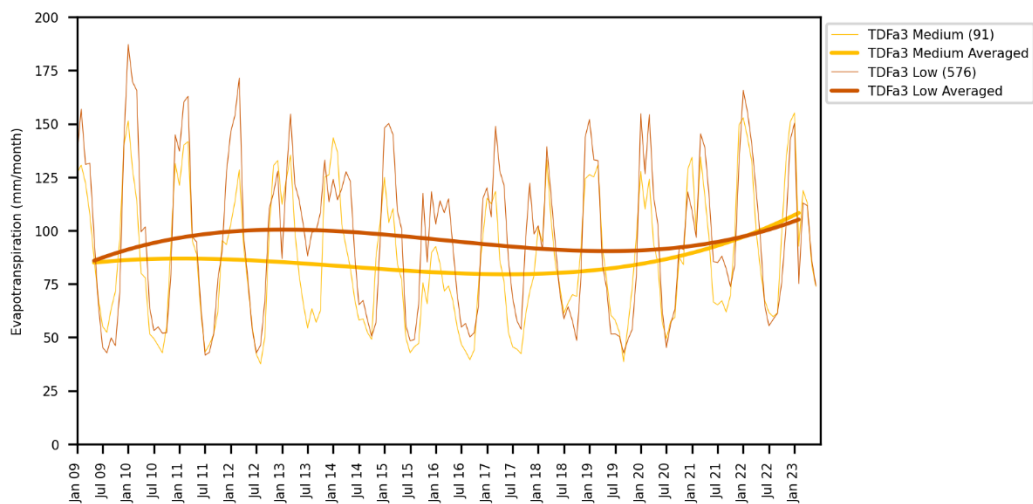


Figure 4-28 Evapotranspiration per rainfall class for TDFa3 Southern African Dry Thicket

It is noticeable that not all forest types were affected by the 2015-2018 drought, which is clearly noticeable in Figure 4-29 to Figure 4-31. In some cases, such as ATF5 Northern Highveld Afrotemperate Forest (Figure 4-23), there is a drop in the polynomial trend in the 2019-2020 period. However, many of the other forest types show no noticeable drop in ET during this period (e. ATF1, Figure 4-20). As can be expected, the water use profile of subtropical Indian Ocean Mangrove (AMAN1, Figure 4-13), was relatively constant from 2010 to 2020.

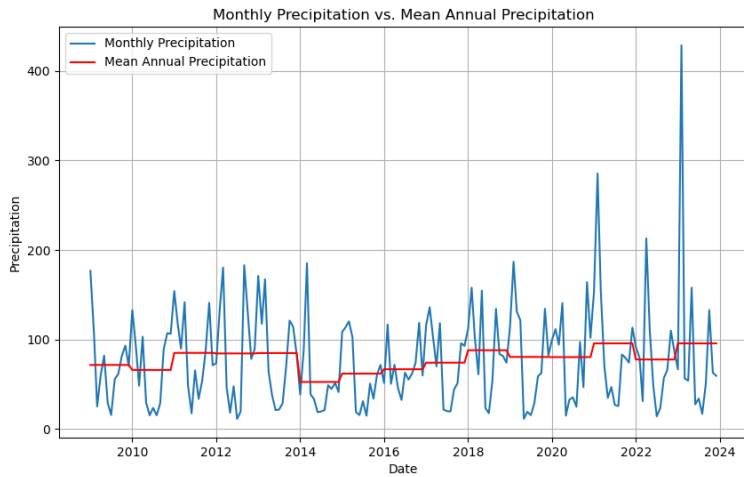


Figure 4-29 Monthly and annual precipitation from 2009 to 2023 at St Lucia (Source: CHIRPS)

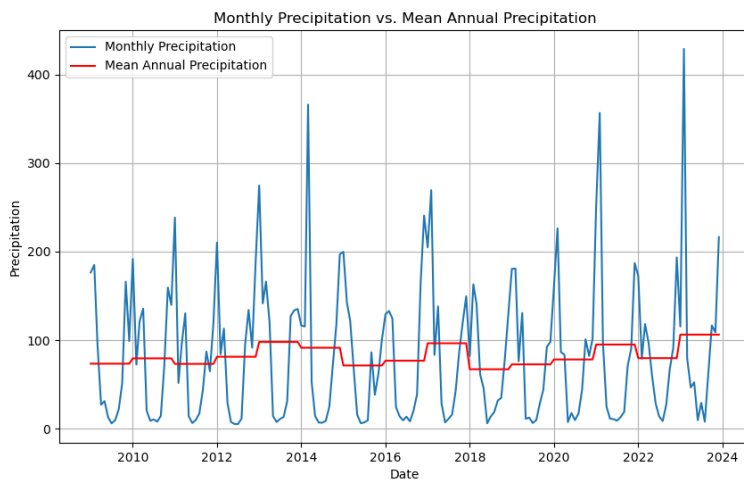


Figure 4-30 Monthly and annual precipitation from 2009 to 2023 at Sabie (Source: CHIRPS)

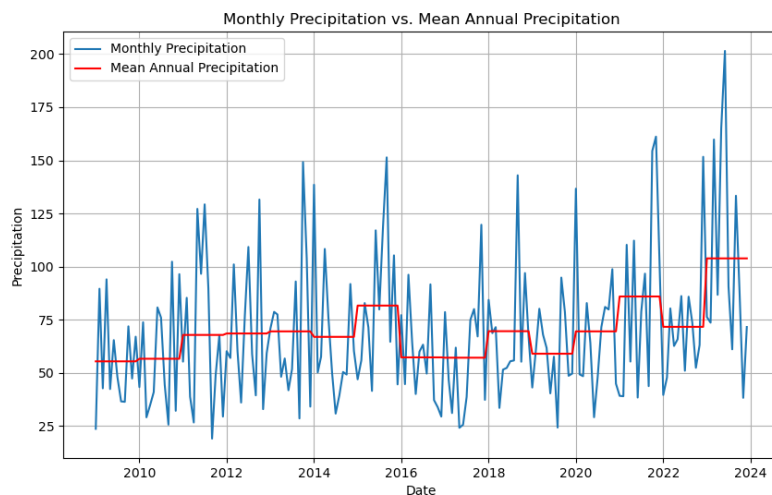


Figure 4-31 Monthly and annual precipitation from 2009 to 2023 at Knysna (Source: CHIRPS)

A recent increase in ET is noticeable for some classes (ACF2, ARF4, ATF5, TDFa2, TDFa3). This is likely attributed to higher rainfall received over the last three years but can also be caused by processes such as bush encroachment and alien plant invasions. More work is needed to investigate the impact of invasive species on the water use of indigenous forests.

The strong relationship found between ET and rainfall is not surprising, as water is recognised as an important driver of plant physiological processes. During photosynthesis, plants open their stomata (pores on leaves) to take in carbon dioxide and release oxygen. However, this stomatal opening also leads to transpiration, the evaporation of water from the leaves. Sufficient soil moisture from rainfall allows plants to maintain this delicate balance, enabling both adequate gas exchange for photosynthesis and efficient water use (Blanco *et al.*, 2022). Trees primarily absorb water through their roots, and sufficient soil moisture is essential for this uptake. During dry periods, plants can become stressed and suffer stunted growth or even death if water is not readily available. During droughts, trees respond by closing their stomata, which reduces the loss of water vapour through transpiration, which has a direct impact on water use (Farquhar & Sharkey, 1982). Different species of trees have adapted to dry climates through evolution, such as having water-saving features like thick waxy leaves to minimise evaporation and deep root systems to tap into deep groundwater reserves (Kramer & Kozlowski, 1979). Trees with smaller leaves lose less water through transpiration compared to those with large, broad leaves. Mangrove trees live in saltwater environments and have adapted to excrete excess salt through their leaves. They also have specialised root structures that help them filter and absorb water from the brackish water (Krishnamurthy, 2008). A strong relationship between the water use of different forest types (composed of different tree and plant species) and rainfall is consequently expected.

4.2.3.2 Solar radiation

Solar radiation during summer (February) was identified as the second most important driver of forest water use, while solar radiation during winter (July) was ranked fourth (Section 4.2.2). The fact that annual solar radiation is also featured in the VIL (12th position) emphasises the importance of solar

radiation on forest water use. Figure 4-32 shows that the solar radiation varies considerably from summer to winter. During summer the solar radiation is relatively low in the areas where indigenous forests typically occur, while the solar radiation in the northeastern parts of South Africa receive relatively high solar radiation during winter.

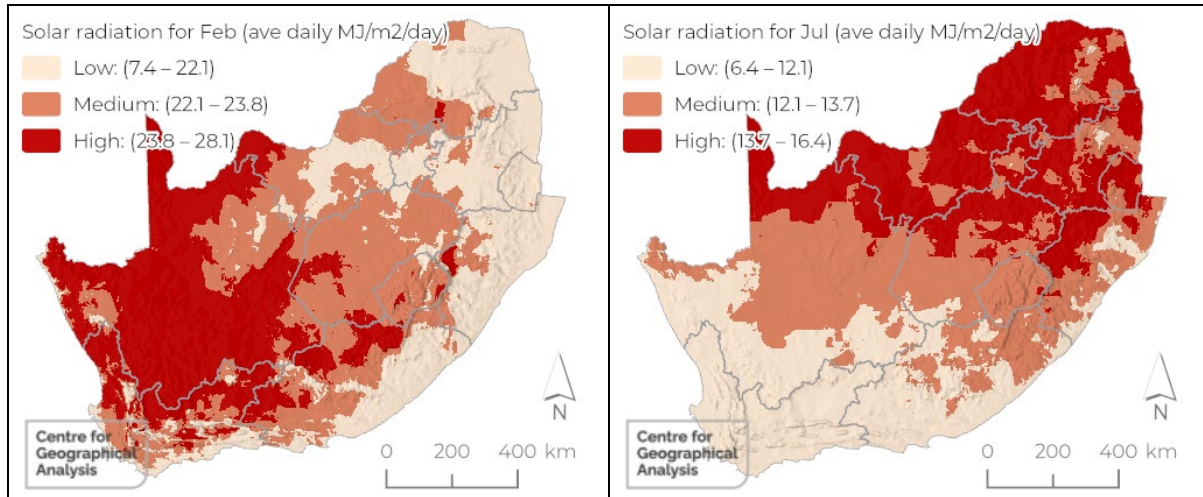


Figure 4-32 Long-term solar radiation classes for February (left) and July (right) Source: Schulze (2007)

Table 4-7 shows that Highland Alluvial Woodland (ARF3) receives the most solar radiation during summer (24.15 MJ/m²/day), while Subtropical Scarp Forest (STFa4) receives the least (17.03 MJ/m²/day). During winter, Bushveld Talus Forest (ATF3) receives the most sunlight (14.21 MJ/m²/day), while Cape Afrotemperate Forest (AF1) receives the least solar radiation (8.01 MJ/m²/day). The low solar radiation of Cape Afrotemperate Forest is likely a combination of cloud cover and shadow caused by terrain. As noted in Section 3.2.14, Cape Afrotemperate Forests are mostly located in the Knysna-Tsitsikamma forest complex and occupy the coastal platform between approximately George and Humansdorp, with outlier forest patches on low-elevation slopes of Outeniqua and Langeberg ranges. These mountain ranges are often covered by clouds due to orographic effects whereby moisture-laden air masses from the ocean are blown by winds towards the mountains. The air is then deflected upward, causing it to cool and form clouds. And on clear days during winter, the mountains cast shadows due to the low solar zenith angle. Consequently, these environmental conditions impact the occurrence and water use of these forests.

Table 4-7 Mean and standard deviation of solar radiation during summer (Feb) and winter (July) per forest type

Forest Type	Code	Solar radiation (average daily MJ/m ² /day)			
		Feb		July	
		Mean	Standard Deviation	Mean	Standard Deviation
Cape Milkwood Woodland	ACF1	20.83	0.80	9.16	0.15
Subtropical Dune Woodland	ACF2	17.74	1.10	11.60	0.94
Subtropical Indian Ocean Mangrove	AMAN1	17.47	1.10	11.37	0.56
Tropical Indian Ocean Mangrove	AMAN2	18.34	0.23	12.38	0.21
Arid Zone Riparian Woodland	ARF1	23.74	0.31	11.40	0.96
Cape Alluvial Woodland	ARF2	22.62	0.48	9.27	0.13
Highland Alluvial Woodland	ARF3	24.15	0.59	12.11	0.28
Subtropical Riparian Woodland	ARF4	20.17	1.39	13.32	0.78
East African Swamp Forest	ASF1	18.36	1.22	11.88	0.64
Cape Talus Forest	ATF1	21.16	1.26	9.12	0.55
Bushveld Talus Forest	ATF3	21.93	0.22	14.21	0.14
Drakensberg Afrot temperate Forest	ATF4	22.54	1.47	13.46	0.63
Northern Highveld Afrot temperate Forest	ATF5	21.48	0.20	13.94	0.13
Cape Afrot temperate Forest	AF1	18.37	1.77	8.01	0.25
Southern Mistbelt Forest	AF2	19.70	1.01	11.15	0.98
Northern Mistbelt Forest	AF3	21.07	0.26	13.99	0.14
African Subtropical Coastal Forest	STFa2	18.41	1.29	12.26	0.61
Subtropical Scarp Forest	STFa4	17.03	2.19	10.96	1.08
Albany Coastal Forest	STFa5	18.91	1.25	9.77	0.52
Southern African Dry Forest	TDFa2	19.92	0.44	13.45	0.50
Southern African Dry Thicket	TDFa3	20.33	0.52	14.19	0.47

The diverse nature of solar radiation can also be seen in Table 4-8 and Table 4-9, which show the relative proportions of forest types that occur in low, medium and high solar radiation areas in summer and winter, respectively. During summer, the majority (67%) of forest types receive low solar radiation, while during winter, only a third (33%) fall in this category, which demonstrates the influence of cloud cover along the coastal areas from George to Mozambique during summer months.

Table 4-8 Solar radiation (February) % class cover per forest type

Forest Type	Code	Low	Medium	High
Cape Milkwood Woodland	ACF1	96	4	0
Subtropical Dune Woodland	ACF2	100	0	0
Subtropical Indian Ocean Mangrove	AMAN1	100	0	0
Tropical Indian Ocean Mangrove	AMAN2	100	0	0
Arid Zone Riparian Woodland	ARF1	0	78	22
Cape Alluvial Woodland	ARF2	5	95	0
Highland Alluvial Woodland	ARF3	2	17	81
Subtropical Riparian Woodland	ARF4	93	7	0
East African Swamp Forest	ASF1	100	0	0
Cape Talus Forest	ATF1	71	29	0
Bushveld Talus Forest	ATF3	37	63	0
Drakensberg Afrot temperate Forest	ATF4	50	24	26
Northern Highveld Afrot temperate Forest	ATF5	100	0	0
Cape Afrot temperate Forest	AF1	100	0	0
Southern Mistbelt Forest	AF2	99	1	0
Northern Mistbelt Forest	AF3	100	0	0

Forest Type	Code	Low	Medium	High
African Subtropical Coastal Forest	STFa2	100	0	0
Subtropical Scarp Forest	STFa4	100	0	0
Albany Coastal Forest	STFa5	100	0	0
Southern African Dry Forest	TDFa2	100	0	0
Southern African Dry Thicket	TDFa3	100	0	0

Table 4-9 Solar radiation (July) % class cover per forest type

Forest Type	Code	Low	Medium	High
Cape Milkwood Woodland	ACF1	100	0	0
Subtropical Dune Woodland	ACF2	64	36	0
Subtropical Indian Ocean Mangrove	AMAN1	91	9	0
Tropical Indian Ocean Mangrove	AMAN2	0	100	0
Arid Zone Riparian Woodland	ARF1	74	22	4
Cape Alluvial Woodland	ARF2	100	0	0
Highland Alluvial Woodland	ARF3	30	70	0
Subtropical Riparian Woodland	ARF4	10	62	28
East African Swamp Forest	ASF1	41	59	0
Cape Talus Forest	ATF1	100	0	0
Bushveld Talus Forest	ATF3	0	0	100
Drakensberg Afrotropical Forest	ATF4	0	67	33
Northern Highveld Afrotropical Forest	ATF5	0	11	89
Cape Afrotropical Forest	AF1	100	0	0
Southern Mistbelt Forest	AF2	76	24	0
Northern Mistbelt Forest	AF3	0	13	87
African Subtropical Coastal Forest	STFa2	27	73	0
Subtropical Scarp Forest	STFa4	83	16	1
Albany Coastal Forest	STFa5	100	0	0
Southern African Dry Forest	TDFa2	0	58	42
Southern African Dry Thicket	TDFa3	0	10	90

On its own, the relationship between solar radiation and forest water use is not strong ($R^2=0.02$).

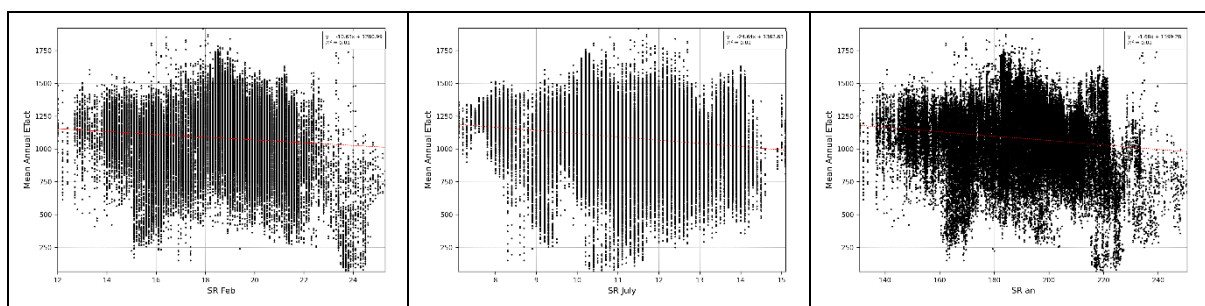


Figure 4-33 Linear regression between forest water use and long-term solar radiation during summer (left), winter (middle) and all year (right)

The relationship is also inconsistent. For instance, Figure 4-34 shows the relationship between winter (July) solar radiation and the water use of Arid Zone Riparian Woodland (ARF1). Within this forest type, patches with low solar radiation used less water than those with medium solar radiation. This is to be expected, given that trees use sunlight as the primary energy source for photosynthesis. Higher solar radiation intensity increases the rate of photosynthesis, meaning more carbohydrates are produced. As

a result, the tree experiences increased metabolic activity, which demands more water for transportation and cellular processes. This leads to increased water uptake through the roots and transpiration (water loss through stomata on leaves). Solar radiation also raises transpiration rates as higher temperatures and sunlight increase the energy available for water evaporation, leading to greater water loss through transpiration (Dagon & Schrag, 2016). A similar relationship exists in Figure 4-34, where the relationship between water use of Subtropical Riparian Woodland (ARF4) and solar radiation in line with what one would expect (i.e. high water use with high solar radiation), but the high variation among forest types and solar radiation classes makes the drawing of conclusions difficult.

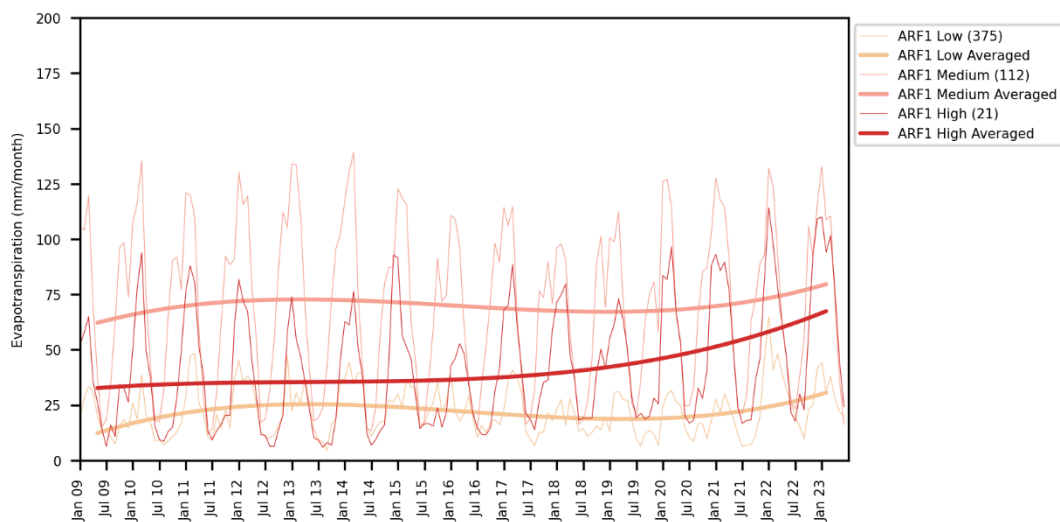


Figure 4-34 Evapotranspiration per solar radiation class during winter for ARF1

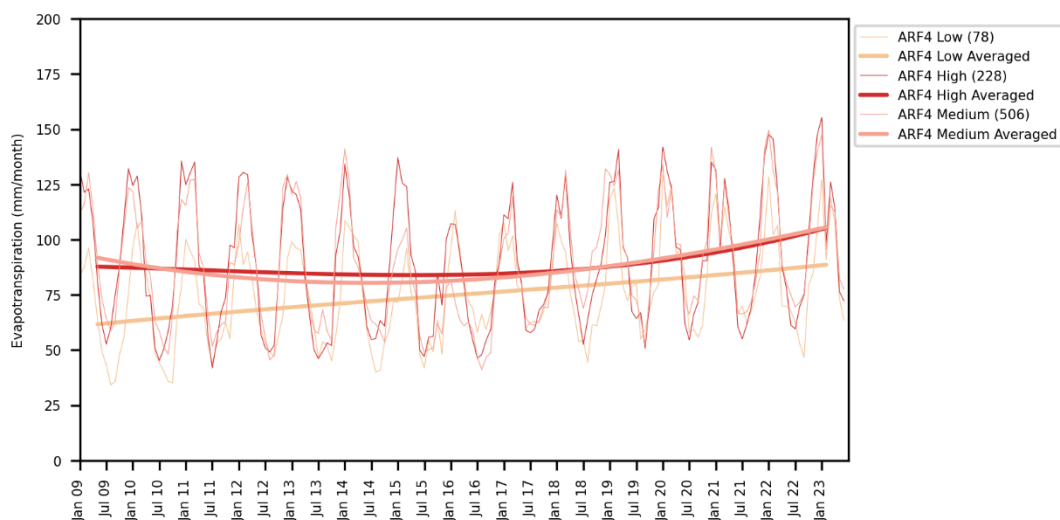


Figure 4-35 Evapotranspiration per solar radiation class during winter for ARF4

4.2.3.3 Heat units (degree days)

Long-term mean annual heat units, or growing degree days (GDD), was identified as the third most

important driver of forest water use (Figure 4-36). GDD is an indicator of ideal conditions for plant growth. As temperatures rise within the optimal range for a specific plant, the metabolic processes of photosynthesis and transpiration accelerate. This means plants demand more water for various functions, potentially increasing overall water use (Smith *et al.*, 2001). Schulze (2007) expresses heat units in degree days, “where these are an accumulation of mean temperatures above a certain lower threshold value (below which active development is considered not to take place), and below an upper limit (above which growth is considered to remain static or even decline), over a period of time. For example, if the threshold temperature is 10°C and the mean temperature of a given day is 22°C, then 12 degree days, or heat units, are accumulated for that day to a previous total.”

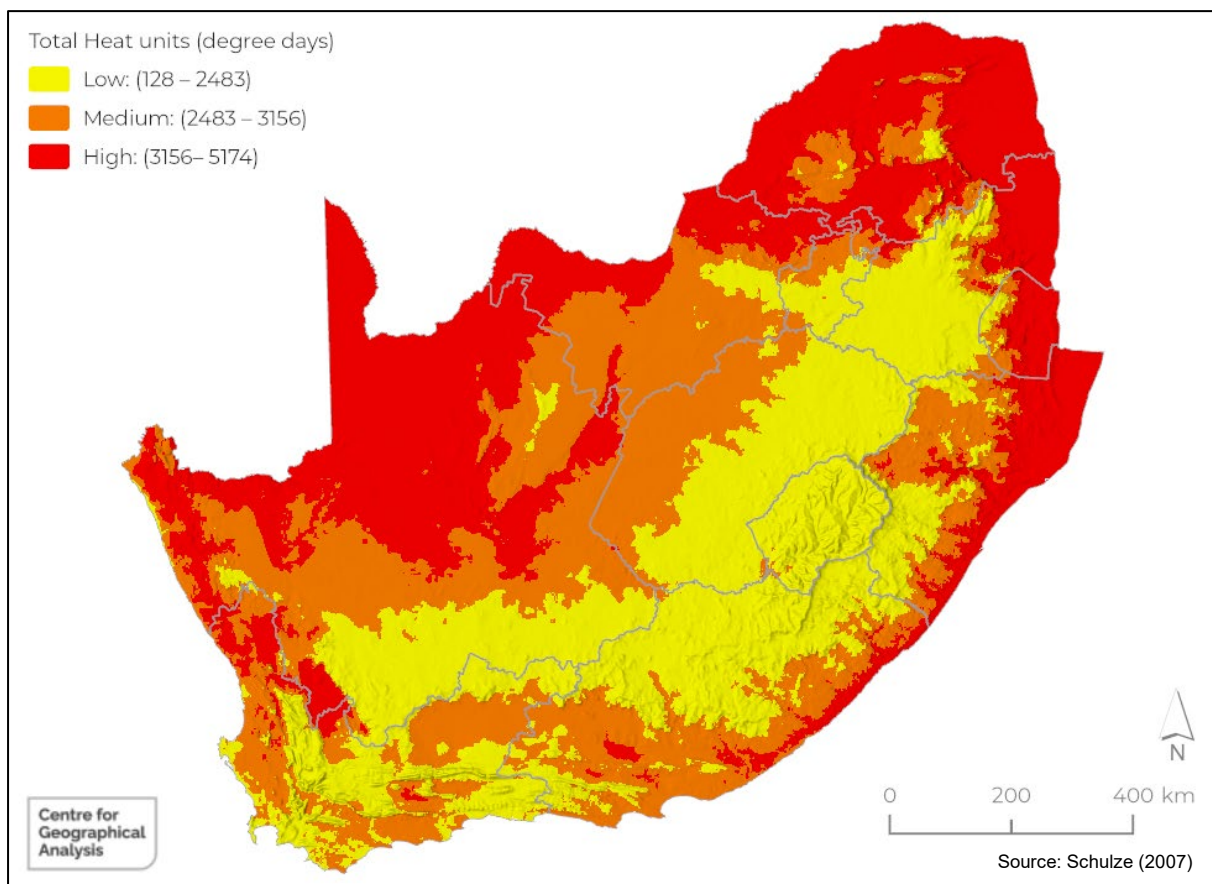


Figure 4-36 Annual heat units (degree days) classes for South Africa

Table 4-10 details the mean annual heat units for each forest type. The number of heat units are the highest (4 645) for Southern African Dry Thicket (TDFa3), while Northern Highveld Afrotperate Forest (ATF5) recorded the lowest (1 890 degree days) heat units. Table 4-11 shows that the forest types are well distributed among the heat unit classes, with the high heat unit class being dominated by subtropical and dry forests.

Table 4-10 Mean and standard deviation of annual heat units (degree days) per forest type

Forest Type	Code	Annual heat units (degree days)	
		Mean	Standard Deviation
Northern Highveld Afrotropical Forest	ATF5	1890	255
Drakensberg Afrotropical Forest	ATF4	1966	352
Southern Mistbelt Forest	AF2	1998	370
Cape Afrotropical Forest	AF1	2330	136
Cape Talus Forest	ATF1	2352	428
Highland Alluvial Woodland	ARF3	2395	91
Cape Alluvial Woodland	ARF2	2545	136
Cape Milkwood Woodland	ACF1	2597	106
Northern Mistbelt Forest	AF3	2726	476
Arid Zone Riparian Woodland	ARF1	2924	220
Albany Coastal Forest	STFa5	3041	40
Bushveld Talus Forest	ATF3	3074	66
Subtropical Scarp Forest	STFa4	3407	302
Subtropical Dune Woodland	ACF2	4213	326
Subtropical Riparian Woodland	ARF4	4239	587
Subtropical Indian Ocean Mangrove	AMAN1	4245	178
African Subtropical Coastal Forest	STFa2	4280	276
East African Swamp Forest	ASF1	4322	172
Southern African Dry Forest	TDFa2	4514	57
Tropical Indian Ocean Mangrove	AMAN2	4538	24
Southern African Dry Thicket	TDFa3	4645	50

Table 4-11 Annual heat units (degree days) % class cover

Forest Type	Code	Low	Medium	High
Cape Milkwood Woodland	ACF1	16	84	0
Subtropical Dune Woodland	ACF2	0	4	96
Subtropical Indian Ocean Mangrove	AMAN1	0	0	100
Tropical Indian Ocean Mangrove	AMAN2	0	0	100
Arid Zone Riparian Woodland	ARF1	0	92	8
Cape Alluvial Woodland	ARF2	23	77	0
Highland Alluvial Woodland	ARF3	91	9	0
Subtropical Riparian Woodland	ARF4	0	10	90
East African Swamp Forest	ASF1	0	0	100
Cape Talus Forest	ATF1	56	44	0
Bushveld Talus Forest	ATF3	0	91	9
Drakensberg Afrotropical Forest	ATF4	91	9	0
Northern Highveld Afrotropical Forest	ATF5	97	3	0
Cape Afrotropical Forest	AF1	93	7	0
Southern Mistbelt Forest	AF2	89	11	0
Northern Mistbelt Forest	AF3	37	47	16
African Subtropical Coastal Forest	STFa2	0	1	99
Subtropical Scarp Forest	STFa4	0	22	77
Albany Coastal Forest	STFa5	0	100	0
Southern African Dry Forest	TDFa2	0	0	100
Southern African Dry Thicket	TDFa3	0	0	100

Figure 4-37 shows that there is no statistical relationship between the water use of forests and heat units. However, the figure includes all of the forest types in combination and does not consider the relationship per forest type.

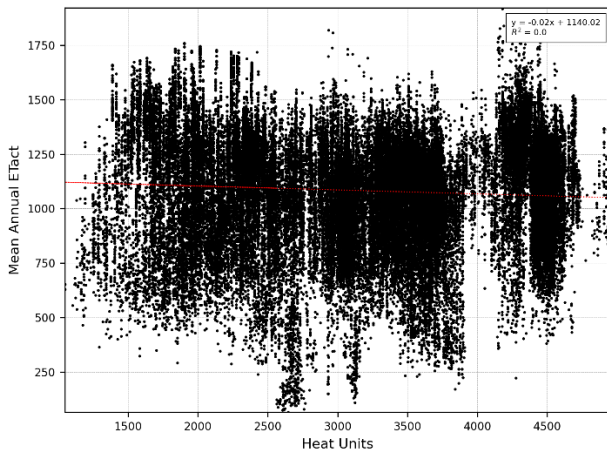


Figure 4-37 Linear regression between forest water use and heat units (degree days).

Figure 4-38 compares the water use of Northern Mistbelt Forest (AF3) to the heat unit classes. There seems to be an increasing water use as heat units increase for this forest type. A similar pattern is observed for Arid Zone Riparian Woodland (ARF1), while for Cape Alluvial Woodland (ARF2) the pattern is absent.

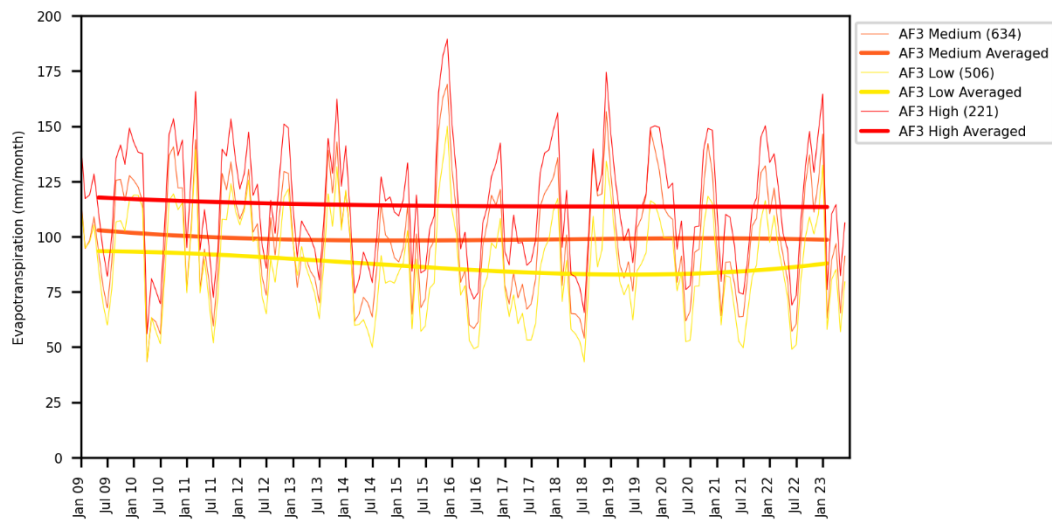


Figure 4-38 Evapotranspiration per heat unit class for AF3

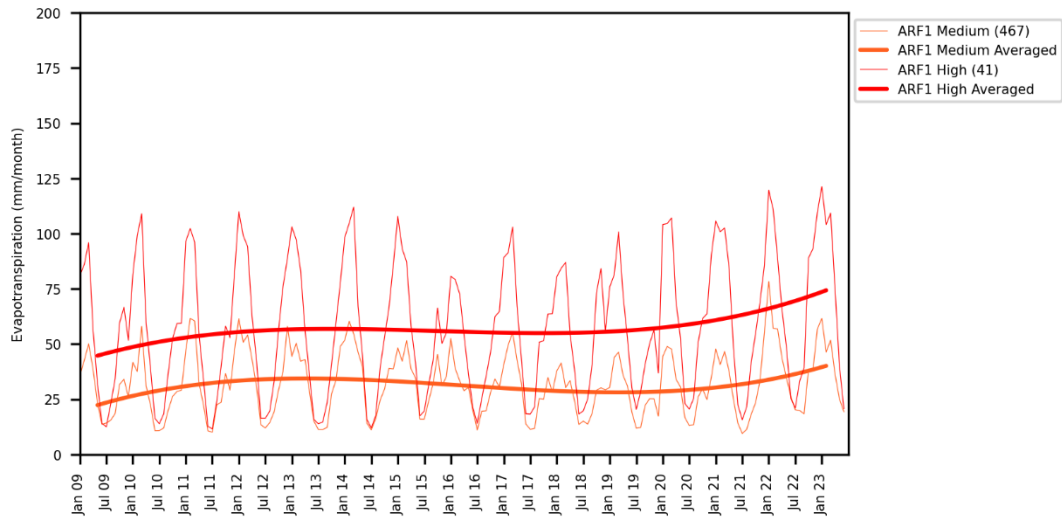


Figure 4-39 Evapotranspiration per heat unit class for ARF1

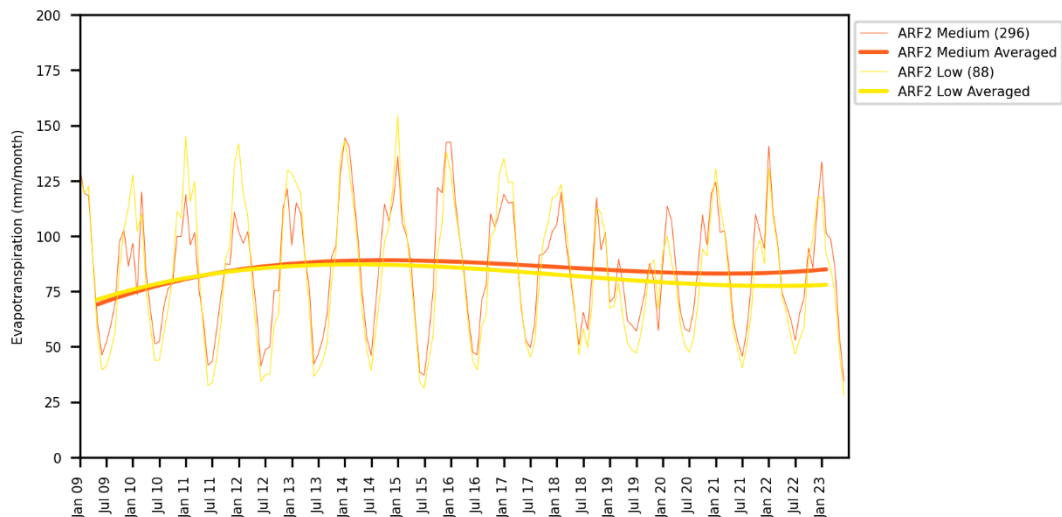


Figure 4-40 Evapotranspiration per heat unit class for ARF2

4.2.3.4 Vapour pressure deficit

The winter (July) vapour pressure deficit (VPD) was identified as the 6th most important driver for forest water use, while summer VPD was rated as the 15th most important driver. Figure 4-41 shows the summer (February) and winter (July) long-term average VPD. The VPD is strongly related to rainfall seasonality, with the summer rainfall regions having a low VPD during the summer months, while winter rainfall regions (e.g. Western Cape) have a low VPD during winter. This is supported by Table 4-12, which shows that only two (10%) forest types are categorised as having a high VPD during summer (Feb). In contrast, six (29%) types fall in this class during winter (Jul) (Table 4-13).

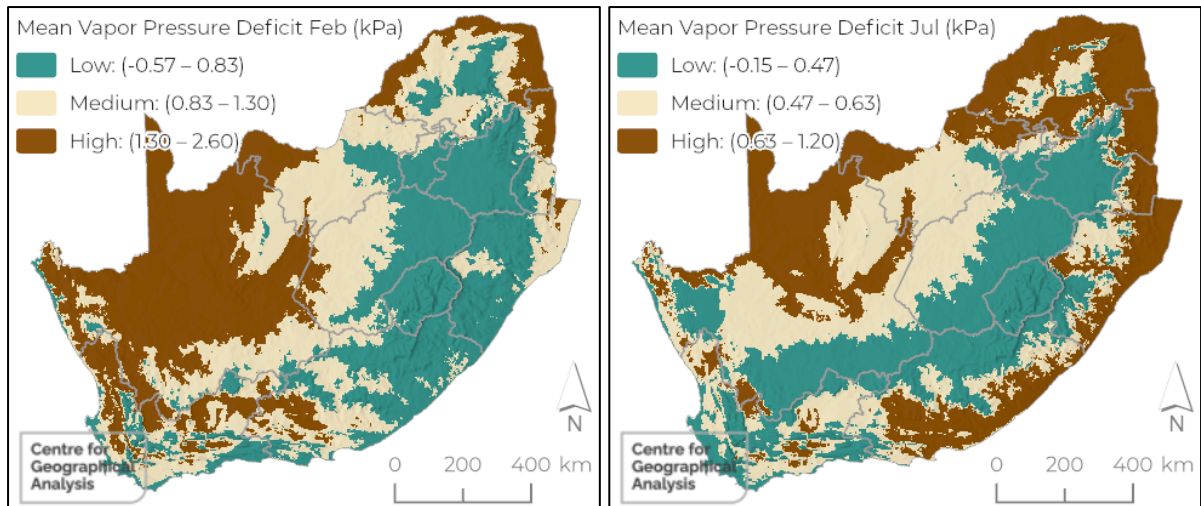


Figure 4-41 Average vapour pressure deficit classes for February (left) and July (right) Source: Schulze (2007)

Table 4-12 Vapour pressure deficit % class cover (Feb)

Forest Type	Code	Low	Medium	High
Cape Milkwood Woodland	ACF1	84	16	0
Subtropical Dune Woodland	ACF2	89	11	0
Subtropical Indian Ocean Mangrove	AMAN1	56	44	0
Tropical Indian Ocean Mangrove	AMAN2	25	75	0
Arid Zone Riparian Woodland	ARF1	0	9	91
Cape Alluvial Woodland	ARF2	0	79	21
Highland Alluvial Woodland	ARF3	2	98	0
Subtropical Riparian Woodland	ARF4	10	42	48
East African Swamp Forest	ASF1	25	75	0
Cape Talus Forest	ATF1	38	61	1
Bushveld Talus Forest	ATF3	0	100	0
Drakensberg Afrotropical Forest	ATF4	91	9	0
Northern Highveld Afrotropical Forest	ATF5	100	0	0
Cape Afrotropical Forest	AF1	100	0	0
Southern Mistbelt Forest	AF2	99	1	0
Northern Mistbelt Forest	AF3	86	14	0
African Subtropical Coastal Forest	STFa2	18	82	0
Subtropical Scarp Forest	STFa4	83	17	0
Albany Coastal Forest	STFa5	91	9	0
Southern African Dry Forest	TDFa2	0	67	33
Southern African Dry Thicket	TDFa3	0	0	100

Table 4-13 Vapour pressure deficit % class cover (July)

Forest Type	Code	Low	Medium	High
Cape Milkwood Woodland	ACF1	66	34	0
Subtropical Dune Woodland	ACF2	5	61	34
Subtropical Indian Ocean Mangrove	AMAN1	0	45	55
Tropical Indian Ocean Mangrove	AMAN2	0	0	100
Arid Zone Riparian Woodland	ARF1	0	67	33
Cape Alluvial Woodland	ARF2	0	100	0
Highland Alluvial Woodland	ARF3	89	11	0
Subtropical Riparian Woodland	ARF4	0	15	85
East African Swamp Forest	ASF1	0	9	91
Cape Talus Forest	ATF1	43	19	38
Bushveld Talus Forest	ATF3	0	98	2
Drakensberg Afrotperate Forest	ATF4	61	32	7
Northern Highveld Afrotperate Forest	ATF5	91	9	0
Cape Afrotperate Forest	AF1	94	6	0
Southern Mistbelt Forest	AF2	58	38	3
Northern Mistbelt Forest	AF3	43	40	16
African Subtropical Coastal Forest	STFa2	0	8	92
Subtropical Scarp Forest	STFa4	1	15	84
Albany Coastal Forest	STFa5	4	66	30
Southern African Dry Forest	TDFa2	0	0	100
Southern African Dry Thicket	TDFa3	0	0	100

Table 4-14 lists the mean and standard deviation VPD during summer (February) and winter (July) for each of the forest types. The lowest VPD during summer (0.27 kPa) and winter (0.35 kPa) was recorded for Northern Highveld Afrotperate Forest (ATF5). Southern African Dry Thicket (TDFa3) and Southern African Dry Forest (TDFa2) had the highest VPD during winter, respectively. Southern African Dry Thicket (TDFa3) occurs in small patches from Ndumo (KwaZulu-Natal) and northwards to the Greater Limpopo Transfrontier Park. Similarly, Southern African Dry Forest (TDFa2) are found mainly in small patches in north Limpopo and along the western piedmonts of the Lebombo mountains. As can be seen in Figure 4-41, these areas have consistently low to medium VPD and have adapted to dry conditions.

Table 4-14 Mean and standard deviation of vapour pressure deficit per forest type during summer (February) and winter (July)

Forest Type	Code	Vapour Pressure Deficit (kPa)			
		Feb		July	
		Mean	Standard Deviation	Mean	Standard Deviation
Cape Milkwood Woodland	ACF1	0.70	0.13	0.42	0.09
Subtropical Dune Woodland	ACF2	0.71	0.12	0.60	0.08
Subtropical Indian Ocean Mangrove	AMAN1	0.77	0.13	0.64	0.06
Tropical Indian Ocean Mangrove	AMAN2	0.86	0.04	0.71	0.03
Arid Zone Riparian Woodland	ARF1	1.39	0.07	0.66	0.08
Cape Alluvial Woodland	ARF2	1.17	0.11	0.58	0.03
Highland Alluvial Woodland	ARF3	1.04	0.11	0.45	0.02
Subtropical Riparian Woodland	ARF4	1.22	0.28	0.95	0.19
East African Swamp Forest	ASF1	0.95	0.17	0.77	0.11
Cape Talus Forest	ATF1	0.79	0.25	0.52	0.15
Bushveld Talus Forest	ATF3	0.95	0.04	0.58	0.02
Drakensberg Afrotemperate Forest	ATF4	0.49	0.22	0.45	0.11
Northern Highveld Afrotemperate Forest	ATF5	0.27	0.09	0.35	0.08
Cape Afrotemperate Forest	AF1	0.47	0.15	0.40	0.04
Southern Mistbelt Forest	AF2	0.39	0.15	0.46	0.09
Northern Mistbelt Forest	AF3	0.56	0.22	0.51	0.13
African Subtropical Coastal Forest	STFa2	0.96	0.21	0.83	0.11
Subtropical Scarp Forest	STFa4	0.58	0.20	0.71	0.09
Albany Coastal Forest	STFa5	0.66	0.12	0.59	0.07
Southern African Dry Forest	TDFa2	1.27	0.06	1.01	0.02
Southern African Dry Thicket	TDFa3	1.40	0.07	0.98	0.04

Figure 4-42 shows that there is very little relationship between the water use of forests and VPD during summer and winter, when all forest types are considered in combination. In addition, Figure 4-1 shows that VPD in February is strongly related mean annual ($R^2=0.9$), February ($R^2=0.89$), annual relative humidity ($R^2=-0.86$) and July ($R^2=0.84$) temperature and heat units ($R^2=0.9$). Similar relationships are present for winter (July) VPD. This highlights the collinearity of VPD with several other climate-related variables.

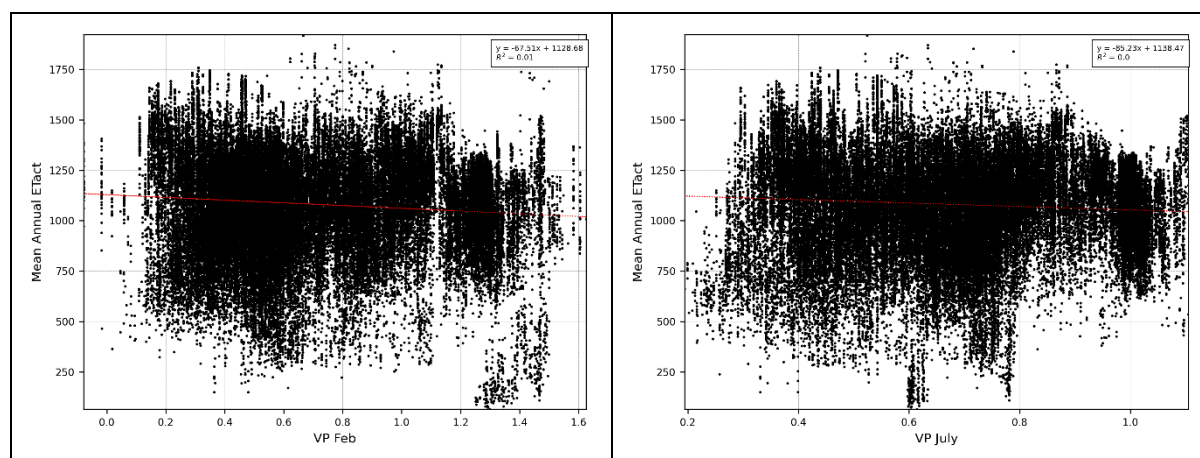


Figure 4-42 Linear regression between forest water use and long-term vapour pressure deficit during summer (left) and winter (right)

At the individual forest type levels, the relationship between VPD and water use is complex. For instance, Figure 4-43 shows that the water use of AF2 is relatively high when VPD is low.

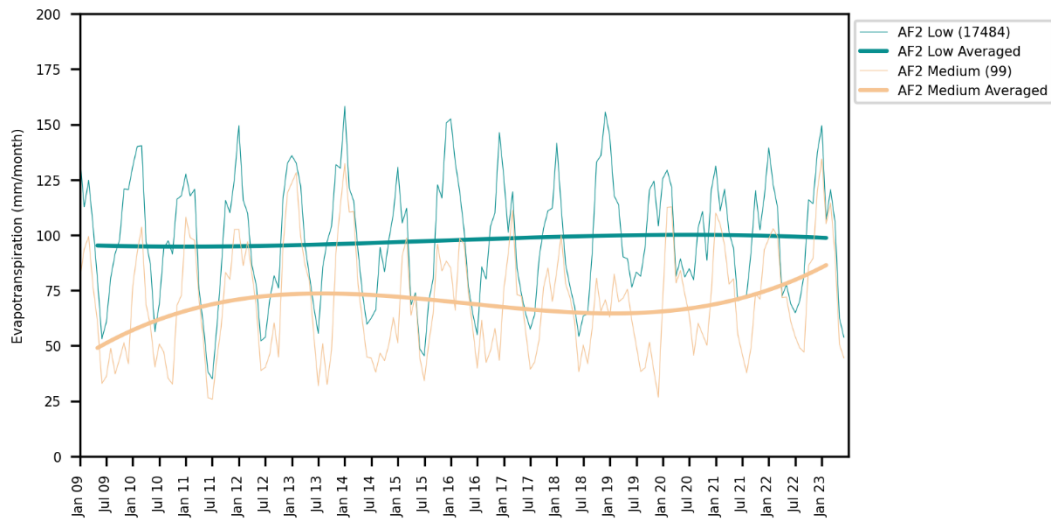


Figure 4-43 Evapotranspiration per vapour pressure deficit class during summer for AF2

VPD is an important concept in understanding the relationship between humidity and evaporation, particularly in the context of plants and their water use. It measures the difference between the actual amount of water vapour present in the air and the maximum amount of water vapour the air can hold at a given temperature (Grossiord *et al.*, 2020). VPD is closely related to temperature because warmer air can hold more water vapour, while high vapour pressure can increase the transpiration of plants, especially if soil moisture is limited. High VPD indicates a drier environment with a larger gap between the actual and potential water vapour content. This drier air has a greater capacity to absorb moisture, including water vapour released by plants through transpiration. Consequently, high VPD conditions can lead to increased water loss from plants, potentially causing stress or hindering growth if they cannot access sufficient water to compensate. However, based on our results, this relationship is inconsistent among the forest types. For instance, Figure 4-44 shows that the water use of AF3 is relatively high for patches falling in the medium VPD class (compared to the low class). Similar observations can be made for other forest types (see Appendix IV). This suggests that the relationship between VPD and water use is complex and depends on a range of other environmental factors.

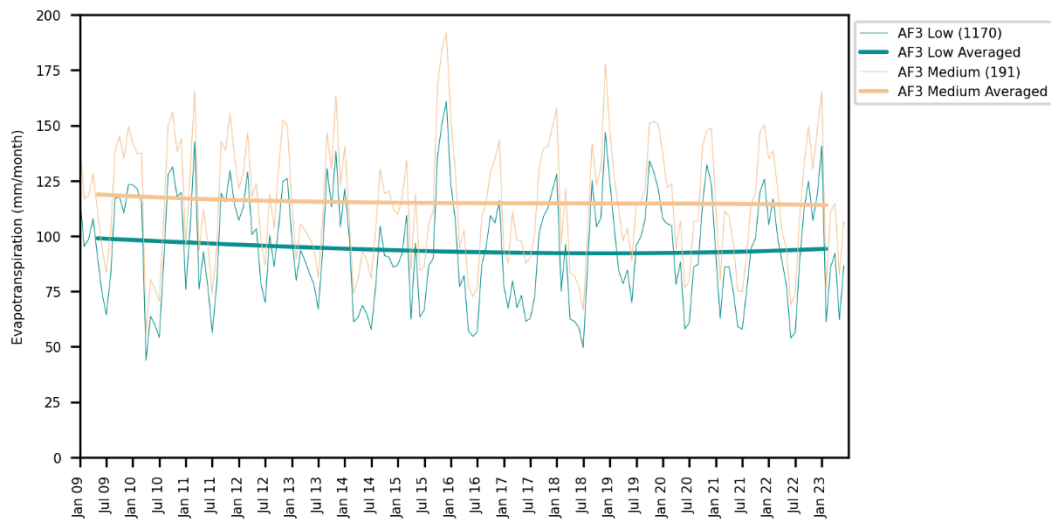


Figure 4-44 Evapotranspiration per vapour pressure deficit class during summer for AF3

4.2.3.5 Relative humidity

Although mean annual relative humidity (RH) ranked relatively low (13th) on the VIL of the water use machine learning model (Section 4.2.2), it was the fifth most important climatic variable. Figure 4-45 shows a map of the long-term annual RH, while Table 4-15 shows the percentage of each forest type that occurs within each humidity class (low, medium and high). Most of the forest types occur in the high RH class, while only two forest types, namely Arid Zone Riparian Woodland (ARF1) and Southern African Dry Thicket (TDFa3) are located in areas with low RH. ARF1 is also recorded as having the lowest mean annual RH (52%) of all classes (

Table 4-16). This can be expected given that these woodlands mainly occur along near-perennial rivers of the southern and eastern Kalahari and the Mesic Savanna. These forests survive in these dry (~223 mm rainfall per year) conditions thanks to water that is transported from higher rainfall areas through hydrological processes.

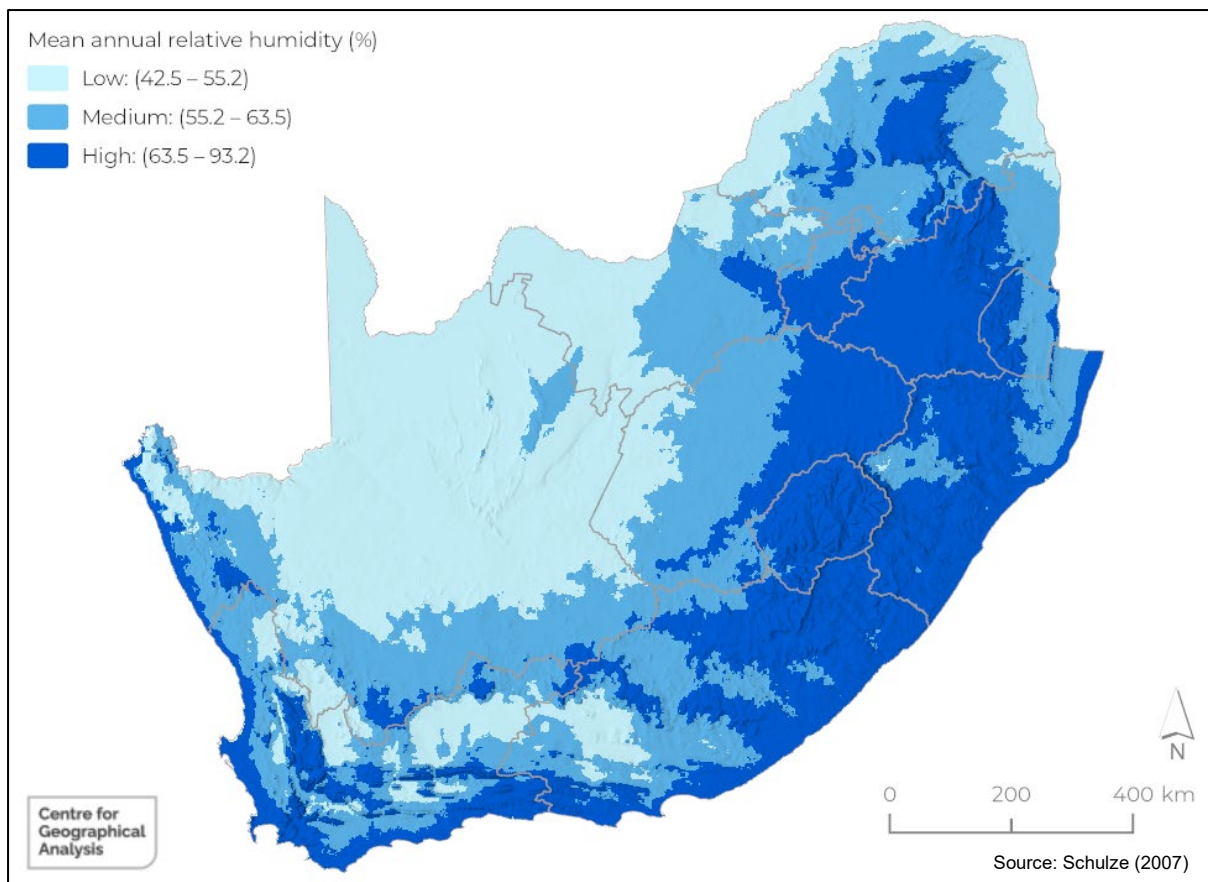


Figure 4-45 Annual relative humidity classes for South Africa

Subtropical Dune Woodland (ACF2) has the highest long-term annual RH (76%). These forests occur along the coast stretching from the Albany region of the Eastern Cape to Mozambique. The high RH is attributed to maritime affects, particularly the warm waters of the Mozambique current, which constantly releases water vapour into the atmosphere through evaporation. Cape Afrotemperate Forest (ACF1), Subtropical Indian Ocean Mangrove (AMAN1), Tropical Indian Ocean Mangrove (AMAN2) and Albany Coastal Forest (STFa5), Cape Milkwood Woodland (AF1) (although, perhaps to a lesser degree) are similarly affected as they are all found along the warm Indian Ocean and explain their high (>70%) RH values.

As with VPD, the relationship between RH and the water use of forests are generally weak (Figure 4-46). A water use graphs per RH class is provided in Appendix IV. As an example, Figure 4-47 shows the water use of East African Swamp Forest (ASF1) from 2009 to 2023. The impact of the drought during 2015-2016 is clearly visible. It seems that the forest patches with medium RH were more affected than those with high RH. But on average, the annual water use of this forest type is not much affected by RH, likely because these forests occur in areas with high soil moisture content.

Table 4-15 Mean annual relativity % class cover

Forest Type	Code	Low	Medium	High
Cape Milkwood Woodland	ACF1	0	0	100
Subtropical Dune Woodland	ACF2	0	0	100
Subtropical Indian Ocean Mangrove	AMAN1	0	0	100
Tropical Indian Ocean Mangrove	AMAN2	0	0	100
Arid Zone Riparian Woodland	ARF1	100	0	0
Cape Alluvial Woodland	ARF2	6	94	0
Highland Alluvial Woodland	ARF3	0	98	2
Subtropical Riparian Woodland	ARF4	0	88	12
East African Swamp Forest	ASF1	0	13	87
Cape Talus Forest	ATF1	0	32	68
Bushveld Talus Forest	ATF3	1	99	0
Drakensberg Afrotperate Forest	ATF4	0	11	89
Northern Highveld Afrotperate Forest	ATF5	0	0	100
Cape Afrotperate Forest	AF1	0	0	100
Southern Mistbelt Forest	AF2	0	1	99
Northern Mistbelt Forest	AF3	0	4	96
African Subtropical Coastal Forest	STFa2	0	11	89
Subtropical Scarp Forest	STFa4	0	1	99
Albany Coastal Forest	STFa5	0	0	100
Southern African Dry Forest	TDFa2	1	98	1
Southern African Dry Thicket	TDFa3	90	10	0

Table 4-16 Mean and standard deviation of annual relative humidity per fores type

Forest Type	Code	Annual relative humidity (%)	
		Mean	Standard Deviation
Arid Zone Riparian Woodland	ARF1	52.04	1.84
Southern African Dry Thicket	TDFa3	54.91	0.9
Cape Alluvial Woodland	ARF2	58.22	1.54
Bushveld Talus Forest	ATF3	58.51	0.93
Highland Alluvial Woodland	ARF3	59.66	1.95
Subtropical Riparian Woodland	ARF4	60.31	4.82
Southern African Dry Forest	TDFa2	60.57	1.48
Cape Talus Forest	ATF1	66.98	5.07
Drakensberg Afrotperate Forest	ATF4	67.83	3.25
African Subtropical Coastal Forest	STFa2	68.42	4.07
Northern Mistbelt Forest	AF3	69.32	2.55
East African Swamp Forest	ASF1	70.25	4.04
Northern Highveld Afrotperate Forest	ATF5	71.26	0.99
Southern Mistbelt Forest	AF2	71.37	2.43
Subtropical Scarp Forest	STFa4	71.62	3.67
Cape Milkwood Woodland	ACF1	71.86	2.65
Albany Coastal Forest	STFa5	72.56	2.2
Tropical Indian Ocean Mangrove	AMAN2	73.92	0.65
Subtropical Indian Ocean Mangrove	AMAN1	74.85	1.79
Cape Afrotperate Forest	AF1	75.28	2.07
Subtropical Dune Woodland	ACF2	75.82	1.51

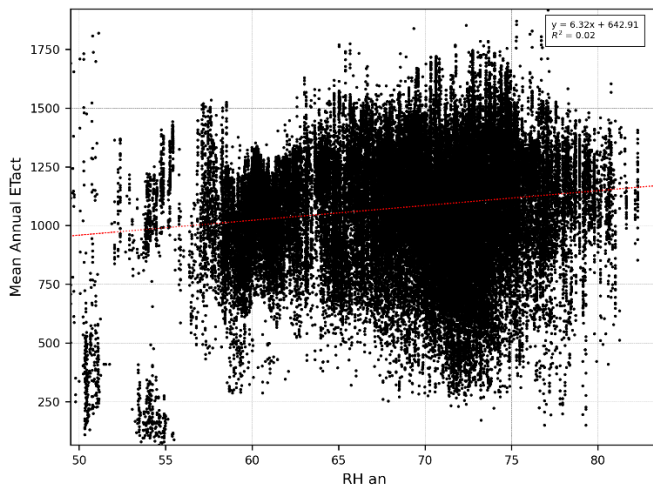


Figure 4-46 Linear regression between forest water use and long-term annual relative humidity

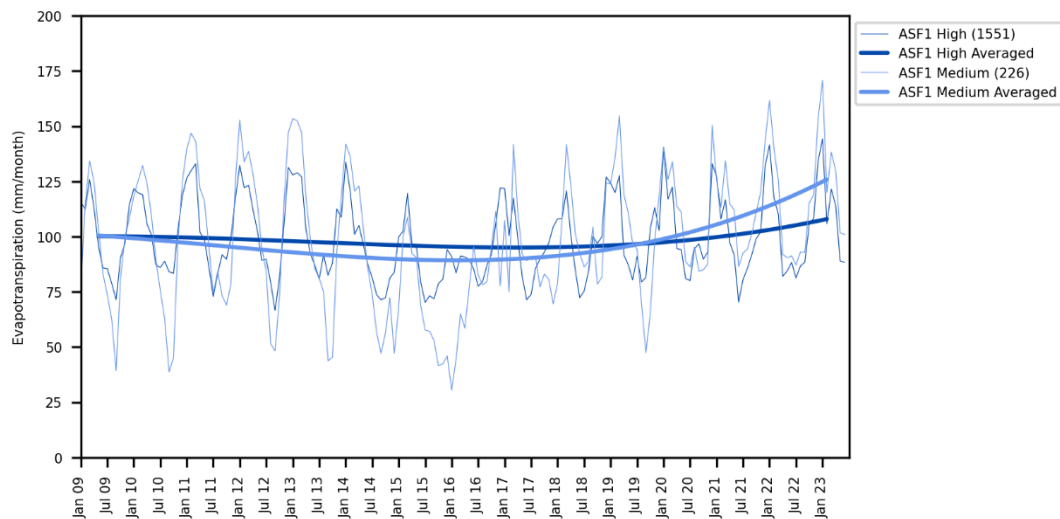


Figure 4-47 Evapotranspiration per annual relative humidity class for ASF1

There's a complex and dynamic relationship between plant water use and RH. When RH is high, the air is already close to saturation with water vapour. This creates a smaller gradient between the water vapour inside the leaf and the air outside, hindering the driving force for transpiration (water loss through leaves). Plants sense high RH through specialised sensors and may partially or completely close their stomata to prevent excessive water loss. This reduces transpiration but also limits CO₂ uptake for photosynthesis. Under high RH, plants can achieve the same level of photosynthesis with less water loss due to reduced transpiration. This improves their WUE. Conversely, when RH is low, there's a large gradient for water vapour, leading to increased transpiration as the plant attempts to balance internal and external water vapour concentrations. This can lead to water loss exceeding absorption, especially if soil moisture is limited (Farquhar & Sharkey, 1982).

This section explored the relationship between climate and the water use of forests. In particular, mean annual rainfall, solar radiation, heat units, vapour pressure deficit, and RH were investigated because these were the most important variables identified during the machine learning process. However, there are countless other climate-related variables that can be analysed. For the sake of brevity, two

additional climate-related variables, namely Köppen climate zones and rainfall seasonally, were analysed but excluded from the discussion. The results of the analyses can be found in Appendix IV. The next section considers the impact of terrain on the water use of forests.

4.2.4 Water use compared to terrain characteristics

Terrain plays an important role in the ecology of forests (Mucina, 2018) and there is a large number of terrain characteristics that can potentially affect forest water use. A total of nine terrain-related environmental variables were analysed and compared to forest water use. This section concentrates on the five most important terrain-related variables, as identified by the machine learning modelling (Section 4.2.2). These are terrain morphology, topographic openness, elevation, slope gradient and topographic position index. The data relating to the other four variables can be found in Appendix IV.

4.2.4.1 Terrain morphology

Terrain morphology was identified by the RF regression analysis (Section 4.2.2) as being the eighth most important environmental factor and the most important terrain-based factor related to water use of indigenous forests. The 27 morphology units covering South Africa, taken from Schulze (2007), were simplified by grouping similar morphology regions, as overviewed in Section 3.4.1. The resulting classification is shown in Figure 4-48.

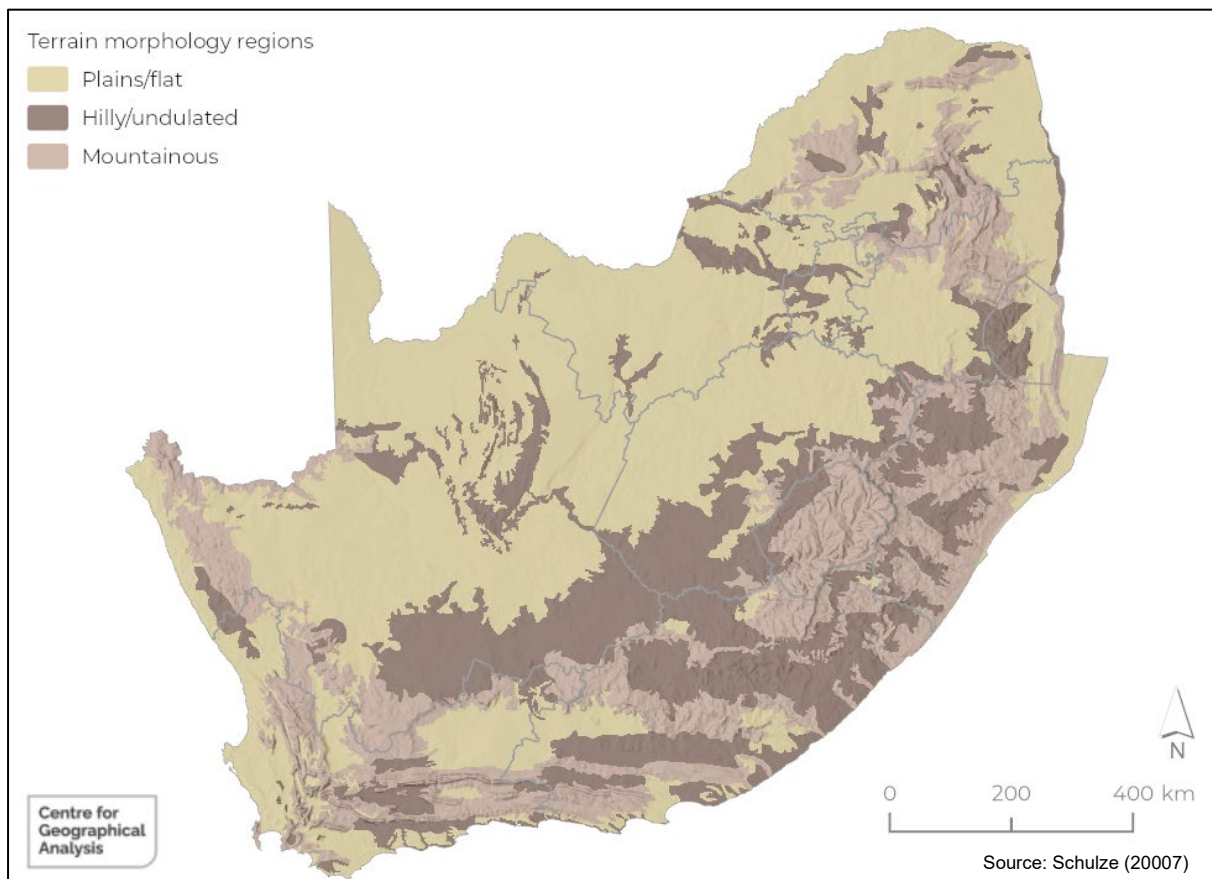


Figure 4-48 Simplified terrain morphology classes

Table 4-17 compares water use of forest types to the simplified terrain morphology types that intersect forests. Ten (48%) of the forest types prefer (>50% cover) plains and flat terrain, while six (29%) forest types (Cape Talus Forest and Northern Highveld Afrotropical Forest) only occur in mountainous landscapes. Cape Milkwood Woodland are found on Plains/flat and Hilly/undulated terrain.

Table 4-17 Terrain morphology type count per forest type (>50% in bold and shaded)

Forest Type	Code	Plains/flat	Hilly/undulated	Mountainous
Cape Milkwood Woodland	ACF1	49	51	0
Subtropical Dune Woodland	ACF2	93	5	2
Subtropical Indian Ocean Mangrove	AMAN1	95	1	4
Tropical Indian Ocean Mangrove	AMAN2	100	0	0
Arid Zone Riparian Woodland	ARF1	70	30	0
Cape Alluvial Woodland	ARF2	0	78	22
Highland Alluvial Woodland	ARF3	0	100	0
Subtropical Riparian Woodland	ARF4	71	6	23
East African Swamp Forest	ASF1	98	2	0
Cape Talus Forest	ATF1	0	0	100
Bushveld Talus Forest	ATF3	25	75	0
Drakensberg Afrotropical Forest	ATF4	0	3	97
Northern Highveld Afrotropical Forest	ATF5	0	0	100
Cape Afrotropical Forest	AF1	73	12	15
Southern Mistbelt Forest	AF2	0	32	68
Northern Mistbelt Forest	AF3	16	0	84
African Subtropical Coastal Forest	STFa2	88	0	12
Subtropical Scarp Forest	STFa4	3	30	68
Albany Coastal Forest	STFa5	14	86	0
Southern African Dry Forest	TDFa2	99	1	0
Southern African Dry Thicket	TDFa3	100	0	0

Figure 4-49 and Figure 4-50 demonstrate the complex relationship between terrain morphology and water use for Arid Zone Riparian Woodland (ARF1) and Cape Alluvial Woodland (ARF2), respectively. For ARF1, forests occurring on plain/flat landscapes used less water than those on hilly/undulated terrain. This difference is, however, not observed for ARF2. Such variations make the identification of patterns difficult.

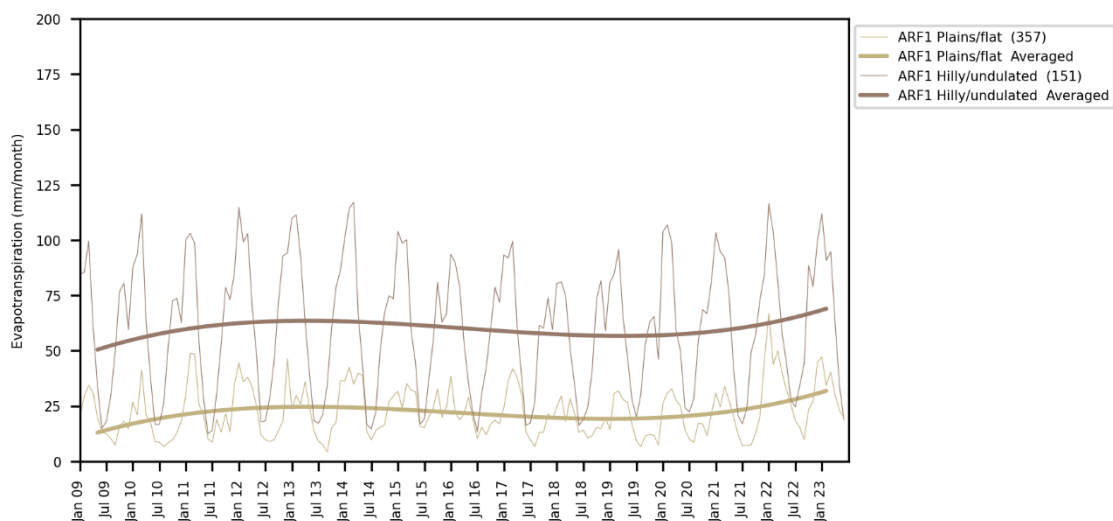


Figure 4-49 Evapotranspiration per terrain morphology class for ARF1

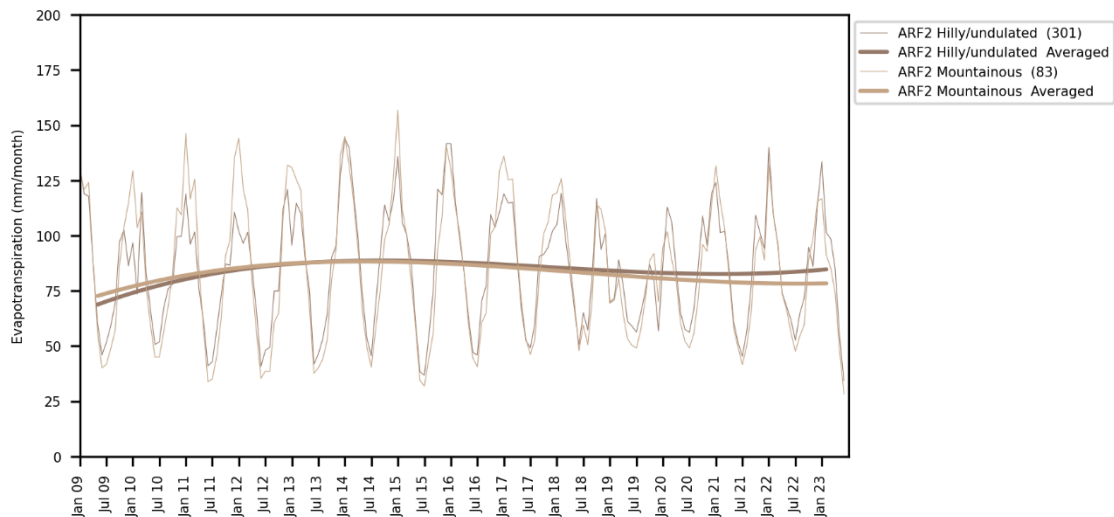


Figure 4-50 Evapotranspiration per terrain morphology class for ARF2

4.2.4.2 Topographic openness

TPO was identified as the second most important terrain-based forest water use driver. Similarly, topographic negative openness was identified as the fourth most important terrain-based forest water use driver. Their overall impact was ranked 9th and 11th respectively.

According to Li and McCarty (2019), topographic openness influences soil water content as it describes the distinction between relief and surrounding topographic features, with convex landforms exhibiting high positive topographic openness values, whereas concave landforms typically have high negative topographic openness values. The low positive openness areas are more likely to be depressional with high soil water contents, while the opposite is true for high positive openness (Figure 4-51). Topographical negative openness (TNO), which is essentially the inverse of TPO, is also featured among the ten most important variables driving water use (Section 4.2.2). Despite the near-inverse relationship between TNO and TPO, a correlation analysis (Figure 4-1) of these two variables showed that they are only moderately related ($R^2=0.54$), which suggests that both factors contributed to the variation of water use among forest types.

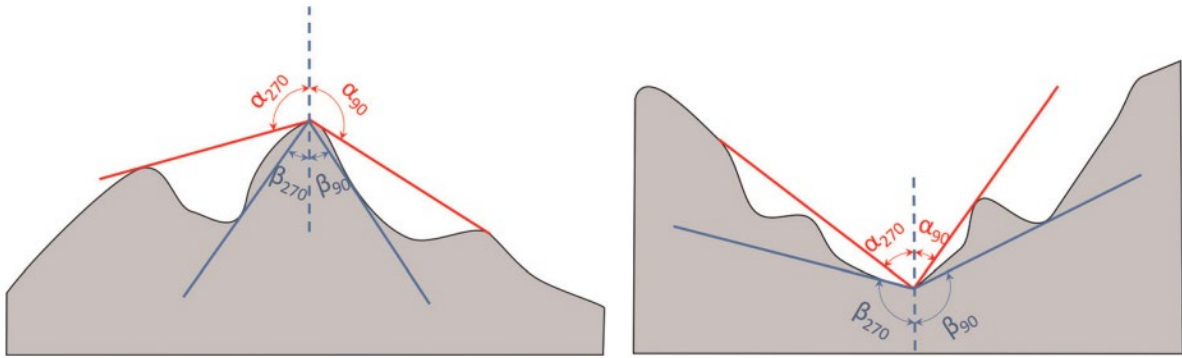


Figure 4-51 Positive (left) and negative (right) topographic openness along two profiles (Li & McCarty, 2019)

Maps of TPO and TNO of a section of the Nyonga forest are shown in Figure 4-52. At a glance one can see that these digital elevation model (DEM) derivatives emphasise crests (TPO) and valleys (TNO), which have been shown to influence the location of forest types in South Africa (Mucina, 2018).

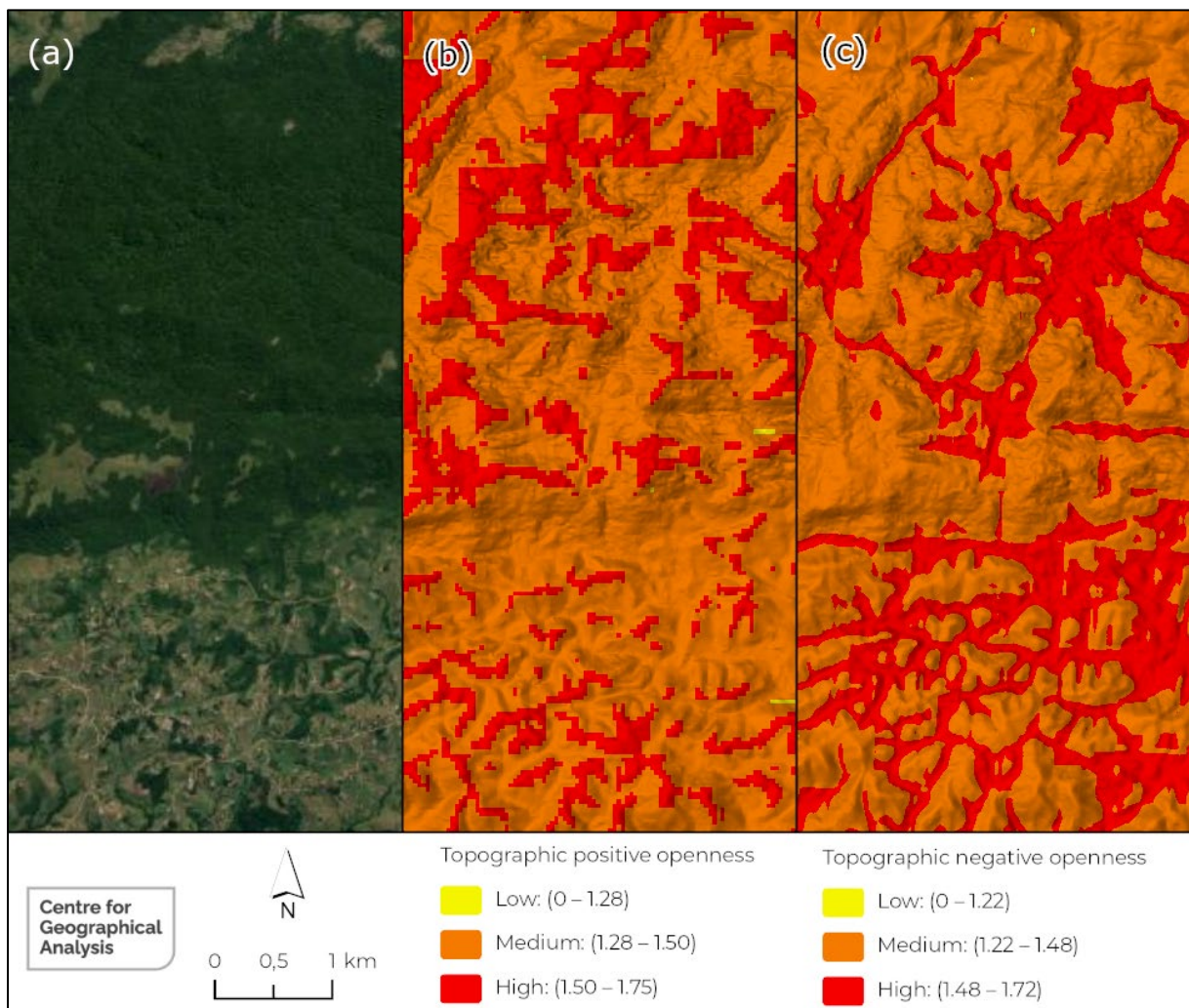


Figure 4-52 Area of Nyonga forest, with aerial view (a), Topographic positive openness (b), and Topographic negative openness (c)

Table 4-18 shows that the Southern African Dry Forest (TDFa2) has the highest TPO and TNO, which means that these forests occur in open areas surrounded by very few hills and mountains. This corresponds well with the known location of these forests on the coastal plains from St Lucia Lake and northward to the Mozambiquan border. In contrast, Northern Mistbelt Forest (AF3) have very low (≤ 1.35) TPO and TNO values, which corresponds well with the location of these forest types on the Lebombo Mountains piedmonts, which are depressional and concave.

Table 4-18 Mean and standard deviation of topographic openness (positive and negative) for each forest type

Forest Type	Code	Topographic Openness			
		Negative		Positive	
		Mean	Standard Deviation	Mean	Standard Deviation
Cape Milkwood Woodland	ACF1	1.51	0.04	1.50	0.06
Subtropical Dune Woodland	ACF2	1.48	0.06	1.50	0.05
Subtropical Indian Ocean Mangrove	AMAN1	1.55	0.02	1.55	0.03
Tropical Indian Ocean Mangrove	AMAN2	1.50	0.06	1.51	0.04
Arid Zone Riparian Woodland	ARF1	1.54	0.02	1.54	0.02
Cape Alluvial Woodland	ARF2	1.49	0.08	1.46	0.08
Highland Alluvial Woodland	ARF3	1.52	0.04	1.51	0.04
Subtropical Riparian Woodland	ARF4	1.53	0.06	1.51	0.07
East African Swamp Forest	ASF1	1.55	0.02	1.54	0.02
Cape Talus Forest	ATF1	1.39	0.09	1.36	0.08
Bushveld Talus Forest	ATF3	1.44	0.05	1.44	0.05
Drakensberg Afrotperate Forest	ATF4	1.40	0.09	1.32*	0.10
Northern Highveld Afrotperate Forest	ATF5	1.40	0.08	1.37	0.07
Cape Afrotperate Forest	AF1	1.44	0.07	1.44	0.08
Southern Mistbelt Forest	AF2	1.43	0.07	1.42	0.06
Northern Mistbelt Forest	AF3	1.35*	0.10	1.33	0.09
African Subtropical Coastal Forest	STFa2	1.53	0.04	1.53	0.04
Subtropical Scarp Forest	STFa4	1.43	0.08	1.41	0.08
Albany Coastal Forest	STFa5	1.44	0.07	1.45	0.07
Southern African Dry Forest	TDFa2	1.56**	0.01	1.56**	0.01
Southern African Dry Thicket	TDFa3	1.54	0.01	1.56	0.01

Table 4-19 and

Table 4-20 show that most of the forest types are classified as having high TNO and TPO values, indicating that they favour open landscapes.

Table 4-19 TNO % class cover per forest type

Forest Type	Code	Low	Medium	High
Cape Milkwood Woodland	ACF1	0	21	79
Subtropical Dune Woodland	ACF2	0	38	62
Subtropical Indian Ocean Mangrove	AMAN1	0	2	98
Tropical Indian Ocean Mangrove	AMAN2	0	31	69
Arid Zone Riparian Woodland	ARF1	0	3	97
Cape Alluvial Woodland	ARF2	1	32	67
Highland Alluvial Woodland	ARF3	0	14	86
Subtropical Riparian Woodland	ARF4	0	12	88
East African Swamp Forest	ASF1	0	1	99
Cape Talus Forest	ATF1	4	79	17
Bushveld Talus Forest	ATF3	0	77	23
Drakensberg Afrotperate Forest	ATF4	4	78	18
Northern Highveld Afrotperate Forest	ATF5	1	81	18
Cape Afrotperate Forest	AF1	1	73	27
Southern Mistbelt Forest	AF2	1	73	26
Northern Mistbelt Forest	AF3	11	81	8
African Subtropical Coastal Forest	STFa2	0	8	92
Subtropical Scarp Forest	STFa4	1	67	31
Albany Coastal Forest	STFa5	0	67	33
Southern African Dry Forest	TDFa2	0	0	100
Southern African Dry Thicket	TDFa3	0	0	100

Table 4-20 TPO % class cover per forest type

Forest Type	Code	Low	Medium	High
Cape Milkwood Woodland	ACF1	1	36	63
Subtropical Dune Woodland	ACF2	0	43	57
Subtropical Indian Ocean Mangrove	AMAN1	0	6	94
Tropical Indian Ocean Mangrove	AMAN2	0	25	75
Arid Zone Riparian Woodland	ARF1	0	4	96
Cape Alluvial Woodland	ARF2	4	48	48
Highland Alluvial Woodland	ARF3	0	33	67
Subtropical Riparian Woodland	ARF4	1	31	67
East African Swamp Forest	ASF1	0	7	93
Cape Talus Forest	ATF1	14	83	3
Bushveld Talus Forest	ATF3	0	92	8
Drakensberg Afrotperate Forest	ATF4	35	63	2
Northern Highveld Afrotperate Forest	ATF5	10	88	2
Cape Afrotperate Forest	AF1	5	73	22
Southern Mistbelt Forest	AF2	3	89	8
Northern Mistbelt Forest	AF3	29	69	1
African Subtropical Coastal Forest	STFa2	0	13	87
Subtropical Scarp Forest	STFa4	7	82	12
Albany Coastal Forest	STFa5	1	75	23
Southern African Dry Forest	TDFa2	0	0	100
Southern African Dry Thicket	TDFa3	0	0	100

Figure 4-53 shows the statistical relationship between topographical openness and water use of all forest types. In both cases, the relationship is weak ($R^2=0$). However, in Figure 4-54 one can see that for Northern Mistbelt Forest (AF3), areas with low TNO tend to use less water, whereas patches with high TNO water use is generally higher. This pattern also holds for some other forest types (see Appendix IV).

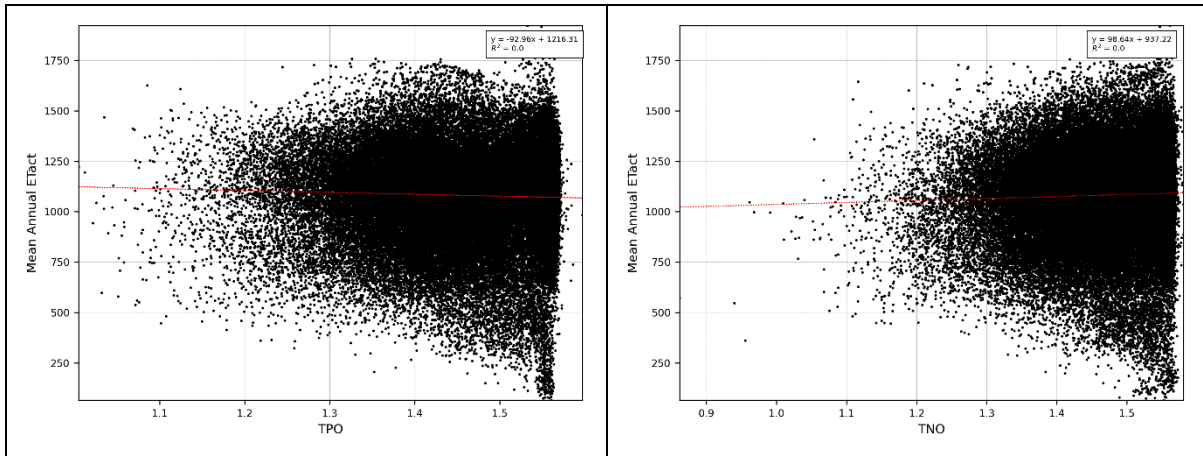


Figure 4-53 Linear regression between forest water use and positive (left) and negative (right) topographic openness, abbreviated as TPO and TNO respectively

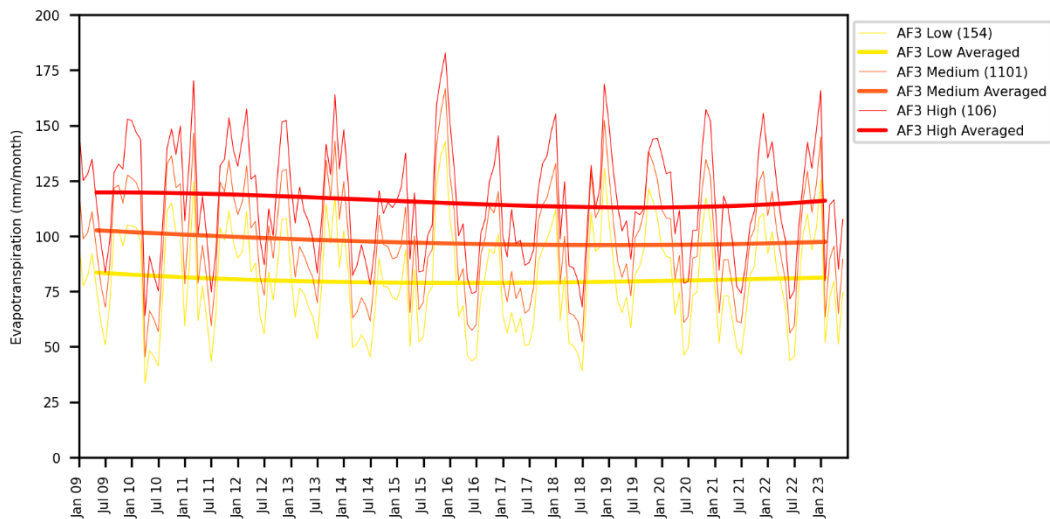


Figure 4-54 Evapotranspiration per topographic negative openness class for AF3

4.2.4.3 Elevation

Elevation (Figure 4-55) was identified as the third most important terrain-based driver for estimating forest type water use. Overall, it is ranked 10th, indicating that, likewise to topographic openness, it is not a major driver for determining forest type water use. Generally, temperatures decrease with increasing elevation, through a process called adiabatic cooling. This leads to lower evaporation rates, potentially increasing soil moisture content compared to lower elevations. However, colder temperatures in very high-lying areas can also limit plant growth and metabolic activity, reducing their overall water demand. Precipitation patterns can also greatly vary with elevation. Some regions experience heavier rainfall at higher altitudes due to atmospheric conditions, while others receive less due to rain shadow effects. This directly affects water availability for plants. Wind speed and direction can be stronger at higher elevations, causing increased evapotranspiration from plants and potentially drying out the soil. As noted in a previous section, likely the biggest way that elevation impact water use of forests is cloud cover (see explanation in Section 4.2.3.2).

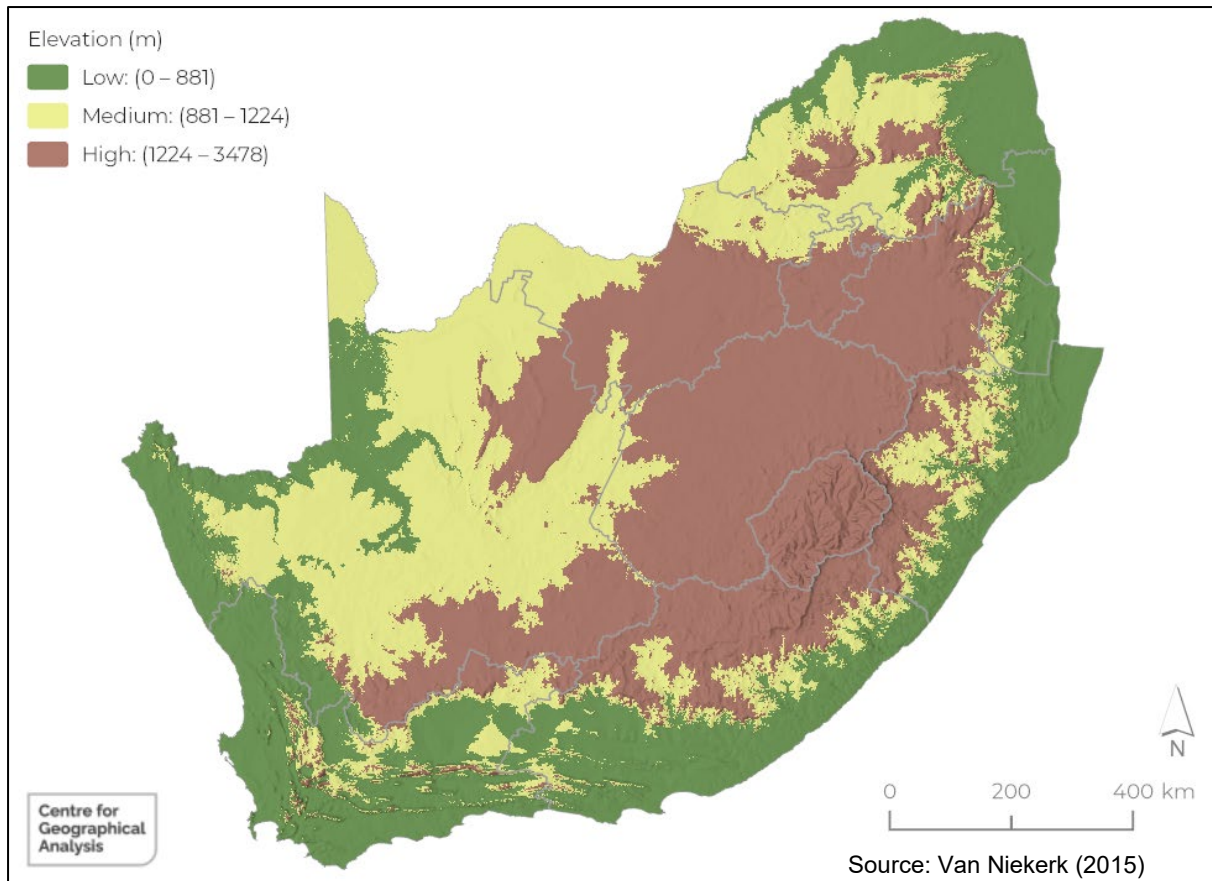


Figure 4-55 Elevation classes of South Africa

Table 4-21 shows the elevation ranges of each forest type. As can be expected, the mangrove and swamp forests are located at low elevations (<110 m on average). The forest types with the highest (>1 000 m on average) elevations are Highland Alluvial Woodland (ARF3) and Northern Mistbelt Forest (AF3). The Northern Mistbelt Forests are located in highly-lying areas from the Mpumalanga Escarpment (Barberton, Long Tom Pass, Blyde and Mariepskop areas), northwards along the northeastern Escarpment as far as Soutpansberg, while Highland Alluvial Woodlands are found in the Highveld along major rivers such as Vaal and upper Gariep. These two forest types are also the only types that were classified as being located in areas with high altitudes (Table 4-22). All the other forest types occur in low altitude areas.

Table 4-21 Mean and standard deviation of elevation per forest type

Forest Type	Code	Elevation (m)	
		Mean	Standard Deviation
Subtropical Indian Ocean Mangrove	AMAN1	30.62	33.53
Tropical Indian Ocean Mangrove	AMAN2	53.55	32.38
Northern Highveld Afrotperate Forest	ATF5	95.90	250.25
East African Swamp Forest	ASF1	109.36	294.3
Cape Milkwood Woodland	ACF1	111.60	58.31
Southern African Dry Forest	TDFa2	116.55	239.47
Subtropical Riparian Woodland	ARF4	171.3	257.48
Cape Alluvial Woodland	ARF2	211.52	89.65
Albany Coastal Forest	STFa5	215.83	64.67
Subtropical Dune Woodland	ACF2	227.73	466.47
Arid Zone Riparian Woodland	ARF1	235.19	96.61
African Subtropical Coastal Forest	STFa2	261.97	423.29
Cape Afrotperate Forest	AF1	334.56	149.81
Subtropical Scarp Forest	STFa4	355.49	378.94
Bushveld Talus Forest	ATF3	367.26	220.68
Cape Talus Forest	ATF1	383.08	191.66
Southern African Dry Thicket	TDFa3	443.90	119.46
Drakensberg Afrotperate Forest	ATF4	487.07	393.59
Southern Mistbelt Forest	AF2	849.66	359.85
Northern Mistbelt Forest	AF3	1281.97	231.07
Highland Alluvial Woodland	ARF3	1376.20	193.02

Table 4-22 Elevation % class cover per forest type

Forest Type	Code	Low	Medium	High
Cape Milkwood Woodland	ACF1	100	0	0
Subtropical Dune Woodland	ACF2	89	2	9
Subtropical Indian Ocean Mangrove	AMAN1	100	0	0
Tropical Indian Ocean Mangrove	AMAN2	100	0	0
Arid Zone Riparian Woodland	ARF1	100	0	0
Cape Alluvial Woodland	ARF2	100	0	0
Highland Alluvial Woodland	ARF3	2	0	98
Subtropical Riparian Woodland	ARF4	98	1	2
East African Swamp Forest	ASF1	96	1	3
Cape Talus Forest	ATF1	98	2	0
Bushveld Talus Forest	ATF3	100	0	0
Drakensberg Afrotperate Forest	ATF4	90	0	10
Northern Highveld Afrotperate Forest	ATF5	97	0	3
Cape Afrotperate Forest	AF1	99	1	0
Southern Mistbelt Forest	AF2	54	32	14
Northern Mistbelt Forest	AF3	4	38	58
African Subtropical Coastal Forest	STFa2	88	7	5
Subtropical Scarp Forest	STFa4	87	7	6
Albany Coastal Forest	STFa5	100	0	0
Southern African Dry Forest	TDFa2	97	2	2
Southern African Dry Thicket	TDFa3	100	0	0

Figure 4-56 shows a scatter plot of the water use of all forests and elevation above mean sea level. Although there seems to be slight positive relationship between water use and elevation, the model is weak ($R^2=0.0$).

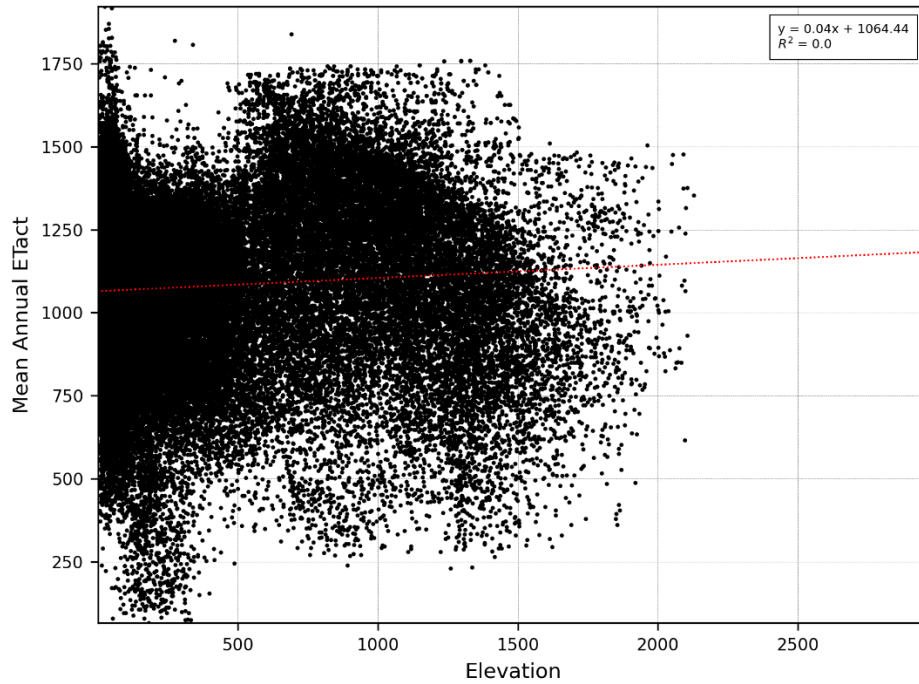


Figure 4-56 Linear regression between forest water use and elevation

The water use graphs for each forest type from 2009 to 2023 can be found in Appendix IV. For example, in the case of AF3 (Figure 4-57), water use is generally low at low altitudes and high at higher altitudes. But this tendency is not present for many of the other forest types that occur on multiple elevation classes (e.g. ACF2, AF2, ASF1, ATF1).

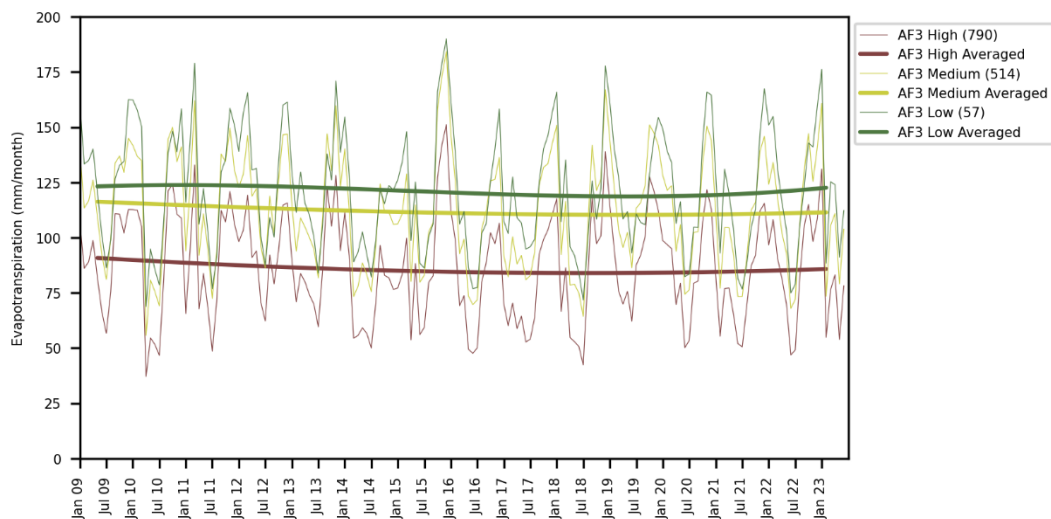


Figure 4-57 Evapotranspiration per elevation class for AF3

4.2.4.4 Slope gradient

Slope gradient was identified as being the 14th most important variable in the RF regression modelling of forest water use, and was the fourth most important terrain-based factor. Figure 4-58 is a slope gradient map, classified into level/gently inclined (0-5.7 degrees), moderately inclined/steep (5.7-29.25 degrees) and very steep (>29.25 degrees) slopes. The map effectively highlights the mountainous areas in South Africa. According to the correlation analysis (Figure 4-1) slope gradient had a negative relationship ($R^2=-0.55$) with soil depth. In other words, soil depth decreases as the slope gradient increases. There was also a negative relationship ($R^2=-0.48$) between heat units and slope gradient.

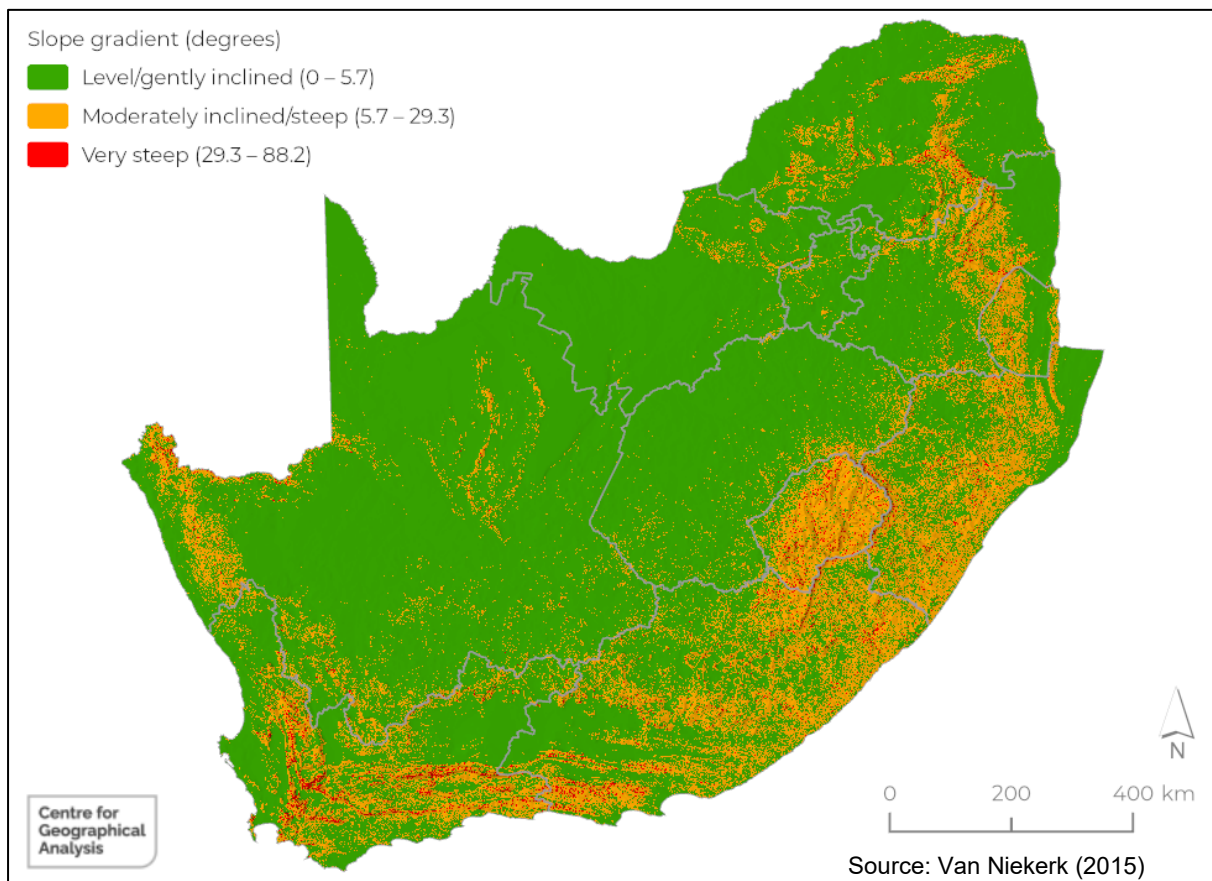


Figure 4-58 Slope gradient classes of South Africa

According to Table 4-23, the mean slope gradient of forest types ranges from less than one degree (Southern African Dry Thicket, 0.9°) to more than 20 degrees (Northern Mistbelt Forest, 22°). However, the standard deviation of the latter type is more than 10°, which suggests that Northern Mistbelt Forest (AF3) occurs in extremely rugged terrain.

Table 4-23 Mean and standard deviation of slope gradient per forest type

Forest Type	Code	Slope gradient (deg)	
		Mean	Standard Deviation
Southern African Dry Thicket	TDFa3	0.9	0.4
Southern African Dry Forest	TDFa2	1.3	1.1
Arid Zone Riparian Woodland	ARF1	1.6	1.6
Subtropical Indian Ocean Mangrove	AMAN1	1.8	2.9
East African Swamp Forest	ASF1	2.4	2.2
African Subtropical Coastal Forest	STFa2	3.7	3.8
Subtropical Riparian Woodland	ARF4	3.9	5.7
Highland Alluvial Woodland	ARF3	4.8	5.1
Cape Milkwood Woodland	ACF1	6.3	4.8
Tropical Indian Ocean Mangrove	AMAN2	6.6	6.1
Subtropical Dune Woodland	ACF2	7.7	6.5
Cape Alluvial Woodland	ARF2	7.9	8.4
Bushveld Talus Forest	ATF3	10.9	7
Albany Coastal Forest	STFa5	12.2	6.4
Cape Afrotropical Forest	AF1	12.6	7.5
Southern Mistbelt Forest	AF2	14.5	7.8
Subtropical Scarp Forest	STFa4	14.6	8.5
Cape Talus Forest	ATF1	17.9	8.5
Northern Highveld Afrotropical Forest	ATF5	19	8.5
Drakensberg Afrotropical Forest	ATF4	19.3	11.2
Northern Mistbelt Forest	AF3	22	10.9

Table 4-24 shows that a very small proportion of forests occur on very steep slopes. Most (57%) forest types are found on moderately inclined or steep slopes, while several (38%) also occur in level and gently included landscapes. The relationship between slope gradient and forest water use is multifaceted. Steeper slopes generally have faster water runoff, leaving less time for infiltration and reducing water accessibility for plants. This can lead to drier conditions compared to gentle slopes, where water has more time to soak into the soil. Depending on the aspect (the direction the slope faces), steeper slopes may receive more or less direct sunlight. North-facing slopes tend to be drier due to higher solar radiation and evaporation, while south-facing slopes might retain moisture better. Trees on steeper slopes often develop deeper and more extensive root systems to reach deeper water sources and anchor themselves against erosive forces (Temgoua *et al.*, 2016). In drier conditions, plants on steeper slopes often adopt water-saving mechanisms like smaller leaves, thicker cuticles to minimise evaporation, and stomatal control to regulate water loss. Different plant species are adapted to thrive on specific slope gradients based on their water requirements and tolerance to dryness. Some specialised plants excel in colonising steep, rocky slopes, while others prefer gentler slopes with better water availability (Asselin *et al.*, 2006).

Table 4-24 Mean slope % class cover per forest type.

Forest Type	Code	Moderately Inclined/Steep	Level/Gently Inclined	Very Steep
Cape Milkwood Woodland	ACF1	58.2	41.7	0.2
Subtropical Dune Woodland	ACF2	50.8	48.9	0.3
Subtropical Indian Ocean Mangrove	AMAN1	95.8	4.2	0.0
Tropical Indian Ocean Mangrove	AMAN2	56.3	43.8	0.0
Arid Zone Riparian Woodland	ARF1	97.2	2.8	0.0
Cape Alluvial Woodland	ARF2	57.3	40.4	2.3
Highland Alluvial Woodland	ARF3	77.6	22.4	0.0
Subtropical Riparian Woodland	ARF4	80.9	18.5	0.6
East African Swamp Forest	ASF1	93.0	7.0	0.0
Cape Talus Forest	ATF1	7.6	82.9	9.5
Bushveld Talus Forest	ATF3	27.4	71.0	1.5
Drakensberg Afrotperate Forest	ATF4	13.4	66.2	20.4
Northern Highveld Afrotperate Forest	ATF5	6.0	82.1	11.9
Cape Afrotperate Forest	AF1	16.0	80.3	3.8
Southern Mistbelt Forest	AF2	12.0	83.7	4.3
Northern Mistbelt Forest	AF3	3.4	74.4	22.3
African Subtropical Coastal Forest	STFa2	80.7	19.2	0.0
Subtropical Scarp Forest	STFa4	16.1	78.2	5.7
Albany Coastal Forest	STFa5	17.6	82.3	0.1
Southern African Dry Forest	TDFa2	99.0	1.0	0.0
Southern African Dry Thicket	TDFa3	100.0	0.0	0.0

The water use profiles for each forest type vs. slope gradient class are provided in Appendix IV. These graphs demonstrate the complexity of this relationship. For instance, Figure 4-59 to Figure 4-61 compare the impact of slope gradient on three forest types, namely Cape Afrotperate Forest (AF1), Southern Mistbelt Forest (AF2) and Northern Mistbelt Forest (AF3). In the first two cases (AF1 and AF2), slope gradient seems to have no impact, but for AF3 there seems to be a pattern of high water use as slope gradient decrease, likely because soils in flatter areas will likely retain more moisture for uptake by the tree roots.

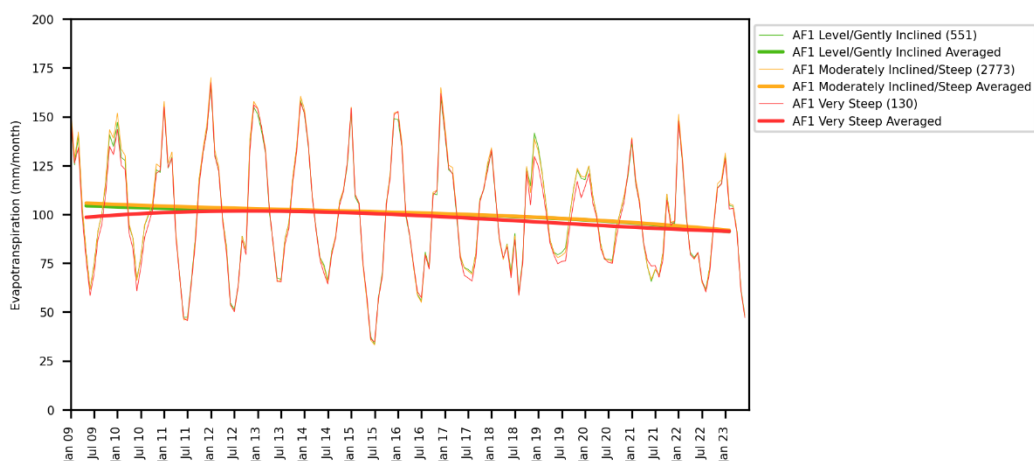


Figure 4-59 Evapotranspiration per slope gradient class for AF1

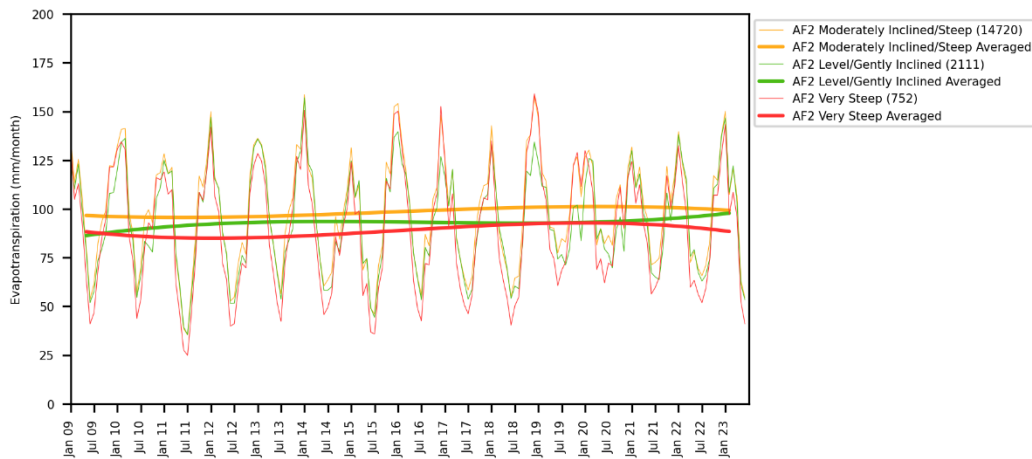


Figure 4-60 Evapotranspiration per slope gradient class for AF2

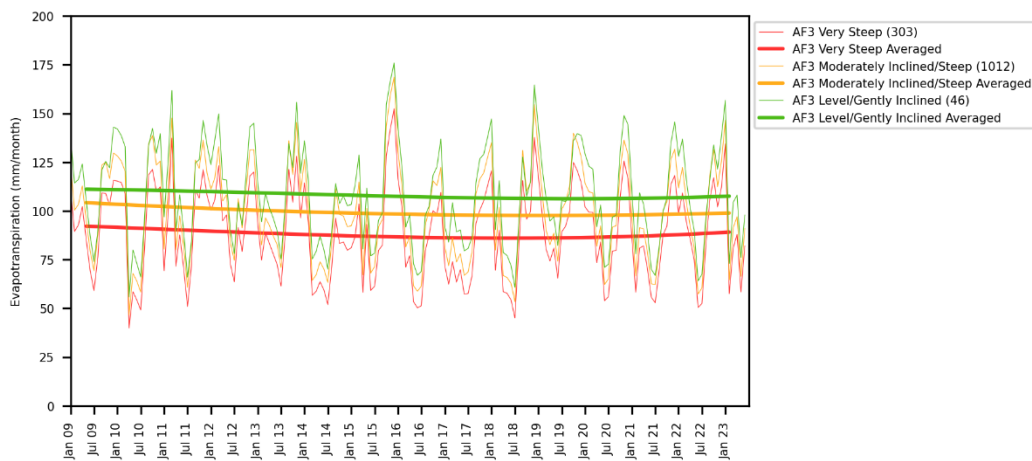


Figure 4-61 Evapotranspiration per slope gradient class for AF3

4.2.4.5 Topographic position index

Topographic position index (TPI) was identified as a less important driver in determining mean annual ET for forest types, ranking as the 6th most important terrain-based variable. Overall, however, it was ranked 17th. TPI is calculated as follows:

$$\text{TPI} = \text{Elevation}_{\text{central}} - \text{Average}(\text{Elevation}_{\text{surrounding}}) \quad \text{Equation 4-1}$$

where $\text{Elevation}_{\text{central}}$ is the elevation value in the centre of a region; and $\text{Average}(\text{Elevation}_{\text{surrounding}})$ is the average elevation if a region, excluding the central value.

Figure 4-62 shows the TPI for the Ngoya forest area. High TPI values represent crests, ridges and outcrops, while low TPI values represent valley bottoms. At a glance it would seem that TPI is similar to TPO and TNO, but the correlation between TPI and these two variables is not high ($R^2=0.37$ and $R^2=-0.27$ respectively), suggesting that TPI can be regarded as an important factor in the water use of forests.

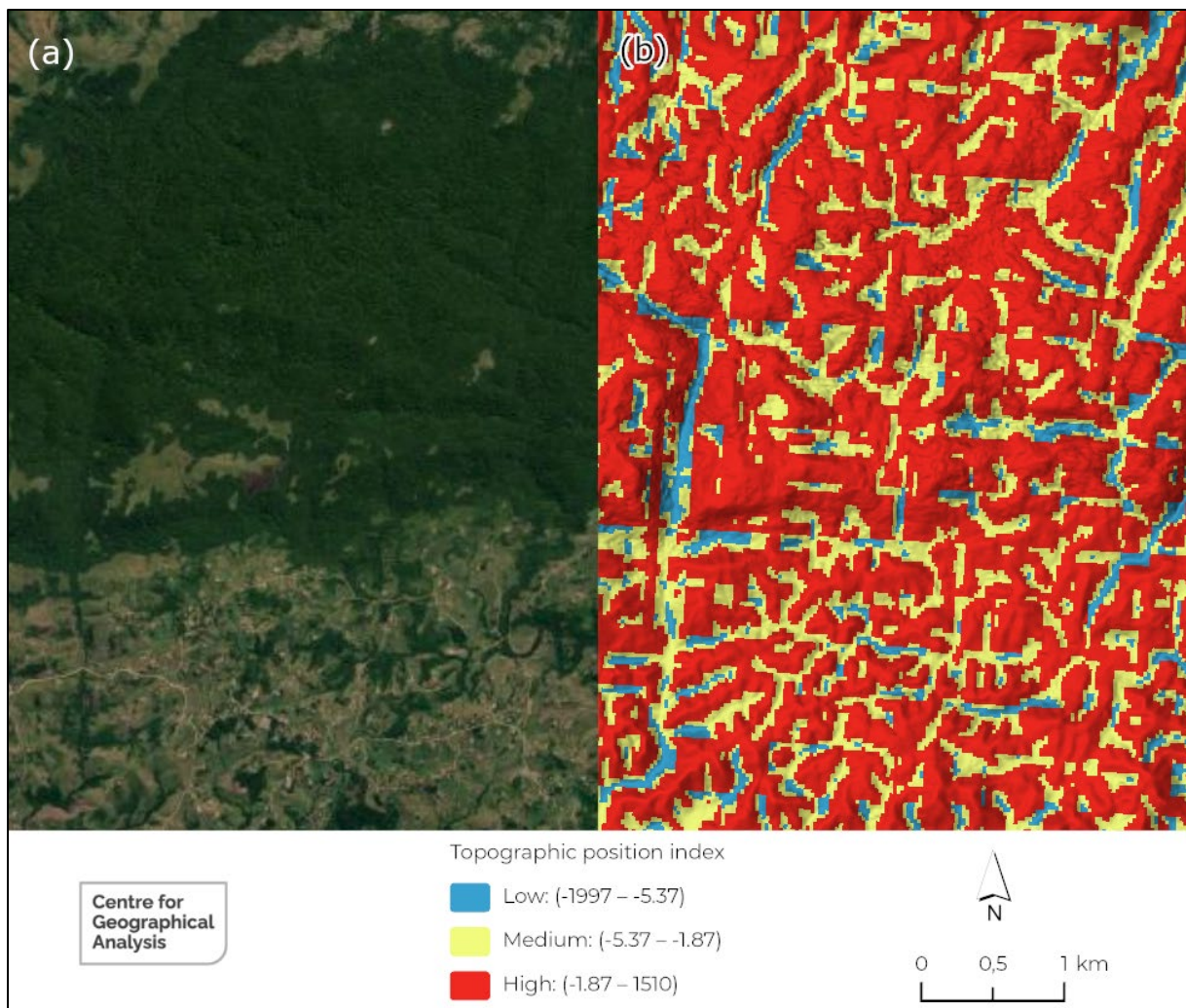


Figure 4-62 Ngoya forest area, with aerial image view (a) and topographic position index (b)

Table 4-25 shows that Drakensberg Afrotropical Forest (ATF4) had the lowest TPI values, which suggests that these forest types typically occur in narrow valley bottoms. However, the standard deviation of TPI for this class is very high (2.93), which means that the mean is not a good representation of the variance. In fact, most of the standard deviations in Table 4-25 are high compared to the mean values. Tropical Indian Ocean Mangrove (AMAN2) has by far the highest TPI values, suggesting that they occur on crests and high-lying areas. This is, however, not a true reflection of the ecology of these forests as they typically occur in very flat, inundated areas along the coast (which should have values close to zero). The high values reported here were caused by a few outlier patches of mangrove forest occurring on steeper slopes.

Table 4-25 Mean and standard deviation of topographic position index per forest type

Forest Type	Code	Topographic position index	
		Mean	Standard Deviation
Drakensberg Afrotropical Forest	ATF4	-1.31	2.93
Northern Highveld Afrotropical Forest	ATF5	-0.92	2.54
Cape Talus Forest	ATF1	-0.58	2.76
Northern Mistbelt Forest	AF3	-0.57	3.21
Cape Alluvial Woodland	ARF2	-0.45	1.78
Bushveld Talus Forest	ATF3	-0.36	1.62
Subtropical Scarp Forest	STFa4	-0.34	2.27
Cape Milkwood Woodland	ACF1	-0.23	1.48
Cape Afrotropical Forest	AF1	-0.19	1.90
Southern Mistbelt Forest	AF2	-0.12	1.84
Subtropical Riparian Woodland	ARF4	-0.12	1.11
East African Swamp Forest	ASF1	-0.07	0.55
Highland Alluvial Woodland	ARF3	-0.05	0.93
Arid Zone Riparian Woodland	ARF1	-0.01	0.35
Southern African Dry Thicket	TDFa3	0.00	0.17
African Subtropical Coastal Forest	STFa2	0.01	0.79
Southern African Dry Forest	TDFa2	0.03	0.28
Subtropical Indian Ocean Mangrove	AMAN1	0.04	0.47
Albany Coastal Forest	STFa5	0.04	1.84
Subtropical Dune Woodland	ACF2	0.08	1.36
Tropical Indian Ocean Mangrove	AMAN2	0.54	1.56

Table 4-26 shows that all of the forest types fall predominately in the high TPI category. This suggests that TPI is not such a good discriminator of forest types and explains why its importance in the RF model was lower than many of the other terrain variables.

Table 4-26 Topographic position index % class cover per forest type

Forest Type	Code	Low	Medium	High
Cape Milkwood Woodland	ACF1	1	8	91
Subtropical Dune Woodland	ACF2	0	4	96
Subtropical Indian Ocean Mangrove	AMAN1	0	1	99
Tropical Indian Ocean Mangrove	AMAN2	0	6	94
Arid Zone Riparian Woodland	ARF1	0	0	100
Cape Alluvial Woodland	ARF2	3	7	90
Highland Alluvial Woodland	ARF3	0	4	96
Subtropical Riparian Woodland	ARF4	0	4	96
East African Swamp Forest	ASF1	0	1	99
Cape Talus Forest	ATF1	4	21	75
Bushveld Talus Forest	ATF3	0	12	88
Drakensberg Afrotropical Forest	ATF4	7	25	67
Northern Highveld Afrotropical Forest	ATF5	6	18	76
Cape Afrotropical Forest	AF1	2	12	86
Southern Mistbelt Forest	AF2	1	9	90
Northern Mistbelt Forest	AF3	6	20	74
African Subtropical Coastal Forest	STFa2	0	2	98
Subtropical Scarp Forest	STFa4	2	16	82
Albany Coastal Forest	STFa5	1	9	90
Southern African Dry Forest	TDFa2	0	0	100
Southern African Dry Thicket	TDFa3	0	0	100

Graphs showing the relationship between forest water use and TPI is provided in Appendix IV. For instance, Figure 4-63 and Figure 4-64 show the profiles for African Subtropical Coastal Forest (STFa2) and Subtropical Scarp Forest (STFa4). In the case of African Subtropical Coastal Forest, there is a

noticeable difference in water use among low, medium and high TPI classes. However, for Subtropical Scarp Forest, there seems to be no difference among these classes.

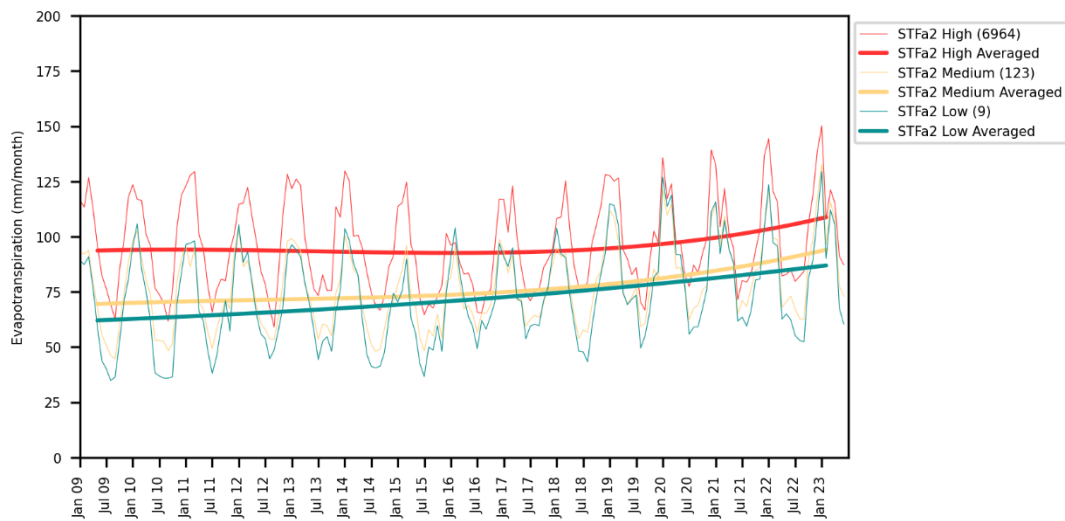


Figure 4-63 Evapotranspiration per TPI class for STFa2

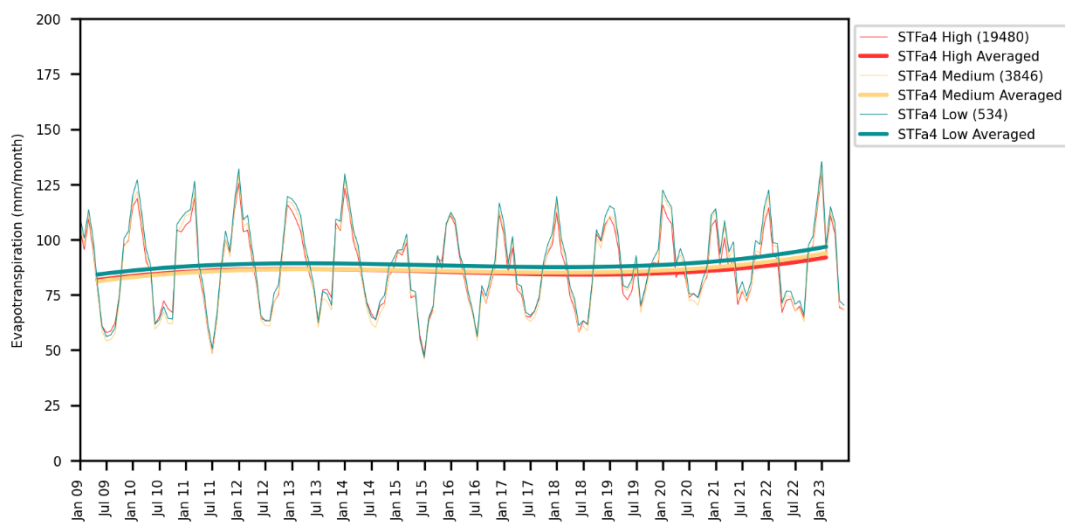


Figure 4-64 Evapotranspiration per TPI class for STFa4

Based on the machine learning analysis, there is a relationship between the water use of forests and terrain characteristics. However, based on the preceding sections, this relationship is highly complex, and it is very difficult to pinpoint exactly how terrain impacts water use. It is clear that terrain on its own does not drive water use but plays a role among other variables such as climate and soil. The next section delves deeper into the relationship between soil characteristics and the water use of forests.

4.2.5 Water use compared to soil characteristics

Different tree species are adapted to thrive in specific soil types based on their water requirements and tolerance to drought or waterlogging. Some specialise in colonising sandy soils with rapid drainage, while others excel in clay soils with high water retention capacity. The impact of soil characteristics, in particular soil depth and soil clay content, on the distribution of indigenous forest

types in South Africa is explored in the following two subsections.

4.2.5.1 Soil depth

Soil depth was ranked seventh in the VIL for determining mean annual ET for forests and was the most important soil-related variable. Figure 4-65 shows the soil depth distribution in South Africa, while Table 4-27 lists the mean and standard deviation of soil depth per forest type. Highland Alluvial Woodland (ARF3) has the lowest mean soil depth (399 mm). These forests occur on the banks of major rivers such as the Vaal and Gariep. The relatively shallow soils in these areas are likely attributed to erosional forces caused by seasonal flooding. Subtropical Dune Woodland (ACF2) has the deepest soils (1 290 mm). As the name suggests, these forests are established on dunes along the eastern coast. These dunes are characterised by deep, sandy soils.

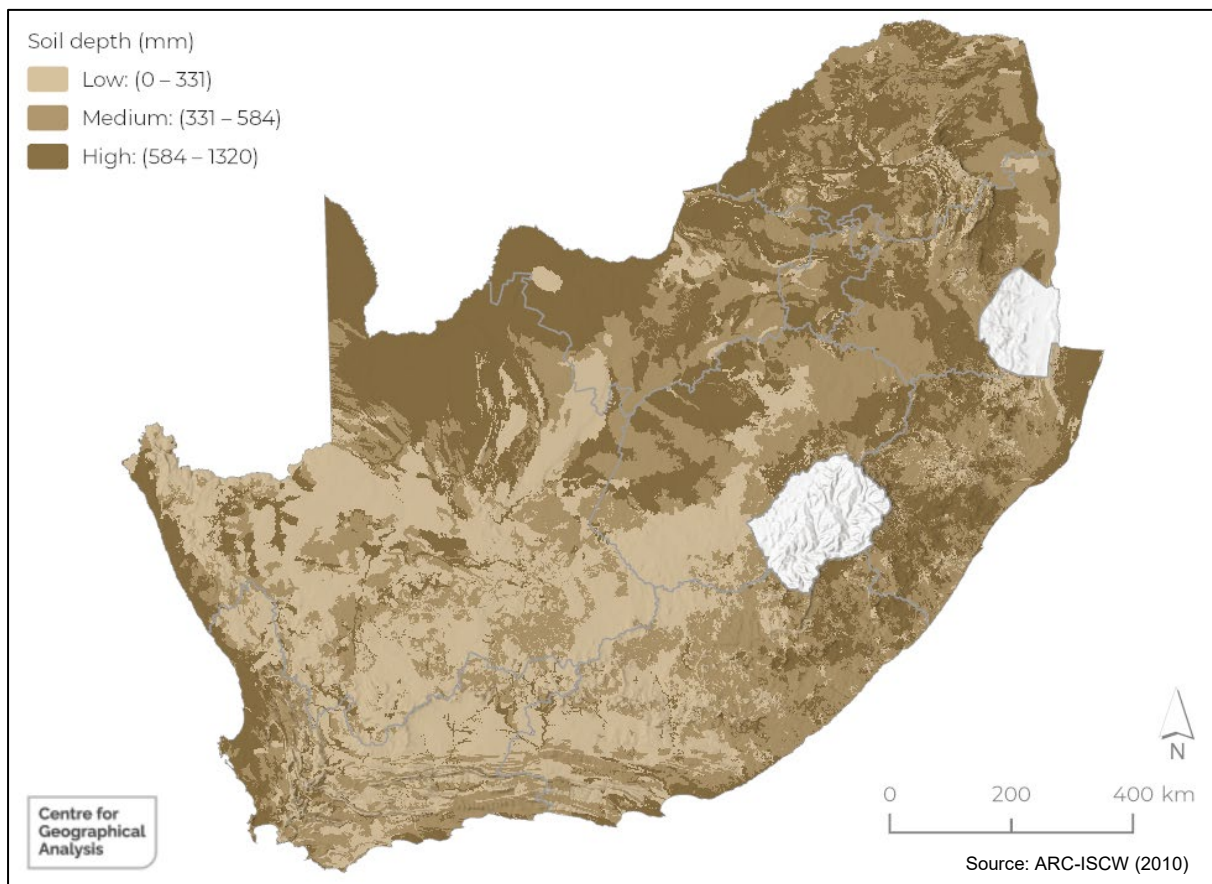


Figure 4-65 Soil depth classes of South Africa

Table 4-27 Mean and standard deviation of soil classes per forest type

Forest Type	Code	Soil depth (mm)	
		Mean	Standard Deviation
Highland Alluvial Woodland	ARF3	399.08	214.68
Cape Afrotperate Forest	AF1	401.98	133.02
Bushveld Talus Forest	ATF3	432.99	60.41
Cape Talus Forest	ATF1	448.15	181.51
Cape Alluvial Woodland	ARF2	453.92	185.30
Northern Mistbelt Forest	AF3	496.80	270.52
Subtropical Scarp Forest	STFa4	502.16	170.99
Drakensberg Afrotperate Forest	ATF4	559.34	122.36
Southern Mistbelt Forest	AF2	566.50	149.71
Northern Highveld Afrotperate Forest	ATF5	581.69	94.64
Arid Zone Riparian Woodland	ARF1	634.22	302.79
Subtropical Riparian Woodland	ARF4	727.62	315.82
Cape Milkwood Woodland	ACF1	729.78	264.93
Albany Coastal Forest	STFa5	938.09	99.31
African Subtropical Coastal Forest	STFa2	1054.51	415.30
Tropical Indian Ocean Mangrove	AMAN2	1069.22	513.68
Southern African Dry Thicket	TDFa3	1096.34	267.10
Subtropical Indian Ocean Mangrove	AMAN1	1174.75	307.60
East African Swamp Forest	ASF1	1228.18	220.21
Southern African Dry Forest	TDFa2	1260.50	160.25
Subtropical Dune Woodland	ACF2	1289.72	114.06

Table 4-28 shows that most (57%) of the forest types occur in soils that were classified as being deep (high), with Highland Alluvial Woodland being the only forest type occurring on shallow soils.

Table 4-28 Soil depth % class cover per forest type

Forest Type	Code	Low	Medium	High
Cape Milkwood Woodland	ACF1	0	30	70
Subtropical Dune Woodland	ACF2	0	1	99
Subtropical Indian Ocean Mangrove	AMAN1	4	2	94
Tropical Indian Ocean Mangrove	AMAN2	19	0	81
Arid Zone Riparian Woodland	ARF1	30	0	70
Cape Alluvial Woodland	ARF2	44	34	21
Highland Alluvial Woodland	ARF3	50	6	45
Subtropical Riparian Woodland	ARF4	12	26	61
East African Swamp Forest	ASF1	1	5	94
Cape Talus Forest	ATF1	28	40	32
Bushveld Talus Forest	ATF3	0	98	2
Drakensberg Afrotperate Forest	ATF4	5	48	47
Northern Highveld Afrotperate Forest	ATF5	1	21	79
Cape Afrotperate Forest	AF1	0	96	4
Southern Mistbelt Forest	AF2	3	54	44
Northern Mistbelt Forest	AF3	34	32	34
African Subtropical Coastal Forest	STFa2	7	17	76
Subtropical Scarp Forest	STFa4	12	68	20
Albany Coastal Forest	STFa5	0	1	99
Southern African Dry Forest	TDFa2	0	2	98
Southern African Dry Thicket	TDFa3	0	13	87

Figure 4-66 shows the statistical relationship between forest water use (all types) and soil depth is weak ($R^2=0.0$).

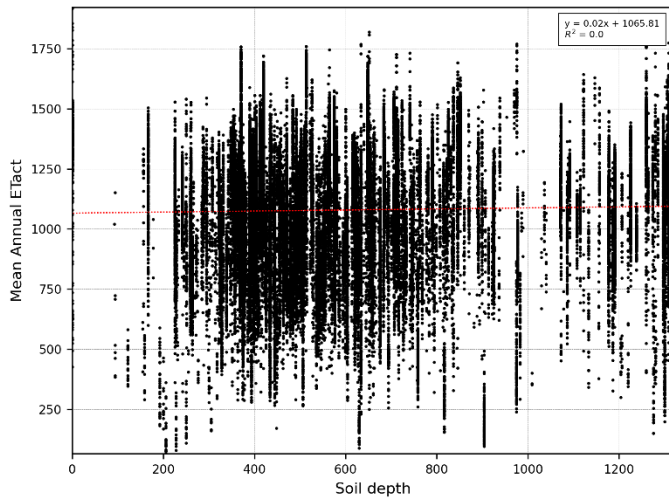


Figure 4-66 Linear regression between forest water use and soil depth

A range of graphs were created to better understand the relationship between soil depth and the water use of each individual forest type. These graphs are available in Appendix IV. As an example, Figure 4-67 shows that water use in Southern Mistbelt Forest (AF2) is lower where soils are shallow (low). This relationship holds for Northern Mistbelt Forest (AF3) (Figure 4-68), but there are among these forest types that occur in areas with soils classified as medium.

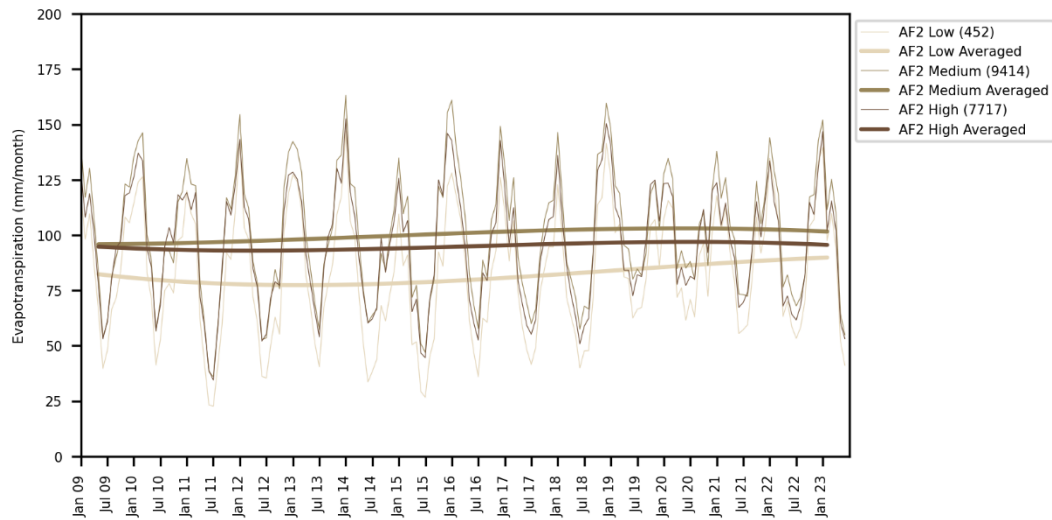


Figure 4-67 Evapotranspiration per soil depth class for AF2

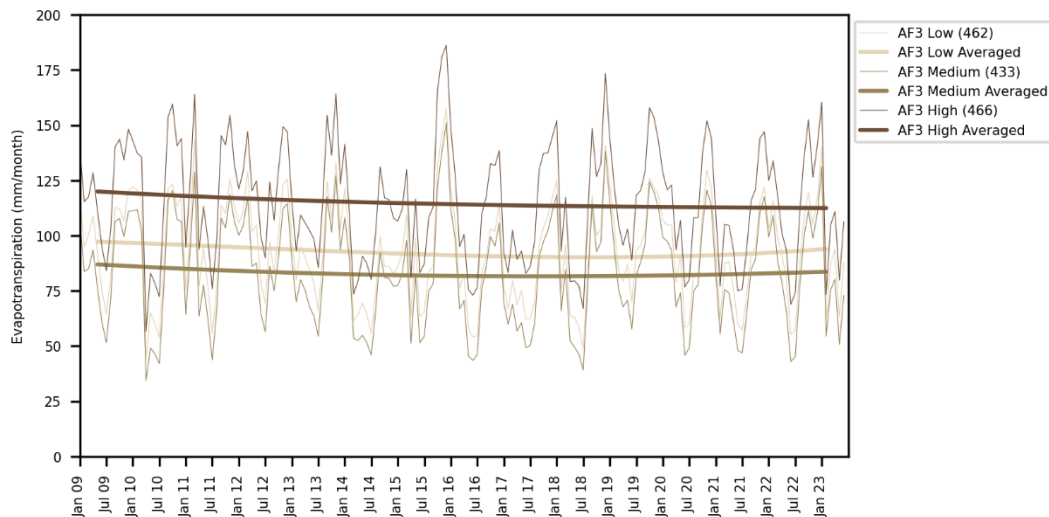


Figure 4-68 Evapotranspiration per soil depth class for AF3

Soils act as water storage mechanisms for plant life. Generally, deeper soils allow for a higher soil moisture content as they are less susceptible to evapotranspiration. Furthermore, deeper soils allow for plants and trees to tap into groundwater reserves via their root systems (Brevik *et al.*, 2017). Shallow soils offer limited water reserves, forcing plants to rely on frequent water uptake or adaptations to access deeper sources. Deeper soils have larger reservoirs, potentially requiring less frequent water use by plants. Shallow soils with less pore space tend to have faster drainage, reducing water retention and potentially leading to higher plant water use due to increased demand (Nimmo *et al.*, 2009). Deeper soils often allow for better infiltration and storage of water, potentially providing more readily available reserves for trees.

4.2.5.2 Soil clay percentage

Soil clay percentage was identified to be a significant driver in determining mean annual ET for forest types, ranking 5th in the VIL. Figure 4-69 shows a clay content map of South Africa. In general, soils are noticeably clayey in the eastern and northern parts of the country, while the Western Cape and Northern Cape have less clay content.

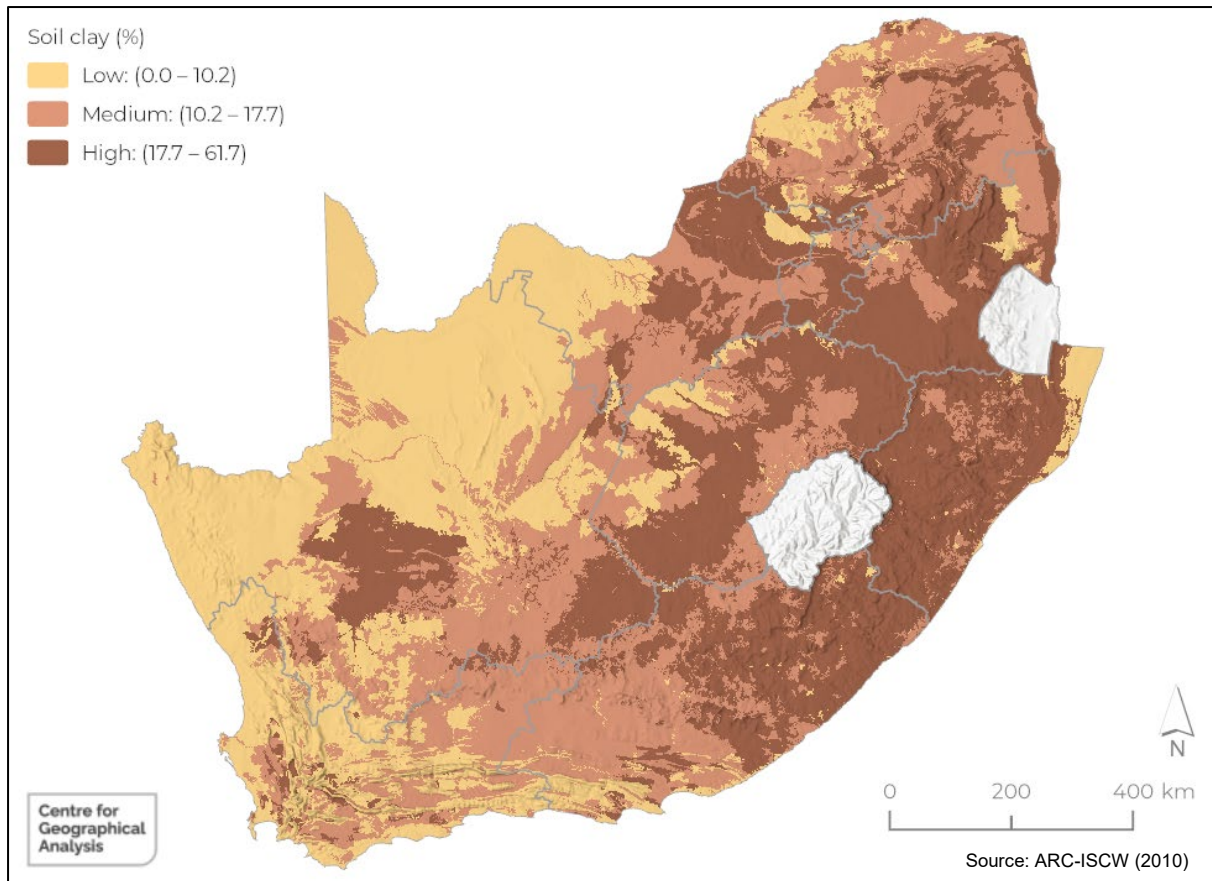


Figure 4-69 Soil clay % classes of South Africa

Table 4-29 shows that the soils of Tropical Indian Ocean Mangroves (AMAN2) have the lowest mean clay content (2.4%), while Northern Highveld Afrotropical Forest (ATF5) have the highest (35%).

Table 4-29 Mean and standard deviation of soil clay % per forest type

Forest Type	Code	Soil Clay (%)	
		Mean	Standard Deviation
Tropical Indian Ocean Mangrove	AMAN2	2.4	1.2
Cape Milkwood Woodland	ACF1	3.6	0.9
Subtropical Dune Woodland	ACF2	3.9	4.2
Southern African Dry Forest	TDFa2	5	6.2
Albany Coastal Forest	STFa5	7	2.4
Cape Alluvial Woodland	ARF2	7.7	2.5
Cape Afrotperate Forest	AF1	7.8	2.4
African Subtropical Coastal Forest	STFa2	8.9	10.1
East African Swamp Forest	ASF1	10.9	11.9
Arid Zone Riparian Woodland	ARF1	11.1	3.4
Cape Talus Forest	ATF1	12	6.2
Southern African Dry Thicket	TDFa3	13.9	9.7
Highland Alluvial Woodland	ARF3	15.7	4.5
Drakensberg Afrotperate Forest	ATF4	23.5	3.7
Subtropical Scarp Forest	STFa4	24.6	8
Subtropical Riparian Woodland	ARF4	27	11.4
Bushveld Talus Forest	ATF3	27.6	4.9
Subtropical Indian Ocean Mangrove	AMAN1	29.5	12.6
Southern Mistbelt Forest	AF2	30	5.6
Northern Mistbelt Forest	AF3	33.3	8.3
Northern Highveld Afrotperate Forest	ATF5	35.2	3.9

According to Table 4-30, most (57%) of the forest types occur on soils that were classified as having low clay content. Only Highland Alluvial Woodland is dominated by soils with a medium clay content, while Drakensberg Afrotperate Forest (ATF4) only occurs on soils with high clay content.

Table 4-30 Soil clay % class cover per forest type

Forest Type	Code	Low	Medium	High
Cape Milkwood Woodland	ACF1	100	0	0
Subtropical Dune Woodland	ACF2	97	0	2
Subtropical Indian Ocean Mangrove	AMAN1	16	1	83
Tropical Indian Ocean Mangrove	AMAN2	100	0	0
Arid Zone Riparian Woodland	ARF1	60	27	13
Cape Alluvial Woodland	ARF2	96	2	2
Highland Alluvial Woodland	ARF3	0	61	39
Subtropical Riparian Woodland	ARF4	7	4	89
East African Swamp Forest	ASF1	75	3	23
Cape Talus Forest	ATF1	57	8	35
Bushveld Talus Forest	ATF3	0	1	99
Drakensberg Afrotperate Forest	ATF4	0	0	100
Northern Highveld Afrotperate Forest	ATF5	0	1	99
Cape Afrotperate Forest	AF1	82	18	0
Southern Mistbelt Forest	AF2	0	3	97
Northern Mistbelt Forest	AF3	0	3	97
African Subtropical Coastal Forest	STFa2	75	5	19
Subtropical Scarp Forest	STFa4	1	21	78
Albany Coastal Forest	STFa5	97	2	1
Southern African Dry Forest	TDFa2	95	2	3
Southern African Dry Thicket	TDFa3	81	0	19

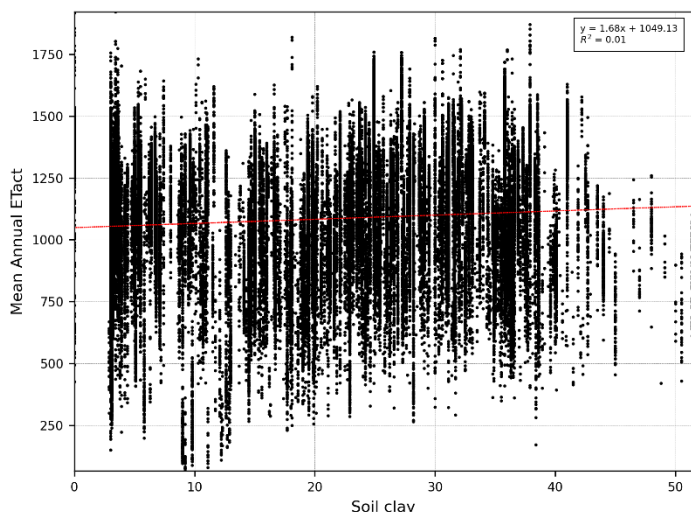


Figure 4-70 Linear regression between forest water use and soil clay

The 2009-2023 water use graphs in Appendix IV compare the impact of soil clay content on water use. Using Southern Mistbelt Forest (AF2) as an example (compared to soil depth graphs in the previous section), it seems that forests on soils classified as having a high clay content used more water than those classified as having a medium clay content.

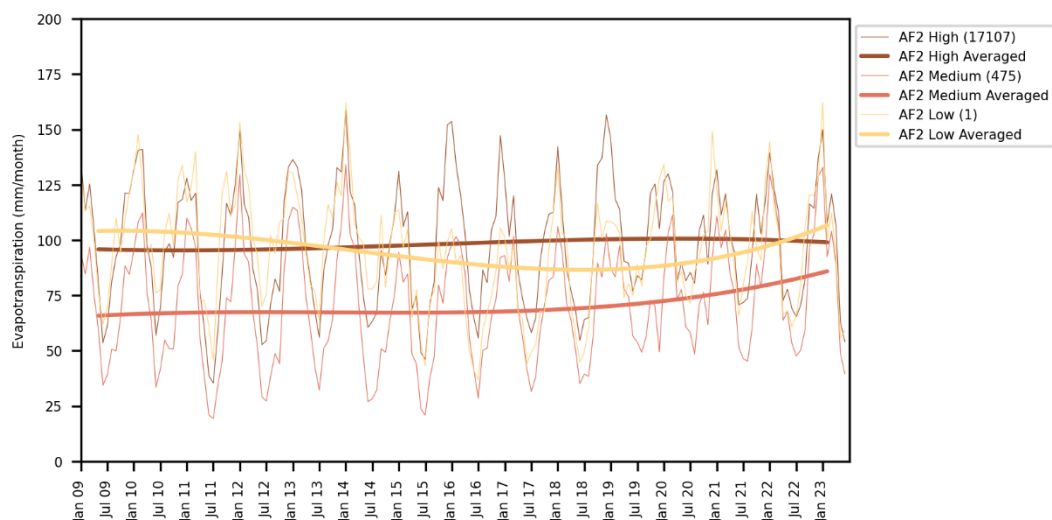


Figure 4-71 Evapotranspiration per soil clay % class for AF2

The forests with high clay content were also unaffected by the 2015-2017 drought. This can be expected as clayey soils have a higher capacity to retain soil moisture. The clay content of soils has a significant effect on the soil's water-holding capacity. Clay soils have smaller particles with larger total surface area than sandy soils, enabling them to hold more water compared to sandy soils (Nimmo *et al.*, 2009). This means there is potentially more water available for plants in clay soils. However, clay soils also tend to have smaller pore spaces and lower saturated hydraulic conductivity. This can lead to slower drainage and waterlogging after heavy rainfall, making the water less readily available for plant uptake. Reduced drainage in clay soils can negatively impact plant growth by limiting oxygen availability to roots. Poor aeration can hinder root development and function, ultimately affecting plant water uptake

efficiency. Trees in clay soils may develop shallower and denser root systems to maximise access to readily available water near the surface. This strategy balances the risk of waterlogging with efficient water capture. In well-drained clay soils with abundant water, plants may not face significant water stress. However, in poorly drained clay soils, some trees may adopt water-saving mechanisms like smaller leaves, thicker cuticles, and stomatal control to minimise water loss through transpiration (Hillel, 2003). Different plant species are adapted to thrive in specific clay content ranges based on their water requirements and tolerance to waterlogging. Some specialise in dry, sandy soils, while others excel in clay soils with abundant but potentially less accessible water.

4.2.6 Indigenous forest water use validation

Field-based measurements to validate the remotely sensed ET were not within the scope of this project. Instead, the project team had to rely on comparing the estimated WaPOR ET values to existing data and knowledge. The following subsections overview the extracted WaPOR ET values for indigenous forests and compare them to previous studies on the water use of indigenous forests, plantations and agriculture. A comparison of extracted WaPOR ET and reference ET is also included.

4.2.6.1 Comparison to literature and reference evapotranspiration

Few studies have focussed on quantifying the water use of indigenous forests of South Africa, and hence, limited transpiration (T) and ET data are available. Table 4-31 lists some of the relevant studies found in the literature and summarises the results. The studies represent a combination of field measurements and modelling. Some T data were collected for individual trees within indigenous forest patches and reported as L/tree/period. Often, this data were not upscaled to an entire forest stand, making comparison with the WaPOR ET data (used in this study) difficult. Another factor limiting direct comparisons between the WaPOR ET data and previous estimates is that the latter are often expressed in mm/period. Also, matching the forest types used in this study to the past forest type classifications and study locations from previous studies proved to be difficult.

Despite these challenges, some comparisons were possible. For instance, annual ET data are available for Cape Afrotemperate Forest (AF1) and Subtropical Scarp Forest (STFa4). Although the forest type classifications differ, we could also find relevant estimations for Arid Zone Riparian Woodland (ARF1) and Southern African Dry Thicket (TDFa3).

The ET of Cape Afrotemperate Forest was estimated in two past studies to be 933 and 1 175 mm/yr (Table 4-31). In our study, the WaPOR-based annual ET for Cape Afrotemperate Forest ranged from 428 to 1 713 mm/yr, with a median of 1 224 mm/yr (Table 4-3). The WaPOR ET estimate is consequently higher than what was estimated in previous studies.

This study's WaPOR ET for Subtropical Scarp Forest ranged between 129 and 1 913 mm/yr with a median annual ET of 1 054 mm/yr (Table 4-3). These estimates are substantially higher than the 668 mm/yr estimated by Dye *et al.* (2008c) (Table 4-31). In terms of Arid Zone Riparian Woodland, Dye *et al.* (2008a) estimated the ET of this forest type to be 1 094 mm/yr (Table 4-31), whereas the WaPOR

ET ranged from 29 to 2 106 mm/yr, with a substantially lower median of (296 mm/yr). As the name suggests, this forest type is typically found in riparian zones in an arid region and hence coarse resolution spatial data may present a mixed pixel effect and ET estimate. ET estimates from past studies on Southern African Dry Thicket (621 and 469 mm/yr, Table 4-31) were within the range of the WaPOR estimated ET (443 to 1 775 mm/yr) but were substantially lower than the median WaPOR ET value (1 153 mm/yr) (Table 4-3).

Direct comparisons of past studies with the long-term WaPOR data present challenges, but the large ranges in annual ET estimates are particularly concerning, as are the ET ranges across regions of different rainfall (summer vs all-year rainfall). The very high ET ranges suggest uncertainties in the WaPOR ET estimates used in this study.

According to Stanhill (2019), ET higher than 1400 mm/yr is rare and mainly occurs in equatorial regions. Specific conditions and combinations thereof (plant, climatic and environment) are required for very high ET to occur, including solar radiation, available water, vapour pressure deficit, plant leaf area, plant physiological control and advective conditions. The ETLook model used in the WaPOR ET estimates has been shown to produce very high ET (~2000 mm/yr) values for water bodies (Van Niekerk *et al.*, 2018). Consequently, it is likely that the water bodies surrounding forest patches may have influenced (increased) the extracted ET values in this project. For instance, Figure 4-72 shows a forested area where the extracted ET values exceed 1600 mm/yr. In most cases, the pixels contain a mixture of forests and water bodies, which could explain why ET is so high for these pixels. Although Van Niekerk *et al.* (2018) showed that, on average, such overestimations are balanced out by underestimations in pixels mixed with other land covers (e.g. bare ground), the location, sparse distribution and often small sizes of the forest patches evaluated in this study may have resulted in biases (under- or overestimations) within specific forest types.

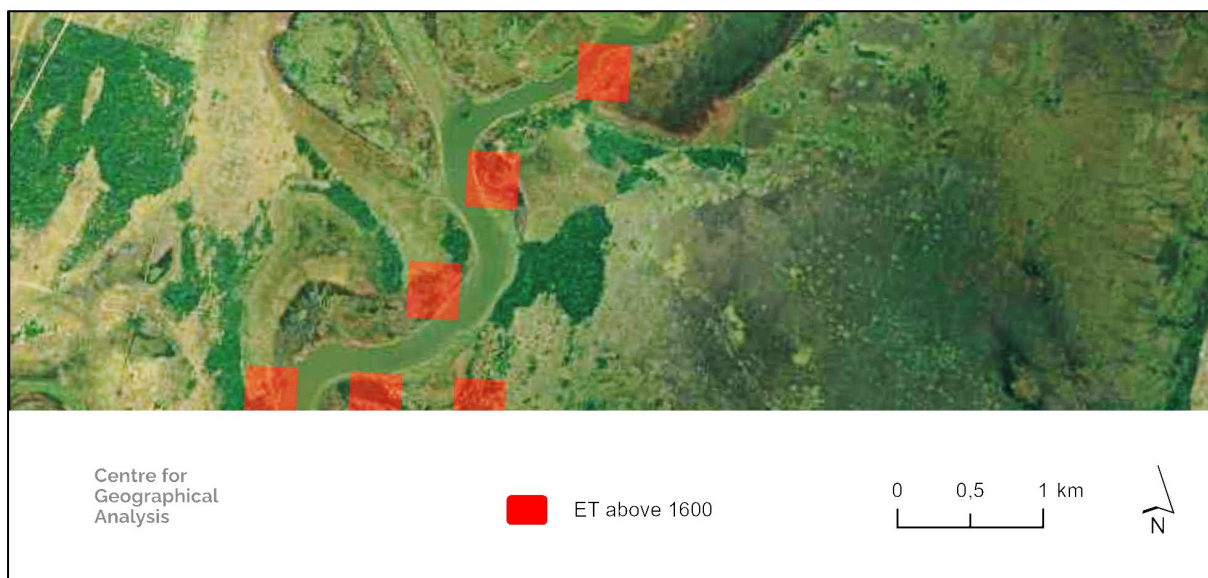


Figure 4-72 Examples of forested pixels with evapotranspiration values exceeding 1600 mm/yr

Figure 4-73 compares the international standard reference ET (ET_o) with WaPOR ET_a extracted at two

locations (pixels): one pixel that is fully covered by indigenous forest (green line) and a pixel that is only partly covered by indigenous forest (red line). The ETo was calculated for the 2020-2023 period from a nearby weather station. The monthly ETa data from the two pixels differed greatly, with the ET Actual (Forest) pixel estimates much higher than the ET Actual (Mixed pixel) values. There seems to be a reasonable temporal agreement between the ETa and ETo values. The ETa often exceeds the ETo estimates, which is likely since ETo represent ET from a well-watered grass surface with no water or nutrient limitations and a specific leaf area, contrasted to species rich indigenous forests often occurring in riparian zones.

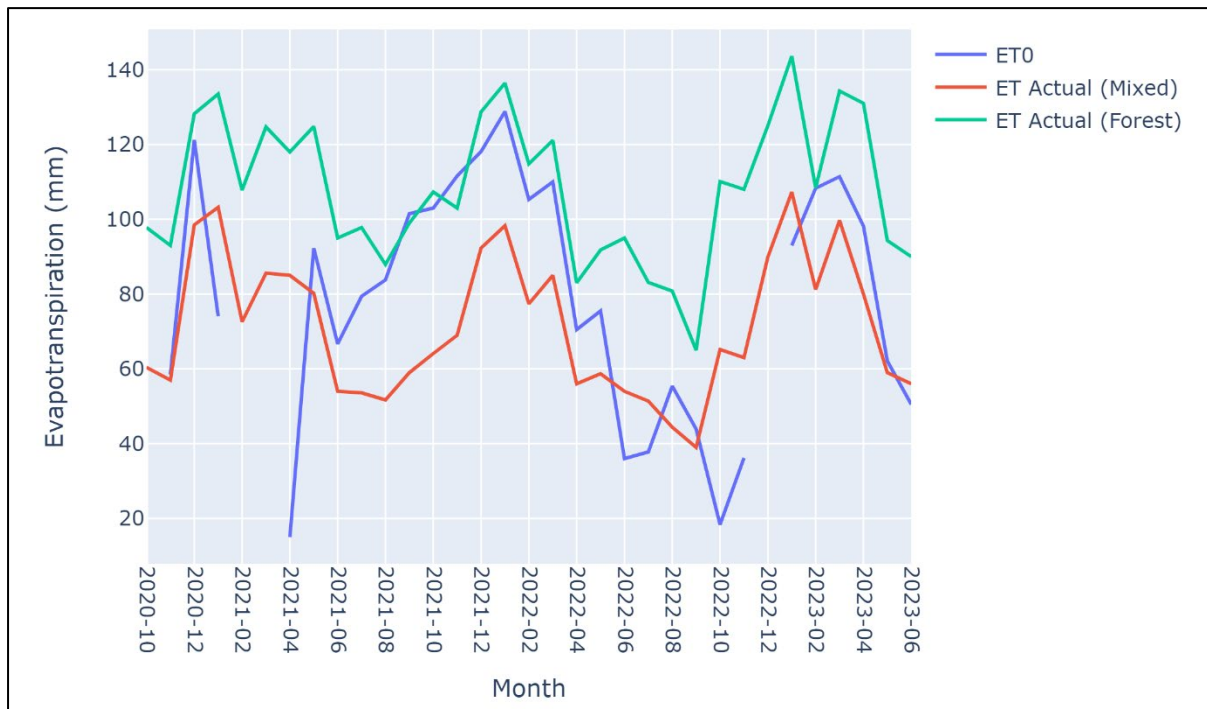


Figure 4-73 WaPOR actual evapotranspiration (ET Actual) extracted at two locations (Mixed and Forest) compared to reference evapotranspiration (ETo) obtained from a nearby a weather station

It is not possible to draw definite conclusions on the accuracy of the WaPOR ET estimates because there are a range of potential factors that can contribute to the uncertainties. Previous field studies were location-specific, and (until this study) no attempts have been made to study regional variations of ET within the context of indigenous forests. Nevertheless, it would be worthwhile to share the data from this study with the providers of the WaPOR data.

It is important that the uncertainties of the WaPOR data be taken into consideration when the water use estimations reported in this study are used. In the context of this study – in which the focus was not to definitively quantify the water use of indigenous forests but rather to enhance our understanding of how water use among different forest types vary and how such differences are influenced by environmental factors – these uncertainties will likely have minimal impact. Consequently, although it seems that the WaPOR product overestimates the ET of forests, the relative differences in ET among forest types are likely sufficient for the purposes of this project.

Table 4-31 List of South African studies estimating transpiration (T) and evapotranspiration (ET) from forest types. ET/T estimates are shown where available in mm, alternatively in L.

Reference	Title	Forest type listed in Reference	Current forest type	Coordinates	T/ET	Method
Clulow <i>et al.</i> (2013)	Water use dynamics of a peat swamp forest and a dune forest in Maputaland, South Africa	Peat swamp forest	ASF1 East African Swamp Forest	28° 10.1760' S 32° 30.0700' E	Peat swamp forest: Overstorey: 15800 L/20 months Mid-storey: 3500 L/20 months	Sapflow of individual trees
		Dune forest	ACF2 Subtropical Dune Woodland	28° 12.0170' S 32° 31.6330' E	Dune forest: Overstorey tree: 10400 L Mid-canopy: 6400 L Understorey tree water: 1100 L	
Dye <i>et al.</i> (2008b)	Water use in relation to biomass of indigenous tree species in woodland, forest and /or plantation conditions	Coastal Platform Forest	AF1 Cape Afrotropical Forest	33° 56.5' S 22° 33' E	Coastal platform forest: 933 mm/yr	Scintillometry, HPV, modelling
		Karkloof Mistbelt forest (3 trees) (<i>Celtis Africana</i> , <i>Podocarpus falcatus</i> , <i>Ptaeroxylon obliquum</i>)	AF2 Southern Mistbelt Forest	29° 18.230' S 30° 13.699' E	<i>Celtis</i> : 8.396 m ³ <i>Podocarpus</i> : 6.571 m ³ <i>Ptaeroxylon</i> : 4.407 m ³	Heat pulse velocity
		Weenen: Valley thicket <i>Euphorbia</i> , <i>Acacia</i> , <i>Cussonia</i> and <i>Olea</i>	No forest found	28° 50.842' S 30° 01.549' E	<i>Olea europaea</i> subsp. <i>Africana</i> : 5.223 m ³ <i>Berchemia zeyheri</i> : 6.103 m ³	
Dye <i>et al.</i> (2008a)	The potential of woodlands and reed beds for control of acid mine drainage in the Witwatersrand Gold Fields	<i>Rhus lancea</i> woodland	ARF1 Arid Zone Riparian Woodland (Trees within 1.5 km of)	26° 55.828' S 26° 46.810' E	Transpiration: Mean: 1094 mm/yr (976 to 1211 mm/yr)	Sapflow from 3 individual trees (scaled to leaf area)
Dye <i>et al.</i> (2008c)	Modelling vegetation water use for general application in different categories of vegetation	Sandveld Savanna	Kruger National park savanna	24° 39' S 28° 42' E	ET 469 mm/yr	Modelling, supported by measurement

Table continued from previous page

Reference	Title	Forest type listed in Reference	Current forest type	Coordinates	T/ET	Method
Dye <i>et al.</i> (2008c)	Modelling vegetation water use for general application in different categories of vegetation	Valley thicket	STFa4 Subtropical Scarp Forest (closest forest)		ET 668 mm/yr	
		Groenkop moist high forest/ southern Cape evergreen indigenous forests	AF1 Cape Afrotropical Forest	29° 19' S 30° 49' E (same as below)	ET: 1175 mm/yr	
Jarman <i>et al.</i> (2004)	Improving the basis for predicting total evaporation from natural veld types in South Africa: A focus on Moist Upland Grassland, Valley Thicket and Coastal Bushveld/Grassland.	Valley Thicket	STFa4 Subtropical Scarp Forest (closest forest)	29° 19' S 30° 49' E	Winter: <1 mm/d Summer: >6 mm/d	Bowen ratio, modelling ET
		Coastal bushveld/grassland	Unknown	-28.063981° 32.309516°	Winter: <2 mm/d Summer: 5-8 mm/d	
Pearson (2017)	An assessment of the water use of indigenous and introduced tree spp. and varying land uses around Vasi Pan, Maputaland, KwaZulu-Natal	Vasi pan indigenous forest	Unknown	Unknown	4.7 to 10 L/d	Heat pulse, eddy covariance
Scott-Shaw <i>et al.</i> (2017)	Water use dynamics of an alien-invaded riparian forest within the summer rainfall zone of South Africa	Eastern Mistbelt forest zone	AF2 Southern Mistbelt Forest (close to)	29° 28.03000' S 29° 52.04800' E	Individual trees: 283 (G. buxifolia) to 4307 L/yr (C. africana)	Sapflow

4.2.6.2 Comparison to agriculture

In a previous WRC study, Van Niekerk *et al.* (2018) estimated the mean annual ET for various agricultural crops in South Africa, both dryland and irrigated. The ET estimates were based on EO data for one year, and summary statistics are shown in Table 4-16. Median ET estimates ranged between 500 and 911 mm/yr, considering all data. Irrigated crop ET ranged between 911 (irrigated citrus) and 553 mm/yr (other irrigated fruit). These median ET estimates are generally substantially lower than the indigenous forest median ET estimates from this study, ranging from 296 (Arid Zone Riparian Woodland) and 1 338 mm/yr (Subtropical Indian Ocean Mangrove) (Table 4-3). The exceptions were Arid Zone Riparian Woodland, Highland Alluvial Woodland and Cape Milkwood Woodland, with median annual ET estimates of < 520 mm/yr.

Table 4-32 Estimated water use (ET) statistics for selected crop types (Van Niekerk *et al.*, 2018)

Crop type	Rainfall season	Group	# samples / pixels	Max ET (mm/yr)	Median ET (mm/yr)	Mean ET (mm/yr)	Standard deviation (mm/yr)	Area considered (ha)
Maize	Summer	All	72 969	1 385	615	618	113	1 771 083
		Irrigated	3 689	1 385	737	764	187	76 246
		Rainfed	69 280	1 378	611	610	102	1 694 837
Wheat	Summer	All	1 558	1 088	600	591	109	40 907
		Irrigated	217	1 088	658	655	136	4 038
		Rainfed	1 341	1 069	597	581	100	36 870
Other small grains	Summer	All	3 335	1 290	590	590	93	50 934
		Irrigated	184	1 129	660	663	189	4 050
		Rainfed	3 151	1 290	589	586	82	46 884
Vegetables	Summer	All	30 085	1 380	637	646	100	545 822
		Irrigated	1 445	1 380	771	789	180	18 843
		Rainfed	28 640	1 354	634	639	89	526 979
Grapes – Table	Winter	All	5 726	1 368	782	788	261	12 381
		Irrigated	5 638	1 368	786	791	260	12 192
Grapes – Wine	Winter	All	41 315	1 399	571	595	190	106 022
		Irrigated	39 937	1 399	574	598	190	103 010
		Rainfed	1 378	1 126	500	528	172	3 012
Grapes – Other	Summer	Irrigated	145	1 315	793	754	254	403
Fruit – Citrus	Winter	Irrigated	5 708	1 400	678	696	221	11 731
	Summer	Irrigated	164	1 396	911	925	206	403
Fruit – Stone	Winter	Irrigated	11 145	1 399	632	655	256	21 918
Fruit – Pome	Winter	Irrigated	15 702	1 398	833	828	237	31 322
Fruit – Other	Winter	Irrigated	1 425	1 331	553	572	210	3 002
Oil seeds	Summer	All	11 656	1 386	508	510	102	290 047
		Irrigated	589	1 386	619	628	173	8 257
		Rainfed	11 067	941	504	504	93	281 790
Lucerne	Summer	Irrigated	1 001	1 396	825	831	251	17 875
Other pastures & forages	Summer	All	199 861	1 397	539	537	123	2 157 027
		Irrigated	7 213	1 394	612	630	175	42 749
		Rainfed	192 648	1 397	536	534	119	2 114 279
Sugarcane	Summer	All	208 095	1 400	756	744	155	279 414
		Irrigated	13 031	1 400	906	914	196	55 929
		Rainfed	195 064	1 399	750	732	145	223 485

4.2.6.3 Comparison to commercial forestry

In a WRC study by Van Niekerk *et al.* (2023), long-term WaPOR ET estimates were extracted for three major commercial forestry genera of South Africa, namely *Acacia*, *Eucalyptus* and *Pinus*. The ET statistics are shown in Table 4-33. Long-term median ET for the three genera did not vary greatly, with the highest estimate for *Eucalyptus* (1 123 mm/yr), followed by *Acacia* (1 096 mm/yr) and *Pinus* trees (1 035 mm/yr). These median ET estimates are within the range of most indigenous forest type ET estimates, except for some woodlands (Arid Zone Riparian Woodland, Highland Alluvial Woodland, Cape Milkwood Woodland) and the Afrotropical forests (Drakensberg Afrotropical Forest and Northern Highveld Afrotropical Forest) which had substantially lower median ET estimates. As mentioned before, care should be taken in comparing the ET estimates from this indigenous forest study with any past data set since the ET ranges appear unusually large and may suggest an overestimation of water use of indigenous forests.

Table 4-33 Summary statistics of evapotranspiration (ET) for selected *Acacia*, *Eucalyptus* and *Pinus* compartments from 1 Jan 2009 to 31 Dec 2020 (Van Niekerk *et al.*, 2023)

MONTH	ACACIA			EUCALYPTUS			PINUS		
	Median	Mean	SD	Median	Mean	SD	Median	Mean	SD
Jan	122	123	25	120	119	28	115	116	30
Feb	109	111	23	109	110	26	104	104	26
Mar	105	107	21	106	108	27	99	100	26
Apr	81	82	17	82	85	24	77	78	22
May	74	74	17	76	78	24	68	69	21
Jun	58	59	16	61	65	24	53	54	20
Jul	57	59	18	63	66	26	52	54	22
Aug	74	74	20	81	82	27	68	69	25
Sep	87	88	23	93	95	32	82	84	30
Oct	93	93	25	97	99	31	91	92	30
Nov	103	103	25	104	105	31	101	101	30
Dec	115	115	24	115	115	29	111	111	31
Annual	1096	1091	196	1123	1131	256	1038	1035	260

5 SYNTHESIS

5.1 Revisiting the project aim and objectives

The aim of the project was to quantify and characterise the water use (evapotranspiration) of indigenous forests throughout South Africa. Objective 1 was to produce a geographical database of indigenous forests in South Africa. The knowledge review revealed that the most up-to-date and accurate indigenous forest map is the recently produced IF2021 (Mucina *et al.*, 2022). Section 3.1 explains that the IF2021 is based on previous maps (e.g. VegMap 2006), expert knowledge and manual digitisation and includes 21 forest types in South Africa.

Despite its overall quality, upon close examination, the IF2021 exhibited spatial accuracy inconsistencies stemming from digitisation at different spatial scales. The project team consequently set out to improve the IF2021 for the purpose of this project by making use of a fully automated KBIC procedure developed to differentiate indigenous forests from other land covers. The KBIC makes use of a range of EO data, including multispectral satellite imagery (Sentinel-2), very high spatial resolution (50 cm) and low spectral (RGB) aerial imagery, as well as a 2 m resolution DSM. The KBIC procedure was applied to areas with known indigenous forests to produce a highly accurate indigenous forest cover map, internally referred to as IF2022, which was further refined through manual correction into the IF2023. The IF2023 was subsequently disaggregated into forest types using the forest type classification IF2021 as basis. A proximity-based geospatial methodology was developed for this purpose. The resulting map is called IF2024. The final step in the indigenous forest mapping procedure was to manually check and edit the IF2024, which was facilitated by an in-house web application designed for this purpose.

Objective 2 of the project was to determine the consumptive water use (actual ET) of indigenous forests using existing RS data. The knowledge review revealed that the WaPOR product (FAO 2024) is the most suitable for this purpose, and monthly WaPOR ET values from 2009 to 2023 were extracted for the IF2024.

Objective 3 was to validate (ground truth) the RS-based consumptive water use of indigenous forests using historical field-based measurements. The extracted ET values were consequently compared to published measurements of ET. Unfortunately, such data was scant, and only a handful of historical measurements could be directly related to the extracted WaPOR ET data. Nevertheless, the information helped to get a sense of the uncertainties in the WaPOR ET data (see discussion in the next section).

The final objective of this project was to describe, analyse and interpret location-specific differences in water use between indigenous forest types at specific locations in South Africa. A total of 24 climate, terrain and soil characteristics were collated at a national scale and compared to the ET values for all forest types. Univariate statistical analyses (correlation analyses and regression modelling) were carried out to find relationships between each environmental variable and the ET values extracted per forest patch. In addition, multivariate machine learning modelling was used to determine which

environmental factors are the most important drivers of forest water use. The results of these analyses were interpreted within the ecological and biophysical context of the various forest types.

5.2 Main findings

One of the main findings of this project is that there is a dire need for an up-to-date and accurate indigenous forest map of South Africa. The absence of such a map makes studies about water use impossible. More importantly, without such a map, there is no way to assess whether our forests are being managed sustainably and determine the rate at which forests are lost. Based on international trends and the growing pressures relating to the reporting of greenhouse gas emissions from different land uses, an accurate and up-to-date indigenous forest map will be critical to quantify the carbon stocks and fluxes of forests and their relationship to biodiversity. This project updated and refined the latest indigenous forest map (Mucina *et al.*, 2022), referred to as the IF2021. The refined map, called IF2024, is an invaluable resource, not only for this project but for future research.

The IF2024 was used to extract water use profiles – using WaPOR ET data – for each forest type. It was found that the ET of forests is, on average, 989 mm/yr (all forest types) and ranged (on average) from 296 mm/yr in the case of Arid Zone Riparian Woodland (ARF1) to 1 338 mm/yr in the case of Subtropical Indian Ocean Mangrove (AMAN1). The WaPOR ET estimations were compared to previous field-based ET estimates and were found to compare well for some forest types while deviating considerably in others. For instance, the annual ET for Cape Afrotropical Forest was estimated as 933 mm/yr and 1 175 mm/yr in previous studies (Table 4-31), while the median WaPOR ET for this forest type is 1 224 mm/yr. In contrast, the ET for Subtropical Scarp Forest was estimated by Dye *et al.* (2008b) to be 668 mm/yr, while the WaPOR ET median for this forest type is 1 054 mm/yr. The ET of Arid Zone Riparian Woodland was estimated by (Dye *et al.*, 2008c) to be 1 094 mm/yr, while the median ET of this forest type is 296 mm/yr according to the WaPOR data. These large deviations are concerning and requires closer inspection.

Given that the focus of this project was on studying regional water use variations and relating these variations to a selection of environmental factors, and since no other long-term ET dataset was available, the WaPOR ET data was used. Univariate statistical analyses and multivariate machine learning were used to better understand the regional variations in the water use of indigenous forests and to relate these variations to environmental conditions. None of the univariate statistical methods produce strong models, which suggests that water use of indigenous forests is complex and not determined by a single factor considered or that other important controlling variable(s) were not included in this analysis.

In contrast, multivariate (random forest regression) machine learning (using the WaPOR ET as the target variable and 24 climatic, terrain and soil-related variables as predictors) produced a very strong model ($R^2 = 0.98$). The random forest algorithm identified long-term mean annual rainfall as the most important driver of water use. This finding was not surprising, given the known relationship between soil moisture and ET. Solar radiation in summer was identified as the second most important driver of forest

ET. Where sufficient soil moisture is available and if plant physiological thresholds are not exceeded, increased solar radiation will result in increased transpiration and evaporation since more energy is available to drive these processes. The other climate-related variables that were identified as being important drivers of forest water use included heat units (3rd), solar radiation during winter (4th) and vapour pressure deficit (7th). These relationships are investigated in Section 4.2.3.

A range of terrain-related variables were also compared to the WaPOR ET values extracted per forest type. Terrain morphology was identified as the most important terrain-related variable (ranked 8th overall), positive topographic openness (9th), elevation (10th) and negative topographic openness (11th). The impact that these and other terrain-based variables have on the water use of forests are reported and discussed in Section 4.2.4. In general, it was difficult to find consistent relationships between terrain-based variables and water use. It seems that the relationships depend on the forest type, likely because forest types are composed of many different species. As such, it is conceivable that habitat variations, including terrain, affect where individual species grow and that this causes intra-class variations.

Two variables, namely soil depth and soil clay content, were considered drivers of forest water use. The importance of soil characteristics on forest water use was confirmed by machine learning modelling, which indicated that soil clay content was the fifth most important variable, and soil depth was the seventh most important variable for explaining the regional variance in forest water use. As with terrain-related variables, it was difficult to find consistent patterns in the relationship between soil characteristics and forest water use. However, in some cases, such as Southern Mistbelt Forest (AF2) and Northern Mistbelt Forest (AF3), water use was consistently lower in shallow soils compared to deeper soils.

The main finding of this research is that EO is an invaluable technology for studying how water use vary among forest types and within the same forest type from the one region to another. Coupled with machine learning, the complex interrelationships between of EO-based forest ET and GIS-based environmental conditions were modelled to a very high accuracy (235 mm/yr). To our knowledge, this finding is novel and a contribution to new knowledge.

The next section delves into some of the challenges experienced during this study, as well as limitations that need to be considered.

5.3 Study limitations and proposals for future research

Analysing indigenous forest water use turned out to be a much larger undertaking than expected and much more difficult compared to previous studies in which EO methods and data were used to quantify the water use of irrigated crops (Van Niekerk *et al.*, 2018) and commercial plantations (Van Niekerk *et al.*, 2023). The first challenge is that indigenous forests are poorly mapped. Despite our efforts to improve the existing indigenous forest maps, the boundaries of indigenous forests are not as well defined as those of commercial plantations and agricultural fields. In addition, indigenous forests range

from dense Afrotropical Forest to sparse Southern African Dry Thickets. And neighbouring indigenous forest types tend to merge into one another – identifying the boundaries between such forests is near-impossible. The diverse species composition and tree age of indigenous forests make their discrimination (using EO methods) very difficult. In this project, we relied on Prof Mucina's extensive expert knowledge of South Africa's indigenous forests to discriminate among types, but human error and subjectiveness are inevitable. More work is needed to improve the indigenous forest map of South Africa refined in this study (IF2024). This study showed that KBIC can be used to accurately delineate and differentiate indigenous forest patches from other land covers. However, this process is only about 80% accurate and additional (manual) corrections are needed to improve the map. As part of this project, manual refinements were carried out for large forest patches (for the purpose of extracting ET), while small patches were left as is. It is recommended that the map refinements continue until all forest patches are accurately mapped.

Another challenge was that very little is known about the water use of indigenous forests. In the absence of sufficient and reliable field data, it is difficult to assess the accuracy of the WaPOR data. The few studies that have been carried out represent one or two locations within a particular forest patch. It is questionable whether such data are representative of all forest patches within the same forest type. We recommend that more field-based water use studies be carried out, specifically within indigenous forests, to better assess remotely sensed ET products. We also propose formal engagement with the developers of ET data products such as WaPOR or MOD16. These products should be evaluated against newly established fluxed towers in indigenous forests. EFTEON¹⁴ may be able to assist with this endeavour.

A range of variables (climatic, terrain and soil) readily available in GIS format were used as input to machine learning to investigate which of these variables drive ET variance. However, no climatic data for the period corresponding to the extracted ET data (2009-2023) were available, and hence the machine learning was incomplete. As noted in a previous project (Van Niekerk *et al.*, 2023) the lack of climatic data remains a major constraint for water use studies. In this project, we had to rely on long-term climate data (Schulze, 2007), which does not consider the climatic variations that occurred during the period studied in this project. The establishment and maintenance of a weather station network should be a national priority. The data produced from such stations must be cleaned and verified to ensure its quality and completeness. Ideally, interpolated climate surfaces, such as those produced by (Schulze, 2007) should be made available on a regular basis and for different time periods (e.g. long-term, decadal, annual and monthly). The data ought to be made freely available for research purposes. In this regard, initiatives such as Climate Smart Agriculture (CSA)¹⁵ and TerraClim¹⁶ should be supported.

This study only considered two soil-related variables, namely soil depth and clay content. Both these variables were identified as key drivers of forest water use. However, South Africa's soil data sets are

¹⁴ <https://efteon.saeon.ac.za/>

¹⁵ <https://climatesmartagri.co.za/>

¹⁶ <https://www.terraclim.co.za/>

outdated and too generalised for water use analyses. More work is needed to develop soil databases and to produce high-resolution digital soil maps. It is recommended that the WRC consider initiating (in collaboration with state organs such as the Department of Agriculture, Land Reform and Rural Development) digital soil mapping projects, particularly relating to the water-holding capacity of soils, as such data is critical for the efficient use of water.

In this project, no EO data were considered as drivers of ET. Future studies should consider the large sets of EO data available through platforms such as Google Earth Engine (GEE) and the Copernicus Data Ecosystem. However, researchers should be cautious about comparing remotely sensed datasets such as NDVI to ET data, as such variables are often used as input to ET modelling.

A generic plant database of South Africa is urgently needed. Ideally such a database should capture seasonal variations (e.g. to distinguish between deciduous and evergreen systems or a combination thereof) and assess species richness/diversity as such traits will impact water use of indigenous forests. RS can also play a role in establishing such a database. For instance, LiDAR data can be used to investigate the structure of forests which will impact surface roughness that will, in turn, affect ET.

An analysis of how environmental factors influence where particular forests occur was outside the scope of the project. However, using the 24 environmental variables collated in this project, a preliminary machine learning (RF) classification of forest types was carried out (Section 4.1.2). The overall accuracy of the resulting model was more than 85%, which demonstrates the intricate relationship between indigenous forest types and climate, terrain and soil. More work is needed to analyse these relationships. Ideally, the environmental variables should be expanded to include EO data. Based on the high accuracies obtained in the preliminary analysis, it is conceivable that machine learning technologies can greatly assist in forest type differentiations and potentially produce more objective maps.

5.4 Recommendations

A range of recommendations and proposals for future research were made in the preceding section. To summarise, we recommend that:

1. The WaPOR-based estimations of indigenous forest water use be interpreted and used with caution as the available field-based measurements against which it could be compared (for verification purposes) are scant and not sufficient to properly assess its accuracy.
2. More field-based measurements of ET within indigenous forests are needed. Ideally, several forest types should be targeted (the results of this project can be used to assist with selection).
3. The range of analyses carried out in this project highlighted the intricate relationships between environmental conditions and water use of forests. However, much more work can be done. Future studies should consider analysing individual forest types separately as this might reduce the large variations in ET observed. Ideally, such an undertaking should include field-based ET measurements.

4. The long-term climate data used in this study (Schulze, 2007) were last updated in 2007. It is critical that fundamental climate surfaces such as long-term monthly rainfall, temperature, solar radiation, vapour deficit and RH be updated. The capacity to produce climate surfaces is available (e.g. TerraClim), but there is a critical shortage of weather station data. The data that are available are either too costly to obtain (e.g. from providers such as the South African Weather Services and the Agricultural Research Council), too incomplete, or both. The number of active weather stations has also been dropping since the early 2000s. Although private-public partnerships such as CSA (funded by the Technology Innovation Agency) are a step in the right direction, much more work is needed to ensure that the weather station network is expanded and maintained.
5. We strongly recommend that South Africa develop capacity in digital soil mapping. In particular, high-resolution maps of soil water-holding capacity are needed. Such maps will be invaluable for water use studies. In addition, such data are needed to inform decisions about crop plantings and to increase water use efficiencies in agriculture.
6. The indigenous forest map refined in this study is an invaluable resource for ensuring that our indigenous forests are protected and managed. It is recommended that verification and editing processes continue beyond the end of this project. Ideally, indigenous forest mapping should be operationalized and updated on an annual or bi-annual basis.

REFERENCES

- Adam E, Mutanga O, Rugege D & Ismail R 2012. Discriminating the papyrus vegetation (*Cyperus papyrus* L.) and its co-existent species using random forest and hyperspectral data resampled to HYMAP. *International Journal of Remote Sensing* 33: 552-569.
- Agricultural Research Council 2010. Land type inventory of South Africa [online]. Pretoria: Institute for Soil, Climate and Water. Available from <http://www.agis.agric.za/agisweb/landtypes.html> [Accessed 3 September 2013].
- Akumu CE, Baldwin K & Dennis S 2019. GIS-based modeling of forest soil moisture regime classes: Using Rinker Lake in northwestern Ontario, Canada as a case study. *Geoderma* 351: 25-35.
- Albert T 2002. Evaluation of remote sensing techniques for ice-area classification applied to the tropical Quelccaya Ice Cap, Peru. *Polar Geography* 26: 210-226.
- Amani S & Shafizadeh-Moghadam H 2023. A review of machine learning models and influential factors for estimating evapotranspiration using remote sensing and ground-based data. *Agricultural Water Management* 284: 108324.
- Annandale JG, Stizaker RJ, Singels A, Van der Laan M & Laker MC 2011. Irrigation scheduling research: South African experiences and future prospects. *Water SA* 37: 16.
- Arino O, Gross D, Ranera F, Leroy M, Bicheron P, Brockman C, Defourny P, Vancutsem C, Achard F & Durieux L 2007. GlobCover: ESA service for global land cover from MERIS. 2007 IEEE international geoscience and remote sensing symposium.
- Asselin H, Belleau A & Bergeron Y 2006. Factors responsible for the co-occurrence of forested and unforested rock outcrops in the boreal forest. *Landscape Ecology* 21: 271-280.
- Atzberger C 2013. Advances in Remote Sensing of Agriculture: Context Description, Existing Operational Monitoring Systems and Major Information Needs. *Remote Sensing* 5: 949-981.
- Baatuwue N & Van Leeuwen L 2011. Evaluation of three classifiers in mapping forest stand types using medium resolution imagery: a case study in the Offinso Forest District, Ghana. *African Journal of Environmental Science and Technology* 5: 25-36.
- Bangira T, Alfieri MS, Menenti M & van Niekerk A 2019. Comparing thresholding with machine learning classifiers for mapping complex water. *Remote Sensing* 11: 1351.
- Bastiaanssen WGM, Cheema MJM, Immerzeel WW, Miltenburg I & Pelgrum H 2012. Surface energy balance and actual evapotranspiration of the transboundary Indus Basin estimated from satellite measurements and the ETLook model. *Water Resources Research* 48: W11512.
- Bastiaanssen WGM, Noordman E, Pelgrum H, Davids G & Allen RG 2005. SEBAL for spatially distributed ET under actual management and growing conditions. *ASCE Journal of Irrigation and Drainage Engineering* 131: 85-93.
- Bastiaanssen WGM, Pelgrum H, Wang J, Ma Y, Moreno JF, Roerink GJ & Wal TV 1998. A remote sensing surface energy balance algorithm for land (SEBAL) 2. *Validation. Journal of Hydrology* 212-213 213-229.
- Beckline M, Yujun S, Yvette B, John AB, Mor-Achankap B, Saeed S, Richard T, Wose J & Paul C 2017. Perspectives of remote sensing and GIS applications in tropical forest management. *Am. J. Agric. For* 5: 33-39.

- Benz UC, Hofmann P, Willhauck G, Lingenfelder I & Heynen M 2004. Multi-resolution, object-oriented fuzzy analysis of remote sensing data for GIS-ready information. *ISPRS Journal of Photogrammetry and Remote Sensing* 58: 239-258.
- Blanco NE, Gollan PJ, Mengin V, Nikkanen L & Fusari CM 2022. A Novel Perspective for Photosystem I: An Emerging Hub for the Functional Integration of Photosynthesis and Metabolism. *Frontiers in Plant Science* 13: 871623.
- Blaschke T, Lang S, Lorup E, Strobl J & Zeil P 2000. Object-oriented image processing in an integrated GIS/remote sensing environment and perspectives for environmental applications. In Cremers A & Greve K (eds) *Environmental information for planning, politics and the public*, 555-570. Marburg: Metropolis Verlag.
- Bock M, Xofis P, Mitchley J, Rossner G & Wissen M 2005. Object-oriented methods for habitat mapping at multiple scales – Case studies from Northern Germany and Wye Downs, UK. *Journal for Nature Conservation* 13: 75-89.
- Bolstad PV & Lillisand TM 1991. Rapid maximum likelihood classification. *Photogrammetric Engineering and Remote Sensing* 57: 67-74.
- Bosch A, Zisserman A & Muoz X 2007. Image Classification using Random Forests and Ferns. *Computer Vision, 2007. ICCV 2007. IEEE 11th International Conference*. Rio de Janeiro Brazil.
- Breiman L 1996. Bagging Predictors. *Machine Learning* 24: 123-140.
- Breiman L 2001. Random forests. *Machine learning* 45: 5-32.
- Brevik EC, Pereira P, Muñoz-Rojas M, Miller BA, Cerdà A, Parras-Alcántara L & Lozano-García B 2017. Soil mapping and process modeling for sustainable land use management: a brief historical review. EGU General Assembly Conference Abstracts.
- Bristow KL & De Jager JM 1981. A proposed technique to measure evapotranspiration using micrometeorological methods. *Water SA* 7: 49-53.
- Brown de Colstoun EC, Story MH, Thompson C, Comisso K, Smith TG & Irons JR 2003. National park vegetation mapping using multitemporal Landsat 7 data and a decision tree classifier. *Remote Sensing of Environment* 85: 316-327.
- Buddenbaum H, Schlerf M & Hill J 2005. Classification of coniferous tree species and age classes using hyperspectral data and geostatistical methods. *International Journal of Remote Sensing* 26: 5453-5465.
- Budei BC, St-Onge B, Hopkinson C & Audet F-A 2018. Identifying the genus or species of individual trees using a three-wavelength airborne lidar system. *Remote Sensing of Environment* 204: 632-647.
- Campbell GS & Norman JM 2000. *An introduction to environmental biophysics*. Springer Science & Business Media.
- Campbell J 2007. *Introduction to remote sensing*. 4th Edition. London: Taylor & Francis.
- Chang J, Paelinckx D & Alterra-Centrum L 2008. Evaluation of Random Forest and Adaboost tree-based ensemble classification and spectral band selection for ecotope mapping using airborne hyperspectral imagery. *Remote Sensing of Environment* 112: 2999-3011.
- Chen B, Li X, Xiao X, Zhao B, Dong J, Kou W, Qin Y, Yang C, Wu Z & Sun R 2016. Mapping tropical forests and deciduous rubber plantations in Hainan Island, China by integrating PALSAR 25-m and multi-temporal Landsat images. *International journal of applied earth observation and geoinformation* 50: 117-130.

- Cho MA, Malahlela O & Ramoelo A 2015. Assessing the utility WorldView-2 imagery for tree species mapping in South African subtropical humid forest and the conservation implications: Dukuduku forest patch as case study. *International Journal of Applied Earth Observation and Geoinformation* 38: 349-357.
- Choudhary K, Boori MS & Kupriyanov A 2018. Spatial modelling for natural and environmental vulnerability through remote sensing and GIS in Astrakhan, Russia. *The Egyptian Journal of Remote Sensing and Space Science* 21: 139-147.
- Choudhury BJ 1997. Estimating areal evaporation using multispectral satellite observations. *NATO ASI Series*, 364-381. Heidelberg: Springer Verslag
- Clulow A, Everson C, Price J, Jewitt G & Scott-Shaw B 2013. Water-use dynamics of a peat swamp forest and a dune forest in Maputaland, South Africa. *Hydrology and Earth System Sciences* 17: 2053-2067.
- Cohen Y & Shoshany M 2002. A national knowledge-based crop recognition in Mediterranean environment. *International Journal of Applied Earth Observation and Geoinformation* 4: 75-87.
- Courault D, Seguin B & Olioso A 2005. Review on estimation of evapotranspiration from remote sensing data: From empirical to numerical modeling approaches. *Irrigation and Drainage Systems* 19: 223-249.
- Cover T & Hart P 1967. Nearest neighbor pattern classification. *IEEE Transactions on Information Theory* 13: 21-27.
- Cunningham Pa & Delany SJ 2007. K-Nearest Neighbour Classifiers. Technical Report UCD-CSI-2007-4, Dublin.
- Dagon K & Schrag DP 2016. Exploring the effects of solar radiation management on water cycling in a coupled land-atmosphere model. *Journal of Climate* 29: 2635-2650.
- Defries RS, Hansen MC, Townshend JR, Janetos A & Loveland TR 2000. A new global 1-km dataset of percentage tree cover derived from remote sensing. *Global Change Biology* 6: 247-254.
- Dincă L, Sparchez G & Dincă M 2014. Romanian's forest soil GIS map and database and their ecological implications. *Carpathian Journal of Earth and Environmental Sciences* 9: 133-142.
- Dong J, Xiao X, Chen B, Torbick N, Jin C, Zhang G & Biradar C 2013. Mapping deciduous rubber plantations through integration of PALSAR and multi-temporal Landsat imagery. *Remote Sensing of Environment* 134: 392-402.
- Dong J, Xiao X, Sheldon S, Biradar C & Xie G 2012. Mapping tropical forests and rubber plantations in complex landscapes by integrating PALSAR and MODIS imagery. *ISPRS Journal of Photogrammetry and remote sensing* 74: 20-33.
- Duro DC, Franklin SE & Dubé MG 2012. Multi-scale object-based image analysis and feature selection of multi-sensor earth observation imagery using random forests. *International Journal of Remote Sensing* 33: 4502-4526.
- Dye P, Jarmain C, Clulow A, Everson C, Mengistu M & Weiersbye I 2018. Evapotranspiration from mine-affected riparian sites along the Vaal River in central South Africa. *South African Geographical Journal* 100: 62-81.
- Dye P, Jarmain C, Oageng B, Xaba J & Weiersbye I 2008a. The potential of woodlands and reed-beds for control of acid mine drainage in the Witwatersrand Gold Fields, South Africa. Proceedings of the Third International Seminar on Mine Closure, Mine Closure.

- Dye PJ, Gush MB, Everson CS, Jarman C, Clulow AD, Mengistu M, Geldenhuys CJ, Wise R, Scholes RJ, Archibald S & Savage MJ 2008b. Water use in relation to biomass of indigenous tree species in woodland, forest and/or plantation conditions. WRC Report no. TT361/08. Pretoria: Water Research Commission.
- Dye PJ, Jarman C, Le Maitre DC, Everson CS, Gush MB & Clulow AD 2008c. Modelling Vegetation Water Use for General Application in Different Categories of Vegetation. WRC Report no. 1319/1/08. Pretoria: Water Research Commission.
- Dye PJ, Poulter AG, Soko S & Maphanga D 1997. The determination of the relationship between transpiration rate and declining available water for Eucalyptus Grandis. WRC Report no. 441/1/97. Pretoria: Water Research Commission.
- Everson C, Scott-Shaw B, Kelbe B, Starke A, Pearton T, Geldenhuys C, Vather T & Maguire M 2019. Quantifying the water-use of dominant land uses in the Maputaland coastal plain. *WRC Report*.
- Everson CS, Dye PJ, Gush MB & Everson TM 2011. Water use of grasslands, agroforestry systems and indigenous forests. *Water SA* 37: 781-788.
- Fagan ME, DeFries RS, Sesnie SE, Arroyo-Mora JP, Soto C, Singh A, Townsend PA & Chazdon RL 2015. Mapping species composition of forests and tree plantations in Northeastern Costa Rica with an integration of hyperspectral and multitemporal Landsat imagery. *Remote Sensing* 7: 5660-5696.
- Falkowski MJ, Hudak AT, Crookston NL, Gessler PE, Uebler EH & Smith AMS 2010. Landscape-scale parameterization of a tree-level forest growth model: a k-nearest neighbor imputation approach incorporating LiDAR data. *Canadian Journal of Forest Research* 40: 184-199.
- FAO 2024. Water Productivity through Open access of Remotely sensed data (WaPOR) [online]. Available from <http://www.fao.org/in-action/remote-sensing-for-water-productivity/en> [Accessed 21 Jan 2024].
- Farquhar GD & Sharkey TD 1982. Stomatal conductance and photosynthesis. *Annual review of plant physiology* 33: 317-345.
- Fieg G 2024. Personal communication to Jarman C re EFTEON flux towers. Pretoria: SAEON.
- Franco-Lopez H, Ek AR & Bauer ME 2001. Estimation and mapping of forest stand density, volume, and cover type using the k-nearest neighbors method. *Remote Sensing of Environment* 77: 251-274.
- Franklin SE & Ahmed OS 2018. Deciduous tree species classification using object-based analysis and machine learning with unmanned aerial vehicle multispectral data. *International Journal of Remote Sensing* 39: 5236-5245.
- Franklin SE, Ahmed OS & Williams G 2017. Northern conifer forest species classification using multispectral data acquired from an unmanned aerial vehicle. *Photogrammetric Engineering & Remote Sensing* 83: 501-507.
- Gibson LA, Jarman C, Su Z & Eckardt FE 2013. Estimating evapotranspiration using remote sensing and the Surface Energy Balance System – A South African perspective. *Water SA* 39: 477-483.
- Gibson PJ & Power CH 2000. *Introduction to remote sensing: Digital image processing and applications*. London: Taylor and Francis.
- Gislason PO, Benediktsson JA & Sveinsson JR 2006. Random forests for land cover classification. *Pattern Recognition Letters* 27: 294-300.

- Gómez C, Wulder MA, Montes F & Delgado JA 2012. Modeling Forest Structural Parameters in the Mediterranean Pines of Central Spain using QuickBird-2 Imagery and Classification and Regression Tree Analysis (CART). *Remote Sensing* 4: 135-159.
- Goodchild MF 2005. *GIS and modeling overview: GIS, spatial analysis, and modeling*. Redlands: ESRI Press.
- Goudriaan R 2014. An operational service to improve crop water and nitrogen management in grapes and other deciduous fruit trees using satellite technology for the season 2013-14. Cape Town: Western Cape Province Department of Agriculture.
- Green S & Clothier B 1988. Water use of kiwifruit vines and apple trees by the heat-pulse technique. *Journal of Experimental Botany* 39.
- Grossiord C, Buckley TN, Cernusak LA, Novick KA, Poulter B, Siegwolf RT, Sperry JS & McDowell NG 2020. Plant responses to rising vapor pressure deficit. *New Phytologist* 226: 1550-1566.
- Gumbricht T, McCarthy J & Mahlander C 1996. Digital interpretation and management of land-cover: A case study of Cyprus. *Ecological Engineering* 6: 273-279.
- Gush MB, de Lange WJ, Dye PJ & Geldenhuys CJ 2015. *Water use and socio-economic benefit of the biomass of indigenous trees (volume 1)*. Water Research Commission Pretoria.
- Gush MB & Dye PJ 2009. Water-use efficiency within a selection of indigenous and exotic tree species in South Africa as determined using sap flow and biomass measurements. *Acta Horticulturae* 846: 323-330.
- Hagner O & Reese H 2007. A method for calibrated maximum likelihood classification of forest types. *Remote Sensing of Environment* 110: 438-444.
- Hansen M, DeFries R, Townshend J, Carroll M, Dimiceli C & Sohlberg R 2003. Global percent tree cover at a spatial resolution of 500 meters: First results of the MODIS vegetation continuous fields algorithm. *Earth Interactions* 7: 1-15.
- Hansen MC & Loveland TR 2012. A review of large area monitoring of land cover change using Landsat data. *Remote Sensing of Environment* 122: 66-74.
- Hansen MC, Townshend JR, DeFries RS & Carroll M 2005. Estimation of tree cover using MODIS data at global, continental and regional/local scales. *International Journal of Remote Sensing* 26: 4359-4380.
- Hardisty J, Taylor DM & Metcalfe SE 1993. *Computerised environmental modelling: a practical introduction using Excel*. Chichester, West Sussex: John Wiley & Sons.
- Hay GJ, Castilla G, Wulder MA & Ruiz JR 2005. An automated object-based approach for the multiscale image segmentation of forest scenes. *International Journal of Applied Earth Observation and Geoinformation* 7: 339-359.
- Heinzel J & Koch B 2011. Exploring full-waveform LiDAR parameters for tree species classification. *International Journal of Applied Earth Observation and Geoinformation* 13: 152-160.
- Hepner F, Logan T, Ritter N & Bryant N 1990. Artificial neural network classification using a minimal training set: Comparison to conventional supervised classification. *Photogrammetric Engineering and Remote Sensing* 56: 469-473.
- Heydari SS & Mountrakis G 2019. Meta-analysis of deep neural networks in remote sensing: A comparative study of mono-temporal classification to support vector machines. *ISPRS journal of photogrammetry and remote sensing* 152: 192-210.

- Heywood I, Cornelius S & Carver S 2006. *An introduction to geographical information systems, 3rd edition*. Harlow, England: Pearson Education Limited.
- Higgs C & van Niekerk A 2022. Impact of Training Set Configurations for Differentiating Plantation Forest Genera with Sentinel-2 Imagery and Machine Learning. *Remote Sensing* 14: 3992.
- Higgs C & van Niekerk A 2024. Signature extension as a machine learning strategy for mapping plantation forest genera with Sentinel-2 imagery. *Remote Sensing Applications: Society and Environment*: 101136.
- Hillel D 2003. *Introduction to environmental soil physics*. Elsevier.
- Hladik C & Alber M 2014. Classification of salt marsh vegetation using edaphic and remote sensing-derived variables. *Estuarine, Coastal and Shelf Science* 141: 47-57.
- Huang C, Davis LS & Townshend JRG 2002. An assessment of support vector machines for land cover classification. *International Journal of Remote Sensing* 23: 725-749.
- Hubert-Moy L, Cotonnec A, Le Du L, Chardin A & Perez P 2001. A Comparison of Parametric Classification Procedures of Remotely Sensed Data Applied on Different Landscape Units. *Remote Sensing of Environment* 75: 174-187.
- Huete A, Didan K, Miura T, Rodriguez EP, Gao X & Ferreira LG 2002. Overview of the radiometric and biophysical performance of the MODIS vegetation indices. *Remote sensing of environment* 83: 195-213.
- Immitzer M, Atzberger C & Koukal T 2012. Tree Species Classification with Random Forest Using Very High Spatial Resolution 8-Band WorldView-2 Satellite Data. *Remote Sensing* 4: 2661-2693.
- Jackson RD & Huete AR 1991. Interpreting vegetation indices. *Preventive veterinary medicine* 11: 185-200.
- Jain AK, Duin RPW & Jianchang M 2000. Statistical pattern recognition: a review. *IEEE Transactions on Pattern Analysis and Machine Intelligence* 22: 4-37.
- Jarmain C, Everson C, Savage M, Mengistu M, Clulow A, Walker S & Gush M 2009a. Refining tools for evaporation monitoring in support of water resources management. *Water Research Commission Report*: 08.
- Jarmain C, Everson C, Savage M, Mengistu M, Clulow A, Walker S & Gush M 2009b. Refining tools for evaporation monitoring in support of water resources management, WRC Report No. K5/1567/08. Pretoria: Water Research Commission.
- Jarmain C, Govender M & Everson C 2004. Improving the basis for predicting total evaporation from natural veld types in South Africa. *Water Research Commission Report* 1219: 04.
- Jarmain C, Mengitsu M, Jewitt G, Kongo V & Bastiaanssen W 2009c. A methodology for near-real time spatial estimation of evaporation. *Water Research Commission, Pretoria, South Africa*.
- Jarmain C, Singels A, Bastidas-Obando E, Paraskevopoulos A, Olivier F, Van der Laan M, Taverna-Turisan D, Dlamini M, Munch Z, Bastiaanssen WGM, Annandale J, Everson C, Savage M & Walker S 2014. Water use efficiency of selected irrigated crops determined with satellite imagery. WRC Report no. TT 602/14. Pretoria: Water Research Commission.
- Kalma JD, McVicar TR & McCabe MF 2008. Estimating land surface evaporation: A review of methods using remotely sensed surface temperature data. *Surveys in Geophysics* 29: 421-469.

- Karssenberg D, Schmitz O, De Vries LM & De Jong K 2008. A tool for construction of stochastic spatio-temporal models assimilated with observational data. 11th AGILE International Conference on Geographic Information Science, Girona, Spain.
- Ke Y, Quackenbush LJ & Im J 2010. Synergistic use of QuickBird multispectral imagery and LIDAR data for object-based forest species classification. *Remote Sensing of Environment* 114: 1141-1154.
- Kidane DK 2005. Rule-based land cover classification model: expert system integration of image and non-image spatial data. MSc thesis. Stellenbosch: Stellenbosch University.
- Koskinen J, Leinonen U, Vollrath A, Ortmann A, Lindquist E, d'Annunzio R, Pekkarinen A & Käyhkö N 2019. Participatory mapping of forest plantations with Open Foris and Google Earth Engine. *ISPRS Journal of Photogrammetry and Remote Sensing* 148: 63-74.
- Kramer PJ & Kozlowski TT 1979. *Physiology of woody plants*. London: Elsevier.
- Krishnamurthy R 2008. *Integrated coastal zone management*. Research Publishing Services.
- Kustas WP & Norman JM 1996. Use of remote sensing for evapotranspiration monitoring over land surfaces. *Hydrological Sciences Journal* 41: 495-516.
- Laipelt L, Kayser RHB, Fleischmann AS, Ruhoff A, Bastiaanssen W, Erickson TA & Melton F 2021. Long-term monitoring of evapotranspiration using the SEBAL algorithm and Google Earth Engine cloud computing. *ISPRS Journal of Photogrammetry and Remote Sensing* 178: 81-96.
- Lang S 2008. Object-based image analysis for remote sensing applications: Modelling reality – dealing with complexity. In Blaschke T, Lang S & Hay G (eds) *Object-based image analysis: Spatial concepts for knowledge-driven remote sensing applications*, 3-26. Berlin/Heidelberg: Springer Verlag.
- Lawrence L & Wright A 2001. Rule-based classification systems using classification and regression tree (CART) analysis. *Photogrammetric Engineering and Remote Sensing* 67: 1137-1142.
- Lawrence RL 2006. Mapping invasive plants using hyperspectral imagery and Breiman Cutler classifications (RandomForest). *Remote sensing of environment* v. 100: pp. 356-362-2006 v.100 no.3.
- Lennartz SP & Congalton RG 2004. Classifying and mapping forest cover types using IKONOS imagery in the Northeastern United States. Proceedings of the ASPRS Annual Conference, Denver, Colorado.
- Li H, Gu H, Han Y & Yang J 2010. Object-oriented classification of high-resolution remote sensing imagery based on an improved colour structure code and a support vector machine. *International Journal of Remote Sensing* 31: 1453-1470.
- Li J, Hu B & Noland TL 2013a. Classification of tree species based on structural features derived from high density LiDAR data. *Agricultural and forest meteorology* 171: 104-114.
- Li X & McCarty GW 2019. Application of topographic analyses for mapping spatial patterns of soil properties. *Geospatial Analyses of Earth Observation (EO) data*.
- Li ZL, Tang BH, Wu H, Ren H, Yan G, Wan Z, Trigo IF & Sobrino JA 2013b. Satellite-derived land surface temperature: Current status and perspectives. *Remote Sensing of Environment* 131: 14-37.
- Lira J & Maletti G 2002. A supervised contextual classifier based on a region-growth algorithm. *Computers and Geosciences* 25: 951-959.

- Lizarazo I 2008. SVM-based segmentation and classification of remotely sensed data. *International Journal of Remote Sensing* 29: 7277-7283.
- Luck W 2018. Generating automated forestry geoinformation products from remotely sensed imagery. Stellenbosch: Stellenbosch University.
- Lui X, Skidmore AK & Van Oosten H 2002. Integration of classification methods for improvement of land-cover map accuracy. *ISPRS Journal of Photogrammetry and Remote Sensing* 56: 257-268.
- Martinuzzi S, Gould WA, Vierling LA, Hudak AT, Nelson RF & Evans JS 2013. Quantifying Tropical Dry Forest Type and Succession: Substantial Improvement with LiDAR. *Biotropica* 45: 135-146.
- Mather PM 2004. *Computer Processing of Remotely-Sensed Images*. 3rd. Chichester, West Sussex: Wiley.
- Mauya EW, Koskinen J, Tegel K, Hämäläinen J, Kauranne T & Käyhkö N 2019. Modelling and Predicting the Growing Stock Volume in Small-Scale Plantation Forests of Tanzania Using Multi-Sensor Image Synergy. *Forests* 10: 279.
- McRoberts RE & Tomppo EO 2007. Remote sensing support for national forest inventories. *Remote Sensing of Environment* 110: 412-419.
- McRoberts RE, Wendt DG, Nelson MD & Hansen MH 2002. Using a land cover classification based on satellite imagery to improve the precision of forest inventory area estimates. *Remote Sensing of Environment* 81: 36-44.
- Morell-Monzó S, Estornell J & Sebastiá-Frasquet M-T 2020. Comparison of Sentinel-2 and high-resolution imagery for mapping land abandonment in fragmented areas. *Remote Sensing* 12: 2062.
- Mucina L (ed) 2018. *Vegetation survey and classification of subtropical forests of Southern Africa*. Dordrecht: Springer.
- Mucina L, Lötter MC, Rutherford MC, van Niekerk A, Macintyre PD, Tsakalos JL, Timberlake J, Adams JB, Riddin T & McCarthy LK 2022. Forest biomes of Southern Africa. *New Zealand Journal of Botany* 60: 377-428.
- Mucina L, Mucina L, Dold AP, Tichý L & van Niekerk A 2018. Classification of the Albany Coastal Forests. *Vegetation Survey and Classification of Subtropical Forests of Southern Africa*: 59-90.
- Mucina L, Pienaar E, Van Niekerk A & Lötter MC 2007. Habitat-level Classification of the Albany Coastal, Pondoland Scarp and Eastern Scarp Forests. Project No. 2006-064. Stellenbosch: DWAF.
- Mucina L & Rutherford M 2006. The vegetation of South Africa, Lesotho and Swaziland. Pretoria: South African National Biodiversity Institute.
- Myburgh G & Van Niekerk A 2013. Effect of feature dimensionality on object-based land cover classification: A comparison of three classifiers. *South African Journal of Geomatics* 2: 13-27.
- Nangendo G, Skidmore AK & van Oosten H 2007. Mapping east African tropical forests and woodlands – A comparison of classifiers. *ISPRS Journal of Photogrammetry and Remote Sensing* 61: 393-404.
- Neusch T & Grussenmeyer P 2003. Remote sensing object-oriented image analysis applied to half-timbered houses. Proceedings of the CIPA XIXth International symposium, Antalya, Turkey.

- Nimmo JR, Perkins KS, Schmidt KM, Miller DM, Stock JD & Singha K 2009. Hydrologic Characterization of Desert Soils with Varying Degrees of Pedogenesis: 1. Field Experiments Evaluating Plant-Relevant Soil Water Behavior. *Vadose Zone Journal* 8: 480-495.
- Novack T, Esch T, Kux H & Stilla U 2011. Machine learning comparison between WorldView-2 and QuickBird-2-simulated imagery regarding object-based urban land cover classification. *Remote Sensing* 3: 2263-2282.
- O'Sullivan D & Unwin DJ 2010. *Geographic data analysis, 2nd edition*. Hoboken: John Wiley & Sons, Inc.
- Olaode A, Naghdy G & Todd C 2014. Unsupervised classification of images: a review. *International Journal of Image Processing* 8: 325-342.
- Oruc M, Marangoz AM & Buyuksalih G 2004. Comparison of pixel-based and object-oriented classification approaches using Landsat-7 ETM spectral bands. Proceedings of the ISPRS 2004 Annual Conference, Istanbul, Turkey.
- Pal M 2005. Random forest classifier for remote sensing classification. *International Journal of Remote Sensing* 26: 217-222.
- Pal M & Mather PM 2003. An assessment of the effectiveness of decision tree methods for land cover classification. *Remote Sensing of Environment* 86: 554-565.
- Pearton TA 2017. An assessment of the water use of indigenous and introduced tree SPP. and varying land uses around Vasi Pan, Maputaland, KwaZulu-Natal.
- Peerbhay KY, Mutanga O & Ismail R 2013. Commercial tree species discrimination using airborne AISA Eagle hyperspectral imagery and partial least squares discriminant analysis (PLS-DA) in KwaZulu-Natal, South Africa. *ISPRS Journal of Photogrammetry and Remote Sensing* 79: 19-28.
- Peled A & Gilichinsky M 2010. Knowledge-based classification of land cover for the quality assessment of GIS database. *The International Archives of the Photogrammetry, Remote Sensing and Spatial Information Sciences* 38: 217-222.
- Pelgrum H, Miltenburg IJ, Cheema MJM, Klaasse A & Bastiaanssen WGM 2011. ETLook: A novel continental evapotranspiration algorithm. *Remote Sensing and Hydrology*, Jackson Hole, Wyoming, USA.
- Petropoulos GP, Kalaitzidis C & Prasad Vadrevu K 2012. Support vector machines and object-based classification for obtaining land-use/cover cartography from Hyperion hyperspectral imagery. *Computers & Geosciences* 41: 99-107.
- Pu R, Landry S & Yu Q 2011. Object-based urban detailed land cover classification with high spatial resolution IKONOS imagery. *International Journal of Remote Sensing* 32: 3285-3308.
- Punia M, Joshi PK & Porwal MC 2011. Decision tree classification of land use land cover for Delhi, India using IRS-P6 AWiFS data. *Expert Syst. Appl.* 38: 5577-5583.
- Rego FL & Koch B 2003. Automatic classification of land cover with high resolution data of the Rio de Janeiro city Brazil comparison between pixel and object classification. In Carstens J (ed) *Remote Sensing of Urban Areas*, 153-157.
- Rodriguez-Galiano VF, Chica-Olmo M, Abarca-Hernandez F, Atkinson PM & Jeganathan C 2012. Random Forest classification of Mediterranean land cover using multi-seasonal imagery and multi-seasonal texture. *Remote Sensing of Environment* 121: 93-107.
- San Juan RFdV & Domingo-Santos JM 2018. The role of gis and lidar as tools for sustainable forest management. *GIS-An Overview of Applications* 1: 124-148.

- Savage MJ, Everson CS & Metelerkamp BR 1997. Evaporation measurement above vegetated surfaces using micrometeorological techniques. WRC Report no. 349/1/97. Pretoria: Water Research Commission.
- Savage MJ, Everson CS, Odhiambo GO, Mengistu MJ & Jarman C 2004. Theory and practice of evaporation measurement, with special focus on SLS AS AN operational tool for the estimation of the spatially-averaged evaporation. WRC Report no. 1335/1/04. Pretoria: Water Research Commission.
- Savage MJ, Odhiambo G, Mengistu MG, Everso C & Jarman C 2010. Measurement of grassland evaporation using a surface-layer scintillometer. *Water Sa* 36.
- Schimper AFW 1898. *Pflanzen-geographie auf physiologischer Grundlage*. G. Fischer.
- Scholes RJ, Gureja N, Giannecchini M, Dovie D, Wilson B, Davidson N, Piggot K, McLoughlin C, Van der Velde K, Freeman A, Bradley S, Smart R & Ndala S 2001. The environment and vegetation of the flux measurement site near Skukuza, Kruger National Park, Koedoe – African Protected Area. *Conservation and Science* 44: 73-83.
- Schulze RE 2007. *South African atlas of climatology and agrohydrology*. WRC Report No. 1489/1/06. Pretoria: Water Research Commission.
- Scott-Shaw BC, Everson CS & Clulow AD 2017. Water-use dynamics of an alien-invaded riparian forest within the Mediterranean climate zone of the Western Cape, South Africa. *Hydrology and Earth System Sciences* 21: 4551-4562.
- Shiba M & Itaya A 2006. Using eCognition for improved forest management and monitoring systems in precision forestry. Proceedings of the International Precision Forestry Symposium, Stellenbosch, South Africa.
- Shugart H, Macko S, Lesolle P, Szuba T, Mukelabai M, Dowty P & Swap R 2004. The SAFARI 2000-Kalahari transect wet season campaign of year 2000. *Global Change Biology* 10: 273-280.
- Smith BN, Harris LC, McCarlie VW, Stradling DL, Thygerson T, Walker J, Criddle RS & Hansen LD 2001. Time, plant growth, respiration, and temperature. *Handbook of plant and crop physiology*, 23-34. CRC Press.
- Sonti S 2015. Application of geographic information system (GIS) in forest management. *Journal of Geography & Natural Disasters* 5: 1000145.
- Stanhill G 2019. Evapotranspiration☆. *Reference Module in Earth Systems and Environmental Sciences*: Elsevier.
- Stephenson G & Van Niekerk A 2009. A cost-effective, rule-based technique to improve forestry inventory on a national scale. Geoscience and Remote Sensing Symposium, 2009 IEEE International, IGARSS 2009.
- Temgoua AGT, Kokutse NK & Kavazović Z 2016. Influence of forest stands and root morphologies on hillslope stability. *Ecological engineering* 95: 622-634.
- Tomppo E, Olsson H, Ståhl G, Nilsson M, Hagner O & Katila M 2008. Combining national forest inventory field plots and remote sensing data for forest databases. *Remote Sensing of Environment* 112: 1982-1999.
- Tseng M-H, Chen S-J, Hwang G-H & Shen M-Y 2008. A genetic algorithm rule-based approach for land-cover classification. *ISPRS Journal of Photogrammetry and Remote Sensing* 63: 202-212.
- Tzotsos A & Argialas D 2008. A support vector machine approach for object based image analysis. *Object-Based Image Analysis*: 663-667.

- Van Aardt J & Norris-Rogers M 2008. Spectral-age interactions in managed, even-aged Eucalyptus plantations: application of discriminant analysis and classification and regression trees approaches to hyperspectral data. *International Journal of Remote Sensing* 29: 1841-1845.
- Van Coillie FMB, Verbeke LPC & De Wulf RR 2007. Feature selection by genetic algorithms in object-based classification of IKONOS imagery for forest mapping in Flanders, Belgium. *Remote Sensing of Environment*. 110: 476-487.
- Van Niekerk A 2016. Stellenbosch University Digital Elevation Model (SUDEM): 2016 Edition (v16.xx). Stellenbosch: Stellenbosch University.
- Van Niekerk A, Jarman C, Goudriaan R, Muller J, Ferreira F, Munch Z, Pauw T, Stephenson GR & Gibson LA 2018. An earth observation approach towards mapping irrigated areas and quantifying water use by irrigated crops in South Africa. WRC Report TT 745/17. Pretoria: Water Research Commission.
- Van Niekerk A, Jarman C, Stephenson G, du Plessis J, Higgs C, Ndyafi V & Mashimbye Z 2023. *The application of national scale remotely sensed evapotranspiration (ET) estimates to quantify water use and differences between plantations in commercial forestry regions of South Africa. WRC Report No. 2966/1/23* Pretoria: Water Research Commission.
- Van Niekerk A, Stephenson G, Pauw T, Boonzaaier I, Myburgh G, Muller J, Vermeulen D, Boshoff A, Van Wyk J & Van den Heever D 2014. Land cover mapping in the Eastern Cape (series of seven reports for Bisho, Butterworth, Flagstaff, Grahamstown, Port Elizabeth, Steytlerville and Willowmore areas). Report to Department of Rural Development and Land Redistribution. Cape Town: Stellenbosch University.
- Vapnik VN 1995. *The nature of statistical learning theory*. Springer-Verlag.
- Verstraeten WW, Veroustraete F & Feyen J 2005. Estimating evapotranspiration of European forests from NOAA-imagery at satellite overpass time: Towards an operational processing chain for integrated optical and thermal sensor data products. *Remote Sensing of Environment* 96: 256-276.
- Verstraeten WW, Veroustraete F & Feyen J 2008. Assessment of evapotranspiration and soil moisture content across different scales of observation. *Sensors* 8: 70-117.
- Von Maltitz G, Mucina L, Geldenhuys C, Lawes M, Eeley H, Adie H, Vink D, Fleming G & Bailey C 2003. Classification system for South African indigenous forests: An objective classification for the Department of water affairs and forestry. Pretoria: CSIR.
- Voss M & Sugumaran R 2008. Seasonal effect on tree species classification in an urban environment using hyperspectral data, LiDAR, and an object-oriented approach. *Sensors* 8: 3020-3036.
- Wagner F, H, Sanchez A, Tarabalka Y, Lotte R, Ferreira M, Aïdar PM, Gloor M, Phillips O & Aragão L 2019. Using the U-net convolutional network to map forest types and disturbance in the Atlantic rainforest with very high resolution images. *Remote Sensing in Ecology and Conservation*.
- Wicks TE, Smith GM & Curran PJ 2002. Polygon-based aggregation of remotely sensed data for regional ecological analyses. *International Journal of Applied Earth Observation and Geoinformation* 4: 161-173.
- Xie Z, Chen Y, Lu D, Li G & Chen E 2019. Classification of land cover, forest, and tree species classes with ZiYuan-3 multispectral and stereo data. *Remote Sensing* 11: 164.
- Xu Y, Yang Y, Chen X & Liu Y 2022. Bibliometric analysis of global NDVI research trends from 1985 to 2021. *Remote Sensing* 14: 3967.

- Yao W, Krzystek P & Heurich M 2012. Tree species classification and estimation of stem volume and DBH based on single tree extraction by exploiting airborne full-waveform LiDAR data. *Remote Sensing of Environment* 123: 368-380.
- Ying L & Bo C 2009. An improved k-nearest neighbor algorithm and its application to high resolution remote sensing image classification. 2009 17th International Conference on Geoinformatics.
- Zambelli P, Lora C, Spinelli R, Tattoni C, Vitti A, Zatelli P & Ciolli M 2012. A GIS decision support system for regional forest management to assess biomass availability for renewable energy production. *Environmental Modelling & Software* 38: 203-213.
- Zhang K, Kimball JS & Running SW 2016. A review of remote sensing based actual evapotranspiration estimation. *Wiley Interdisciplinary Reviews: Water* 3: 834-853.

APPENDIX I: CAPACITY BUILDING

Although the product budget makes provision for only two MSc students, four students are or have been directly contributing to or have been benefitting from this project, namely Messrs Hanu Mostert, Mhlangabezi Mdwai, Ayaaz Mullajie and Zandre Nieuwoudt.

Mr Hanu Mostert registered for MSc Geoinformatics at Stellenbosch University at the beginning of 2021 in a part-time capacity (he is working full-time at GeoSmart Space). Mr Mostert is being supervised by Dr Eric Mashimbye and Mr Kyle Loggenberg (with Prof Van Niekerk as adviser). The focus of his work is on the linkages between terrain and indigenous forests. Specifically, he is using object-based image analysis (OBIA) and machine learning to develop a methodology for mapping detailed landforms (e.g. crests, hillslopes, foot slopes, pediments, valley bottom, flood plains) maps for selected forested areas throughout South Africa. The aim is to compare the location and types of indigenous forests to these landforms to better understand the forests' topographic and environmental profiles. Two articles are targeted. The first article will focus on developing an automated workflow for classifying landforms. This will ultimately be achieved by using object-based image analysis combined with machine learning methods. The first step is to investigate the effect of DEM source and resolution on landform classification in the Western Cape. Several digital elevation models (DEMs) were evaluated, namely ASTER DEM, ALOS DEM, SRTM DEM, and SUDEM were evaluated. The impact of resolution was also assessed by resampling the DEMs to 30 m and 90 m. The landform classification method was automated according to the widely known Hammond classification methodology. A second set of experiments were carried out that used the Dikau *et al.* classification methodology. Validation points were created and it is currently in the process of being assessed by a geomorphologist, Dr. Grenfell, for validation. The timeline is to submit the first article for publication by the end of 2023 and the second article by the end of March 2024. The final write-up will happen thereafter and hand-in of the thesis is planned for July 2024.

Mr Mhlangabezi Mdwai registered as a BSc Hons Geoinformatics student at Stellenbosch University in 2021. The spectral properties of indigenous and plantation forests are often very similar, which makes their differentiation difficult (Stephenson and Van Niekerk 2009). However, indigenous forests are invariably much older than plantation forests. If the latter's age can be estimated using historical satellite imagery (e.g. MODIS or Landsat), this (age) information could be used to improve plantation and indigenous forest maps. For his research project, supervised by Prof Van Niekerk, he investigated how multitemporal Landsat imagery can be used to estimate the age of forests. Given that the ages of indigenous forests are unknown (well outside the timeframe for when imagery was available), the focus was to estimate the ages of plantation forests. Any forests with ages of less than 40 years can consequently be discarded as indigenous forests. The results are very promising, with an average error of less than one year. The intention was that Mr Mdwai would continue with an MSc in 2022 (as part of this project), but unfortunately, Mr Mdwai was not accepted (did not qualify) for MSc studies.

Mr Ayaaz Mullajie joined the project team in February 2022. His full-time MSc Geoinformatics study aimed to compare the effectiveness of convolutional neural networks (CNN) trained on medium resolution hyperspectral (HS), high-resolution MS and very high-resolution RGB imagery for mapping indigenous forest cover. Until September 2022, he was being supervised by Dr Munch and Prof Van Niekerk, but despite significant progress made, he decided to drop out from the programme citing personal reasons. This was a great loss for the project from a financial and progress point of view.

Mr Zandre Nieuwoudt joined the project team in February 2023. His MSc in Geoinformatics is being supervised by Prof Van Niekerk. Mr Nieuwoudt aims to continue with Mr Mullajie's research on the use of CNNs and the fusion of very high spatial resolution (50 cm) and low spectral resolution (RGB) aerial photography, high spatial resolution (10 m) and medium spectral resolution (multispectral), and low spatial resolution (30 m) and very high spectral resolution (hyperspectral) data for forest mapping. His project also forms part of the BiosCape campaign (<https://www.bioscape.io/science>) in collaboration with NASA. To date, Mr Nieuwoudt has been focussing on updating Mr Mullajie's proposal and literature review, but data collection and preparation will soon commence.

In addition to the students working on the project, a number of interns were appointed to assist with the indigenous forest digitising and quality control. Mr Given Nqoto, a GIS Mentor at Gert Sibande District Municipality in Mpumalanga requested that two GIS trainees, **Ms Nozipho Xaba** and **Mr Tshegofatso Moche** intern at the CGA as part of a programme called Infrastructure Skills Development Grant (ISDG), funded by the National Treasury department. The main aim of this programme is to develop capacity within municipalities by creating a long-term and sustainable pool of young professionals with built environment-related technical skills (engineering, town planning, architecture, quantity surveying, geographic information system (GIS) and project/operations management skills) and improve infrastructure management. Ms Xaba and Mr Moche were heavily involved with the indigenous forest digitising in 2022 and completed their internships in late November 2022.

In addition to the interns from outside Stellenbosch University, GIS assistance was provided in late 2022 and early 2023 from the following Stellenbosch University (SU) students: **Mr Emile Burger, Mr Andre Williams, Mr Niekus Fourie, Mr Charles Mudima, Ms Nokwazi Ngubo, Mr Daniel Timpson, Mr Rutger van Huyssteen, Mr Zander Lourens, Mr Farhaan Essop Ahmed and Mr Johan O Kennedy**. The majority of these students were in the second or third year of their geoinformatics degrees in late 2022 and the internships afforded them a level of real-world project exposure and practical experience in the advanced geographical information technology (GIT) software used for the digitising (eCognition) going into their final year, honours or masters studies.

APPENDIX II: PUBLICATIONS

No publications have emanated from this project at the time of writing this report.

APPENDIX III: ACCESS TO DATA GENERATED THROUGH THIS PROJECT

The remotely sensed WaPOR data used in this study can be freely downloaded from <https://wapor.apps.fao.org/>. The IF2021 indigenous forest map is available at <https://bit.ly/forests2021>. The refined indigenous forest map (IF2024) is still being edited, but will be released through a dedicated web app (link pending).

All of the data used in this project will be archived and stored for at least five years.

APPENDIX IV: SUPPLEMENTARY MATERIAL

The supplementary material for this report can be obtained from: https://bit.ly/indigenous_supp